CELL SURFACE ENGINEERING AND ITS APPLICATIONS

IN CANCER THERAPY

by

Daniel Yongwon Lee

A dissertation submitted to the faculty of
The University of Utah
in partial fulfillment of the requirements for the degree of

Doctor of Philosophy

Department of Pharmaceutics and Pharmaceutical Chemistry

The University of Utah

August 2017

The University of Utah Graduate School

STATEMENT OF DISSERTATION APPROVAL

The dissertation of **Daniel Yongwon Lee**

has been approved by the following supervisory committee members:

David A. Bull	, Chair	**June 02, 2017** Date Approved
David W. Grainger	, Member	**June 07, 2017** Date Approved
Hamidreza S. Ghandehari	, Member	**June 07, 2017** Date Approved
Mingnan Chen	, Member	**June 07, 2017** Date Approved
Matthew A. Williams	, Member	**June 07, 2017** Date Approved
Young-Wook Won	, Member	**June 02, 2017** Date Approved

and by **Carol S. Lim** , Chair of

the Department of **Pharmaceutics and Pharmaceutical Chemistry**

and by David B. Kieda, Dean of The Graduate School.

ABSTRACT

Remodeling of cell surface to install new features has continuously attracted attention for cell therapy. This dissertation focuses on a method of cell surface engineering using bioactive molecules to transiently award distinct functions to ordinary cells. Spontaneous incorporation of lipid-conjugated biomaterials to the cell membrane through hydrophobic interaction provides the basis for noninvasive cell surface modification.

First, mesenchymal stem cells (MSCs) were surface-engineered to embed a recombinant protein, stromal-derived factor 1 (SDF-1), for an enhanced target-specific homing effect. The SDF-1-embedded MSCs showed augmented migration towards the concentration gradient of their molecular target, CXC chemokine receptor 4 (CXCR4). Next, Jurkat cells were surface-engineered with magnetic resonance imaging (MRI) contrast agents to demonstrate the suitability of surface engineering in cell tracking. The contrast agent-embedded Jurkat cells were detectable by MRI.

To demonstrate the applicability of this technology in translational research, immune effector cells were surface-engineered with antibody-drug conjugates (ADCs) and their combined efficacy was examined in animal tumor models. This combination of chemotherapy and immunotherapy showed significant efficacy in treating cancers; however, the immunomodulatory effects of chemotherapy were difficult to control. This observation was due to the off-target toxicity of chemotherapy that damages the host immune cells: many cancer patients often require replenishment of immune cells after a

series of chemotherapy in order to benefit from immunotherapy. In order to overcome the challenge, new chemoimmunotherapeutic strategies require sufficient immunomodulatory ability of chemotherapy, targeted chemotherapy for reduced toxicity, and enhanced recruitment of immune cells to the tumor tissue. Surface engineering to affix chemotherapeutic agents on the cell membrane of immune effector cells is therefore an attractive approach.

In the main study of this dissertation, natural killer 92 (NK92) cells were surface-engineered to carry ADCs on their membranes. A lipid-conjugated model ADC, trastuzumab-DM1 (T-DM1), homogeneously modified the allogeneic NK92 cells without affecting the viability of NK92 cells. T-DM1-embedded NK92 (SE-NK/T-DM1) cells exerted strong anti-cancer activity through targeted chemoimmunotherapy. Although a wide range of experimental observations has proven that the SE-NK/T-DM1 cells are effective over the co-treatment of T-DM1 and NK92 cells, further investigations should be conducted to validate their potential for clinical application.

TABLE OF CONTENTS

ABSTRACT ……..iii

LIST OF FIGURES ……viii

LIST OF TABLES ……...…xiii

LIST OF ABBREVIATIONS …….…….xiv

Chapters

1. INTRODUCTION 1

1.1. Cell Surface Engineering…….....1
1.1.1. Covalent Conjugation 2
1.1.2. Electrostatic Interactions 6
1.1.3. Hydrophobic Interaction 7
1.1.4. Genetic Modification 10
1.2. Challenges in Surface Engineering of Living Cells 16
1.2.1. Cell Membrane Dynamics 17
1.2.2. *In Vivo* System 18
1.3. Applications of Surface-Engineered Cells Prepared by Hydrophobic Interaction..... 20
1.3.1. Islet Cell Transplantation..... 20
1.3.2. Mesenchymal Stem Cell Delivery for Myocardial Infarction 22
1.3.3. Enhancing Antigen Presentation for Dendritic Cells 23
1.4. Conclusions 25
1.5. References 29

2. CELL SURFACE ENGINEERING TO EMBED TARGETING LIGANDS OR TRACKING AGENTS ON THE CELL MEMBRANE..... …….44

2.1. Abstract…… 44
2.2. Introduction…….45
2.3. Materials and Methods…….46
2.3.1. Materials……... .46
2.3.2. Characteristics of MSCs……47
2.3.3. Cell Culture…….. 47

2.3.4. Surface Engineering with a Homing Peptide .... ……..48
2.3.5. Modification of MSCs with SDF-1 48
2.3.6. Migration Assay 49
2.3.7. Tests in Various Cell Lines 49
2.3.8. Modification with Tracking Agents 50
2.3.9. MRI 50
2.3.10. Statistical Analysis 51
2.4. Results 51
2.4.1. Modification of MSCs with a Homing Peptide 51
2.4.2. Modification of MSCs with a Protein..... 53
2.4.3. Migration of Modified MSCs 53
2.4.4. Normalization 56
2.4.5. Modification with Tracking Agents 61
2.5. Discussion 61
2.6. Conclusion..... 68
2.7. References 70

3. ADC-EMBEDDED NK92 CELLS TO COMBINE CHEMOTHERAPY AND IMMUNOTHERAPY IN A SINGLE CELL……73

3.1. Abstract 73
3.2. Introduction ..……...74
3.3. Materials and Methods …….....77
3.3.1. Study Design..……...77
3.3.2. Materials ..……78
3.3.3. Cell Culture ……...……...79
3.3.4. Generation of Recombinant Trastuzumab..…….....79
3.3.5. Synthesis of T-DM1..……...…….80
3.3.6. Antibody Activity ...…….……80
3.3.7. Cytotoxicity of T-DM1 ……81
3.3.8. Surface Engineering of Jurkat Cells and NK92 Cells.……..81
3.3.9. Characterization of Surface-Engineered Effector Cells……81
3.3.10. Selective Binding and Transfer of TZ and T-DM1 from Surface-Engineered Effector Cells to Cancer Cells …….....82
3.3.11. Internalization of Transferred T-DM1 into Cancer Cells……..83
3.3.12. Cytotoxicity Assay……84
3.3.13. Mechanistic Studies ..……..85
3.3.14. *In Vivo* Tumor Efficacy Study…….. 86
3.3.15. Biodistribution ……...86
3.3.16. Statistical Analysis..…….....……87
3.3.17. Animal Ethics ……...87
3.4. Results ..……...88
3.4.1. Design of the SE-NK/ADC Cells as Chemoimmunotherapy.....…….....88
3.4.2. Synthesis of T-DM1……..88
3.4.3. Generation of Surface-Engineered Cells……...97
3.4.4. Selective Binding and Transfer of TZ and T-DM1….……107

3.4.5. Anti-Cancer Activity of SE-NK/T-DM1 Cells……112
3.4.6. Mechanistic Studies ……..……..123
3.4.7. *In Vivo* Efficacy Studies ……126
3.5. Discussion ……..137
3.6. Conclusion ...……..141
3.7. References...……...143

4. RESULTS, CONCLUSIONS, AND FUTURE STUDIES ……..……..149

4.1. Summary of Chapter 2……..……..……149
4.1.1. Study Motivation ……149
4.1.2. Hypothesis …...……..……150
4.1.3. Key Study Results ……..……..……150
4.1.4. Conclusion ……..……...…151
4.2. Summary of Chapter 3……..……....152
4.2.1. Study Motivation ……152
4.2.2. Hypothesis ..…..……159
4.2.3. Key Study Results…...……..……...160
4.2.4. Conclusion ...……..……...162
4.3. Future Studies ...……..163
4.3.1. Risk of Differentiation and *In Vivo* Migration of SDF-1 Modified MSCs ……..163
4.3.2. Relaxivity of SPIONs on Surface Modified Jurkat Cells……..166
4.3.3. Internalization of Surface-Embedded SPIONs through Endocytosis...168
4.3.4. Real-Time Tracking of Therapeutic Cells Modified with SPIONs…....168
4.3.5. Degree of DMPE-PEG Conjugation on SPIONs and T-DM1……170
4.3.6. Concentration-Dependent DMPE-PEG Toxicity……171
4.3.7. Quantification of Internalized T-DM1……172
4.3.8. Mechanism of SE-NK/T-DM1 Cells……..……..172
4.3.9. Pharmacokinetics of SE-NK/T-DM1 Cells...……..173
4.3.10. Chou-Talalay Method of Combinatorial Effects……175
4.3.11. Improving Cytotoxicity of NK92 Cells ……176
4.3.12. Her2-Positive Breast Cancer and Hematological Cancers..……177
4.4. References...……179

APPENDIX: DIRECT INCORPORATION OF FUNCTIONAL PEPTIDE INTO M-DNA THROUGH LIGAND-TO-METAL CHARGE TRANSFER…..……...188

LIST OF FIGURES

1.1. Cell surface engineering with biomaterials……..…...……..3

1.2. SPR sensorgram of (a) DMPE-PEG-NH_2, (b) DPPE-PEG-NH_2, and (c) DSPE-PEG-NH_2 incorporation into supported lipid layer…….....8

2.1. MSCs modified with a homing peptide……52

2.2. Viability (a) and proliferation rate (b) of MSCs after the modification with DMPE-PEG-CRPPR-FITC ..……54

2.3. Confocal micrograph and FACS analysis of the SDF-1-modified MSCs.....…….....55

2.4. Migration of CRPPR modified MSCs towards CRIP2. ……57

2.5. Migration of the MSCs modified with DMPE-PEG-SDF-1 toward CXCR4 gradient ($^{\#}P$<0.01)....……...58

2.6. Surface modification of various cell types. Confocal micrographs of DMPE-PEG-FITC modified cell surface of different cell types…….……...59

2.7. Adhesion of different types of cells on a tissue culture plate after the surface modification with DMPE-PEG-FITC ……60

2.8. Confocal images of the SPION-modified Jurkat cells ……62

2.9. Degree of Jurkat cell modification with SPIONs ..……63

2.10. MRI of agar phantoms containing Jurkat cells modified with different amounts of DMPE-PEG-SPION-FITC ...…….64

2.11. Viability (a) and cell proliferation (b) of Jurkat cell after modification with DMPE-PEG-SPION-FITC ...…….65

3.1. Illustration of SE-NK/ADCs cells and their mechanism of actions ….……89

3.2. Synthesis of T-DM1, DMPE-TZ, and DMPE-T-DM1……90

3.3. FPLC purification of (a) TZ, (b) T-DM1 R=5, (c) T-DM1 R=10, (d) T-DM1 R=15……...91

3.4. ESI/MS spectra of T-DM1 synthesized with 5 molar excess of SMCC-DM1……..92

3.5. ESI/MS spectra of T-DM1 synthesized with 10 molar excess of SMCC-DM1……93

3.6. ESI/MS spectra of T-DM1 synthesized with 15 molar excess of SMCC-DM1……94

3.7. Cytotoxicity of Kadcyla® and T-DM1s synthesized with different ratio of SMCC-DM1 in SK-BR-3 cells ……..……..95

3.8. Cytotoxicity of Kadcyla® and T-DM1s synthesized with different ratio of SMCC-DM1 in MDA-MB-231 cells ……..…….96

3.9. Antigen-specific binding of TZ and T-DM1……98

3.10. Confocal images of SE-JK/TZ cells. ……99

3.11. Cell viability (a) and cell proliferation (b) of SE-JK/TZ cells compared to unmodified Jurkat cells..……..100

3.12. Retention time of TZ on the surface of SE-JK/TZ cells in the presence of 10% serum…..…….…..101

3.13. Confocal images of SE-JK/T-DM1 cells and SE-NK/T-DM1 cells…..……..103

3.14. Influence of surface modification with T-DM1 on NK92 cell viability and proliferation.....104

3.15. Retention time of T-DM1 on the surface of SE-NK/T-DM1 cells …..……105

3.16. Expression of NK92 cell receptors ……..106

3.17. TZ and T-DM1 on the surface of SE-JK/TZ cells and SE-NK/T-DM1 cells, respectively, increased the number of cancer-bound Jurkat and NK92 cells..……108

3.18. Confocal images showing the binding of SE-JK/TZ-FITC cells, SE-NK/TZ-FITC cells, or SE-NK/T-DM1-FITC cells to SK-BR-3 cells or MDA-MB-231 cells ..……109

3.19. Internalization of transferred T-DM1 into Her2-positive SK-BR-3 cells……111

3.20. Internalization of transferred T-DM1 into Her2-negative MDA-Mb-231 cells.…..113

3.21. Amounts of T-DM1 embedded on the cell membrane ……114

3.22. Long-term incubation of SE-NK/T-DM1 cells with (a) Her2-positive SK-BR-3 cells or (b) Her2-negative MDA-MB-231 cells ……...……115

3.23. Short-term incubation of SE-NK/T-DM1 cells with (a) SK-BR-3 cells and (b) MDA-MB-231 cells demonstrated targeted anti-cancer activity. ….……..117

3.24. Effects of DM1 on cancer cell death……118

3.25. Anti-cancer activity of T-DM1 contained in the SE-NK/T-DM1 cells against (a) SK-BR-3 cells and (b) MDA-MB-231 cells ...……120

3.26. Cancer cell death induced by SE-NK/TZ cells and SE-JK/TZ cells in (a) SK-BR-3 cells and (b) MDA-MB-231 cells……..……...121

3.27. Anti-cancer effects of SE-NK/T-DM1 cells and SE-JK/T-DM1 cells against (a) SK-BR-3 cells and (b) MDA-MB-231 cells …...……122

3.28. Effects of IL-2 on the anti-cancer activity of SE-NK/T-DM1 cells …..……..124

3.29. Degranulation of NK92 cells ……...……...125

3.30. Cytotoxicity of Kadcyla® and T-DM1s synthesized with different ratios of SMCC-DM1 in Calu-3 cells…….……127

3.31. Confocal images showing the binding of SE-JK/TZ cells, SE-NK/TZ cells, or SE-NK/T-DM1 cells to Calu-3 cells ……...…….....128

3.32. Internalization of transferred T-DM1 into Her2-positive Calu-3 cells….……129

3.33. Long-term incubation of SE-NK/T-DM1 cells with Calu-3 cells ….……..130

3.34. Targeted binding of SE-NK/T-DM1 cells to Calu-3 cells……131

3.35. Short-term incubation of SE-NK/T-DM1 cells with Calu-3 cells demonstrated the enhanced anti-cancer activity through targeted binding. …..……....132

3.36. Expression of CD107a on NK92 cells, T-DM1+NK92 cells, or SE-NK/T-DM1 cells following the co-incubation with Calu-3 cells ……...……..133

3.37. *In vivo* anti-cancer efficacy of SE-NK/T-DM1 cells in Her2-positive Calu-3 models……..135

3.38. *In vivo* anti-cancer efficacy of SE-NK/T-DM1 cells in Her2-negative MDA-MB-231 models…...……...136

3.39. Biodistribution of SE-NK/T-DM1 cells in Calu-3 model …..……..138

A.1. Schematic illustration showing the binding of cysteine-contained peptides to plasmid DNAs through the LMCT transition…….191

A.2. Effects of Zn^{2+} concentration and incubation time on M-DNA formation.…….…195

A.3. Cytotoxicity of M-DNA generated using various concentrations of $ZnCl_2$……...196

A.4. Characterization of PEI/M-DNA polyplex ……..197

A.5. EtBr replacement assays of PEI/M-DNA polyplex....……...198

A.6. EtBr replacement assays of PEI/B-DNA polyplex...…….200

A.7. Luciferase gene transfection by PEI/M-DNA polyplex or PEI/B-DNA polyplex….201

A.8. Spectrophotometric titration of C-9R-C with Zn^{2+}……203

A.9. The free cysteine concentration in C-9R-C and the free cysteine concentration after the addition of different amounts of C-9R-C peptide to M-DNA, or $ZnCl_2$ containing reaction buffers…...……..204

A.10. Agarose gel electrophoresis of C-9R-C/M-DNA complex and G-9R-G/M-DNA complex……205

A.11. Transfection of HEK293 cells with C-9R-C/M-DNA complex and C-9R-C/B-DNA complex.…….....……..207

A.12. Cellular uptake of C-9R-C/B-DNA complex or C-9R-C/M-DNA complex in HEK293 cells...…….……...208

A.13. HEK293 cell viability following the transfection with C-9R-C/M-DNA complex or C-9R-C/B-DNA complex ….…….....209

A.14. Transfection efficiency of C-9R-C/M-DNA complex relative to that of G-9R-G/M-DNA complex in HEK293 cells.……...……211

A.15. Agarose gel electrophoresis of M-DNA or B-DNA modified with C-RGD-C peptide…….213

A.16. Spectrophotometric analysis of C-RGD-C/M-DNA complex formation ……..…214

A.17. Changes in absorbance at 230 nm as a function of Zn/Cys ratio..……215

A.18. Luciferase activity (a) and cell viability (b) of MDA-MB-231 cells transfected with C-RGD-C/M-DNA complex……218

A.19. Luciferase activity (a) and cell viability (b) of HEK293 cells transfected with C-RGD-C/M-DNA complex..……..……219

A.20. Cellular uptake of C-RGD-C/B-DNA complex or C-RGD-C/M-DNA complex in (a) MDA-MB-231 cells or (b) HEK293 cells.……220

LIST OF TABLES

1.1. Methods for cell surface engineering…….……..……..4

1.2. Currently ongoing CAR-T cell clinical trials..…….…..……..12

1.3. Preclinical and clinical studies on CAR-NK cells.……15

4.1. Immunomodulatory functions of chemotherapeutic agents and antibodies……...154

4.2. Comparison of T cells, peripheral blood NK cells, and NK92 cells….…….158

A.1. Size and zeta potential ……...……...….……...…216

LIST OF ABBREVIATIONS

ADCC	Antibody-dependent cellular cytotoxicity
ADCs	Antibody-drug conjugates
Annexin V/PI kit	Annexin V Alexa Fluor® 488 and propidium iodide kit
bFGF	Basic fibroblast growth factor
BSA	Bovine serum albumin
CAR	Chimeric antigen receptor
CCK-8	Cell Counting kit-8
CDC	Complement-dependent cytotoxicity
CPP	Cell penetrating peptide
CRIP2	Cysteine-rich intestinal protein 2
CXCR4	CXC chemokine receptor 4
DAMP	Damage-associated molecular patterns
DCs	Dendritic cells
DMEM	Dulbecco's Modified Eagle's Medium
DMPE	1,2-dimyristoyl-sn-glycerol-3-phosphatidylethanolamine
DMPE-T-DM1	Lipid-PEG-conjugated T-DM1
DMPE-T-DM1-FITC	Lipid-PEG conjugated FITC labeled T-DM1

DMPE-TZ	Lipid-PEG-conjugated TZ
DMPE-TZ-FITC	Lipid-PEG conjugated FITC labeled TZ
DMSO	Dimethyl sulfoxide
DOPE	1,2-Dioleoyl-sn-glycero-3-phosphatidylethanolamine
DPBS	Dulbecco's phosphate-buffered saline
DPPE	1,2-dipalmitoyl-sn-glycerol-3-phosphatidylethanolamine
DSPE	1,2-distearoyl-sn-glycerol-3-phosphatidylethanolamine
EDC	1-ethyl-3-(3-dimethylaminopropyl) carbodiimide hydrochloride
EGFR	Epidermal growth factor receptor
ELISA	Enzyme-linked immunosorbent assay
EtBr	Ethidium bromide
FACS	Fluorescence-activated cell sorting
FBS	Fetal bovine serum
FITC	Fluorescein isothiocyanate
FLASH	MRI fast-low-shot-angle
FPLC	Fast protein liquid chromatography
FRAP	fluorescent recovery after photobleaching
GA	Geldanamycin
GD2	Ganglioside GD2
GPCR	G-protein-coupled receptors
GVHD	Graft-versus-host diseases
HA	Hyaluronic acid

HBSS	Hank's Balanced Salt Solution
HEK293 cells	Human Embryonic Kidney cell line
Her2 (ErbB2)	Human epidermal growth factor receptor 2
HLA	Human leukocyte antigen
IFN-γ	Interferon-γ
IgG	Immunoglobulin G
IL-2	Interleukin-2
LC-ESI/MS	Liquid chromatography-electrospray ionization mass spectrometry
LMCT	Ligand-to-metal charge transfer
mAb	Monoclonal antibody
ManNAz	*N*-α-azidoacetylmannosamine
MCP-1	Monocyte chemoattractant protein-1
M-DNA	Metal-bound DNA
MHC	Major histocompatibility complex
MI	Myocardial infarction
MOPS	3-(N-morpholino)propanesulfonic acid
MRI	Magnetic resonance imaging
MSC	Mesenchymal stem cells
MTT	3-(4,5-dimethylthiazol-2-yl)-2,5-diphenyltetrazolium bromide cytotoxicity assay
MWCO	Molecular weight cut-off
ncAA	Non-canonical amino acids
NHS	*N*-hydroxyl-succinimidyl ester
NK cell	Natural killer cells

NK92 cells	Natural killer 92 cells
NKG2D	Natural killer group 2D receptor
PAA	Poly(acrylic acid)
PAH	Poly(allylamine hydrochloride)
PBS	Phosphate-buffered saline
PDADMAC or PDDA	Poly(diallydimethylammonium) chloride
PEG	Poly(ethylene glycol)
PEI	Branched poly(ethyleneimine)
PET	Position emission tomography
PIGF	Placental growth factor
PLL	Poly-L-lysine
PLL-*g*-PEG	Poly-L-lysine -*graft*-poly(ethylene glycol)
PPP	Polyphosphoric acid
PSS	Poly(styrene) sulfate
PSS	Poly(styrene) sulfate
PVA	Poly(vinyl alcohol)
RS	Aminoacyl-tRNA synthetase
scFv	Single-chain antibody fragment
SDF-1	Stromal derived factor 1
SE-JK/T-DM1 cells	Surface-engineered Jurkat cells with trastuzumab-DM1
SE-JK/TZ cells	Surface-engineered Jurkat cells with trastuzumab
SE-NK/ADC cells	Surface-engineered NK cells with antibody-drug conjugates

SE-NK/T-DM1 cells	Surface-engineered NK92 cells with T-DM1
SE-NK/T-DM1-FITC	Surface-engineered NK92 cells with FITC labeled T-DM1
SE-NK/TZ cells	Surface-engineered NK92 cells with Trastuzumab
SiaNAz	N-α-azidoacetyl sialic acid
SMCC-DM1	4-(N-maleimidomethyl)cyclohexane-1-carboxylate linked DM1
SPIONs	Superparamagnetic iron oxide nanoparticles
SPR	Surface plasmon resonance
TAA	Tumor associated antigen
TCR	T cell receptor
T-DM1	Trastuzumab-DM1
T-DM1+Jurkat cells	Jurkat cells with T-DM1 co-treatment
T-DM1+NK92 cells	NK92 cells with T-DM1 co-treatment
T-DM1-FITC	FITC-labeled T-DM1
TZ	Trastuzumab
TZ+Jurkat cells	Jurkat cells with TZ co-treatment
TZ+NK92 cells	NK cells with TZ co-treatment
UV	Ultraviolet
VEGF	Vascular endothelial growth factor

CHAPTER 1

INTRODUCTION

1.1. Cell Surface Engineering

Cell surface engineering to provide new characteristics and functions to cells has drawn continual interest from researchers in biomedical science. Biomaterials including proteins, surface receptors, antibodies, peptides, genetic materials, and protective polymers have been used to endow specific functions to cells.[1-8] The research areas that have benefitted from cell surface modification are (1) investigation of adding new functions, (2) reducing graft rejection for transplantation by masking the surface antigens, (3) creation of heterogeneous cluster of cells by cell-to-cell attachment, and (4) enhancing immune effector functions for therapeutic benefits. Inarguably, the last area has become one of the most intensively investigated topics involving genetically engineered immune cells for cancer therapy.[9] In order to introduce the new functionalities, cell surface was initially modified through covalent conjugation,[5,6,8,10] electrostatic interaction,[11-13] and hydrophobic interaction.[4,14-18] Continuous research on cell surface modification has ultimately arrived at genetic modification that permanently reprograms cells.[3,19,20] Ideal surface engineering methods should provide control over the fate and functions of the modified cells without interfering with cell survival, proliferation, and cellular activities. Therefore, the methods listed above should be carefully selected to meet the purpose of modifying the cell surface

properties. Biomaterials commonly used for all surface engineering techniques and their representative applications are summarized in Figure. 1.1 and Table 1.1.

1.1.1. Covalent Conjugation

Covalent conjugation chemically, metabolically, or enzymatically attaches bioactive substances to the cell membrane.[5-8,21-23] Chemical conjugation is the most straightforward method that takes advantage of surface-exposed functional groups, such as amines and thiols, on the membrane proteins as grafting points. Currently, *N*-hydroxyl-succinimidyl ester (NHS) groups,[5-8] maleimide,[23] and pyridyldithiol[24,25] are the most frequently used chemical cross-linkers (Figure 1.1a). Metabolic surface modification has been reported by Saxon et al. and Prescher et al.[21,22] Interestingly, human cells undergo unnatural sialic acid biosynthesis when exposed to unnatural sugar *N*-α-azidoacetylmannosamine (ManNAz), an analog of the native sugar *N*-acetylmannosamine (Figure 1.1b). This process incorporates *N*-α-azidoacetyl sialic acid (SiaNAz), a metabolite of ManNAz, to the membrane glycoconjugates. The added azide groups further provide attachment points for biomaterials through Staudinger ligation[21,22] or click-chemistry.[26,27] Covalent conjugation can be also achieved through enzymatic conjugation. As reported by Swee et al., transpeptidase sortase A from *Staphylococcus aureus* efficiently conjugates peptides or proteins with LPETG motif to the N-terminal glycine exposed on the surface of different types of cells (Figure 1.1c).[28] Although chemical conjugation provided stable modification, conjugated biomaterials gradually disappeared over time.[5,8,16] Moreover, the degree of modification is difficult to control with covalent conjugation and higher degree of modification using bioactive molecules, both small or large, may cause significant

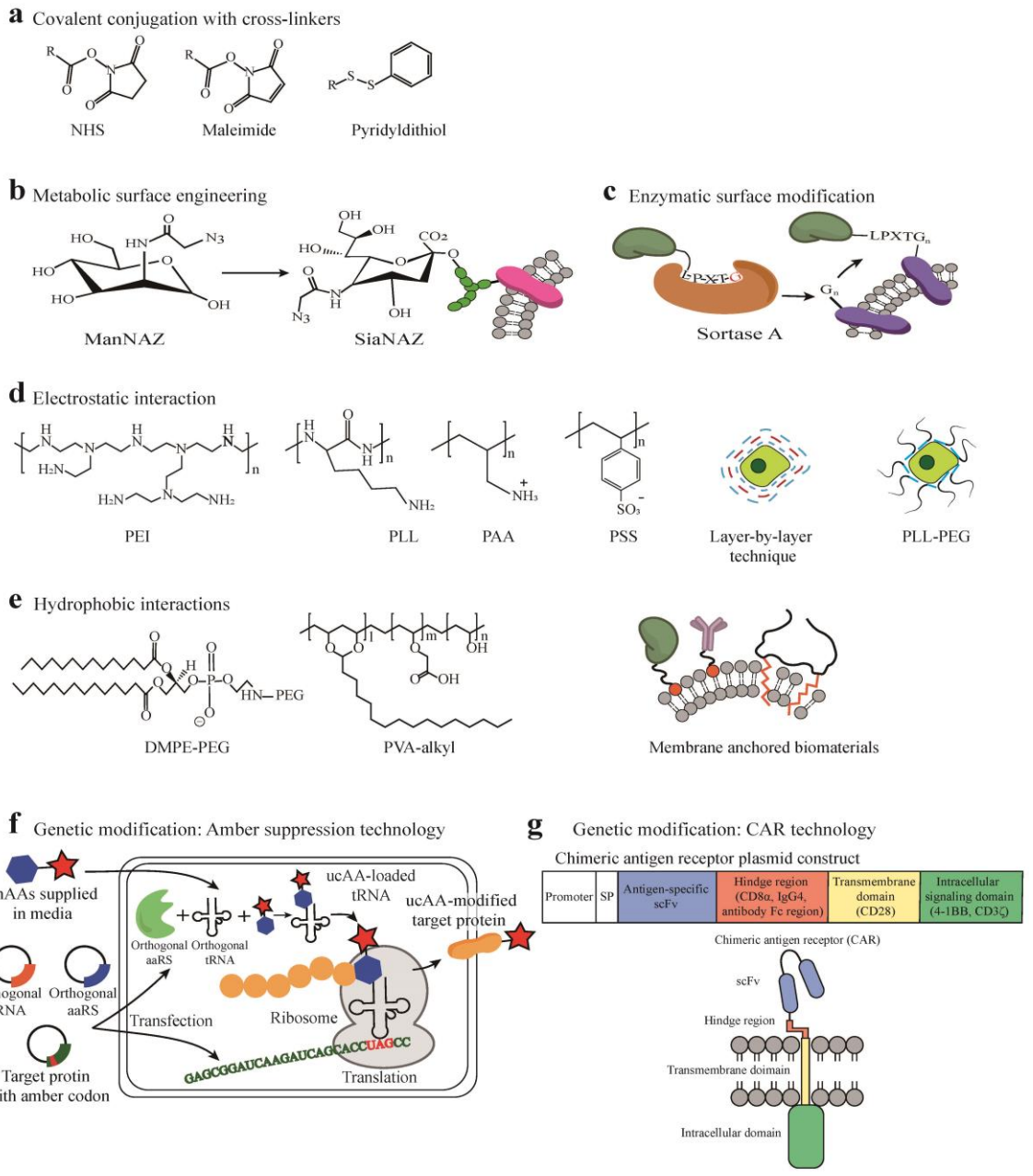

Figure 1.1 Cell surface engineering with biomaterials. (a) Incorporation of cross-linkers, such as NHS, Maleimide, or pyridyldithiol, allows cell surface modification with biomaterials. Cell metabolism of unnatural sugar (b) and enzymatic reactions (c) can be exploited to attach functional groups on the cell surface. (d) Electrostatic interactions between the cell surface and the charged polymers such as PEI, PLL, PAA, and PSS can modify cells through layer-by-layer technique. Also, charged block-co-polymers, such as PLL-PEG, can modify the cell surface through electrostatic interaction. (e) Lipid-conjugated bioactive molecules or polymers with long alkyl chains can be embedded into the cell membrane through hydrophobic interaction. Genetic modifications can remodel the cell surface by means of amber suppression (f) and CAR technology (g).

Table 1.1. Methods for cell surface engineering

	Modification sites	Treatment	Cells	Introduced biomaterials	Reference
Covalent conjugation	Primary amines of membrane protein	Chemical reaction	Islet cells	PEG-NHS	6, 7, 8
				PEG-Biotin/avidin then heparin-conjugated polymers	5
				Phosphine-PEG-NHS followed by Staudinger ligation of thrombomodulin	10
	Thiol groups of membrane protein		K562, C6, B16	Pyridyldithiol conjugated Gd(III) chelates	24
	Surface exposed thiols		T cells	Maleimide cross-linking of lipid nanocapsules loaded with SN-38	23
	Membrane protein	Metabolic reaction of unnatural sialic acid biosynthesis	Jurkat cells HeLa cells	Peracetylated ManNaz followed by Staudinger ligation of phosphine-biotine conjugate	21
			Splenocyte	Peracetylated ManNaz followed by Staudinger ligation of phos-Flag peptide	22
	Membrane proteins and peptides with exposed N-terminal glycine	Enzymatic conjugation	Yeast cells, 293T cells, splenocytes, *Toxoplasma gondii*, CD8 T cells	Biotin-LPETG peptide TAMRA-LPETG peptide Antibody-LPETG peptide	28
Electrostatic interaction	Negatively charged cell surface	Non-covalent reaction	Islet cells	PDDA, PAH, and PSS; layer-by-layer	13
			MCF-7	PEI, PPP, PAH, PS, PLL, PDDA, and PSS; layer-by-layer	11
			Porcine brain capillary endothelial cells	PDDA, PAH, and PSS; layer-by-layer	30
			Human fibroblast cells	PLL, PAA, and alginate; layer-by-layer	12
			Mouse mesenchymal stem cells	PLL and HA; layer-by-layer	33
			Islet cells	PLL-*g*-PEG, PLL-*g*-PEG-biotin, PLL-*g*-PEG-hydrzide PLL-*g*-PEG-azide	31, 36

Table 1.1. (Continued)

	Modification sites	Treatment	Cells	Introduced biomaterials	Reference
Hydrophobic interaction	Cell membrane	Non-covalent reaction	Islet cells	DPPE-PEG-maleimide followed by thiolated-PVA	15
			Islet cells, HEK293	DPPE-PEG-NH_2 followed by alginate and PLL; layer-by-layer	37
			HEK293 cells CCRF-CEM	DPPE-PEG-NH_2, PVA-alkyl	16
			Islet cells, CCRF-CEM	DPPE-PEG-Biotin followed by Biotin-BSA and streptavidin; layer-by-layer; heparin and urokinase immobilization	38
			HEK293, Islet cells	Thiolated PVA-alkyl followed by maleimide-conjugated urokinase	15
			HEK293, Islet cells	DPPE-PEG-Bitin followed by streptavidin	39
			Islet cells	DPPE-PEG-maleimide terminated with cystein	40
			HeLa cells, HepG2, B16, Ba/F3	DOPE-PEG-Mouse IgG1	4
			Mesenchymal stem cells	DMPE-PEG-FITC, DMPE-PEG-GFP, DMPE-PEG-CXCR4	18
			Mesenchymal stem cells, Jurkat cells	DMPE-CRPPR peptide, DMPE-SDF-1, DMPE-SPIONs	41
Genetic modification	Membrane proteins	Amber suppression technology	HEK293T cells	Insulin receptor with ncAA for click chemistry	49
			HEK293T cells	GPCR with photoactivatable cross-linkers	54
			HEK293 cells	EGFR with ncAA for TAMRA labeling	53
	Membrane	Gene transfection and transduction	T cell	ErbB2-CAR, CD19-CAR, VEGF2-CAR	64, 66, 67, 75, 77
			NK cell	ErbB2-CAR, GD2-CAR CD19-CAR, CD20-CAR	71, 72, 73
			T cell	CD16, NKG2D	79, 80
			NK cell	CD16, NKG2D	81, 83

Adapted from Teramura et al.[2]

physiological alterations, such as reduction of membrane mobility and diffusion kinetics to the modified cells.[2,14,29]

1.1.2. Electrostatic Interactions

Electrostatic interactions modify the cell surface by establishing self-assembled structures between the negatively charged cell surface and cationic polymers (Figure 1.1d). Cells initially modified with cationic polymers can be further engineered *via* a layer-by-layer technique by sequentially applying anionic and cationic polymers.[11,13,30-32] Because modified cells encapsulated by multiple polymeric layers can reduce molecular recognition, the electrostatic layer-by-layer approach has been often investigated in cell transplantation research.[13,31] Many cationic/anionic polymers and poly electrolytes, such as poly-L-lysine, (PLL), poly(styrene) sulfate (PSS), poly(allylamine hydrochloride) (PAH), poly(diallydimethylammonium) chloride (PDADMAC or PDDA), poly(ethyleneimine) (PEI), polyphosphoric acid (PPP), and poly(acrylic acid) (PAA), and hyaluronic acid (HA) have been used to generate multiple layers on cell membrane.[11,13,30-33] Thickness of the polymer layer can be controlled by changing the number of layers. The new surface properties of the modified cells rely on the polymer characteristics of the outermost layer. Despite the advantage of cell surface modification through electrostatic interaction, the high charge density of cationic polymers significantly reduces the viability of modified cells.[30,34,35] In an attempt to reduce the toxicity, PLL-*graft*-poly(ethylene glycol) (PLL-*g*-PEG) was introduced to coat the surface islet cells.[31,36] Surface modification of PLL-*g*-PEG was further developed to incorporate functional groups, such as biotin, hydrazide, and azide, to capture streptavidin, aldehyde,

and cyclooctyne.[36] While the cytotoxicity of cationic polymers was improved through PEG conjugations on primary amines of PLL, biocompatibility of cationic polymers has not been fully resolved.

1.1.3. Hydrophobic Interaction

Amphiphilic polymers polymerized with long alkyl chains, such as phospholipid-conjugated PEGs and poly(vinyl alcohol) (PVA), provide noninvasive modifications of the cell surface through hydrophobic interaction (Figure 1.1e). Similarly, a large number of different cell types have been modified *via* hydrophobic interaction with lipid-conjugated biomaterials for specific function.[4,14-18,29,37-42] Most lipophilic membrane dyes currently available in the market, such as DiI, DiD, DiR, and DiO, are developed upon cell surface modification through hydrophobic interaction. Interaction of lipid-conjugated PEGs with lipid bilayers was examined by Yamamoto et al. using surface plasmon resonance (SPR) spectroscopy.[43] Lipids with different lengths of alkyl chains—1,2-dimyristoyl-sn-glycerol-3-phosphatidylethanolamine (DMPE, 14 carbons), 1,2-dipalmitoyl-sn-glycerol-3-phosphatidylethanolamine (DPPE, 16 carbons), and 1,2-distearoyl-sn-glycerol-3-phosphatidylethanolamine (DSPE, 18 carbons)—were conjugated with PEG (5 kDa) and applied onto the lipid bilayer. Out of all lipid-PEG conjugates, DMPE showed the most rapid incorporation to the membrane (Figure 1.2). Insertion of DPPE showed concentration-dependent behavior; however, incorporation of DSPE was only observed at high concentration. Dissociation of DMPE was more rapid compared to DPPE when modified lipid bilayer was washed with PBS. No dissociation was observed once DSPE was incorporated into the membrane. Thus, it was noted that

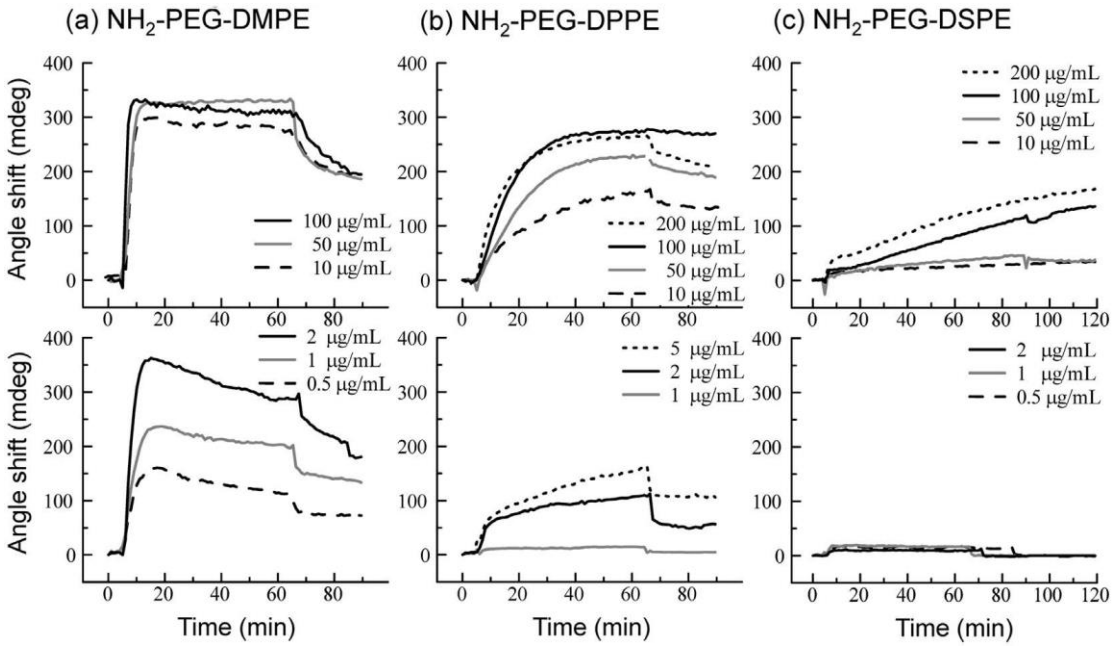

Figure 1.2. SPR sensorgram of (a) DMPE-PEG-NH_2, (b) DPPE-PEG-NH_2, and (c) DSPE-PEG-NH_2 incorporation into supported lipid layer. The upper panels show lipid-PEG concentrations above 5 µg/ml and lower panels show lipid-PEG concentrations below 5 µg/ml. Adapted from Yamamoto et al.[43]

longer hydrophobic chains reduce the incorporation rate and the dissociation rate of lipid molecules.[43] Interestingly, fluorescence of FITC-labeled lipid-PEGs was recovered in a few minutes in fluorescent recovery after photobleaching (FRAP) assay.[43] This observation indicates that lipid-PEGs embedded in the lipid bilayer were able to diffuse laterally within the lipid bilayer. Unlike covalent conjugation and electrostatic interaction, surface modification with hydrophobic interaction allows membrane-anchored bioactive molecules to participate in the dynamic movement of cell membrane. Most importantly, cells modified with lipid-conjugated biomaterials showed negligible toxicity, and the modified cells resumed normal cellular activities.[37-39] Instead of preparing the lipid-conjugated molecules, modification of cell surface can be achieved by liposomal fusion strategy.[44] Because liposomes are vesicles composed of lipids and lipid-conjugated molecules, large sections of the liposomes containing specialized lipids can be incorporated into the membrane without causing severe toxicity.[44-46] Fate of the lipid-conjugated bioactive molecules has not been fully understood, and the exclusion pathway requires further investigation; however, the endocytosis of membrane-anchored lipid-conjugated biomaterials has not been observed.[47] Lipid-conjugated biomolecules are believed to be released from the cells to the surroundings due to equilibrium difference.[16] Although molecules of interest must be hydrophobized by lipid or alkyl chain conjugation and the retention time on the surface is variable, hydrophobic interaction is an attractive surface engineering technology that offers rapid and nontoxic surface modification to virtually any type of cell.

1.1.4. Genetic Modification

Out of all cell modification methods discussed in this section, genetic modification is the most advanced and complicated surface modification technique. Strength of genetic modification lies within its versatility to introduce or knock-out specific surface proteins for desired effects.[48] Amber suppression technology has been developed to introduce noncanonical amino acids (ncAAs) bearing special functional groups for chemical attachments to the surface proteins synthesized by the cells (Figure 1.1f).[49-54] This method involves transfecting cells with plasmids that express a protein of interest containing an amber stop codon at the desired site and aminoacyl-tRNA synthetase/tRNA (RS/tRNA) pair. These orthogonal RS/tRNA pairs do not interfere with the native RS/tRNA pair but rather work in conjunction with the host protein machinery. When native and orthogonal RS/tRNA pairs encounter the amber codon without ncAA supplementation, translation terminates and a truncated protein is synthesized. However, when ncAAs are supplied to the media, the orthogonal RS/tRNA pair adds the corresponding ncAAs to the growing peptide chain and synthesizes the final protein with specific modifications. Various ncAAs have been synthesized to provide biocompatible modifications.[49,55-57] Although amber suppression technology is a fascinating surface modification method, its apparent limitations—including competition between orthogonal and native RS/tRNA pairs, low expression efficiency, and adverse effects of truncated proteins—should be evaluated for therapeutic applications.[50,58]

Advances in genetic engineering, fueled by the growing interest in cell-based immunotherapy, have enabled the expression of new receptors to enhance the efficacy of therapeutic immune cells. Because tumors have evolved to manipulate the

microenvironment as a means of evading the host immune system,[59-62] readministrating a large number of *ex vivo* expanded autologous immune effectors cells, such as T cells and natural killer (NK) cells, is often ineffective against cancers. In order to overcome this major obstacle in cell-based immunotherapy, anti-cancer effects of T cells and NK cells must be activated through a different signaling pathway. Genetic modification to express chimeric antigen receptors (CARs) specific for tumor-associated antigens (TAAs) has redirected T cell and NK cell activity towards tumors in many reported studies (Figure 1.1g).[9,62-77] While genetically modified T cell receptors (TCRs) can recognize both intracellular and cell surface antigens, CARs are more advantageous because they are not restricted by major histocompatibility complex (MHC) and HLA type and can be applied to NK cells.[62,78] Table 1.2 provides a list of CAR-T cells currently undergoing clinical investigation. Also, Table 1.3 shows CAR-NK cells under preclinical and clinical evaluations as an alternative to CAR-T cells. Generally, as shown in Figure 1.1, CARs are composed of a single-chain antibody fragment (scFv), a hinge region connected to transmembrane domain, and tandem intracellular domains. The two most important components are the scFv and the intracellular domains: scFv determines the antigen specificity, and the intracellular domains control the degree and persistency of cytolytic activity and activation.[78] Adoptively transferred CAR-T cells and CAR-NK cells migrate towards the TAAs, bind to their targeted TAAs, stimulate the intracellular domains, and ultimately activate the cytolytic functions of T cells and NK cells. CAR-T cells have targeted many TAAs associated with different types of cancers, and numerous TAAs are currently being evaluated in the clinical setting (Table 1.2).[9,62] Genetic modification is not limited to expression of CARs and can be extended to improve the expression of cytolytic

Table 1.2. Currently ongoing CAR-T cell clinical trials

Target	Indication	Clinical Trials
CD19 or CD20	Leukemia	NCT01860937, NCT02146924, NCT02228096, NCT02435849, NCT02028455, NCT02614066, NCT02625480, NCT01747486, NCT02030847, NCT02535364, NCT01683279
	Leukemia or lymphoma	NCT02443831, NCT02529813, NCT02546739, NCT01430390, NCT01853631, NCT02050347, NCT02456350, NCT02081937, NCT02132624, NCT02349698, NCT01475058, NCT02537977
	Lymphoma	NCT02650999, NCT02431988, NCT02631044, NCT02445248, NCT02277522, NCT02624258, NCT01493453, NCT01840566, NCT02134262, NCT02247609, NCT02348216, NCT02030834
	Multiple myeloma	NCT02135406, NCT02135406
CD22	B cell malignancy	NCT02588456, NCT02315612
Igκ light chain	B cell malignancy	NCT00881920
CD30	Lymphoma	NCT02259556, NCT02274584
CD138	Multiple myeloma	NCT01886976
BCMA	Multiple myeloma	NCT02546167, NCT02215967

Table 1.2. (Continued)

Target	Indication	Clinical Trials
CD33	Myeloid malignancies	NCT01864902
CD123	Myeloid malignancies	NCT02623582, NCT02159495
NKG2D ligands	Various hematological malignancies	NCT02203825
ROR1	Leukemia	NCT02194374
EGFR	EGFR+ solid tumors	NCT02331693, NCT01869166
EGFRvIII	Glioblastoma	NCT02209376, NCT02209376, NCT02209376, NCT01454596,
GD2	Neuroblastoma, Ewing's sarcoma, osteosarcoma and melanoma	NCT01822652, NCT02107963
IL13Rα2	Glioma	NCT02208362
HER2	HER2+ solid tumors	NCT00902044, NCT01109095
Mesothelin	Mesothelioma, pancreatic cancer and ovarian cancer	NCT02159716, NCT02414269, NCT01897415, NCT02580747, NCT02465983
PSMA	Prostate cancer	NCT01140373

Table 1.2. (Continued)

Target	Indication	Clinical Trials
FAP	Malignant pleural mesothelioma	NCT01722149
GPC3	Hepatocellular carcinoma	NCT02395250
MET	Breast cancer	NCT01837602
MUC16	Ovarian cancer	NCT02498912
CEA	Various solid tumors	NCT02349724, NCT01723306
Lewis-Y	Solid tumors and myeloid malignancies	NCT01716364
MUC1	Hepatocellular carcinoma, NSCLC, pancreatic carcinoma, triple-negative invasive breast carcinoma	NCT02617134, NCT02587689

Abbreviations:
BCMA, B cell maturation antigen; CEA, carcinoembryonic antigen; EGFR, epidermal growth factor receptor; EGFRvIII, EGFR variant III; FAP, fibroblast activation protein; GPC3, glypican 3; HER2, human epidermal growth factor receptor 2; Ig, immunogloulin; IL13Rα2, interleukin 13 receptor α2 subunit; MUC, mucin; NSCLC, nonsmall cell lung carcinoma; ROR1, receptor tyrosine kinase-like orphan receptor.

Adapted from Fesnak et al.[9] and www.clinicaltrials.gov.

Table 1.3. Preclinical and clinical studies on CAR-NK cells

Target	Indication	NK cell types	Reference	Clinical trials
CD19	Lymphoid malignancies	PBMC NK / NK92	79, 80-83	NCT00995137 NCT01974479
CD20	Lymphoid malignancies	PBMC NK / NK92	71, 84, 85	
CD38	Multiple myeloma	PBMC NK / NK92	86	
Her2	Breast carcinoma Head and neck cancer Ovarian carcinoma Glioblastoma	PBMC NK / NK92	70, 87, 88	
GD2	Neuroblastoma	NK92	72	
EPCAM	Breast carcinoma Pancreatic cancer	NK92 NK92	89	
EBNA3C	EBV infections	NK92	90	
CS1	Multiple myeloma	NK92	91	

Abbreviations:
PBMC NK, NK cell isolated from the peripheral blood mononuclear cells; EBNA3C, Epstein-Barr nuclear antigen 3C; Her2, human epidermal growth factor receptor 2; EPCAM, epithelial cell adhesion molecule; GD2, ganglioside GD2; CS1, surface glycoprotein.

Adapted from Klingemann et al.[69] Glienke et al.[20] and www.clinicaltrials.gov.

receptors that are constitutively expressed at low levels. In this approach, genes coding for NKG2D, an NK cell activating receptor, and CD16 (FcγRIII), an Fc receptor responsible for antibody-dependent cellular cytotoxicity (ADCC), can be employed for augmented expression on T cell and NK cell membranes.[92-96] There is no doubt that genetic engineering technology empowers unresponsive immune effector cells against cancer and other difficult-to-treat diseases; however, its potential weaknesses should be addressed for smoother clinical application. Viral vectors are readily employed to generate genetically modified T cells and NK cells; however, the transduction efficiency is unimpressive and varies widely. The transduction efficiency was only between 50% to 75% even with the lentiviral transduction.[97,98] Although no observation was reported on oncogenic transformation of genetically modified T cells, manipulation at the gene level yields the potential risk of gene integration regardless of vectors. This consequently leads to gene dysregulation, as seen in gene-modified stem cell transfer.[99] Moreover, current protocols to prepare genetically engineered T cells used in the clinical trials are extremely expensive and time-consuming.[62,100,101]

1.2. Challenges in Surface Engineering of Living Cells

For clinical translation, surface-engineered cells must satisfy several fundamental principles of biocompatibility. Because cells are the most critical component of cell therapy, any modifications applied to the cell surface should not have detrimental effects on cell viability. At any stage of preparation, cell viability should not be altered by changes in pH, osmolality, temperature, pressure, degree of agitation, and exposure to organic solvent.[48] Surface modification should not become a physical barrier that blocks diffusion

of necessary nutrients. This is particularity important for islet cell transplantation, where surface-modified islet cells secrete insulin in response to glucose levels.[15,38,102] Unless the purpose for surface engineering is to mask the surface antigens during transplantation or adoptive transfer of immune cells—for the sake of reducing the occurrence of graft-versus-host disease (GVHD)—surface proteins and receptors should be exposed on the surface without hindrance to bind growth factors and ligands to signal cell survival, proliferation, and activation. For example, binding of interleukin-2 (IL-2) to IL-2 receptors on T cells and NK cells triggers cell expansion.[103] Moreover, surface engineered biomolecules should not reduce the membrane flexibility and elasticity, which are the essential properties of cell membrane that allows cell adhesion, migration, and signaling.[104-107] Lastly, the cost of surface engineering cells for therapeutic purposes must be affordable. Genetic modification of CAR-T cells can be finely tuned to provide personalized cell therapy for many cancers and diseases; however, the cost of treatment is extremely expensive, estimated at $25,000 per treatment.[101] The high cost arises from the labor-intensive and time-consuming certified process to prepare CAR-T cells. The surface modification methods discussed in this chapter have the potential to be applied as an alternative technology to CAR-T cells and are more economical with rapid preparation of therapeutic cells.

1.2.1. Cell Membrane Dynamics

Cell membrane is in a dynamic state. It is subjected to undergo constant remodeling where most of its components—lipids and membrane proteins—are internalized, degraded, recycled, and replaced.[108,109] The rate of these processes is highly dependent on the type of

lipids and proteins and varies widely from hours to weeks.[110] Cell membrane lipids and proteins are routinely internalized through endocytosis, pinocytosis, and phagocytosis. Due to their size, type, and property, biomaterials that are chemically conjugated, electrostatically adsorbed, hydrophobically embedded, or genetically expressed on the membrane, may internalize mostly through endocytosis.[111] The process of endocytosis is initiated as complementary ligands bind to surface receptors or as bioactive substances are absorbed on the cell membrane.[112-114] These events trigger invaginations of small areas containing the receptors and affected regions of cell membrane. Subsequently, the invaginated pockets are closed, and newly formed vesicles are transported to the intracellular compartments. During endocytosis, any molecules and materials on the invaginated cell membrane and in the proximal media will be taken up by the cells, resulting in the loss of desired functions installed *via* surface engineering. Therefore, surface engineering methods should consider cell membrane dynamics in order to improve the surface residence time of the desired biomaterials for prolonged therapeutic effects.

1.2.2. *In Vivo* System

Unlike the *in vitro* experimental settings, the *in vivo* environment is an integrated system of many complex mechanical and biochemical interactions. Transplanted or adoptively transferred surface-engineered therapeutic cells are exposed to sheer stress and hemodynamic forces that can strip off the installed surface modification.[48] Migration in the circulation and endothelial transmigration in the tissues, as demonstrated by leukocytes and stem cells, require extensive reshaping of the cell membrane.[115,116] In the spleen, circulating cells are forced to enter the compact network of sinusoidal capillaries to eliminate damaged

and aged cells.[117] In order to compensate for the mechanical stress from the *in vivo* environment, surface-engineered cells must display unaltered membrane flexibility and elasticity. Surface-engineered cells in blood circulation are also exposed to coagulation factors, the complement immune system, and inflammation mediators that drastically reduce duration of therapeutic effects.[118,119] Macrophages and monocytes of innate immune defense are often stimulated in response to the bioactive substances on surface-modified cells and subsequently eliminate them from the body by phagocytosis.[120] Immunogenic biomaterials, such as proteins synthesized from bacterial host and antibodies isolated from animals, are opsonized by neutralizing antibodies and are cleared by the innate immune system and complement activation.[121-124] Moreover, CAR designs can produce genetically modified cells with a high risk of adverse effects. Hombach et al. described that CAR-T cells bearing constant IgG1 Fc domains in the hinge regions simultaneously activated the CAR-T cells and cross-activated the host immune cells with CD16 receptors.[125] As a result, the off-target activation of CAR-T cells was increased and the undesired proinflammatory cytokines were released from the CD16-expressing host innate immune cells activated against the IgG1 Fc domains of CAR-T cells. Potential adverse effects of unintentionally activated innate immune cells were minimal as they were removed by activated CAR-T cells; however, off-target activation of CAR-T cells reduced the anti-cancer activity of CAR-T cells and increased the risk of cytokine release syndrome (CRS).[126,127] In conclusion, cell surface modification, regardless of the methods employed, must not sacrifice the membrane flexibility and elasticity but rather provide new functionality in addition to the protection against mechanical and biological challenges for clinical applications.

1.3. Applications of Surface-Engineered Cells Prepared by Hydrophobic Interaction

Surface engineering methods discussed in this chapter, (1) covalent conjugation, (2) electrostatic interaction, (3) hydrophobic interaction, and (4) genetic modification, have both advantages and limitations for biomedical applications. Although covalent conjugation provides stable modification on lipids, proteins, glycolipids, and polysaccharides, high degrees of modification may result in impairment of native protein function, altered membrane flexibility, and reduced viability. Electrostatic interaction allows for layer-by-layer techniques, but the cytotoxicity resulting from cationic polymers is too significant to be considered for clinical application. Genetic modification is an attractive method to generate customized surface proteins and receptors; however, gene transfer efficiency, generation process, and the safety of genetically modified cells need to be improved. Although short retention time is a potential limitation, aforementioned in the previous section, cell surface engineering with lipid-conjugated biomaterials through hydrophobic interaction provides noninvasive, nontoxic, and uniform modification of cells. Virtually any cell or structure encapsulated with a lipid bilayer can be rapidly modified with hydrophobized biomaterials. In this section, applications of cell surface modification with lipid-conjugated biomaterials will be presented.

1.3.1. Islet Cell Transplantation

Patients with transplanted cells, tissues, and organs are administered immunosuppressive drugs to reduce the risk of GVHD.[128] Without immunosuppression, the host immune system recognizes the transplanted cells, tissues, and organs as foreign matters, and thus mobilizes immune effector cells, produces antibodies, and destroys them.

Even before the immune recognition, coagulation factors and complement activators in the blood circulation in contact with the transplanted grafts trigger an inflammatory response directed for destruction.[129-134] Both membrane and surface antigens on the graft should be protected and masked in order to reduce the risk of transplant rejection. As shown in Table 1.1, many studies have used hydrophobic interactions to modify the islet cell surface. Teramura and Iwata reported to encapsulate islet cells with multiple protective layers created by DPPE-PEG-biotin, streptavidin, and biotin-conjugated bovine serum albumin (biotin-BSA).[38] First, islet cells were incubated with DPPE-PEG-biotin to install initial biotinylated surface. Next, streptavidin followed by biotin-BSA were applied in sequence 20 times. This layer-by-layer technique produced multiple protective layers with a total thickness of 30 nm on the islet cells without significantly affecting the cell viability.[38] Glucose molecules were able to diffuse through the protective membrane and finally into the cell. In response to glucose levels, surface-engineered islet cells were able to release insulin accordingly. Effects of surface modified islet cells were examined in streptozotocin-induced diabetic mice.[40] Islet cells with DPPE-PEG were transplanted in the liver through the portal vein. Compared to the control mice transplanted with unmodified islet cells, mice transplanted with modified islet cells showed improved graft survival; however, glucose regulatory functions of surface-modified islet cells were achieved only for a short period due to increased cell damage.[40] Teramura and Iwata continued to attach living cells to protect islet cells.[39] The rationale for this approach was that the attachment of vascular endothelial cells or fibroblast isolated from a recipient on islet cells would increase the transplantation compatibility.[39] In order to test the new strategy, both HEK293 cells and islet cells were modified with DPPE-PEG-biotin. Streptavidin was immobilized on

HEK293 cells and subsequently immobilized on biotin-functionalized islet cell surface. Interestingly, HEK293 cells continuously proliferated to completely cover the islet cells a few days after the immobilization. Histological analysis confirmed that islet cells at the core did not undergo necrosis or show signs of damage.[39] Unfortunately, transplantation of living cell-modified islet cells has not been examined in animal models yet.

1.3.2. Mesenchymal Stem Cell Delivery for Myocardial Infarction

Mesenchymal stem cells (MSCs) have been used to remodel the left ventricle and rescue the cardiac function for myocardial infarction (MI) in animal models.[135-137] At the ischemic sites, administrated MSCs secreted arteriogenic cytokines, such as vascular endothelial growth factor (VEGF), basic fibroblast growth factor (bFGF), placental growth factor (PIGF), and monocyte chemoattractant protein-1 (MCP-1), to repair the damaged tissues.[138,139] Unfortunately, systemic delivery of large amount of MSCs to the target site has been difficult to achieve; only 1% of systemically administrated MSCs migrated to the infarct site.[140] Poor migration of MSCs is related to the loss of CXC chemokine receptor 4 (CXCR4).[141] *Ex vivo* expansion of MSCs is necessary to generate a therapeutically relevant number of cells; however, during the expansion, MSCs express heterogeneous CXCR4 with significantly reduced affinity to their corresponding ligands, stromal cell-derived factor 1 (SDF-1). This effect ultimately reduces the chemotaxis of MSCs along the chemokine gradient to specific sites.[142] Systematic administration of MSCs should therefore be improved with a reliable targeting method to enhance therapeutic efficacy.

Immediately after myocardial infarction, injured cardiomyocytes up-regulate SDF-1 expression to recruit stem cells for repair.[143,144] Although many studies have stated that

migration of $CXCR4^+$ bone marrow stem cells along the SDF-1 concentration gradient is critical for cardiac recovery,[143,145,146] it has been suggested that the responsiveness to SDF-1 in these cells may mature over 4-7 days after MI.[147,148] Conversely, expression of SDF-1 in the heart starts to decline 4-7 days after the ischemic injury.[143] Thus, expanding autologous MSCs—which takes several weeks—for the treatment of MI is not ideal due to the small therapeutic window of SDF-1 expression. Previously, CXCR4 expression on MSCs had been induced by hypoxic culture conditions, addition of cytokine cocktails, and viral gene transduction. However, these methods are now discouraged due to the lengthy generation time and risk of altering the MSC properties.[149-152] In order to exploit the SDF-1 gradient for targeted delivery of MSCs to the MI site, pre-expanded MSCs should be rapidly modified with the targeting moiety. To comply with the requirements, Won et al. modified the MSCs with DMPE-PEG conjugated recombinant CXCR4 and examined the behavior of CXCR4-modified MSCs in the presence of SDF-1.[18] Compared to the unmodified MSCs, CXCR4 modified MSCs demonstrated enhanced migration towards the SDF-1 gradient.[18] Although the efficacy of CXCR4 modified MSCs has not been evaluated in the animal models of MI, the reported *in vitro* results imply that surface engineering of therapeutic cells with targeting moieties through hydrophobic interaction may allow specific migration towards the desired site in the living system.

1.3.3. Enhancing Antigen Presentation for Dendritic Cells

Immunotherapy has become one of the central cancer therapeutic strategies; all components of immunotherapy, including T cells, NK cells, dendritic cells (DCs), antibodies and antigens, have been extensively studied to understand the fundamental

mechanisms and to improve efficacy against cancer. From these continuous efforts, advanced immunotherapies, including CAR-T cells,[9] CAR-NK cells,[153,154] antibody-drug conjugates (ADCs),[155] and dendritic cell (DCs) vaccines,[156,157] were developed. DC vaccines are attractive because DCs are the primary antigen presenting cells that can not only activate T cell, B cells, and NK cells, but also induce immunological memory to control tumor relapses for long-term protection.[156,158] In this approach, DCs isolated from patients are challenged with tumor antigens found on their tumors and reinfused back into patients.[159] In turn, DCs degrade the tumor antigens into small peptides and transfer them onto MHC for $CD8^+$ T cells and $CD4^+$ T cells activation.[160,161] Although clinical efficacy of DC vaccines has been demonstrated with MUC1 antigen, it has become clear that the method of loading cancer antigens onto DCs is critical because it determines the efficiency of antigen presentation and magnitude of immune activation.[162,163] Ideally, DCs should be exposed to a wide range of tumor antigens in order to provide extended protective coverage. Unfortunately, the current library of tumor antigen peptides used for DC priming is limited. Also, the fact that tumor cells can escape host immune surveillance by expressing variant antigens further limits the potential to use peptide antigens for DC priming.[164] Alternatively, whole cancer cells can be used for antigen-loading of DCs.[163,165,166] DCs loaded with apoptotic cancer cells enable broad recognition of cancer cells by potentially expressing all known and unknown cancer-associated antigens and activating a repertoire of immune cells, including $CD8^+$ T cells, $CD4^+$ T cells, NK cells and γδ T cells.[4,163,165,166] To demonstrate the *ex vivo* whole cell loading of DCs, Tomita et al. first induced apoptosis in cancer cells by brief ultraviolet (UV) light exposure and then surface engineered the apoptotic cancer cells with antibody conjugated DOPE-PEG.[4] Subsequently, the surface-engineered

apoptotic cells were incubated with the isolated DCs. As a result, DCs recognized the antibodies on the surface of apoptotic cancer cells, captured Fc domains of antibodies *via* Fc receptors, and internalized the apoptotic cells *via* phagocytosis.[4] It is interesting to note that the antibody used in this study was an arbitrary IgG not specific for any particular antigen or DC surface receptor. This process mimics the internalization of neutralizing antibody-opsonized dying cells by Fc receptors on DCs. With the surface modification of apoptotic cancer cells using any antibodies, DCs can be readily and efficiently loaded with all potential antigens associated with specific cancer cells.

1.4. Conclusions

Cell therapy has advanced to the point where it aims to provide treatments for tissue degeneration, chronic inflammation, autoimmunity, genetic disorders, cancer, and infectious diseases.[48] Because the efficacy of cell therapy heavily depends on the fate and function of therapeutic cells, innovative strategies are continuously being introduced to enhance cell survival and improve native functions and therapeutic effects. Synthetic and natural biomaterials were incorporated onto the cell surface through covalent conjugation, electrostatic interaction, hydrophobic interaction, and genetic modification in order to provide unique properties and functionalities to cells. Although covalent conjugation and electrostatic interaction provide stable surface modification, the degree of modification is difficult to control. Excessive modification may disrupt the membrane integrity, resulting in severe cytotoxicity. Genetic modification has an advantage to express heterologous proteins in cells; however, the expression of desired protein heavily depends on the amount of genetic materials internalized by the cells and the efficiency of protein synthesis of the

targeted cells. Nonetheless, viral gene transfer limits the application of genetically modified cells for therapies due to safety and economical concerns, including the use of viral vectors, expensive production cost, and extensive generation time. Compared to other surface engineering methods, hydrophobic interaction is a safer membrane modification method of chemistry that noninvasively modifies the cell surface by inserting lipid-conjugated molecules into the membrane. Limitations of surface engineering through hydrophobic interaction should be addressed for clinical application. Internalization of lipid-conjugated biomaterials can rapidly reduce the therapeutic efficacy and viability of modified cells. Inui and coworkers, however, reported that endocytosis of PEGylated lipids such as DMPE-PEG, DPPE-PEG, and DSPE-PEG was not observed.[47] Despite limited understanding of the fate of lipid-PEG conjugated bioactive substances, surface engineering with hydrophobic interaction is an attractive technique because it can be applied to virtually any cell. Since the modification process is rapid and straightforward, it can be incorporated to "off-the-shelf" cells as "off-the-self" reagents.

The next two chapters of this dissertation concentrate on the applications of cell surface engineering with hydrophobic interaction to improve the target-site homing effects for cell delivery and to integrate special functions to therapeutic cells. Traditionally, therapeutic cells had been directly injected into the accessible target sites, such as the left ventricle for MI and the portal veins of the liver for islet cell transplantation.[167,168] However, systematic administration of therapeutic cells is preferred due to the fact that most diseases and tumor tissues are inaccessible for direct injection. Although therapeutic cells are living drugs that can navigate through the endothelial and stromal barriers to arrive at their pathological sites,[23,169,170] intravenous injections of these cells have shown very low levels

of accumulation at target sites.[171] Therefore, cell delivery must incorporate a targeted mechanism to enhance therapeutic efficacy. In Chapter 2, surfaces of MSCs were modified with SDF-1 protein. This approach aims to take advantage of the CXCR4/SDF-1 axis to deliver MSCs towards injured cardiomyocytes expressing CXCR4 at the late stage of acute MI. In Chapter 3, NK cells were surface-engineered to embed antibody-drug conjugates (ADCs). Trastuzumab-DM1 (T-DM1) was selected as a model ADC. Surface-engineered NK cells with T-DM1 selectively targeted Her2-positive SK-BR-3 cells and Calu-3 cells but not Her2-negative MDA-MB-231 cells. Two experimental studies have demonstrated the ability of cell surface engineering—with different targeting moieties—to redirect therapeutic cells towards the sites of interest.

The ability to empower cells with therapeutic functions—by modifying the cell surface with desired bioactive materials—was investigated in the subsequent chapters. In Chapter 2, imaging agents were used to modify cells for cell tracking purposes. It is important to understand the fate of administered therapeutic cells. Currently, positron emission tomography (PET) imaging and magnetic resonance imaging (MRI) are employed to noninvasively monitor the behavior of therapeutic cells in real-time. In Chapter 2, Jurkat cells were modified to carry superparamagnetic iron oxide nanoparticles (SPIONs) on their surface. These SPION-modified Jurkat cells did not show significant alterations in cell viability and produced a sharp contrast for MRI. In Chapter 3, targeted chemotherapeutic agents were embedded in the immune cells to enhance the anti-cancer efficacy of chemoimmunotherapy. In addition to the tumor homing effect, ADCs delivered powerful cytotoxic agents to the target cells. Cooperative anti-cancer activities of ADC-modified NK cells induced significantly enhanced cancer cell

death: (1) ADCs on the surface delivered NK cells closer to cancer cells; (2) cancer cell death was induced by cytolytic activity of NK cells; (3) internalized ADCs induced apoptosis in cancer cells; and (4) NK cells recognized the apoptotic cancer cells and eliminated them. Moreover, ADC-embedded NK cells induced strong tumor growth suppression in animal models. Experimental approaches are provided in subsequent chapters. To close, concluding remarks and future directions are discussed in Chapter 4.

1.5. References

1. Zhao WA, Teo GSL, Kumar N, Karp JM. 2010. Chemistry and material science at the cell surface. Mater Today **13**(4):14-21.

2. Teramura Y, Iwata H. 2010. Cell surface modification with polymers for biomedical studies. Soft Matter **6**(6):1081-1091.

3. Carlsten M, Childs RW. 2015. Genetic manipulation of NK cells for cancer immunotherapy: Techniques and clinical implications. Front Immunol **6**:266.

4. Tomita U, Yamaguchi S, Sugimoto Y, Takamori S, Nagamune T. 2012. Poly(ethylene glycol)-lipid-conjugated antibodies enhance dendritic cell phagocytosis of apoptotic cancer cells. Pharmaceuticals (Basel) **5**(5):405-416.

5. Cabric S, Sanchez J, Lundgren T, Foss A, Felldin M, Kallen R, Salmela K, Tibell A, Tufveson G, Larsson R, Korsgren O, Nilsson B. 2007. Islet surface heparinization prevents the instant blood-mediated inflammatory reaction in islet transplantation. Diabetes **56**(8):2008-2015.

6. Contreras JL, Xie D, Mays J, Smyth CA, Eckstein C, Rahemtulla FG, Young CJ, Anthony Thompson J, Bilbao G, Curiel DT, Eckhoff DE. 2004. A novel approach to xenotransplantation combining surface engineering and genetic modification of isolated adult porcine islets. Surgery **136**(3):537-547.

7. Lee DY, Lee S, Nam JH, Byun Y. 2006. Minimization of immunosuppressive therapy after islet transplantation: Combined action of heme oxygenase-1 and PEGylation to islet. Am J Transplant **6**(8):1820-1828.

8. Yun Lee D, Hee Nam J, Byun Y. 2007. Functional and histological evaluation of transplanted pancreatic islets immunoprotected by PEGylation and cyclosporine for 1 year. Biomaterials **28**(11):1957-1966.

9. Fesnak AD, June CH, Levine BL. 2016. Engineered T cells: The promise and challenges of cancer immunotherapy. Nat Rev Cancer **16**(9):566-581.

10. Stabler CL, Sun XL, Cui W, Wilson JT, Haller CA, Chaikof EL. 2007. Surface re-engineering of pancreatic islets with recombinant azido-thrombomodulin. Bioconjug Chem **18**(6):1713-1715.

11. Germain M, Balaguer P, Nicolas JC, Lopez F, Esteve JP, Sukhorukov GB, Winterhalter M, Richard-Foy H, Fournier D. 2006. Protection of mammalian cell used in biosensors by coating with a polyelectrolyte shell. Biosens Bioelectron **21**(8):1566-1573.

12. Elbert DL, Herbert CB, Hubbell JA. 1999. Thin polymer layers formed by polyelectrolyte multilayer techniques on biological surfaces. Langmuir **15**(16):5355-5362.

13. Krol S, del Guerra S, Grupillo M, Diaspro A, Gliozzi A, Marchetti P. 2006. Multilayer nanoencapsulation. New approach for immune protection of human pancreatic islets. Nano Lett **6**(9):1933-1939.

14. Rabuka D, Forstner MB, Groves JT, Bertozzi CR. 2008. Noncovalent cell surface engineering: Incorporation of bioactive synthetic glycopolymers into cellular membranes. J Am Chem Soc **130**(18):5947-5953.

15. Teramura Y, Kaneda Y, Iwata H. 2007. Islet-encapsulation in ultra-thin layer-by-layer membranes of poly(vinyl alcohol) anchored to poly(ethylene glycol)-lipids in the cell membrane. Biomaterials **28**(32):4818-4825.

16. Teramura Y, Kaneda Y, Totani T, Iwata H. 2008. Behavior of synthetic polymers immobilized on a cell membrane. Biomaterials **29**(10):1345-1355.

17. Totani T, Teramura Y, Iwata H. 2008. Immobilization of urokinase on the islet surface by amphiphilic poly(vinyl alcohol) that carries alkyl side chains. Biomaterials **29**(19):2878-2883.

18. Won YW, Patel AN, Bull DA. 2014. Cell surface engineering to enhance mesenchymal stem cell migration toward an SDF-1 gradient. Biomaterials **35**(21):5627-5635.

19. Sentman CL, Meehan KR. 2014. NKG2D CARs as cell therapy for cancer. Cancer J **20**(2):156-159.

20. Glienke W, Esser R, Priesner C, Suerth JD, Schambach A, Wels WS, Grez M, Kloess S, Arseniev L, Koehl U. 2015. Advantages and applications of CAR-expressing natural killer cells. Front Pharmacol **6**:21.

21. Saxon E, Bertozzi CR. 2000. Cell surface engineering by a modified Staudinger reaction. Science **287**(5460):2007-2010.

22. Prescher JA, Dube DH, Bertozzi CR. 2004. Chemical remodelling of cell surfaces in living animals. Nature **430**(7002):873-877.

23. Huang B, Abraham WD, Zheng Y, Bustamante Lopez SC, Luo SS, Irvine DJ. 2015. Active targeting of chemotherapy to disseminated tumors using nanoparticle-carrying T cells. Sci Transl Med **7**(291):291ra294.

24. Digilio G, Menchise V, Gianolio E, Catanzaro V, Carrera C, Napolitano R, Fedeli F, Aime S. 2010. Exofacial protein thiols as a route for the internalization of Gd(III)-based complexes for magnetic resonance imaging cell labeling. J Med Chem **53**(13):4877-4890.

25. Torres AG, Gait MJ. 2012. Exploiting cell surface thiols to enhance cellular uptake. Trends Biotechnol **30**(4):185-190.

26. Hong V, Steinmetz NF, Manchester M, Finn MG. 2010. Labeling live cells by copper-catalyzed alkyne--azide click chemistry. Bioconjug Chem **21**(10):1912-1916.

27. Baskin JM, Prescher JA, Laughlin ST, Agard NJ, Chang PV, Miller IA, Lo A, Codelli JA, Bertozzi CR. 2007. Copper-free click chemistry for dynamic in vivo imaging. Proc Natl Acad Sci U S A **104**(43):16793-16797.

28. Swee LK, Lourido S, Bell GW, Ingram JR, Ploegh HL. 2015. One-step enzymatic modification of the cell surface redirects cellular cytotoxicity and parasite tropism. ACS Chem Biol **10**(2):460-465.

29. Paulick MG, Forstner MB, Groves JT, Bertozzi CR. 2007. A chemical approach to unraveling the biological function of the glycosylphosphatidylinositol anchor. Proc Natl Acad Sci U S A **104**(51):20332-20337.

30. Chanana M, Gliozzi A, Diaspro A, Chodnevskaja I, Huewel S, Moskalenko V, Ulrichs K, Galla HJ, Krol S. 2005. Interaction of polyelectrolytes and their composites with living cells. Nano Lett **5**(12):2605-2612.

31. Wilson JT, Cui W, Chaikof EL. 2008. Layer-by-layer assembly of a conformal nanothin PEG coating for intraportal islet transplantation. Nano Lett **8**(7):1940-1948.

32. Martinez JS, Keller TC, 3rd, Schlenoff JB. 2011. Cytotoxicity of free versus multilayered polyelectrolytes. Biomacromolecules **12**(11):4063-4070.

33. Veerabadran NG, Goli PL, Stewart-Clark SS, Lvov YM, Mills DK. 2007. Nanoencapsulation of stem cells within polyelectrolyte multilayer shells. Macromol Biosci **7**(7):877-882.

34. Westman EH, Ek M, Enarsson LE, Wagberg L. 2009. Assessment of antibacterial properties of polyvinylamine (PVAm) with different charge densities and hydrophobic modifications. Biomacromolecules **10**(6):1478-1483.

35. Lv H, Zhang S, Wang B, Cui S, Yan J. 2006. Toxicity of cationic lipids and cationic polymers in gene delivery. J Control Release **114**(1):100-109.

36. Wilson JT, Krishnamurthy VR, Cui W, Qu Z, Chaikof EL. 2009. Noncovalent cell surface engineering with cationic graft copolymers. J Am Chem Soc **131**(51):18228-18229.

37. Miura S, Teramura Y, Iwata H. 2006. Encapsulation of islets with ultra-thin polyion complex membrane through poly(ethylene glycol)-phospholipids anchored to cell membrane. Biomaterials **27**(34):5828-5835.

38. Teramura Y, Iwata H. 2008. Islets surface modification prevents blood-mediated inflammatory responses. Bioconjug Chem **19**(7):1389-1395.

39. Teramura Y, Iwata H. 2009. Islet encapsulation with living cells for improvement of biocompatibility. Biomaterials **30**(12):2270-2275.

40. Teramura Y, Iwata H. 2009. Surface modification of islets with PEG-lipid for improvement of graft survival in intraportal transplantation. Transplantation **88**(5):624-630.

41. Lim KS, Lee DY, Valencia GM, Won YW, Bull DA. 2017. Cell surface-engineering to embed targeting ligands or tracking agents on the cell membrane. Biochem Biophys Res Commun **482**(4):1042-1047.

42. Itagaki T, Arima Y, Kuwabara R, Kitamura N, Iwata H. 2015. Interaction between cells and poly(ethylene glycol)-lipid conjugates. Colloids Surf B Biointerfaces **135**:765-773.

43. Yamamoto T, Teramura Y, Itagaki T, Arima Y, Iwata H. 2016. Interaction of poly(ethylene glycol)-conjugated phospholipids with supported lipid membranes and their influence on protein adsorption. Sci Technol Adv Mater **17**(1):677-684.

44. Pulsipher A, Griffin ME, Stone SE, Brown JM, Hsieh-Wilson LC. 2014. Directing neuronal signaling through cell-surface glycan engineering. J Am Chem Soc **136**(19):6794-6797.

45. Dutta D, Pulsipher A, Luo W, Yousaf MN. 2011. Synthetic chemoselective rewiring of cell surfaces: Generation of three-dimensional tissue structures. J Am Chem Soc **133**(22):8704-8713.

46. Csiszar A, Hersch N, Dieluweit S, Biehl R, Merkel R, Hoffmann B. 2010. Novel fusogenic liposomes for fluorescent cell labeling and membrane modification. Bioconjug Chem **21**(3):537-543.

47. Inui O, Teramura Y, Iwata H. 2010. Retention dynamics of amphiphilic polymers PEG-lipids and PVA-alkyl on the cell surface. ACS Appl Mater Interfaces **2**(5):1514-1520.

48. Stephan MT, Irvine DJ. 2011. Enhancing cell therapies from the outside in: Cell surface engineering using synthetic nanomaterials. Nano Today **6**(3):309-325.

49. Nikic I, Kang JH, Girona GE, Aramburu IV, Lemke EA. 2015. Labeling proteins on live mammalian cells using click chemistry. Nat Protoc **10**(5):780-791.

50. Wals K, Ovaa H. 2014. Unnatural amino acid incorporation in E. coli: Current and future applications in the design of therapeutic proteins. Front Chem **2**:15.

51. Nikic I, Plass T, Schraidt O, Szymanski J, Briggs JA, Schultz C, Lemke EA. 2014. Minimal tags for rapid dual-color live-cell labeling and super-resolution microscopy. Angew Chem Int Ed Engl **53**(8):2245-2249.

52. Grunbeck A, Sakmar TP. 2013. Probing G protein-coupled receptor-ligand interactions with targeted photoactivatable cross-linkers. Biochemistry **52**(48):8625-8632.

53. Lang K, Davis L, Torres-Kolbus J, Chou C, Deiters A, Chin JW. 2012. Genetically encoded norbornene directs site-specific cellular protein labelling via a rapid bioorthogonal reaction. Nat Chem **4**(4):298-304.

54. Coin I, Perrin MH, Vale WW, Wang L. 2011. Photo-cross-linkers incorporated into G-protein-coupled receptors in mammalian cells: A ligand comparison. Angew Chem Int Ed Engl **50**(35):8077-8081.

55. Milles S, Lemke EA. 2013. What precision-protein-tuning and nano-resolved single molecule sciences can do for each other. Bioessays **35**(1):65-74.

56. Lang K, Chin JW. 2014. Cellular incorporation of unnatural amino acids and bioorthogonal labeling of proteins. Chem Rev **114**(9):4764-4806.

57. Wang J, Xie J, Schultz PG. 2006. A genetically encoded fluorescent amino acid. J Am Chem Soc **128**(27):8738-8739.

58. Dumas A, Lercher L, Spicer CD, Davis BG. 2015. Designing logical codon reassignment - Expanding the chemistry in biology. Chem Sci **6**(1):50-69.

59. Zitvogel L, Tesniere A, Kroemer G. 2006. Cancer despite immunosurveillance: Immunoselection and immunosubversion. Nat Rev Immunol **6**(10):715-727.

60. Vinay DS, Ryan EP, Pawelec G, Talib WH, Stagg J, Elkord E, Lichtor T, Decker WK, Whelan RL, Kumara HM, Signori E, Honoki K, Georgakilas AG, Amin A, Helferich WG, Boosani CS, Guha G, Ciriolo MR, Chen S, Mohammed SI, Azmi AS, Keith WN, Bilsland A, Bhakta D, Halicka D, Fujii H, Aquilano K, Ashraf SS, Nowsheen S, Yang X, Choi BK, Kwon BS. 2015. Immune evasion in cancer: Mechanistic basis and therapeutic strategies. Semin Cancer Biol **35** Suppl:S185-198.

61. Stewart TJ, Abrams SI. 2008. How tumours escape mass destruction. Oncogene **27**(45):5894-5903.

62. Kershaw MH, Westwood JA, Darcy PK. 2013. Gene-engineered T cells for cancer therapy. Nat Rev Cancer **13**(8):525-541.

63. Cheadle EJ, Hawkins RE, Batha H, Rothwell DG, Ashton G, Gilham DE. 2009. Eradication of established B-cell lymphoma by CD19-specific murine T cells is dependent on host lymphopenic environment and can be mediated by CD4+ and CD8+ T cells. J Immunother **32**(3):207-218.

64. Milone MC, Fish JD, Carpenito C, Carroll RG, Binder GK, Teachey D, Samanta M, Lakhal M, Gloss B, Danet-Desnoyers G, Campana D, Riley JL, Grupp SA, June CH. 2009. Chimeric receptors containing CD137 signal transduction domains mediate

enhanced survival of T cells and increased antileukemic efficacy in vivo. Mol Ther **17**(8):1453-1464.

65. Chmielewski M, Hahn O, Rappl G, Nowak M, Schmidt-Wolf IH, Hombach AA, Abken H. 2012. T cells that target carcinoembryonic antigen eradicate orthotopic pancreatic carcinomas without inducing autoimmune colitis in mice. Gastroenterology **143**(4):1095-1107 e1092.

66. Zhao Y, Wang QJ, Yang S, Kochenderfer JN, Zheng Z, Zhong X, Sadelain M, Eshhar Z, Rosenberg SA, Morgan RA. 2009. A herceptin-based chimeric antigen receptor with modified signaling domains leads to enhanced survival of transduced T lymphocytes and antitumor activity. J Immunol **183**(9):5563-5574.

67. Chinnasamy D, Yu Z, Kerkar SP, Zhang L, Morgan RA, Restifo NP, Rosenberg SA. 2012. Local delivery of interleukin-12 using T cells targeting VEGF receptor-2 eradicates multiple vascularized tumors in mice. Clin Cancer Res **18**(6):1672-1683.

68. Yvon E, Del Vecchio M, Savoldo B, Hoyos V, Dutour A, Anichini A, Dotti G, Brenner MK. 2009. Immunotherapy of metastatic melanoma using genetically engineered GD2-specific T cells. Clin Cancer Res **15**(18):5852-5860.

69. Klingemann H. 2014. Are natural killer cells superior CAR drivers? Oncoimmunology **3**:e28147.

70. Schonfeld K, Sahm C, Zhang C, Naundorf S, Brendel C, Odendahl M, Nowakowska P, Bonig H, Kohl U, Kloess S, Kohler S, Holtgreve-Grez H, Jauch A, Schmidt M, Schubert R, Kuhlcke K, Seifried E, Klingemann HG, Rieger MA, Tonn T, Grez M, Wels WS. 2015. Selective inhibition of tumor growth by clonal NK cells expressing an ErbB2/HER2-specific chimeric antigen receptor. Mol Ther **23**(2):330-338.

71. Boissel L, Betancur-Boissel M, Lu W, Krause DS, Van Etten RA, Wels WS, Klingemann H. 2013. Retargeting NK-92 cells by means of CD19- and CD20-specific chimeric antigen receptors compares favorably with antibody-dependent cellular cytotoxicity. Oncoimmunology **2**(10):e26527.

72. Esser R, Muller T, Stefes D, Kloess S, Seidel D, Gillies SD, Aperlo-Iffland C, Huston JS, Uherek C, Schonfeld K, Tonn T, Huebener N, Lode HN, Koehl U, Wels WS. 2012. NK cells engineered to express a GD2 -specific antigen receptor display built-in ADCC-like activity against tumour cells of neuroectodermal origin. J Cell Mol Med **16**(3):569-581.

73. Zhang C, Burger MC, Jennewein L, Genssler S, Schonfeld K, Zeiner P, Hattingen E, Harter PN, Mittelbronn M, Tonn T, Steinbach JP, Wels WS. 2016. ErbB2/HER2-specific NK cells for targeted therapy of glioblastoma. J Natl Cancer Inst **108**(5).

74. Kalos M, Levine BL, Porter DL, Katz S, Grupp SA, Bagg A, June CH. 2011. T cells with chimeric antigen receptors have potent antitumor effects and can establish memory in patients with advanced leukemia. Sci Transl Med **3**(95):95ra73.

75. Morgan RA, Yang JC, Kitano M, Dudley ME, Laurencot CM, Rosenberg SA. 2010. Case report of a serious adverse event following the administration of T cells transduced with a chimeric antigen receptor recognizing ERBB2. Mol Ther **18**(4):843-851.

76. Louis CU, Savoldo B, Dotti G, Pule M, Yvon E, Myers GD, Rossig C, Russell HV, Diouf O, Liu E, Liu H, Wu MF, Gee AP, Mei Z, Rooney CM, Heslop HE, Brenner MK. 2011. Antitumor activity and long-term fate of chimeric antigen receptor-positive T cells in patients with neuroblastoma. Blood **118**(23):6050-6056.

77. Ahmed N, Brawley VS, Hegde M, Robertson C, Ghazi A, Gerken C, Liu E, Dakhova O, Ashoori A, Corder A, Gray T, Wu MF, Liu H, Hicks J, Rainusso N, Dotti G, Mei Z, Grilley B, Gee A, Rooney CM, Brenner MK, Heslop HE, Wels WS, Wang LL, Anderson P, Gottschalk S. 2015. Human epidermal growth factor receptor 2 (HER2) -specific chimeric antigen receptor-modified T cells for the immunotherapy of HER2-positive sarcoma. J Clin Oncol **33**(15):1688-1696.

78. Sadelain M, Brentjens R, Riviere I. 2013. The basic principles of chimeric antigen receptor design. Cancer Discov **3**(4):388-398.

79. Boissel L, Betancur M, Wels WS, Tuncer H, Klingemann H. 2009. Transfection with mRNA for CD19 specific chimeric antigen receptor restores NK cell mediated killing of CLL cells. Leuk Res **33**(9):1255-1259.

80. Li L, Liu LN, Feller S, Allen C, Shivakumar R, Fratantoni J, Wolfraim LA, Fujisaki H, Campana D, Chopas N, Dzekunov S, Peshwa M. 2010. Expression of chimeric antigen receptors in natural killer cells with a regulatory-compliant non-viral method. Cancer Gene Ther **17**(3):147-154.

81. Imai C, Mihara K, Andreansky M, Nicholson IC, Pui CH, Geiger TL, Campana D. 2004. Chimeric receptors with 4-1BB signaling capacity provoke potent cytotoxicity against acute lymphoblastic leukemia. Leukemia **18**(4):676-684.

82. Shimasaki N, Fujisaki H, Cho D, Masselli M, Lockey T, Eldridge P, Leung W, Campana D. 2012. A clinically adaptable method to enhance the cytotoxicity of natural killer cells against B-cell malignancies. Cytotherapy **14**(7):830-840.

83. Romanski A, Uherek C, Bug G, Muller T, Rossig C, Kampfmann M, Krossok N, Hoelzer D, Seifried E, Wels W, Ottmann OG, Tonn T. 2004. Re-targeting of an NK cell line (NK92) with specificity for CD19 efficiently kills human B-precursor leukemia cells. Blood **104**(11):751a-751a.

84. Chu YY, Yahr A, Ayello J, van de Ven C, Zhou XZ, Cairo MS. 2013. Anti-CD20 chimeric antigen receptor (CAR) modified expanded natural killer (NK) cells significantly mediate Burkitt lymphoma (BL) regression and improve survival in human BL xenografted NSG mice. Blood **122**(21).

85. Muller T, Uherek C, Maki G, Chow KU, Schimpf A, Klingemann HG, Tonn T, Wels WS. 2008. Expression of a CD20-specific chimeric antigen receptor enhances

cytotoxic activity of NK cells and overcomes NK-resistance of lymphoma and leukemia cells. Cancer Immunol Immunother **57**(3):411-423.

86. Yang SH, An X, Brown RD, Ho J, Gibson J, Joshua DE, Wels W, Sze DM. 2005. Development of retargeted CD38-specific NK-92 cell line for potential anti-myeloma immunotherapy. Blood **106**(11):358b-358b.

87. Uherek C, Tonn T, Uherek B, Becker S, Schnierle B, Klingemann HG, Wels W. 2002. Retargeting of natural killer-cell cytolytic activity to ErbB2-expressing cancer cells results in efficient and selective tumor cell destruction. Blood **100**(4):1265-1273.

88. Kruschinski A, Moosmann A, Poschke I, Norell H, Chmielewski M, Seliger B, Kiessling R, Blankenstein T, Abken H, Charo J. 2008. Engineering antigen-specific primary human NK cells against HER-2 positive carcinomas. Proc Natl Acad Sci U S A **105**(45):17481-17486.

89. Sahm C, Schonfeld K, Wels WS. 2012. Expression of IL-15 in NK cells results in rapid enrichment and selective cytotoxicity of gene-modified effectors that carry a tumor-specific antigen receptor. Cancer Immunol Immunother **61**(9):1451-1461.

90. Tassev DV, Cheng M, Cheung NK. 2012. Retargeting NK92 cells using an HLA-A2-restricted, EBNA3C-specific chimeric antigen receptor. Cancer Gene Ther **19**(2):84-100.

91. Chu J, Deng Y, Benson DM, He S, Hughes T, Zhang J, Peng Y, Mao H, Yi L, Ghoshal K, He X, Devine SM, Zhang X, Caligiuri MA, Hofmeister CC, Yu J. 2014. CS1-specific chimeric antigen receptor (CAR)-engineered natural killer cells enhance in vitro and in vivo antitumor activity against human multiple myeloma. Leukemia **28**(4):917-927.

92. Zhang T, Sentman CL. 2013. Mouse tumor vasculature expresses NKG2D ligands and can be targeted by chimeric NKG2D-modified T cells. J Immunol **190**(5):2455-2463.

93. D'Aloia MM, Caratelli S, Palumbo C, Battella S, Arriga R, Lauro D, Palmieri G, Sconocchia G, Alimandi M. 2016. T lymphocytes engineered to express a CD16-chimeric antigen receptor redirect T-cell immune responses against immunoglobulin G-opsonized target cells. Cytotherapy **18**(2):278-290.

94. Clemenceau B, Vivien R, Pellat C, Foss M, Thibault G, Vie H. 2013. The human natural killer cytotoxic cell line NK-92, once armed with a murine CD16 receptor, represents a convenient cellular tool for the screening of mouse mAbs according to their ADCC potential. MAbs **5**(4):587-594.

95. Hermanson DL, Kaufman DS. 2015. Utilizing chimeric antigen receptors to direct natural killer cell activity. Front Immunol **6**:195.

96. Chang YH, Connolly J, Shimasaki N, Mimura K, Kono K, Campana D. 2013. A chimeric receptor with NKG2D specificity enhances natural killer cell activation and killing of tumor cells. Cancer Res **73**(6):1777-1786.

97. Zhang H, Snyder KM, Suhoski MM, Maus MV, Kapoor V, June CH, Mackall CL. 2007. 4-1BB is superior to CD28 costimulation for generating CD8(+) cytotoxic lymphocytes for adoptive immunotherapy. J Immunol **179**(7):4910-4918.

98. Ligtenberg MA, Mougiakakos D, Mukhopadhyay M, Witt K, Lladser A, Chmielewski M, Riet T, Abken H, Kiessling R. 2016. Coexpressed catalase protects chimeric antigen receptor-redirected T cells as well as bystander cells from oxidative stress-induced loss of antitumor activity. J Immunol **196**(2):759-766.

99. Hacein-Bey-Abina S, von Kalle C, Schmidt M, Le Deist F, Wulffraat N, McIntyre E, Radford I, Villeval JL, Fraser CC, Cavazzana-Calvo M, Fischer A. 2003. A serious adverse event after successful gene therapy for X-linked severe combined immunodeficiency. N Engl J Med **348**(3):255-256.

100. Kaiser AD, Assenmacher M, Schroder B, Meyer M, Orentas R, Bethke U, Dropulic B. 2015. Towards a commercial process for the manufacture of genetically modified T cells for therapy. Cancer Gene Ther **22**(2):72-78.

101. Klingemann H, Boissel L, Toneguzzo F. 2016. Natural killer cells for immunotherapy - Advantages of the NK-92 cell line over blood NK cells. Front Immunol **7**:91.

102. Takemoto N, Teramura Y, Iwata H. 2011. Islet surface modification with urokinase through DNA hybridization. Bioconjug Chem **22**(4):673-678.

103. Boyman O, Sprent J. 2012. The role of interleukin-2 during homeostasis and activation of the immune system. Nat Rev Immunol **12**(3):180-190.

104. Lingwood D, Simons K. 2010. Lipid rafts as a membrane-organizing principle. Science **327**(5961):46-50.

105. Lautenschlager F, Paschke S, Schinkinger S, Bruel A, Beil M, Guck J. 2009. The regulatory role of cell mechanics for migration of differentiating myeloid cells. Proc Natl Acad Sci U S A **106**(37):15696-15701.

106. Novo C, Fonseca E, Freitas AA. 1987. Altered fatty acid membrane composition modifies lymphocyte localization in vivo. Cell Immunol **106**(2):387-396.

107. Curtis AS, Chandler C, Picton N. 1975. Cell surface lipids and adhesion. III. The effects on cell adhesion of changes in plasmalemmal lipids. J Cell Sci **18**(3):375-384.

108. van Meer G, Voelker DR, Feigenson GW. 2008. Membrane lipids: Where they are and how they behave. Nat Rev Mol Cell Biol **9**(2):112-124.

109. Sprong H, van der Sluijs P, van Meer G. 2001. How proteins move lipids and lipids move proteins. Nat Rev Mol Cell Biol **2**(7):504-513.

110. Vellai T, Takacs-Vellai K. 2010. Regulation of protein turnover by longevity pathways. Protein metabolism and homeostasis in aging. Adv Exp Med Biol **694**:69-80.

111. Grant BD, Donaldson JG. 2009. Pathways and mechanisms of endocytic recycling. Nat Rev Mol Cell Biol **10**(9):597-608.

112. Adler AF, Leong KW. 2010. Emerging links between surface nanotechnology and endocytosis: Impact on nonviral gene delivery. Nano Today **5**(6):553-569.

113. McMahon HT, Boucrot E. 2011. Molecular mechanism and physiological functions of clathrin-mediated endocytosis. Nat Rev Mol Cell Biol **12**(8):517-533.

114. Kumari S, Mg S, Mayor S. 2010. Endocytosis unplugged: Multiple ways to enter the cell. Cell Res **20**(3):256-275.

115. Ley K, Laudanna C, Cybulsky MI, Nourshargh S. 2007. Getting to the site of inflammation: The leukocyte adhesion cascade updated. Nat Rev Immunol **7**(9):678-689.

116. Katritsis D, Kaiktsis L, Chaniotis A, Pantos J, Efstathopoulos EP, Marmarelis V. 2007. Wall shear stress: Theoretical considerations and methods of measurement. Prog Cardiovasc Dis **49**(5):307-329.

117. Mebius RE, Kraal G. 2005. Structure and function of the spleen. Nat Rev Immunol **5**(8):606-616.

118. Dobrovolskaia MA, Aggarwal P, Hall JB, McNeil SE. 2008. Preclinical studies to understand nanoparticle interaction with the immune system and its potential effects on nanoparticle biodistribution. Mol Pharm **5**(4):487-495.

119. Nilsson B, Korsgren O, Lambris JD, Ekdahl KN. 2010. Can cells and biomaterials in therapeutic medicine be shielded from innate immune recognition? Trends Immunol **31**(1):32-38.

120. Wang JQ, Sui MH, Fan WM. 2010. Nanoparticles for tumor targeted therapies and their pharmacokinetics. Curr Drug Metab **11**(2):129-141.

121. Dunkelberger JR, Song WC. 2010. Complement and its role in innate and adaptive immune responses. Cell Res **20**(1):34-50.

122. Harding FA, Stickler MM, Razo J, DuBridge RB. 2010. The immunogenicity of humanized and fully human antibodies: Residual immunogenicity resides in the CDR regions. MAbs **2**(3):256-265.

123. Gorbet MB, Sefton MV. 2004. Biomaterial-associated thrombosis: Roles of coagulation factors, complement, platelets and leukocytes. Biomaterials **25**(26):5681-5703.

124. Sperling C, Fischer M, Maitz MF, Werner C. 2009. Blood coagulation on biomaterials requires the combination of distinct activation processes. Biomaterials **30**(27):4447-4456.

125. Hombach A, Hombach AA, Abken H. 2010. Adoptive immunotherapy with genetically engineered T cells: Modification of the IgG1 Fc 'spacer' domain in the extracellular moiety of chimeric antigen receptors avoids 'off-target' activation and unintended initiation of an innate immune response. Gene Ther **17**(10):1206-1213.

126. Tey SK. 2014. Adoptive T-cell therapy: Adverse events and safety switches. Clin Transl Immunology **3**(6):e17.

127. Bonifant CL, Jackson HJ, Brentjens RJ, Curran KJ. 2016. Toxicity and management in CAR T-cell therapy. Mol Ther Oncolytics **3**:16011.

128. Duncan MD, Wilkes DS. 2005. Transplant-related immunosuppression: A review of immunosuppression and pulmonary infections. Proc Am Thorac Soc **2**(5):449-455.

129. Bennet W, Sundberg B, Groth CG, Brendel MD, Brandhorst D, Brandhorst H, Bretzel RG, Elgue G, Larsson R, Nilsson B, Korsgren O. 1999. Incompatibility between human blood and isolated islets of Langerhans - A finding with implications for clinical intraportal islet transplantation? Diabetes **48**(10):1907-1914.

130. Bennet W, Sundberg B, Lundgren T, Tibell A, Groth CG, Richards A, White DJ, Elgue G, Larsson R, Nilsson B, Korsgren O. 2000. Damage to porcine islets of Langerhans after exposure to human blood in vitro, or after intraportal transplantation to cynomologus monkeys - Protective effects of sCR1 and heparin. Transplantation **69**(5):711-719.

131. Johansson H, Lukinius A, Moberg L, Lundgren T, Berne C, Foss A, Felldin M, Kallen R, Salmela K, Tibe A, Tufveson G, Ekdahl KN, Elgue G, Korsgren O, Nilsson B. 2005. Tissue factor produced by the endocrine cells of the islets of Langerhans is associated with a negative outcome of clinical islet transplantation. Diabetes **54**(6):1755-1762.

132. Contreras JL, Eckstein C, Smyth CA, Bilbao G, Vilatoba M, Ringland SE, Young C, Thompson JA, Fernandez JA, Griffin JH, Eckhoff DE. 2004. Activated protein C preserves functional islet mass after intraportal transplantation - A novel link between endothelial cell activation, thrombosis, inflammation, and islet cell death. Diabetes **53**(11):2804-2814.

133. Moberg L, Johansson H, Lukinius A, Berne C, Foss A, Kallen R, Ostraat O, Salmela K, Tibell A, Tufveson G, Elgue G, Ekdahl KN, Korsgren O, Nilsson B. 2002. Production of tissue factor by pancreatic islet cells as a trigger of detrimental thrombotic reactions in clinical islet transplantation. Lancet **360**(9350):2039-2045.

134. Korsgren O, Lundgren T, Felldin M, Foss A, Isaksson B, Permert J, Persson NH, Rafael E, Ryden M, Salmela K, Tibell A, Tufveson G, Nilsson B. 2008. Optimising islet engraftment is critical for successful clinical islet transplantation. Diabetologia **51**(2):227-232.

135. Silva GV, Litovsky S, Assad JA, Sousa AL, Martin BJ, Vela D, Coulter SC, Lin J, Ober J, Vaughn WK, Branco RV, Oliveira EM, He R, Geng YJ, Willerson JT, Perin EC. 2005. Mesenchymal stem cells differentiate into an endothelial phenotype, enhance vascular density, and improve heart function in a canine chronic ischemia model. Circulation **111**(2):150-156.

136. Berry MF, Engler AJ, Woo YJ, Pirolli TJ, Bish LT, Jayasankar V, Morine KJ, Gardner TJ, Discher DE, Sweeney HL. 2006. Mesenchymal stem cell injection after myocardial infarction improves myocardial compliance. Am J Physiol Heart Circ Physiol **290**(6):H2196-2203.

137. Tomita S, Mickle DA, Weisel RD, Jia ZQ, Tumiati LC, Allidina Y, Liu P, Li RK. 2002. Improved heart function with myogenesis and angiogenesis after autologous porcine bone marrow stromal cell transplantation. J Thorac Cardiovasc Surg **123**(6):1132-1140.

138. Kinnaird T, Stabile E, Burnett MS, Shou M, Lee CW, Barr S, Fuchs S, Epstein SE. 2004. Local delivery of marrow-derived stromal cells augments collateral perfusion through paracrine mechanisms. Circulation **109**(12):1543-1549.

139. Kinnaird T, Stabile E, Burnett MS, Lee CW, Barr S, Fuchs S, Epstein SE. 2004. Marrow-derived stromal cells express genes encoding a broad spectrum of arteriogenic cytokines and promote in vitro and in vivo arteriogenesis through paracrine mechanisms. Circ Res **94**(5):678-685.

140. Barbash IM, Chouraqui P, Baron J, Feinberg MS, Etzion S, Tessone A, Miller L, Guetta E, Zipori D, Kedes LH, Kloner RA, Leor J. 2003. Systemic delivery of bone marrow-derived mesenchymal stem cells to the infarcted myocardium: Feasibility, cell migration, and body distribution. Circulation **108**(7):863-868.

141. Wynn RF, Hart CA, Corradi-Perini C, O'Neill L, Evans CA, Wraith JE, Fairbairn LJ, Bellantuono I. 2004. A small proportion of mesenchymal stem cells strongly expresses functionally active CXCR4 receptor capable of promoting migration to bone marrow. Blood **104**(9):2643-2645.

142. Rombouts WJC, Ploemacher RE. 2003. Primary murine MSC show highly efficient homing to the bone marrow but lose homing ability following culture. Leukemia **17**(1):160-170.

143. Askari AT, Unzek S, Popovic ZB, Goldman CK, Forudi F, Kiedrowski M, Rovner A, Ellis SG, Thomas JD, DiCorleto PE, Topol EJ, Penn MS. 2003. Effect of stromal-cell-derived factor 1 on stem-cell homing and tissue regeneration in ischaemic cardiomyopathy. Lancet **362**(9385):697-703.

144. Abbott JD, Huang Y, Liu D, Hickey R, Krause DS, Giordano FJ. 2004. Stromal cell-derived factor-1alpha plays a critical role in stem cell recruitment to the heart after myocardial infarction but is not sufficient to induce homing in the absence of injury. Circulation **110**(21):3300-3305.

145. Tang YL, Qian K, Zhang YC, Shen L, Phillips MI. 2005. Mobilizing of haematopoietic stem cells to ischemic myocardium by plasmid mediated stromal-cell-derived factor-1alpha (SDF-1alpha) treatment. Regul Pept **125**(1-3):1-8.

146. Misao Y, Takemura G, Arai M, Ohno T, Onogi H, Takahashi T, Minatoguchi S, Fujiwara T, Fujiwara H. 2006. Importance of recruitment of bone marrow-derived CXCR4+ cells in post-infarct cardiac repair mediated by G-CSF. Cardiovasc Res **71**(3):455-465.

147. Schachinger V, Erbs S, Elsasser A, Haberbosch W, Hambrecht R, Holschermann H, Yu J, Corti R, Mathey DG, Hamm CW, Suselbeck T, Assmus B, Tonn T, Dimmeler S, Zeiher AM, Investigators R-A. 2006. Intracoronary bone marrow-derived progenitor cells in acute myocardial infarction. N Engl J Med **355**(12):1210-1221.

148. Penn MS. 2009. Importance of the SDF-1:CXCR4 axis in myocardial repair. Circ Res **104**(10):1133-1135.

149. Cheng Z, Ou L, Zhou X, Li F, Jia X, Zhang Y, Liu X, Li Y, Ward CA, Melo LG, Kong D. 2008. Targeted migration of mesenchymal stem cells modified with CXCR4 gene to infarcted myocardium improves cardiac performance. Mol Ther **16**(3):571-579.

150. Ghadge SK, Muhlstedt S, Ozcelik C, Bader M. 2011. SDF-1alpha as a therapeutic stem cell homing factor in myocardial infarction. Pharmacol Ther **129**(1):97-108.

151. Shi M, Li J, Liao L, Chen B, Li B, Chen L, Jia H, Zhao RC. 2007. Regulation of CXCR4 expression in human mesenchymal stem cells by cytokine treatment: Role in homing efficiency in NOD/SCID mice. Haematologica **92**(7):897-904.

152. Liu H, Xue W, Ge G, Luo X, Li Y, Xiang H, Ding X, Tian P, Tian X. 2010. Hypoxic preconditioning advances CXCR4 and CXCR7 expression by activating HIF-1alpha in MSCs. Biochem Biophys Res Commun **401**(4):509-515.

153. Cheng M, Chen Y, Xiao W, Sun R, Tian Z. 2013. NK cell-based immunotherapy for malignant diseases. Cell Mol Immunol **10**(3):230-252.

154. Morvan MG, Lanier LL. 2016. NK cells and cancer: You can teach innate cells new tricks. Nat Rev Cancer **16**(1):7-19.

155. Diamantis N, Banerji U. 2016. Antibody-drug conjugates--an emerging class of cancer treatment. Br J Cancer **114**(4):362-367.

156. Palucka K, Banchereau J. 2012. Cancer immunotherapy via dendritic cells. Nat Rev Cancer **12**(4):265-277.

157. van der Burg SH, Arens R, Ossendorp F, van Hall T, Melief CJ. 2016. Vaccines for established cancer: Overcoming the challenges posed by immune evasion. Nat Rev Cancer **16**(4):219-233.

158. Janikashvili N, Larmonier N, Katsanis E. 2010. Personalized dendritic cell-based tumor immunotherapy. Immunotherapy **2**(1):57-68.

159. Apostolopoulos V, Pietersz GA, Tsibanis A, Tsikkinis A, Stojanovska L, McKenzie IF, Vassilaros S. 2014. Dendritic cell immunotherapy: Clinical outcomes. Clin Transl Immunology **3**(7):e21.

160. Rosalia RA, Quakkelaar ED, Redeker A, Khan S, Camps M, Drijfhout JW, Silva AL, Jiskoot W, van Hall T, van Veelen PA, Janssen G, Franken K, Cruz LJ, Tromp A, Oostendorp J, van der Burg SH, Ossendorp F, Melief CJ. 2013. Dendritic cells process synthetic long peptides better than whole protein, improving antigen presentation and T-cell activation. Eur J Immunol **43**(10):2554-2565.

161. ten Broeke T, Wubbolts R, Stoorvogel W. 2013. MHC class II antigen presentation by dendritic cells regulated through endosomal sorting. Cold Spring Harb Perspect Biol **5**(12):a016873.

162. Nestle FO, Farkas A, Conrad C. 2005. Dendritic-cell-based therapeutic vaccination against cancer. Curr Opin Immunol **17**(2):163-169.

163. Schnurr M, Scholz C, Rothenfusser S, Galambos P, Dauer M, Robe J, Endres S, Eigler A. 2002. Apoptotic pancreatic tumor cells are superior to cell lysates in promoting cross-priming of cytotoxic T cells and activate NK and gammadelta T cells. Cancer Res **62**(8):2347-2352.

164. Jackson HJ, Brentjens RJ. 2015. Overcoming antigen escape with CAR T-cell therapy. Cancer Discov **5**(12):1238-1240.

165. Galea-Lauri J, Darling D, Mufti G, Harrison P, Farzaneh F. 2002. Eliciting cytotoxic T lymphocytes against acute myeloid leukemia-derived antigens: Evaluation of dendritic cell-leukemia cell hybrids and other antigen-loading strategies for dendritic cell-based vaccination. Cancer Immunol Immunother **51**(6):299-310.

166. Kotera Y, Shimizu K, Mule JJ. 2001. Comparative analysis of necrotic and apoptotic tumor cells as a source of antigen(s) in dendritic cell-based immunization. Cancer Res **61**(22):8105-8109.

167. Rangappa S, Makkar R, Forrester J. 2010. Review article: Current status of myocardial regeneration: New cell sources and new strategies. J Cardiovasc Pharmacol Ther **15**(4):338-343.

168. Noguchi H. 2010. Pancreatic stem/progenitor cells for the treatment of diabetes. Rev Diabet Stud **7**(2):105-111.

169. Choi MR, Stanton-Maxey KJ, Stanley JK, Levin CS, Bardhan R, Akin D, Badve S, Sturgis J, Robinson JP, Bashir R, Halas NJ, Clare SE. 2007. A cellular Trojan Horse for delivery of therapeutic nanoparticles into tumors. Nano Lett **7**(12):3759-3765.

170. Power AT, Bell JC. 2008. Taming the Trojan horse: Optimizing dynamic carrier cell/oncolytic virus systems for cancer biotherapy. Gene Ther **15**(10):772-779.

171. Hale SL, Dai W, Dow JS, Kloner RA. 2008. Mesenchymal stem cell administration at coronary artery reperfusion in the rat by two delivery routes: A quantitative assessment. Life Sci **83**(13-14):511-515.

CHAPTER 2

CELL SURFACE ENGINEERING TO EMBED TARGETING LIGANDS OR TRACKING AGENTS ON THE CELL MEMBRANE[†]

2.1 Abstract

Efficient modification of cells with specific molecules or compounds that can guide the cells to the target tissues provides an attractive means of improving the efficacy of cell therapy. To address this, we have developed a cell surface engineering technology to noninvasively modify the cell surface. This technology can embed a wide variety of bioactive molecules on any cell surface and allows for targeting of a wide range of tissues in a variety of disease states. Using cell surface engineering technology, mesenchymal stem cells (MSCs) or Jurkat cells were modified with: 1) a homing peptide or a recombinant protein to facilitate the migration of the cells toward a specific molecular target; or 2) magnetic resonance imaging (MRI) contrast agents to allow for *in vivo* tracking of the cells. The incorporation of a targeting peptide or protein on MSCs facilitated the migration of cells toward their molecular target. MRI contrast agents were successfully embedded on

[†]Modified with the permission from KS Lim, GM Valencia, YW Won, and DA Bull. Biochemical and Biophysical Research Communications 2017; 482: 1042-1047. Copyright © 2016 Elsevier Inc. Lee and Lim co-managed this project and co-authored the research article. Lee contributed to the modification of MSCs with SDF-1, migration of SDF-1 modified MSCs, modification with tracking agents, and MRI imaging. Lim contributed to the surface engineering with CRPPR peptide, migration of CRPPR-modified MSCs, and modification tests in various cell lines. Bull and Won are the PIs responsible for the project.

the cell surface without adverse effects and the contrast agent-labeled cells were detectable by MRI. Our technology is a promising method of cell surface engineering that provides a broad range of applicability for cell therapies.

2.2. Introduction

Cell therapy typically involves systemic infusion of living cells to exert a direct or indirect effect against human disease.[1] The efficacy of cell therapy may be improved by the following measures: increasing the injection dose and the graft yield, reducing immune-mediated rejection, enhancing circulation time, and/or facilitating migration toward the target tissues.[2] The modification of cells to present targeting ligands and the encapsulation of cells in delivery vehicles have improved the yield of engraftment to the target tissues.[3,4] Such methods, however, still face one or more of the following limitations: (1) exposure of the cells to harsh conditions, (2) use of viral-gene transfer, (3) complicated processes, and (4) permanent modification.[5]

Cell preconditioning requires *ex vivo* expansion of cells in the presence of toxic chemicals or under a specific condition.[6] Gene-based approaches to induce expression of a particular ligand against the target receptor are highly versatile; however, poor transfection efficiency and uncontrolled gene expression remain to be critical challenges.[7,8] Conjugation of targeting ligands to proteins or polysaccharides present on the cell membrane can alter the membrane structure permanently, suggesting that the activity of surface-modified cells can be unpredictable.[9,10] Electrostatic interaction may be an alternative to chemical conjugation.[11] Because molecules bound to the cell surface through charge interaction are able to dissociate and internalize into the cells, this method has the

potential to affect cell metabolism and viability.[12] Thus, there is a need for an alternative technology that can noncovalently modify cells without altering the cellular viability, metabolism or function.

We have developed a cell surface engineering technology based on hydrophobic interaction, allowing any biological molecule to be noninvasively embedded on the cell membrane, while maintaining the inherent cellular activiity.[13] This technology allows for homogeneous and rapid modification of cell surface with a variety of biological molecules such as homing peptides, proteins, antibodies, and tracking agents, regardless of the cell type. In this study, the applicability of our surface engineering method to mesenchymal stem cells (MSCs) and Jurkat cells with a homing peptide, a small protein, and magnetic resonance imaging (MRI) contrast agents, was examined.

2.3. Materials and Methods

2.3.1. Materials

All 1,2-dimyristoyl-sn-glycero-3-phosphoethanolamine-poly (ethylene glycol) conjugates (DMPE-PEG-NHS, DMPE-PEG-Maleimide, DMPE-PEG-NH_2, 5 kDa), NHS-activated PEG (5 kDa), and FITC-labeled carboxyl-terminated SPIONs (SPIONs-FITC, 25-30 nm) were purchased from Nanocs (New York, NY). Recombinant human SDF-1 was obtained from Peprotech (Rocky Hill, NJ), and recombinant human CXCR4 was purchased from SPEED BioSystems (Rockville, MD). CRPPR-FITC and CRPPR peptide were synthesized by the University of Utah Peptide Core Facility. Recombinant cysteine-rich protein 2 (CRIP2) was purchased from Sino Biological Inc. (Beijing, China). The anti-SDF-1 antibody and FITC-conjugated secondary antibody were

obtained from R&D systems (Minneapolis, MN). All cell culture products—FBS, DPBS, PBS, HBSS, DMEM, and RPMI 1640—were obtained from Invitrogen (Carlsbad, CA). Cell Counting kit-8 (CCK-8) was purchased from Dojindo (Kumamoto, Japan). All other materials were purchased from Thermo Fisher Scientific (Waltham, MA).

2.3.2. Characteristics of MSCs

MSCs obtained from the Pharmicell Co., Ltd. (Sungnam, Korea) were isolated from the bone marrow aspiration in healthy adult male donors under informed consent. Mononuclear cells isolated from the bone marrow aspirate by density gradient centrifugation were briefly cultured with DMEM containing low glucose, 10% FBS, and 20 μg/mL gentamicin for 5 to 7 days. Nonadherent cells were removed while the culture flask-adhering cells displaying fibroblast-like spindle-shapes were continuously enriched. MSCs were subcultured at 80% confluency and maintained up to four passages. Flow cytometric analysis showed that the cultured MSCs were positive for mesenchymal stem cell markers, such as CD105 and CD73, but negative for hematopoietic markers, such as CD45, CD34, and CD14.

2.3.3. Cell Culture

All cells were cultured in DMEM containing 20% FBS and 1% antibiotics at 37ºC under 5% CO_2 atmosphere. Jurkat cells were grown in the same conditions with RPMI-1640 containing 10% FBS and 1% antibiotics. At 90% cell confluency, the cells were detached, washed and suspended at 7.5×10^5 cells/mL concentration in HBSS.

2.3.4. Surface Engineering with a Homing Peptide

DMPE-PEG-maleimide was conjugated to a CRPPR or CRPPR-FITC peptide. DMPE-PEG-maleimide dissolved in PBS at 1 mg/mL concentration and a 1 mg/mL stock solution of CRPPR in PBS were mixed and produced a final molar ratio of DMPE-PEG to CRPPR=15:1. After 1 hour of incubation at room temperature, impurities were removed by using Amicon Ultra Centrifugal Filters (3 kDa; Millipore, Billerica, MA). Conjugates were kept at -80°C until use. MSCs were cultured as described above, and the DMPE-PEG-CRPPR was added directly to the cell suspension. The modified MSCs were collected, washed, and suspended in HBSS for confocal microscopy (Nikon A1R, Nikon, Japan) and FACS analysis (BD FACSCanto, BD Bioscience, USA). The cell viability and the proliferation after the modification were determined by the MTT assay and CCK-8 assay, respectively.

2.3.5. Modification of MSCs with SDF-1

To prepare DMPE-PEG-SDF-1, 0.5 mg/mL SDF-1 in PBS was mixed with a 15-molar excess amount of DMPE-PEG-NHS, followed by 2 hours of reaction at room temperature. The resulting DMPE-PEG-SDF-1 was dialyzed (MWCO: 20 kDa) against PBS for 24 hours, sterilized by filtration, and stored at -80°C until use. DMPE-PEG-SDF-1 amounts ranging from 5 to 100 μg were added to 7.5×10^5 cells of MSCs. The modified MSCs were labeled with primary mouse anti-SDF-1 antibodies and secondary FITC-goat anti-mouse antibodies. These labeled cells were observed by confocal microscopy to visualize the location of SDF-1 on the cell surface and analyzed by FACS to quantify the percentage of the modified cells.

2.3.6. Migration Assay

The CRPPR-modified MSCs were placed in the insert of a transwell system, and the outer wells were filled with culture media with or without CRIP2. After 24 hours of incubation, MSCs remaining on the topside of the insert were removed, and the MSCs on the bottom of the insert were harvested and counted. To determine the dose effect of the CRPPR on the migration, different amounts of the DMPE-PEG-CRPPR were added to a fixed number of MSCs. The modified MSCs were plated in the transwell system as described above. The effect of CRIP2 dose on MSC migration was investigated. The MSCs modified with 60 μg of the DMPE-PEG-CRPPR were seeded in the transwell system. Subsequently, the outer wells were filled with the culture media with increasing concentrations of CRIP2. After 24 hours of incubation, the number of migrated MSCs was determined by measuring the viable cells on the bottom of the insert using a MTT assay. To test the CXCR4 concentration-dependent migration, MSCs were mixed with 100 μg of the DMPE-PEG-SDF-1 and seeded in the inserts of transwell system at a density of 2×10^4 cells in complete culture media. The lower reservoirs were filled with complete culture media containing 0, 50, 100, 200, or 300 ng/mL of CXCR4. After 24 hours of incubation, cells remaining on the topside of the insert were removed, and cells that had migrated to the bottom of the insert were also counted by MTT assay.

2.3.7. Tests in Various Cell Lines

DMPE-PEG-FITC was added directly to various cell lines, including 293T, Jurkat, A549, BT-474, MCF-7, MDA-MB-231, and SK-BR-3. After 10 minutes of incubation, cells were harvested, washed, and suspended in HBSS for confocal microscopy and FACS

analysis. The modified cells were seeded on 24-well plates and incubated for 18 hours. The cell adhesion and the morphology of the cells were observed using an optical microscope (Olympus IX51, Olympus, Japan).

2.3.8. Modification with Tracking Agents

Carboxyl-terminated SPION-FITCS were attached to DMPE-PEG-NH_2 through NHS/EDC conjugation chemistry. Briefly, 5 mg of EDC and 10 mg of sulfo-NHS were reacted with 1 mL of SPION-FITC containing 2 mg of iron in MES buffer (pH 6.0) for 30 minutes at room temperature. After EDC and sulfo-NHS were removed using a spin column (MWCO: 10 kDa), the NHS-activated SPIONs were mixed with 20 mg of DMPE-PEG-NH_2 to saturate the NHS-activated sites for 2 hours at room temperature. The DMPE-PEG-SPION-FITC was dialyzed (MWCO: 10 kDa) against PBS (pH 7.4) for 24 hours. For a negative control, PEG-conjugated SPIONs (5 kDa) were generated in the same way. Amounts of the DMPE-PEG-SPION-FITC ranging from 10 μL to 200 μL were used tomodify 7.5×10^5 Jurkat cells. SPION-modified Jurkat cells were analyzed by confocal microscopy and FACS analysis. Jurkate cells labeled with PEG-SPIONs were analyzed with FACS analysis. Viability and proliferation of SPION-modified Jurkat cells were analyzed by the CCK-8 assay.

2.3.9. MRI

For MRI imaging, 7.5×10^5 Jurkat cells were modified with 50, 100, or 200 μL of the DMPE-PEG-SPION-FITC. One hundred thousand SPION-modified or unmodified Jurkat cells were seeded into a premolded agar gel prepared in an 8-chamber coverglass with

0.5% (w/v) of low melting agarose in PBS. Before the gel completely solidified, cooled 0.5% agarose solution was added on the top of the seeded cells and kept at 4°C to solidify. Agar phantom-containing unmodified or SPION-modified Jurkat cells were examined with a Bruker 7T scanner (Bruker Biospin; Ettlingen, Germany). Samples were analyzed using T2*-weighted sequences (TR/TE/flip-angle = 323 ms/7.5 ms/30 degrees) with fast low-angle shot (FLASH). Images were taken in 25 slices (slice thickness = 0.5 mm) in plane resolution 0.195 mm x 0.195 mm.

2.3.10. Statistical Analysis

All data are presented as the mean ± standard deviation (n=3). Results, including the images and plots, were reported from one of two independent experiments. Statistical analysis was performed with Student's *t*-test, and the threshold value was set at $^{\#}P<0.01$.

2.4. Results

2.4.1 Modification of MSCs with a Homing Peptide

To determine the minimal amount of DMPE-PEG-conjugated peptide necessary to achieve homogeneous coating of the cell surface, DMPE-PEG-CRPPR-FITC was added incrementally to a constant number of MSCs. DMPE-CRPPR-FITC was incorporated homogeneously into the surface of MSCs; the degree of modification was directly proportional to the amount of added conjugates up to 30 μg (Figure 2.1a, b). When the amount of DMPE-PEG-CRPPR-FITC exceeded 60 μg, the fluorescence intensity in the cytosol increased significantly, indicating that the internalization had occurred. As little as 5 μg of DMPE-PEG-CRPPR was enough to completely modify 7.5×10^5 MSCs.

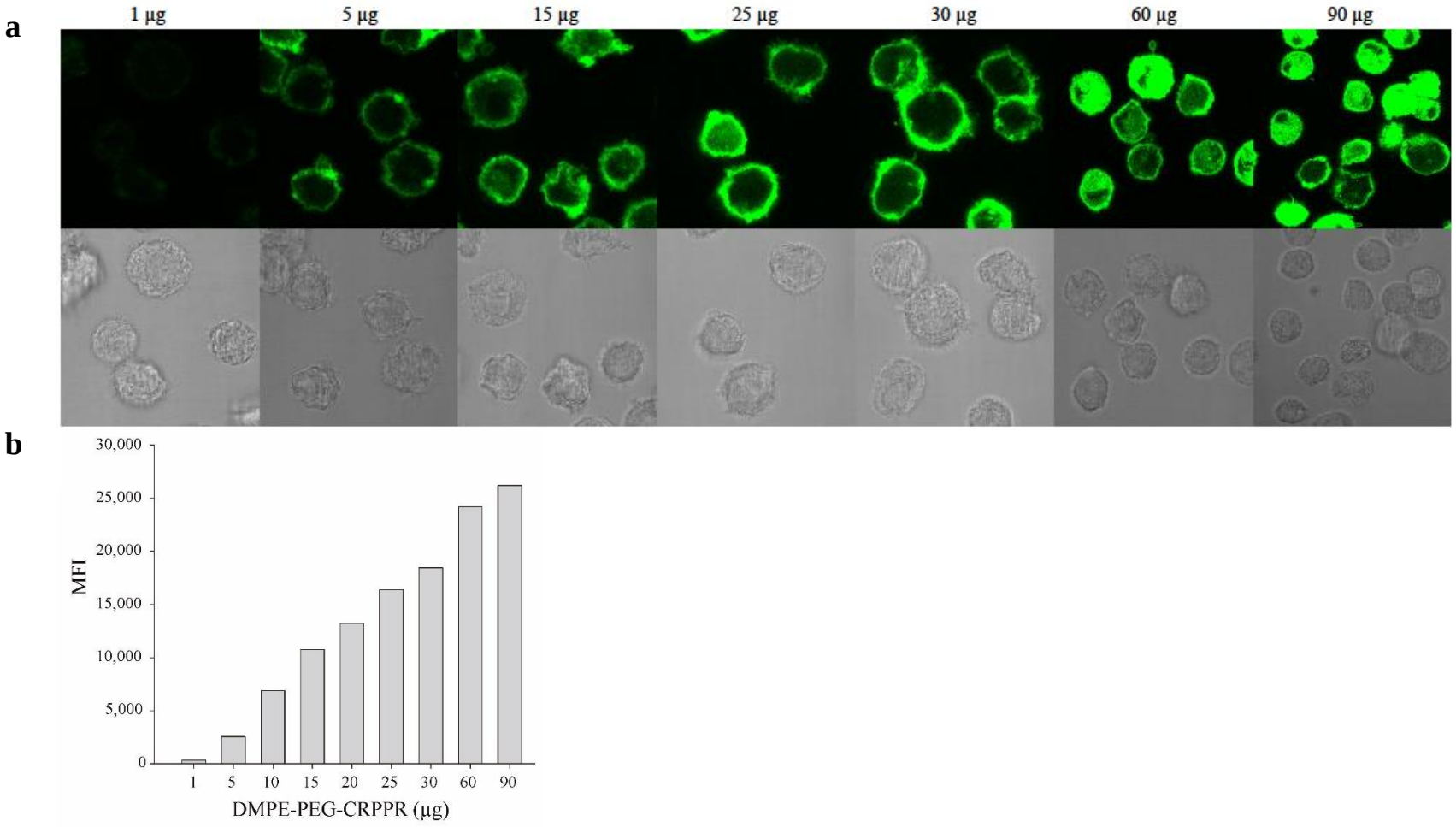

Figure 2.1. MSCs modified with a homing peptide. (a) Confocal micrograph (60×) showing the modified MSCs with DMPE-CRPPR- FITC. FICT was excited at 495 nm and emission was recorded at 520 nm. Images were selected from three independent experiments. (b) The mean fluorescence intensity (MFI) of the modified MSCs determined by FACS analysis (Ex/Em= 495/520 nm). Data were selected from three independent experiments.

To determine the effect of surface modification on cell viability and proliferation, CRPPR-modified MSCs and unmodified MSCs were plated and cultured for 48 hours. The viabilities and proliferation rates were measured at 24 hours and 48 hours post-seeding. No differences in cell viability and proliferation were observed between the modified MSCs and the unmodified MSCs (Figure 2.2a, b), verifying that the modified MSCs retained the ability to proliferate. These results confirmed that our cell surface engineering technology does not hinder cell growth.

2.4.2. Modification of MSCs with a Protein

SDF-1 was chosen to modify MSCs through hydrophobic interaction seeing that the CXCR4/SDF-1 axis is a well-established chemotaxis signal for MSC migration. The MSCs were modified to anchor SDF-1 on the cell surface in order to verify uniform cell modification with a protein and reconfirm the enhanced migration that we observed in the prior study.[13] Although 5 μg of DMPE-PEG-SDF-1 was sufficient to modify the given number of cells, the degree of modification was increased with an increasing amount of added DMPE-PEG-SDF-1 in comparison to the control group and the 0 μg-treated group (nonmodified cells incubated with anti-SDF-1 antibody) (Figure 2.3a, b).

2.4.3. Migration of Modified MSCs

Migration of MSCs modified with DMPE-PEG-CRPPR or DMPE-PEG-SDF-1 toward their complementary homing signals was verified. First, MSCs were modified with increasing amounts of DMPE-PEG-CRPPR to investigate the effect of dosing on migration. The migration of CRPPR-modified MSCs was examined in the presence of

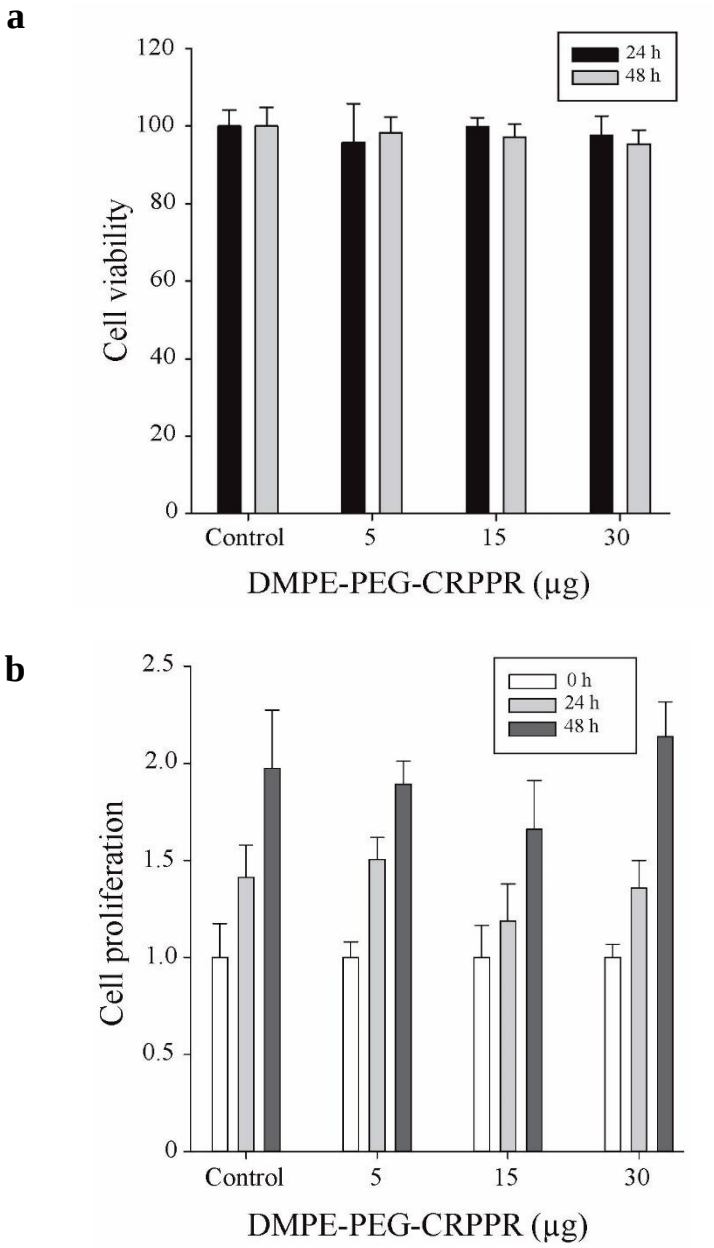

Figure 2.2. Viability (a) and proliferation rate (b) of MSCs after the modification with DMPE-PEG-CRPPR-FITC. Each condition was tested in triplicate and one representative experimental result is presented. No significant difference in cell viability (a) and proliferative activity (b) was observed between the unmodified MSCs and the MSCs modified with CRPPR-FITC.

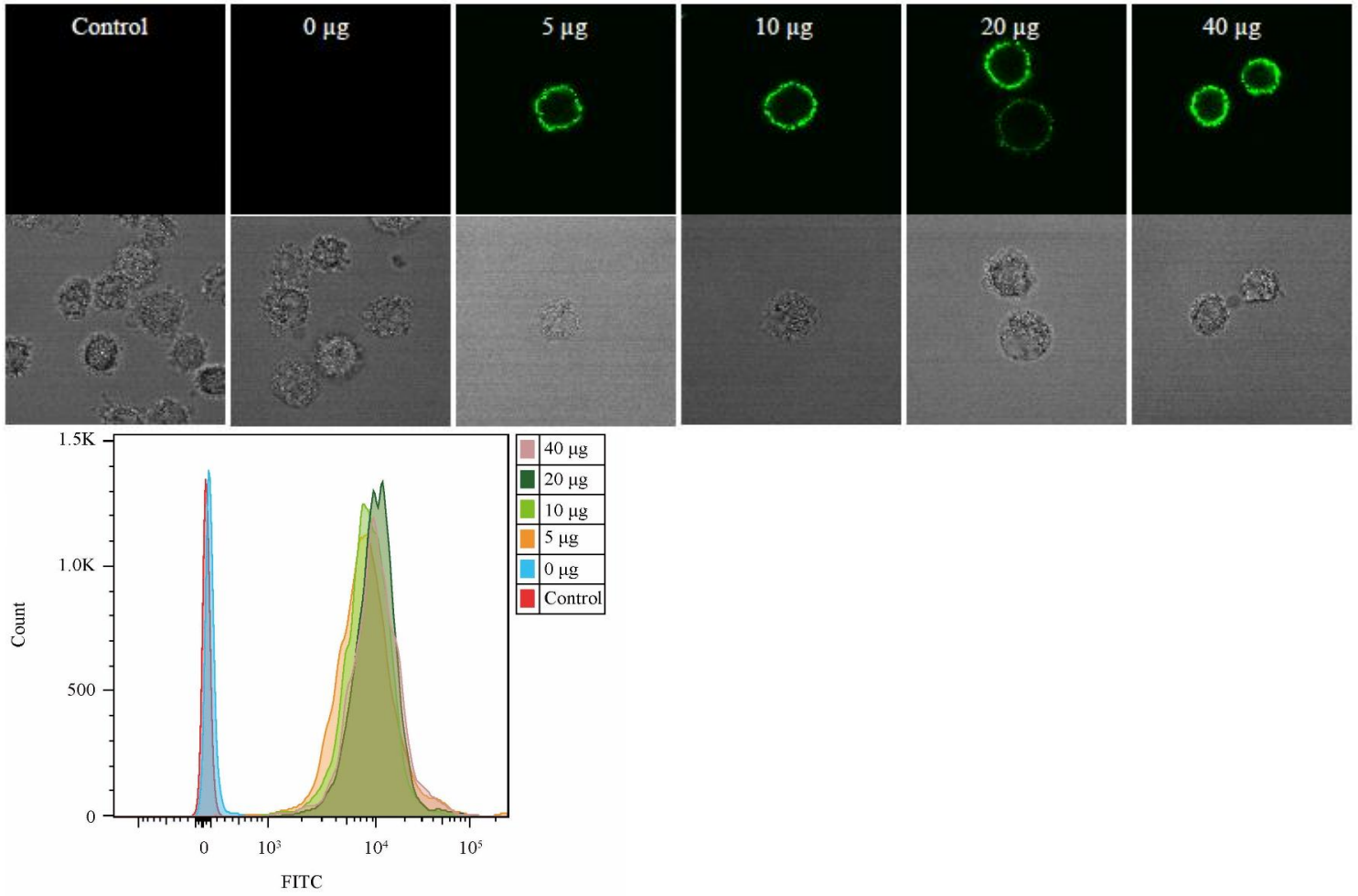

Figure 2.3. Confocal micrograph and FACS analysis of the SDF-1-modified MSCs. (a) MSCs presenting SDF-1 on the surface observed by confocal microscopy (60×). (b) The degree of modification determined by the FACS analysis. FITC-labeled SDF-1 on MSC surface were excited 495 nm and emission was recorded at 520 nm. One representative result from three independent experiments is reported.

CRIP2 protein—the molecular target of the CRPPR peptide. The number of MSCs migrating towards CRIP2 was significantly increased compared to that of the nonmodified MSCs (Figure. 2.4a). The extent of migration was observed to be directly proportional to the amount of embedded DMPE-PEG-CRPPR on the surface of the MSCs. Todemonstrate the CRIP2 gradient-dependent increase in migration, MSCs modified with 60 μg of DMPE-PEG-CRPPR were exposed to increasing concentrations of CRIP2.The migration of the modified MSCs increased in a CRIP2 dose-dependent manner (Figure. 2.4b). As shown in Figure 2.5, migration of the modified MSCs with the DMPE-PEG-SDF-1 increased toward CXCR4, which is the target receptor for SDF-1.

2.4.4. Normalization

In order to demonstrate the feasibility of our surface engineering technology to serve as a platform that can be applied to the modification of a wide variety of cells, 293T, Jurkat, A549, BT-474, MCF-7, MDA-MB-231, and SK-BR-3 cells were modified with DMPE-PEG-FITC through the optimized method and then observed by confocal microscopy. DMPE-PEG-FITC was detected on the surface of the cells (Figure 2.6). Although the degree of the surface modification varies by cell type, 100% of the given cell population was modified with DMPE-PEG-FITC. The modified cells were seeded on a cell culture plate to evaluate the ability of the modified cells to adhere to the plate. There was no difference in cell adhesion between the modified cells and the nonmodified parent cells (Figure 2.7). Jurkat cells showed proliferative clumps, indicating no change in cell behavior after the surface modification.

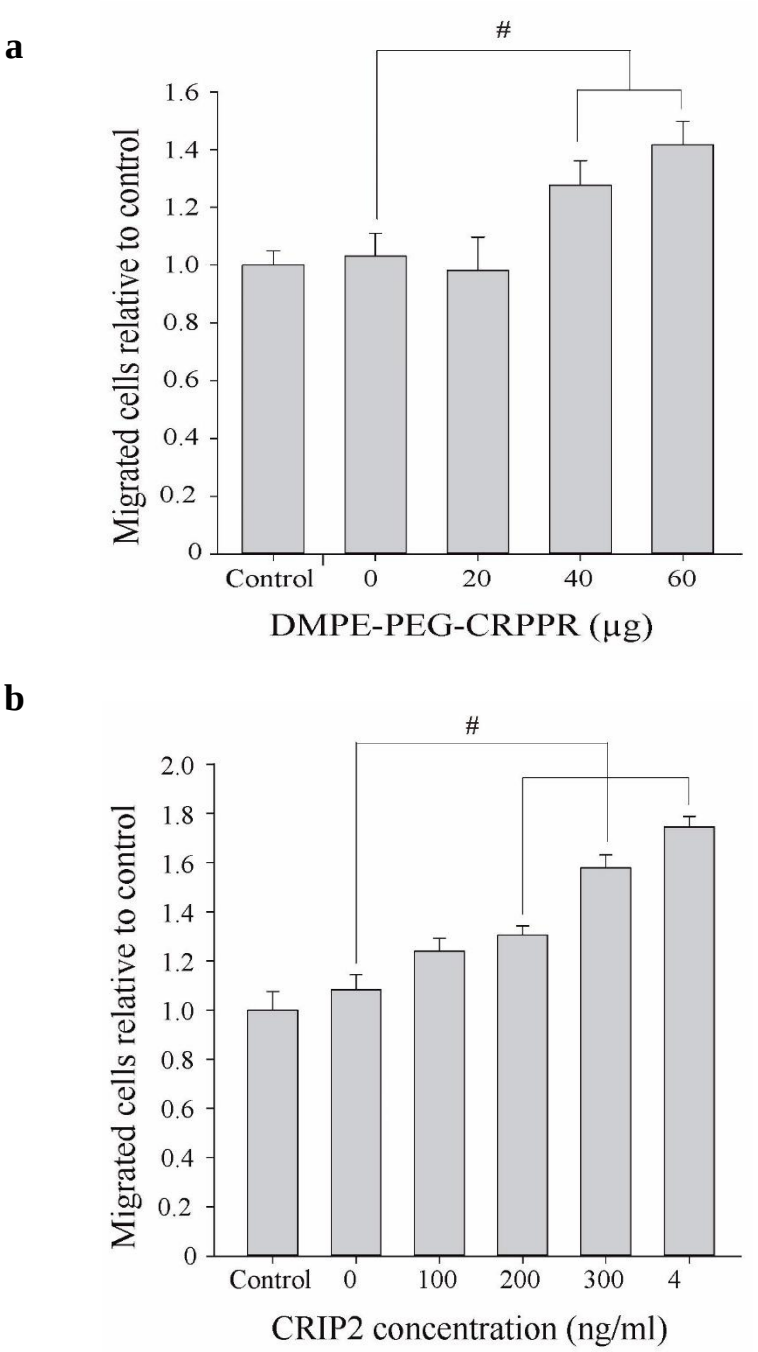

Figure 2.4. Migration of CRPPR modified MSCs towards CRIP2. (a) Migration of the MSCs modified with increasing amounts of DMPE-PEG-CRPPR toward CRIP2 ($^{\#}P<0.01$). (b) Migration of the MSCs modified with DMPE-PEG-CRPPR toward CRIP2 gradient ($^{\#}P<0.01$). Data were selected from three independent experiments. All experiments were conducted in triplicate.

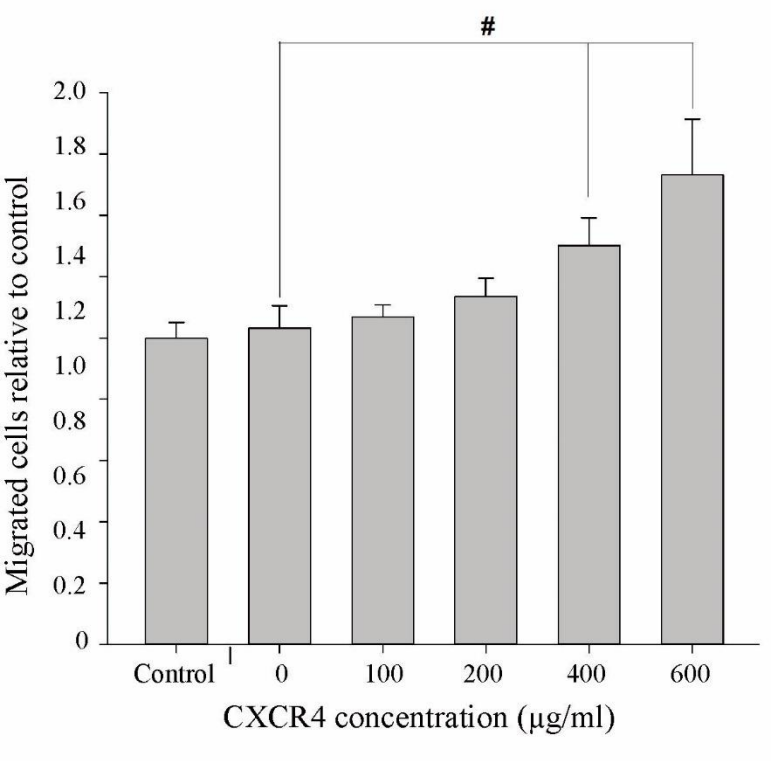

Figure 2.5. Migration of the MSCs modified with DMPE-PEG-SDF-1 toward CXCR4 gradient (n=3, $^{\#}P$<0.01). MSCs modified with 100 μg of DMPE-PEG-SDF-1 were able to migrate across the transwell membrane when they were exposed to increasing concentration of CXCR4. Data were selected from three independent experiments.

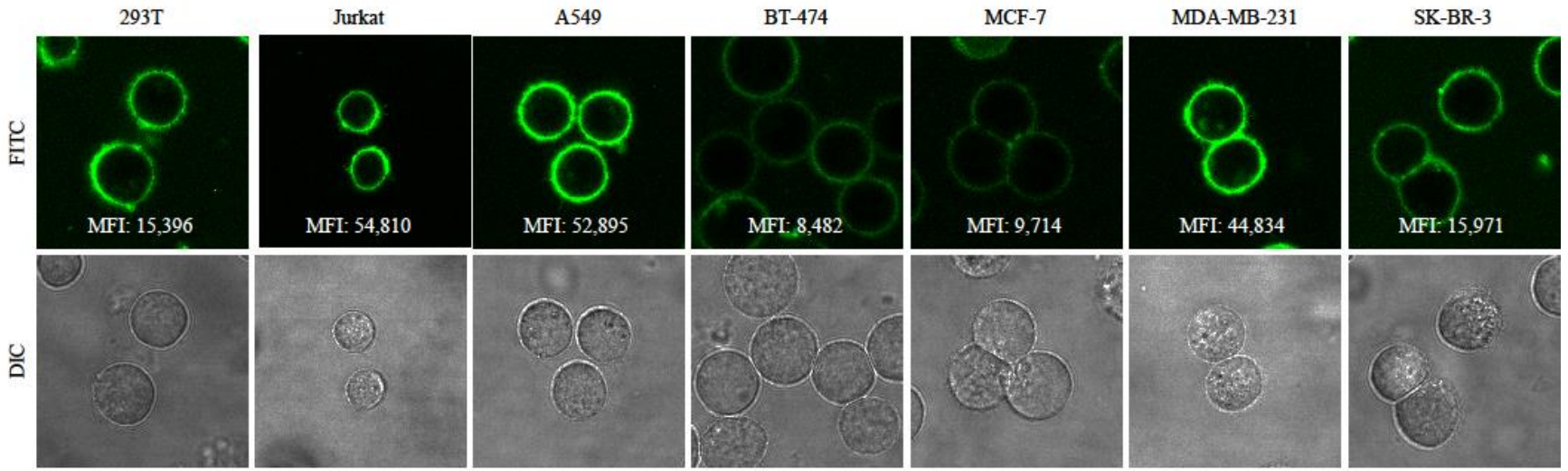

Figure 2.6. Surface modification of various cell types. Confocal micrographs (60×) of DMPE-PEG-FITC modified cell surface of different cell types. FITC-surface modified cells were excited at 495 nm and fluorescence emission was detected at 520 nm. Images were selected from three independent experiments. MFI: Mean Fluorescence Intensity determined using FACS.

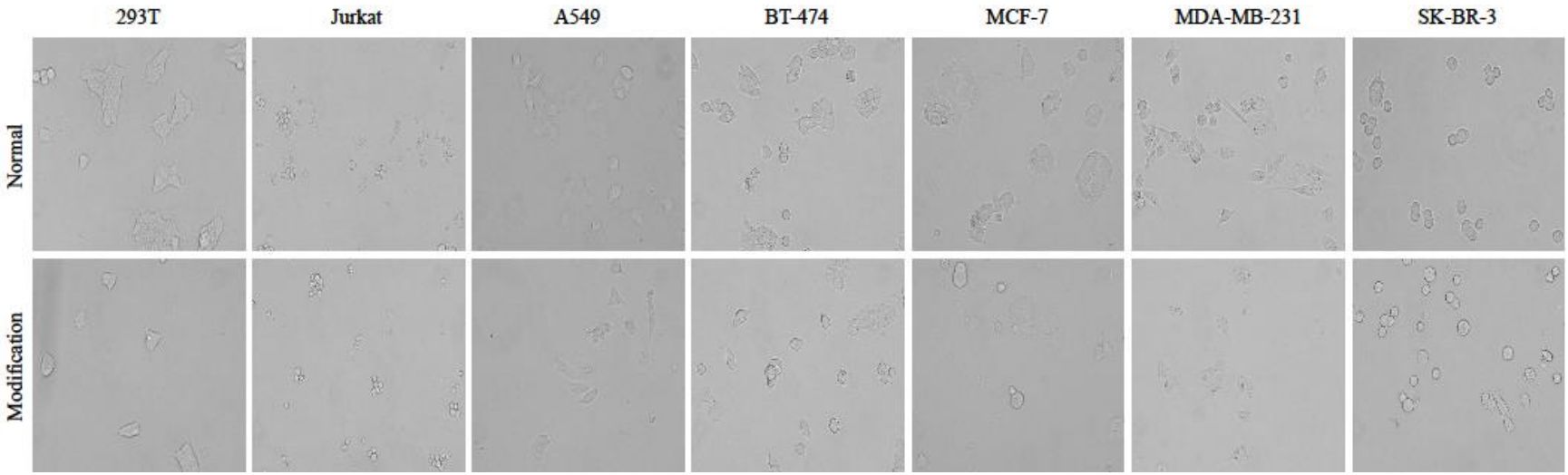

Figure 2.7. Adhesion of different types of cells on a tissue culture plate after the surface modification with DMPE-PEG-FITC. No difference in cell adhesion pattern was observed between unmodified cells and DMPE-PEG-FITC modified cells. Also, behavior of suspension cells, such as Jurkat cells, was not altered after the modification with DMPE-PEG-FITC. Images were selected from three independent experiments.

2.4.5. Modification with Tracking Agents

To test whether or not our surface engineering technology can be used to label cells with tracking agents, Jurkat cells were modified with DMPE-PEG-SPION-FITC. Jurkat cells modified with increasing amounts of DMPE-PEG-SPION-FITC showed fluorescent emission on the cell surface, but not in the cytosol (Figure. 2.8), while FITC emission was not observed in the unmodified Jurkat cells. Jurkat cells showed a high degree of modification when surface-engineered with DMPE-PEG-SPION-FITC; however, considerably low fluorescent intensity was observed when Jurkat cells were treated with PEG-SPION-FITC (Figure 2.9a, b). This observation confirmed that the conjugated lipids allowed SPION incorporation into the cell surface. As shown in Figure 2.10, SPION-modified Jurkat cells were detectable by MRI and displayed a positive MRI signal; the signal intensity increased as the dosage of SPION increased. Modification of Jurkat cells with DMPE-PEG-SPION had no influence on cell viability or proliferative capacity of the cells (Figure 2.11a, b). These results demonstrate that surface engineering technology can be employed to embed tracking agents in the surfaces of cells without the creation of covalent bonds or internalization of imaging agents.

2.5. Discussion

Surface modification through hydrophobic interaction requires preconjugation of lipid-PEG with the desired biological molecule prior to cell incubation. This method generates modified cells more quickly, reduces the amount of conjugate required, increases the yield of modified cells, improves cell viability, and minimizes any adverse effects on cellular activity compared to other cell surface modification techniques. Surface

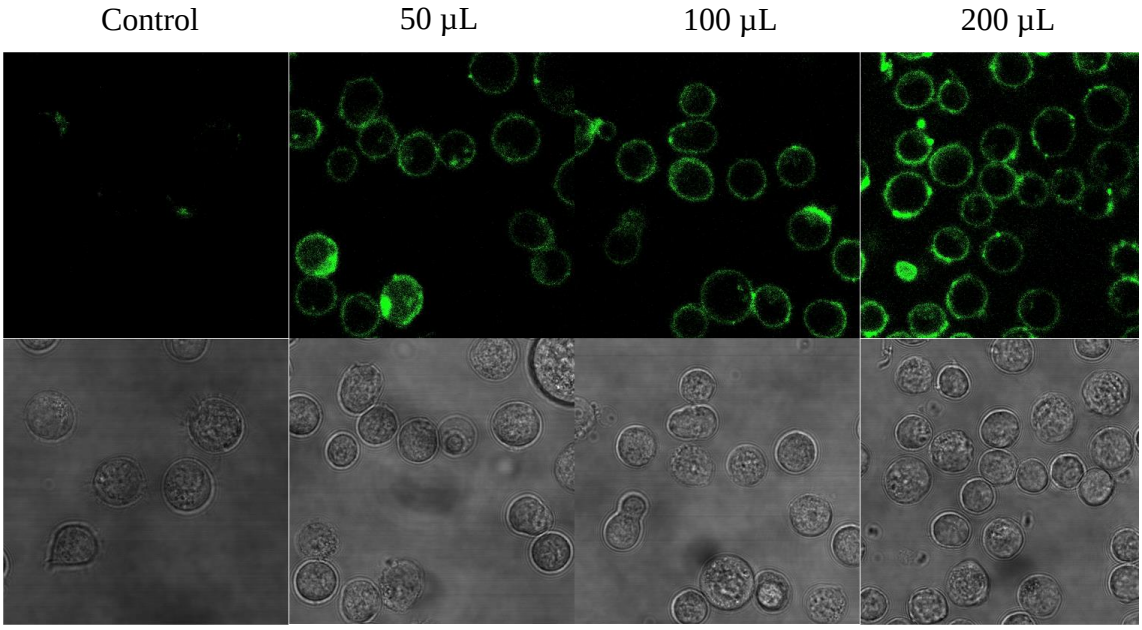

Figure 2.8. Confocal images (60×) of Jurkat cells modified with DMPE-PEG-SPION-FITC. FITC-labeled SPIONs were excited at 495 nm and emission was detected at 520 nm. Internalization of SPIONs was not observed after the modification. Images were selected from three independent experiments.

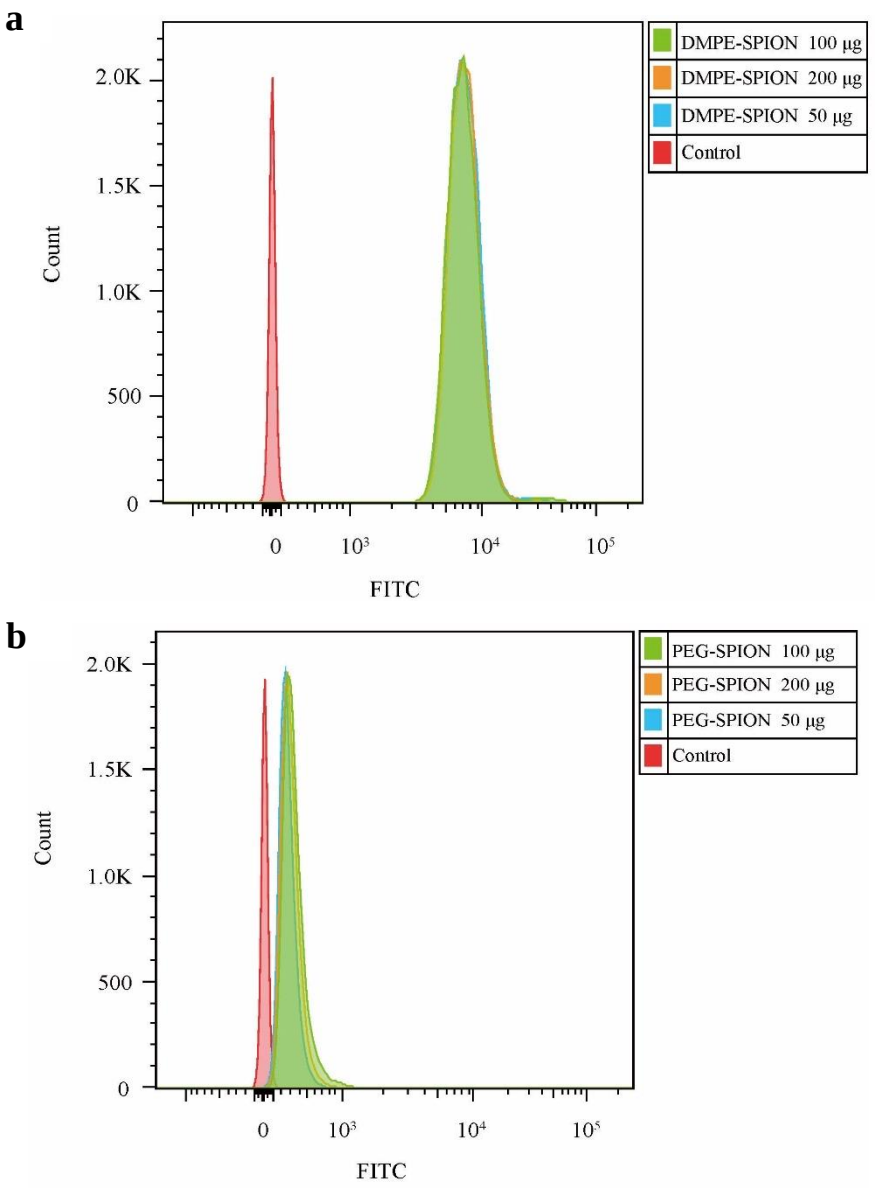

Figure 2.9. Degree of Jurkat cell modification with SPIONs. (a) FACS analysis of Jurkat cells modified with DMPE-PEG-SPION-FITC. (b) FACS analysis of Jurkat cells modified with PEG-SPION-FITC. FITC-labeled SPIONs on the Jurkat cell membrane was excited at 495 nm and fluorescent emission was recorded at 520 nm. One representative result from three independent experiments is presented.

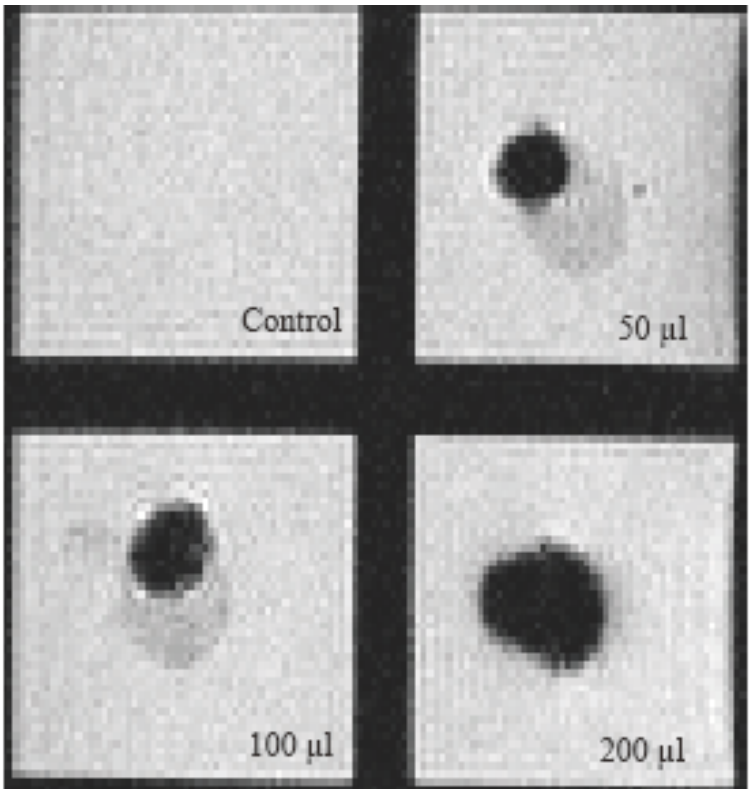

Figure 2.10. MRI of agar phantoms containing Jurkat cells modified with different amounts of DMPE-PEG-SPION-FITC. Each agar phantom was seeded with 1×10^5 SPION-modified Jurkat cells and resulting MRI signal was recorded. Images were selected from three independent experiments.

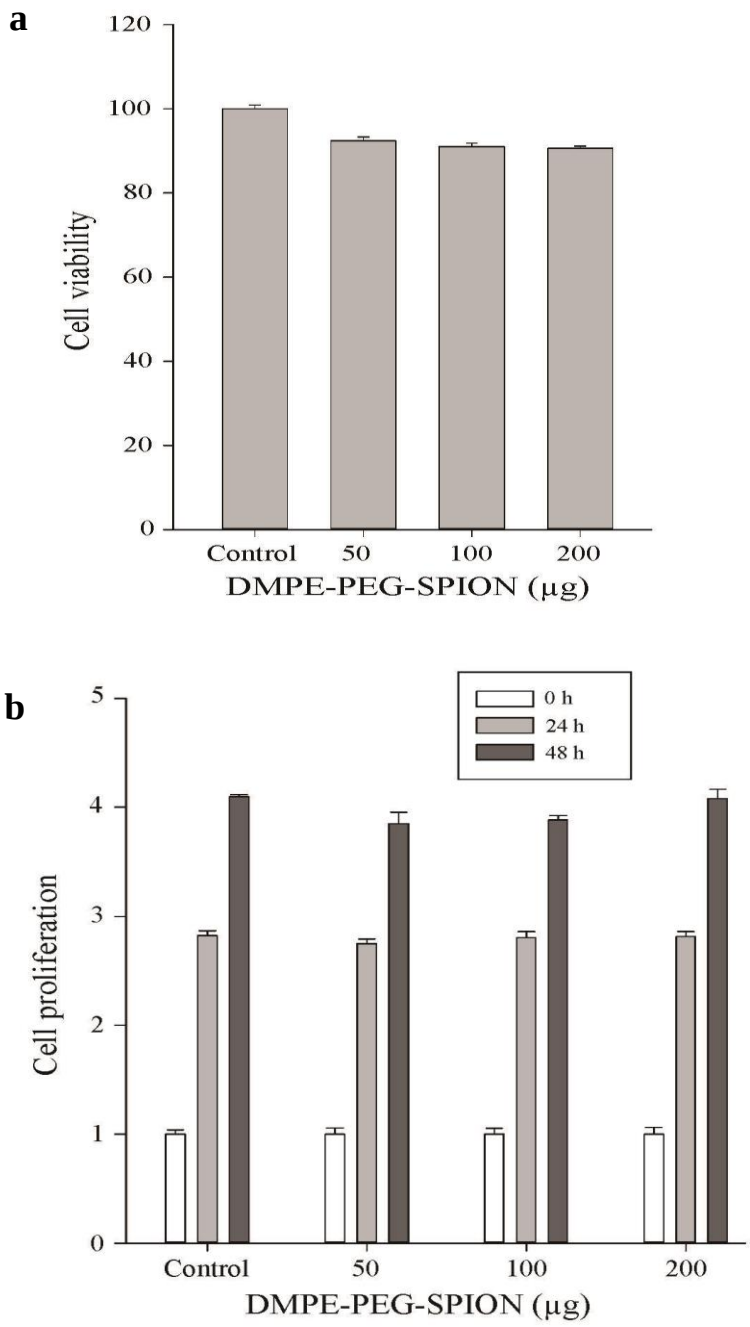

Figure 2.11. Viability (a) and cell proliferation (b) of Jurkat cell after modification with DMPE-PEG-SPION-FITC. No significant difference was observed in cell viability (a) or proliferative activity (b) between unmodified Jurkat cells and SPION-modified Jurkat cells. All experiments were conducted in triplicate. The results were selected from three independent experiments.

modification with hydrophobic interaction is therefore broadly applicable to many types of cell therapy.

The percentage of MSCs engrafted into a target organ following systemic injection is typically very low. For example, generally only 1% of injected MSCs that have been expanded *ex vivo* reach the acutely infarcted myocardium.[14] Although MSC-based cell therapies have shown promising outcomes in several clinical settings,[1,15] the homing of injected MSCs to their target tissues must improve. To this end, polymeric scaffolds, microspheres, and hydrogels have been tested. The results, however, have been unsatisfactory due to reduced activity, viability, and differentiation potential of the MSCs following *ex vivo* expansion.[16,17] This proposes the need for tremendous numbers of MSCs to be administered in order to achieve a therapeutic benefit.[18] On the other hand, the surface modification of MSCs using the lipid-PEG platform has minimal effects on the intrinsic activity of cells and a high recovery yield, regardless of the type of bioactive molecule planted on the cell surface. More importantly, MSCs modified by this method can migrate toward the gradients of their corresponding ligands. Consequently, modification of the cell surface of MSCs with homing molecules provides a safe means to improve the migration of MSCs toward their target tissues, resulting in enhanced efficacy of cell therapy.

Given their ability to produce a sharp contrast with MRI, SPIONs have become well-established imaging agents for a variety of biomedical applications.[19,20] SPION-based imaging provides real-time noninvasive tracking of cells to monitor their distribution throughout the living body. There are a number of methods currently in use to label cells with SPIONs. Cellular uptake of imaging agents has been the most commonly used labeling technique for the reason that surface-modified SPIONs can easily internalize into

cells at high concentrations.[21,22] Even though surface-coated SPIONs are generally regarded as safe, adverse effects associated with the internalized SPIONs have been observed. Within a cell, SPIONs are often found in the acidic environments of lysosomes[23,24] that can promote the degradation of both the protective coat and iron oxide core of the SPIONs to release iron ions,[21,25] which in turn can disrupt cell homeostasis and lead to cytotoxicity.[21,26] Recent studies suggest that the long-term adverse effects of SPIONs should not be neglected, especially when stem cells or immune cells are labeled and administered for therapeutic purposes.[24,27] Cationic polyelectrolyte-stabilized SPIONs appear to stay bound to the cell surface.[28] The cytotoxicity of cationic SPIONs is generally higher than that of neutral or slightly negatively charged SPIONs.[29,30] Thus, a method that can noninvasively and rapidly label cells without the use of positively charged SPIONs would offer significant advantages.

Labeling cells with SPIONs using a lipid-PEG platform offers several advantages over the methodologies discussed above. The generation of lipid-PEG-conjugated SPIONs is inexpensive and straightforward. A variety of target cells can be instantly functionalized using lipid-PEG-SPIONs without employing a complicated modification process. Cell-surface modification with lipid-PEG-SPIONs is biocompatible because the modification is transient, the degree of modification is controllable by adjusting the dosage, cell viability is unaffected, and the internalization of SPIONs is substantially reduced. Hence, cell surface modification using lipid-PEG-SPIONs allows efficient tracking of cells without altering their therapeutic functions.

Although cell surface modification with hydrophobic interaction using lipid-conjugated exogenous materials provides a noninvasive and rapid generation of therapeutic cells, the surface retention time of biomaterials embedded in the cell membrane should be taken into account when evaluating for potential *in vivo* studies and clinical applications. Many factors, such as physical shape, size, surface charge of the bioactive molecules, and their patterns of chemical conjugation with the lipid molecules, can affect the surface retention time.[10] Previously, our group reported that DMPE-PEG-FITC on the cell surface could be detected up to 3 hours in the presence of 20% serum.[13] Lipid-conjugated antibody examined in Chapter 3 of this dissertation displayed 48-hour long surface retention time on NK cells. Moreover, Deno et al. showed the detection of vitamin E-loaded liposomes (118 ± 12 nm) on the surface of HUVEC cells in the presence of serum for up to 72 hours.[31] These liposomes were modified with 20-mer of deoxyadenylic acid and immobilized on the HUVEC cell surface modified with lipid conjugated 20-mer of complementary deoxythymidylic acid though DNA hybridization. Cell surface-embedded CRPPR peptides, SDF-1 proteins, and SPIONs may display surface retention times similar to FITC dyes, antibodies and liposomes, respectively. Surface retention time, dissociation mechanism, and the fate of dissociated biomaterials should be further studied for the designed therapeutic purpose.

2.6. Conclusion

In conclusion, this study has explored the applicability of cell surface engineering to embed various types of bioactive molecules in the surfaces of a variety of cell types. Using this technology, homing peptides, targeting ligands, or contrast agents may be embedded

noninvasively and transiently on the surface of a cell membrane without adversely affecting the cell or compromising cell function. Therefore, cell surface engineering can improve and extend the therapeutic application of cell therapy to many different types of diseases.

2.7. References

1. Ankrum J, Karp JM. 2010. Mesenchymal stem cell therapy: Two steps forward, one step back. Trends Mol Med **16**(5):203-209.

2. Hare JM, Fishman JE, Gerstenblith G, Velazquez DLD, Zambrano JP, Suncion VY, Tracy M, Ghersin E, Johnston PV, Brinker JA. 2012. Comparison of allogeneic vs autologous bone marrow–derived mesenchymal stem cells delivered by transendocardial injection in patients with ischemic cardiomyopathy: The POSEIDON randomized trial. Jama **308**(22):2369-2379.

3. Wynn RF, Hart CA, Corradi-Perini C, O'Neill L, Evans CA, Wraith JE, Fairbairn LJ, Bellantuono I. 2004. A small proportion of mesenchymal stem cells strongly expresses functionally active CXCR4 receptor capable of promoting migration to bone marrow. Blood **104**(9):2643-2645.

4. Karp JM, Teo GSL. 2009. Mesenchymal stem cell homing: The devil is in the details. Cell Stem Cell **4**(3):206-216.

5. Teramura Y, Kaneda Y, Totani T, Iwata H. 2008. Behavior of synthetic polymers immobilized on a cell membrane. Biomaterials **29**(10):1345-1355.

6. Srijaya TC, Ramasamy TS, Kasim NH. 2014. Advancing stem cell therapy from bench to bedside: Lessons from drug therapies. J Transl Med **12**:243.

7. Cheng Z, Ou L, Zhou X, Li F, Jia X, Zhang Y, Liu X, Li Y, Ward CA, Melo LG. 2008. Targeted migration of mesenchymal stem cells modified with CXCR4 gene to infarcted myocardium improves cardiac performance. Mol Ther **16**(3):571-579.

8. Shi M, Li J, Liao L, Chen B, Li B, Chen L, Jia H, Zhao RC. 2007. Regulation of CXCR4 expression in human mesenchymal stem cells by cytokine treatment: Role in homing efficiency in NOD/SCID mice. Haematologica **92**(7):897-904.

9. Goddard JM, Hotchkiss J. 2007. Polymer surface modification for the attachment of bioactive compounds. Prog Polym Sci **32**(7):698-725.

10. Stephan MT, Irvine DJ. 2011. Enhancing cell therapies from the outside in: Cell surface engineering using synthetic nanomaterials. Nano Today **6**(3):309-325.

11. Boylan NJ, Zhou W, Proos RJ, Tolbert TJ, Wolfe JL, Laurence JS. 2013. Conjugation site heterogeneity causes variable electrostatic properties in Fc conjugates. Bioconjug Chem **24**(6):1008-1016.

12. Won YW, Lim KS, Kim YH. 2011. Intracellular organelle-targeted non-viral gene delivery systems. J Control Release **152**(1):99-109.

13. Won YW, Patel AN, Bull DA. 2014. Cell surface engineering to enhance mesenchymal stem cell migration toward an SDF-1 gradient. Biomaterials **35**(21):5627-5635.

14. Barbash IM, Chouraqui P, Baron J, Feinberg MS, Etzion S, Tessone A, Miller L, Guetta E, Zipori D, Kedes LH. 2003. Systemic delivery of bone marrow–derived mesenchymal stem cells to the infarcted myocardium: Feasibility, cell migration, and body distribution. Circulation **108**(7):863-868.

15. Williams AR, Hare JM. 2011. Mesenchymal stem cells biology, pathophysiology, translational findings, and therapeutic implications for cardiac disease. Circ Res **109**(8):923-940.

16. Lim SH, Mao H-Q. 2009. Electrospun scaffolds for stem cell engineering. Adv Drug Deliv Rev **61**(12):1084-1096.

17. Rustad KC, Wong VW, Sorkin M, Glotzbach JP, Major MR, Rajadas J, Longaker MT, Gurtner GC. 2012. Enhancement of mesenchymal stem cell angiogenic capacity and stemness by a biomimetic hydrogel scaffold. Biomaterials **33**(1):80-90.

18. Ikebe C, Suzuki K. 2014. Mesenchymal stem cells for regenerative therapy: Optimization of cell preparation protocols. Biomed Res Int **2014**:951512.

19. Kelm JM, Fussenegger M. 2010. Scaffold-free cell delivery for use in regenerative medicine. Adv Drug Deliv Rev **62**(7-8):753-764.

20. Bull E, Madani SY, Sheth R, Seifalian A, Green M, Seifalian AM. 2014. Stem cell tracking using iron oxide nanoparticles. Int J Nanomedicine **9**:1641-1653.

21. Singh N, Jenkins GJ, Asadi R, Doak SH. 2010. Potential toxicity of superparamagnetic iron oxide nanoparticles (SPION). Nano Rev **1**.

22. Li L, Jiang W, Luo K, Song H, Lan F, Wu Y, Gu Z. 2013. Superparamagnetic iron oxide nanoparticles as MRI contrast agents for non-invasive stem cell labeling and tracking. Theranostics **3**(8):595-615.

23. Arbab AS, Wilson LB, Ashari P, Jordan EK, Lewis BK, Frank JA. 2005. A model of lysosomal metabolism of dextran coated superparamagnetic iron oxide (SPIO) nanoparticles: Implications for cellular magnetic resonance imaging. NMR Biomed **18**(6):383-389.

24. Chen CC, Ku MC, D MJ, Lai JS, Hueng DY, Chang C. 2013. Simple SPION incubation as an efficient intracellular labeling method for tracking neural progenitor cells using MRI. PLoS One **8**(2):e56125.

25. Shen Y, Huang Z, Liu X, Qian J, Xu J, Yang X, Sun A, Ge J. 2015. Iron-induced myocardial injury: An alarming side effect of superparamagnetic iron oxide nanoparticles. J Cell Mol Med **19**(8):2032-2035.

26. Bulte JW, Douglas T, Witwer B, Zhang SC, Strable E, Lewis BK, Zywicke H, Miller B, van Gelderen P, Moskowitz BM, Duncan ID, Frank JA. 2001. Magnetodendrimers allow endosomal magnetic labeling and in vivo tracking of stem cells. Nat Biotechnol **19**(12):1141-1147.

27. Verma VK, Kamaraju SR, Kancherla R, Kona LK, Beevi SS, Debnath T, Usha SP, Vadapalli R, Arbab AS, Chelluri LK. 2015. Fluorescent magnetic iron oxide nanoparticles for cardiac precursor cell selection from stromal vascular fraction and optimization for magnetic resonance imaging. Int J Nanomedicine **10**:711-726.

28. Dzamukova MR, Zamaleeva AI, Ishmuchametova DG, Osin YN, Kiyasov AP, Nurgaliev DK, Ilinskaya ON, Fakhrullin RF. 2011. A direct technique for magnetic functionalization of living human cells. Langmuir **27**(23):14386-14393.

29. Lv H, Zhang S, Wang B, Cui S, Yan J. 2006. Toxicity of cationic lipids and cationic polymers in gene delivery. J Control Release **114**(1):100-109.

30. Frohlich E. 2012. The role of surface charge in cellular uptake and cytotoxicity of medical nanoparticles. Int J Nanomedicine **7**:5577-5591.

31. Deno S, Takemoto N, Iwata H. 2014. Introduction of antioxidant-loaded liposomes into endothelial cell surfaces through DNA hybridization. Bioorg Med Chem **22**(1):350-357.

CHAPTER 3

ADC-EMBEDDED NK92 CELLS TO COMBINE CHEMOTHERAPY AND IMMUNOTHERAPY IN A SINGLE CELL

3.1 Abstract

Conventional combinatorial therapy of chemotherapy and immunotherapy has shown promising outcomes; still, a significant interest in developing new methods to reinforce the efficacy of chemoimmunotherapy persists for the purpose of effective cancer therapy. These potential chemoimmunotherapeutic strategies focus on attaining the following: incorporating a strong chemotherapy that is nontoxic to immune cells, targeted delivery of potent chemotherapeutic agents to avoid adverse effects, enhancing stimulation of the host immune cells to mobilize towards the tumor sites, and preserving the intense cytotoxic activities of immune cells against tumor cells. Unfortunately, efforts to achieve these objectives with the current combinatorial therapies are often frustrated by the health and medical conditions of cancer patients. To overcome this challenge, an antibody-drug conjugate (ADC), T-DM1, was embedded in the membrane of NK92 cells through hydrophobic interaction to produce a single-cell formulation of targeted chemoimmunotherapy. These surface-engineered NK92 cells with T-DM1 (SE-NK/T-DM1 cells) were able to specifically recognize and destroy the target cancer cells. With the combined anti-cancer effects of targeted deliveries of chemotherapeutic

agents and cytolytic NK92 cells, SE-NK/T-DM1 cells significantly suppressed the tumor growth in mice bearing Her2-postive tumors compared to the NK92 cells co-treated with T-DM1. These results suggest that ADC-embedded NK92 cells provide therapeutic advantages as new chemoimmunotherapeutic agents that can simultaneously deliver antibodies, cytotoxic agents, and immune effector cells to their target tissues.

3.2 Introduction

It has been widely acknowledged that the combinatorial therapy of chemotherapy and immunotherapy is beneficial for the treatment of many clinical cancers.[1,2] Conventional chemoimmunotherapy typically utilizes the ability of the host immune system to recognize the immunogenic apoptotic cancer cells induced by chemotherapy.[3,4] For better outcomes, chemoimmunotherapy requires both the immunomodulating ability of chemotherapy and the recruitment of a sufficient number of immune effector cells to the tumor site.[5,6] However, the immunomodulatory effects of cytotoxic agents appear only when patients are exposed to low-dose chemotherapy because high-dose chemotherapy can simultaneously shatter the host immune cells and destroy the cancer cells.[7-10] Although the host immune system is involved in the suppression of abnormal tumor growth, cytolytic activity of these immune cells is inhibited by the evasive mechanism of tumor cells to bypass the immune surveillance.[11,12] In order for chemoimmunotherapeutic agents to be effective, the following criteria should be satisfied: (1) chemotherapeutic agents should be able to induce cancer cell death, (2) components must signal the host immune system to discharge immune effector cells at the tumor site, (3) the chemotherapeutic agent should be nontoxic to immune cells or targeted delivery of cytotoxic drugs should be incorporated

to avoid off-tumor toxicity, and (4) immune effector cells must maintain their cytolytic activity against the cancer cells.[1,13,14]

The adoptive cell transfer of *ex vivo* expanded immune cells is a clinically proven method to provide large amounts of effector cells to boost the anti-cancer immunity. Recent fatal adverse effects reported from clinical studies on chimeric antigen receptor T (CAR-T) cells have contributed to the increased interest in using natural killer (NK) cells as an alternative to T cells.[12,15,16] However, obtaining a sufficient amount of autologous NK cells seems difficult because the number of autologous NK cells that can be isolated from a patient is limited.[12] Allogeneic NK cells have demonstrated advantages over autologous NK cells in terms of convenient *ex vivo* expansion and consistent cytolytic activity.[11,12,16] Among the various types of allogeneic NK cells, NK92 cells constitute the only cell line that is currently being tested in patients with solid organ malignancies, but the clinical outcomes have been disappointing.[11,12,17,18] Genetic modification to express CARs, CD16, or NKG2D—in the interest of empowering NK92 cells—is continuously being studied to improve the anti-cancer activity of NK92 cells.[12,19,20]

Monoclonal antibodies (mAbs) have been established as the mainstream mode of immunotherapy in clinical oncology as well as excellent vehicles for targeted delivery of cytotoxic agents.[21-23] Antibodies can induce cancer cell death through their direct activity, antibody-dependent cellular cytotoxicity (ADCC), and/or complement-dependent cytotoxicity (CDC).[21] As immunomodulators, antibodies bind to the target cancer cells, initiating the migration of many effector cells—including NK cells, DCs, cytotoxic T cells, and tumor-associated macrophages—towards the tumor tissue.[11,13,14] Nevertheless, the fact that mAbs must be used in combination with standard chemotherapy in order to produce

more potent anti-cancer effects indicates the weak therapeutic efficacy of mAb treatment as a monotherapy.[24-26] The need to amplify the anti-cancer effects of mAb has encouraged the development of antibody-drug conjugates (ADCs).[21,27,28]

ADCs exert anti-cancer activity through dual functions: mAbs act as immunomodulators to stimulate the host immune system, and chemotherapeutic agents directly induce cancer cell death.[22,23] ADCs lower the dosage of chemotherapeutic agents and reduce the adverse effects on both normal tissues and immune cells, making ADCs ideal therapeutic agents for chemoimmunotherapy. Unfortunately, the efficacy of ADCs may be reduced due to the distribution of host immune cells and ADCs in the body. It has been shown that the number of active immune cells in tumor tissues is not significantly different from that in normal tissues.[29] Also, poor accumulation of ADCs in the tumor sites has been reported.[30] Consequently, the host immune system may be unable to detect the ADCs bound to cancer cells for ADCC; future studies should address these critical challenges. Integrating the ability of ADCs to deliver cytotoxic agents to the target cancer cells with the cytolytic activity of NK cells is therefore of great interest, especially when considering an innovative strategy to combine ADCs and NK cells in a single formulation.

We have developed a cell surface engineering technology that enables the embedment of a variety of biomaterials in the cell surface.[31,32] In this study, NK92 cells were engineered to carry ADCs on their membrane in order to generate surface-engineered NK92 cells capable of homing toward target tumor tissues and exerting enhanced anti-cancer effects through chemoimmunotherapy. We hypothesized that (1) ADC-embedded NK92 (SE-NK/ADC) cells would specifically migrate towards the target tumor site through the recognition of tumor antigens by ADCs, (2) ADCs would

induce apoptosis in the target cancer cells, (3) NK92 cells concurrently delivered at the tumor tissues with ADCs would recognize the apoptotic cancer cells, and (4) NK92 cells would further destroy the dying cancer cells through direct cytolytic activities. We have generated the surface-engineered NK92 cells with a model ADC, Trastuzumab-DM1 (T-DM1; SE-NK/T-DM1 cells), and investigated the potential therapeutic benefits as a novel means of chemoimmunotherapy.

3.3. Materials and Methods

3.3.1 Study Design

We hypothesized that the NK92 cells modified with ADCs would migrate toward the antigen-expressing target cancer cells *via* antigen-specific binding. Following the migration toward the tumor, ADCs would induce cancer cell death, and NK92 cells would destroy the apoptotic cancer cells through a number of mechanisms. All *in vitro* studies were performed at least twice in triplicate. *In vivo* experiments were designed to demonstrate the tumor-targeted efficacy of SE-NK/T-DM1 cells, which would be difficult to determine in the *in vitro* models. NOD scid gamma (NSG, NOD-*scid* IL2Rg^{null}) mice were selected because they lack mature T cells, B cells, and NK cells that can interact and eliminate the infused allogeneic cells. In order to isolate the therapeutic effects of SE-NK/T-DM1 cells, interference from the murine immune system had to be minimized. The *in vivo* study sample size was calculated from a similar study reported in a literature demonstrating the efficacy of Her2-specific CAR-NK cells.[20] Efficacy studies and biodistribution studies were completed with four mice per group (three mice for the control group in Her2-negative MDA-MB-231 models) and three mice per group, respectively.

Animals were injected once per week for 3 weeks, and tumor growth was monitored for 21 days. To compensate for the different growth rates of inoculated tumors, the initial volume normalized the recorded tumor volume. Animal experiments were terminated when the tumor volume reached 1,500 mm^3 according to the IACUC-approved protocol. Biodistribution was also normalized by counting 1×10^5 cells using flow cytometry from the total cell suspension prepared for each harvested organ. Data analysis was not blinded, but rather crosschecked by all lab members, and outliers were not excluded.

3.3.2. Materials

Trastuzumab (Herceptin®) and ado-trastuzumab emtansine (Kadcyla®) were purchased from Genentech (San Francisco, CA). Plasmid DNA-encoding trastuzumab, pVITRO1-Trastuzumab-IgG1/$_{K,}$ was obtained from Addgene (plasmid # 61883 deposited by Andrew Beavil). A DNA isolation kit was purchased from Clonetech (Mountain View, CA). Succinimidyl 4-(N-maleimidomethyl)cyclohexane-1-carboxylate linked DM1 (SMCC-DM1) was acquired from MedKoo Bioscience (Morrisville, NC). 1,2-Dimyristoyl-*sn*-glycero-3-phosphoethanolamine-poly(ethylene glycol)-NHS (DMPE-PEG-NHS, MW= 5 kDa) was purchased from Nanocs (New York, NY). All other materials were purchased from Thermo Fisher Scientific (Waltham, MA). All cancer cell lines and NK92 cells were purchased from ATCC (Manassas, VA). X-VIVO 15 and IL-2 were purchased from Lonza (Walkersville, MD) and Peprotech (Rocky Hill, NJ), respectively. Cell counting kit (CCK-8) was obtained from Dojindo Molecular Technologies (Kumamoto, Japan). Cell activation cocktail, brefeldin A, and monensin were acquired from Biolegend (San Diego, CA). All other cell culture products were purchased from Thermo Fisher Scientific (Waltham, MA). All antibodies were acquired from Miltenyi

Biotec (Bergisch Gladbach, Germany), except for the Alexa 488-conjugated goat anti-human IgG (H+L) antibody (Thermo Fisher). Human IgG total ELISA kit and human IFN-γ ELISA kit were acquired from eBioscience (San Diego, CA) and R&D Systems (Minneapolis, MN), respectively. Matrigel™ Matrix HC was obtained from Fisher Scientific (Bedford, MA). Tissue dissociation kit, gentleMACS Dissociator, and associated materials were purchased from Miltenyi Biotec (Bergisch Gladbach, Germany).

3.3.3. Cell Culture

Human SK-BR-3 and MDA-MB-231 breast cancer cells were maintained in McCoy's 5A media and RPMI 1640 media, respectively. Human Calu-3 lung cancer cells were maintained with RPMI 1640 media. Jurkat cells were grown in RPMI 1640. Cancer cell and Jurkat cell media were supplemented with 10% FBS, 100 U/mL penicillin, and 100 μg/mL streptomycin. Human NK92 cells were maintained in X-VIVO 15, containing 500 U/mL IL-2, 10% FBS, 100 U/mL penicillin, and 100 μg/mL streptomycin. FreeStyle™ 293-F cells were grown in a shaker incubator with FreeStyle™ 293 expression media according to the manufacturer's instructions.

3.3.4. Generation of Recombinant Trastuzumab

Freestyle™ 293-F cells were transfected with pVITRO1-Trastuzumab-IgG1/$_K$ under the conditions specified by the Expi293 expression kit (Thermo Fisher Scientific). Transfected cells were grown over 72 hours, and the culture media—containing secreted trastuzumab (TZ)—was collected. The culture media was dialyzed against PBS for 24 hours at 4°C, passed through 0.22 μm filter, and purified by FPLC (NGC Scout™ System, Bio-Rad, Hercules, CA) equipped with a protein G affinity column (Thermo Fisher

Scientific). FPLC-purified TZ was dialyzed against PBS at 4°C using a Slide-A-Lyzer G2 dialysis cassette (MWCO 20 kDa) and stored at -80°C until use.

3.3.5. Synthesis of T-DM1

T-DM1 was prepared by conjugating SMCC-DM1 to TZ. SMCC-DM1 was dissolved in DMSO at a concentration of 2 mg/mL, and a 5, 10, or 15 molar excess of SMCC-DM1 was added to 2 mg of TZ dissolved in PBS. The reaction mixture was stirred for 2 hours at room temperature. Unconjugated SMCC-DM1 was removed *via* overnight dialysis (MWCO 20 kDa) against PBS at 4°C. The resulting T-DM1 was further purified by FPLC using a protein G affinity column followed by an additional dialysis (MWCO 20 kDa). Samples of T-DM1 were submitted to the University of Utah Mass Spectrometry & Proteomics Core, and the drug-to-antibody ratio (DAR) of each synthesized T-DM1 was calculated from the LC-ESI/MS spectrum. DAR was calculated with Equation 3.1.

$$DAR = \sum (number\ of\ drugs \times AUC) / Total\ AUC \quad (3.1)$$

3.3.6. Antibody Activity

Her2-binding was determined for TZ and T-DM1 synthesized with different molar ratios. All antibodies and ADCs were labeled with FITC. SK-BR-3 cells and MDA-MB-231 cells were incubated with 5 μg of FITC-conjugated TZ, T-DM1, Herceptin®, and Kadcyla® and the resulting fluorescent signal was measured by flow cytometry (FACSCanto™, BD Bioscience). Collected data were analyzed by FlowJo software.

3.3.7. Cytotoxicity of T-DM1

Cytotoxicity of all synthesized T-DM1 was compared to Kadcyla®. Her2-positive SK-BR-3 cells and Her2-negative MDA-MB-231 cells—1×10^4 cells/well—were seeded on a 48-well plate, and serially diluted T-DM1 or Kadcyla® was added to the media. After 48-hour incubation, the resulting cancer cell death was analyzed by MTT assay. Data were analyzed with GraphPad Prism 6 software using a four-parameter logistic nonlinear regression model. Subsequent studies used the T-DM1 prepared with a molar ratio of 10.

3.3.8. Surface Engineering of Jurkat Cells and NK92 Cells

Lipid-PEG-conjugated TZ (DMPE-TZ) or T-DM1 (DMPE-T-DM1) was prepared by mixing 2 mg of TZ or T-DM1 dissolved in PBS with 15 molar excess of DMPE-PEG-NHS dissolved in DMSO. The reaction mixture was stirred at room temperature for 2 hours. Unconjugated DMPE-PEGs were removed *via* overnight dialysis (MWCO: 20 kDa) against PBS at 4°C. Jurkat cells and NK92 cells were modified with DMPE-TZ and DMPE-T-DM1 to generate SE-JK/TZ cells, SE-JK/T-DM1 cells, SE-NK/TZ cells, and SE-NK/T-DM1 cells. Briefly, 5×10^5 Jurkat cells or NK92 cells were incubated with different amounts of DMPE-TZ or DMPE-T-DM1 in 100 μL PBS at room temperature for 15 minutes. After the modification, cells were washed twice with 1 mL PBS.

3.3.9. Characterization of Surface-Engineered Effector Cells

Jurkat cells and NK92 cells were modified with FITC-labeled DMPE-TZ and DMPE-T-DM1 according to the procedure described above. Surface-engineered effector

cells were visualized by confocal microscopy (Nikon A1R, Nikon). Collected images were processed with ImageJ software. Changes in cell viability and proliferative functions after the modification were determined using CCK-8. Changes in absorbance were recorded over 48 hours. Surface retention times of TZ and T-DM1 on the cells membrane were measured using Alexa 488-conjugated goat anti-human (H+L) antibodies (Ex/Em= 495/520 nm). The SE-JK/TZ cells and SE-NK/T-DM1 cells were incubated in complete media. At each time point, a portion of cells were withdrawn and labeled with 10 μg of Alexa 488-conjugated goat anti-human (H+L) antibodies. Fluorescent signal was measured by flow cytometry and analyzed by FlowJo software.

The amount of T-DM1 embedded on the cell membrane was determined using a Human IgG total ELISA kit (detection limit: 15.6 - 1,000 pg/mL). Proteins from 1×10^5 SE-NK/T-DM1 cells or SE-JK-T-DM1 cells prepared with different amounts of T-DM1 were extracted through differential lysis, and the lysate collected from the membrane fraction was analyzed. The amount of human IgG was calculated using the T-DM1 standard curve. NK92 cells and Jurkat cells were modified with 100 μg DMPE-TZ or DMPE-T-DM1 in all subsequent studies. The amounts of TZ and T-DM1 were scaled up according to the effector-to-target (E:T) ratio for each experimental condition involving single or co-treatment.

3.3.10. Selective Binding and Transfer of TZ and T-DM1 from Surface-Engineered Effector Cells to Cancer Cells

To test the selective binding of surface-engineered effector cells, SK-BR-3 cells, Calu-3 cells, and MDA-MB-231 cells were labeled with 2 μM of CellTracker™ Red CMTPX (Ex/Em= 577/602 nm). Cancer cells— 4×10^4 cells/well—were seeded 24-well

plate. Jurkat cells and NK92 cells were labeled with 1 μM of CellTracker™ Blue CMAC (Ex/Em= 353/466 nm) prior to modification. Cancer cells were co-incubated with SE-JK/TZ cells, SE-NK/T-DM1 cells, Jurkat cells with TZ co-treatment (TZ+Jurkat cells), NK92 cells with T-DM1 co-treatment (T-DM1+NK92 cells), unmodified Jurkat cells, and unmodified NK92 cells at E:T ratio of 5:1 or 10:1. After 2 hours, unbound Jurkat cells and NK92 cells were removed, and all remaining cells were collected. The number of effector cells was quantified per 1×10^4 cancer cells by flow cytometry and the remaining E:T ratio was calculated.

An experimental approach similar to the selective binding study has been used to demonstrate the transfer of TZ and T-DM1 from the surface-engineered effector cells to target cancer cells. SK-BR-3 cells, Calu-3 cells, and MDA-MB-231 cells were labeled with 2 μM of CellTracker™ Red CMTPX and seeded on a Lab-Tek™ II 8-chambered coverglass at a density of 1×10^4 cells/well. Jurkat cells and NK92 cells were labeled with 1 μM of CellTracker™ Blue CMAC and subsequently modified with 100 μg of DMPE-TZ-FITC and DMPE-T-DM1-FITC. After the modification, 1×10^5 effector cells were incubated with the cancer cells for 30 minutes at room temperature and washed twice to remove the unbound effector cells. Co-incubated cells were imaged by confocal microscopy (60×) and collected images were processed by ImageJ software.

3.3.11. Internalization of Transferred T-DM1 into Cancer Cells

Cancer cells were seeded on a Lab-Tek™ II 8-chambered coverglass at a density of 1×10^4 cells/well and labeled with NucBlue® Live ReadyProbe Reagent (Ex/Em= 360/460 nm). Cancer cells were treated with T-DM1-FITC or CMPTX-labeled

SE-NK/T-DM1-FITC cells at E:T ratio of 10:1. Unbound T-DM1-FITC and SE-NK/T-DM1-FITC cells were removed after 30 minutes. As a positive control, geldanamycin (GA) was added to the wells treated with T-DM1-FITC at a final concentration of 3 μM. Internalization of T-DM1-FITC (Ex/Em= 495/520 nm) was imaged by confocal microscopy (60×) at the initial time point and 6 hours later. Collected images were processed with ImageJ software.

3.3.12. Cytotoxicity Assay

SK-BR-3 cells, Calu-3 cells, and MDA-MB-231 cells were labeled with CellTracker™ Blue CMAC and seeded at 1×10^4 cells/well on a 48-well plate 24 hours before the treatment. Cancer cells were co-incubated with SE-JK/TZ cells, SE-JK/T-DM1 cells, SE-NK/TZ cells, and SE-NK/T-DM1 cells at E:T ratio of 5:1 or 10:1 in 600 μl of complete media. As control treatments, cancer cells were co-incubated with unmodified Jurkat cells, unmodified NK92 cells, TZ, T-DM1, TZ+Jurkat cells, Jurkat cells with T-DM1 co-treatment (T-DM1+JK cells), T-DM1+NK92 cells, or NK92 cells with TZ co-treatment (TZ+NK92 cells). All cells were harvested, labeled with the Annexin V Alexa Fluor® 488 and propidium iodide (Annexin V/PI) kit, and analyzed by flow cytometry after 24 hours of co-incubation. To determine the targeted anti-cancer efficacy, all treatments were washed 2 hours after the co-culture, and the remaining cancer-bound effector cells were further incubated for 24 hours. All cells were collected and labeled with the Annexin V/PI kit. Cancer cell death was analyzed by flow cytometry. To distinguish the effects of T-DM1 and NK92 cells, cancer cells were co-incubated with SE-JK/TZ cells, SE-JK/T-DM1 cells, SE-NK/TZ cells, SE-NK/T-DM1 cells, and other corresponding

control treatments for 6 hours. Resulting cancer cell death was identified with the Annexin V/PI kit under flow cytometry. All collected results were analyzed by FlowJo software.

3.3.13. Mechanistic Studies

SK-BR-3 cells were labeled with CellTracker™ Blue CMAC and seeded at 1×10^4 cells/well on a 48-well plate. SK-BR-3 cells were co-incubated with SE-NK/T-DM1 cells, NK92 cells, T-DM1, and T-DM1+NK92 cells in the presence or absence of 50 U/mL of IL-2 at E:T ratio of 10:1. After 2 hours, unbound effector cells were removed, and the remaining cells were continuously incubated for 24 hours. Cancer cell death induced by each treatment was analyzed by flow cytometry as described above. Culture media from each well was applied to a human INF-γ ELISA to determine the level of secreted INF-γ.

Expression of CD107a was detected by co-incubating the effector cells with SK-BR-3 cells, Calu-3 cells, or MDA-MB-231 cells. Cancer cells were seeded on a 96-well plate at a density of 2×10^4 cells/well; SE-NK/T-DM1 cells, NK92 cells and T-DM1+NK92 cells were added to each well at E:T ratio of 10:1. Unmodified NK92 cells stimulated with cell activation cocktail containing phorbol-12-myristate-13-acetate (PMA) and ionomycin were included as a positive control. Anti-CD107a-FITC antibodies (Clone: H4A3), 10 μg, were added directly into each well. After the cells were incubated at 37°C for 1 hour, brefeldin A and monensin were added to each well according to the manufacturer's protocol and incubated for an additional 5 hours. All cells were collected, stained with anti-CD56-APC antibodies (clone: REA196) to identify NK92 cells, and examined by flow cytometry. Collected results were analyzed with FlowJo software.

3.3.14. *In Vivo* Tumor Efficacy Study

In vivo studies were conducted with 6-week-old female NSG mice. Each mouse was inoculated with 1×10^7 cells of Her2-positive Calu-3 cells or Her2-negative MDA-MB-231 cells suspended in PBS with 10% (v/v) Matrigel™. Tumor-inoculated mice were randomly assigned to each experimental group upon tumor establishment. The control group (n=4 for Calu-3 model and n=3 for MDA-MB-231 model) received no treatment, but the study groups (n=4 per group) were administered weekly with 0.21 mg of T-DM1, 1×10^7 NK92 cells, 0.21 mg of T-DM1+1×10^7 NK92 cells, 5×10^6 SE-NK/T-DM1 cells, or 1×10^7 SE-NK/T-DM1 cells *via* tail vein infusion. The tumor size was measured three times per week, and the tumor volume was calculated using Equation 3.2: where a is the long diameter, and b is the short diameter of the tumor. Tumor progression was monitored for

$$V = 0.5ab^2 \tag{3.2}$$

21 days, and the relative tumor volume was calculated by dividing the recorded volumes with the initial volume.

3.3.15. Biodistribution

Biodistribution of SE-NK/T-DM1 cells was analyzed using a flow cytometry technique that quantifies organ-trafficking cells.[20,33-35] This approach provides an analysis that agrees well with image-based biodistribution analyses, such as radiolabeling and bioluminescent imaging.[33,34] NSG mice bearing Calu-3 tumors were randomly assigned to each experimental group. The control group (n=3)

received no treatment, and the study groups (n=3) were treated with 1×10^7 NK92 cells, 0.21 mg of T-DM1+1×10^7 NK92 cells, or 1×10^7 SE-NK/T-DM1 cells *via* tail vein infusion. Animals were sacrificed 24 hours after the injection, and the heart, kidneys, liver, lungs, spleen, and tumor were harvested. Single-cell suspension of each harvested organ was prepared using the gentleMACS dissociator and tissue dissociation kits. Half of each cellmixture was incubated with 30 μg of an anti-CD56-APC antibody (clone: REA196,Ex/Em= 650/660 nm) for 30 minutes at 4°C. Cells were washed twice with coldPBS, and the presence of NK92 cells was detected by counting 1×10^5 total cells using flow cytometry. Collected results were analyzed by FlowJo.

3.3.16. Statistical Analysis

Statistical analysis was performed using Graphpad Prism 6. All data are presented in mean ± SD. All data were analyzed with one-way ANOVA with Tukey post-hoc tests or two-way ANOVA with Bonferroni post-hoc tests. Statistical significance threshold of each test was set at $P < 0.05$: ns = not significant; $P > 0.05$; *, $P < 0.05$; **, $P < 0.01$; ***, $P < 0.001$; ****, $P < 0.0001$.

3.3.17. Animal Ethics

All animal experiments were approved by the University of Utah Institutional Animal Care and Use Committee. Described animal procedures were conducted according to the guidelines and regulations.

3.4. Results

3.4.1. Design of SE-NK/ADC Cells as Chemoimmunotherapy

We recently described that bioactive molecules including proteins, peptides, and imaging agents could be incorporated into the cell surface for targeted delivery or *in vivo* real-time tracking.[31,32] With this understanding, we have generated the SE-NK/ADC cells to combine targeted chemotherapy and cell-based immunotherapy in a single formulation (Figure 3.1). Allogeneic NK92 cells that expand to a large population in *ex vivo* conditions can be rapidly transformed into SE-NK/ADC cells. These surface-engineered NK92 cells with ADCs can induce a combinatorial anti-cancer efficacy at the tumor site through the cytotoxicity of ADCs and direct cytolytic activity of NK92 cells.

3.4.2. Synthesis of T-DM1

SMCC-DM1 was conjugated to the recombinant anti-Her2 mAb (Trastuzumab, TZ) at molar ratios (SMCC-DM1/TZ) of 5, 10, or 15 (Figure 3.2). FPLC purification profiles of TZ and T-DM1 products are shown in Figure 3.3. The resulting species of T-DM1 were analyzed using ESI/MS to calculate the drug-to-antibody ratios (DARs) (Figure 3.4, 3.5, 3.6). The calculated DARs for T-DM1 R=5, R=10, or R=15 were 1.04, 2.18, or 3.18, respectively. Synthesized T-DM1 and Kadcyla® induced cell death in SK-BR-3 cells, but not in MDA-MB-231 cells (Figure 3.7, 3.8). The LC50 of T-DM1 R=5, 10, and 15 were 0.275 μg/mL, 0.044 μg/mL, and 0.024 μg/mL, respectively, on SK-BR-3 cells. T-DM1 R=10 demonstrated comparable anti-cancer activity to Kadcyla®, whose LC50 was 0.040 μg/ml in SK-BR-3 cell T-DM1 R=10 was therefore selected for the cell surface engineering. Although T-DM1 R=15 showed higher DAR, it was not selected because

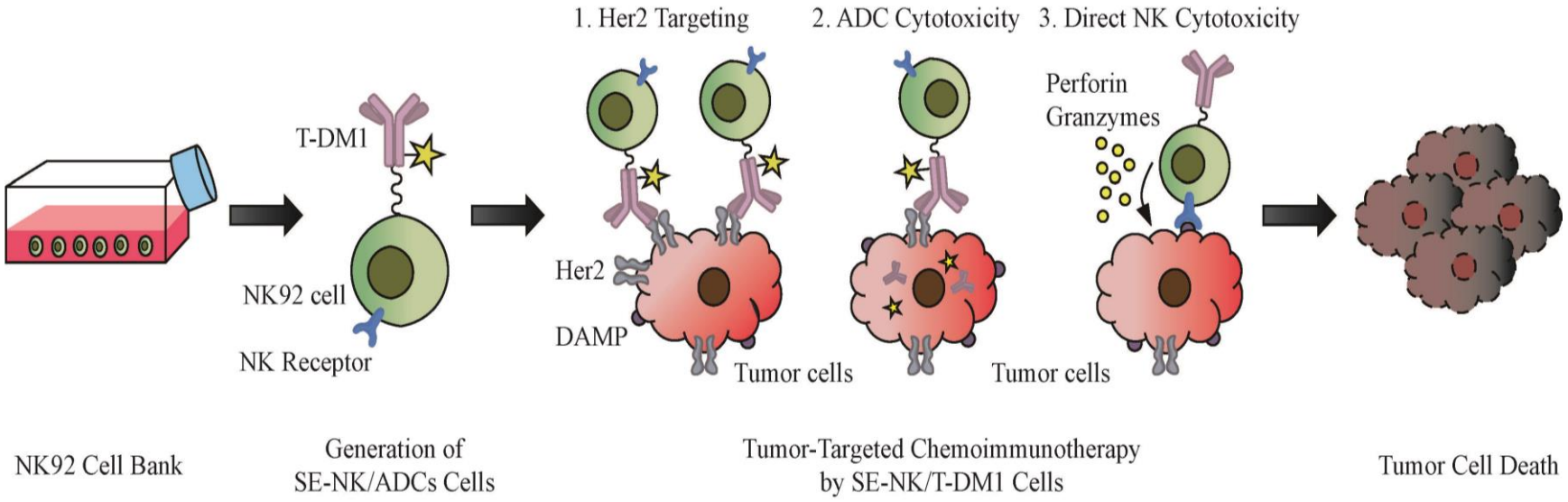

Figure 3.1. Illustration of SE-NK/ADC cells and their mechanism of actions. As a model ADC, T-DM1 specific for Her2 has been selected. The lipid-PEG-conjugated ADCs are prepared as a ready-to-use formulation while allogeneic NK92 cells are available from a cell bank. The surface-engineered NK92 cells engrafted with ADCs migrate toward the target tumor site guided by the recognition of target antigen. In the target tumor tissues, ADCs induce apoptosis in cancer cells and NK92 cells present in proximity destroy the apoptotic target cancer cells by recognizing the damage associated molecular patterns (DAMPs).

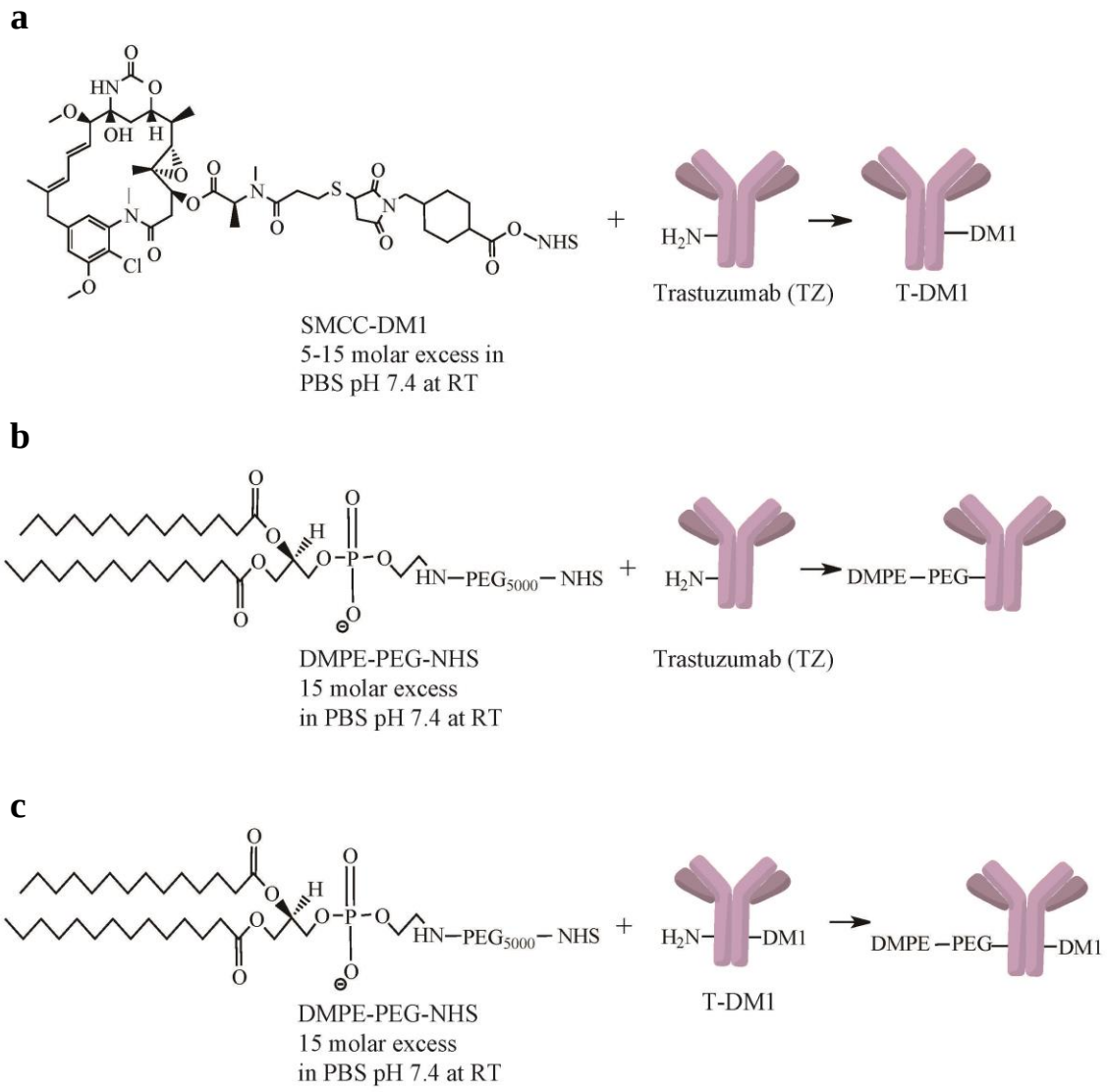

Figure 3.2. Synthesis of T-DM1, DMPE-TZ, and DMPE-T-DM1. (a) Different molar excess of SMCC-DM1 reconstituted in DMSO was added to TZ dissolved in PBS. Mixtures were continuously stirred at room temperature for 2 hours. Product was dialyzed (MWCO 20 kDa) overnight against PBS at 4°C and further purified by FPLC using a protein G affinity column. FPLC-purified T-DM1 was dialyzed (MWCO 20 kDa) overnight against PBS at 4°C. (b, c) TZ or T-DM1 was mixed with 15 molar excess of DMPE-PEG-NHS dissolved in DMSO. Each mixture was stirred at room temperature for 2 hours and dialyzed (MWCO 20 kDa) overnight against PBS at 4°C.

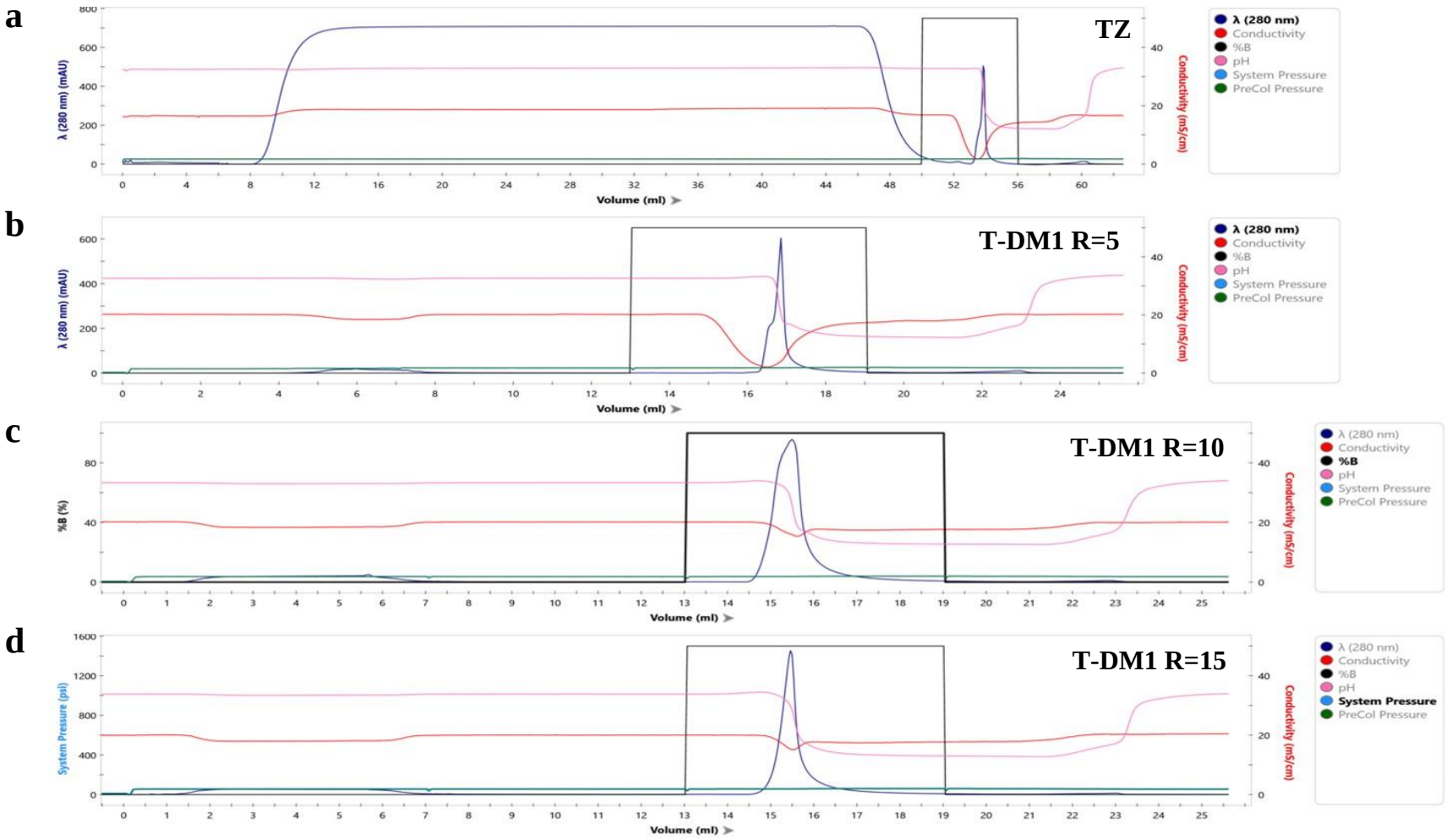

Figure 3.3. FPLC purification of (a) TZ, (b) T-DM1 R=5, (c) T-DM1 R=10, (d) T-DM1 R=15.

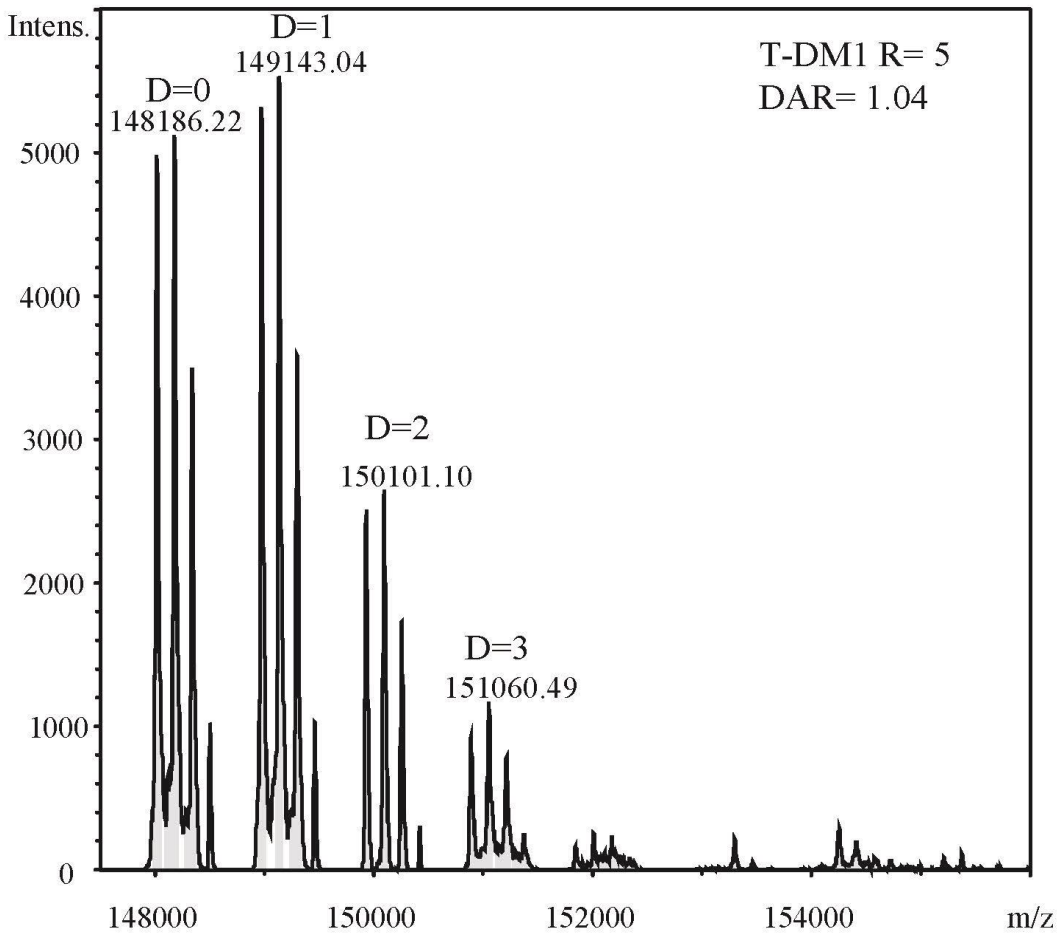

Figure 3.4. ESI/MS spectra of T-DM1 synthesized with 5 molar excess of SMCC-DM1.

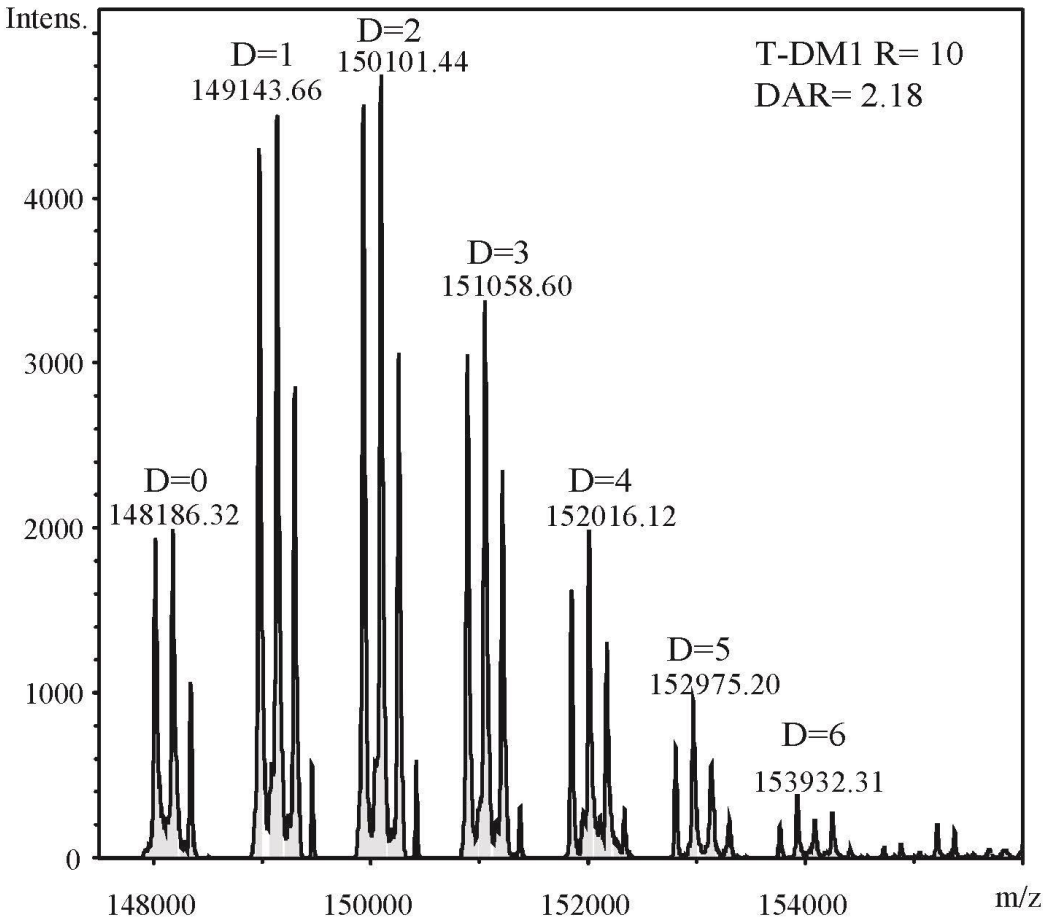

Figure 3.5. ESI/MS spectra of T-DM1 synthesized with 10 molar excess of SMCC-DM1.

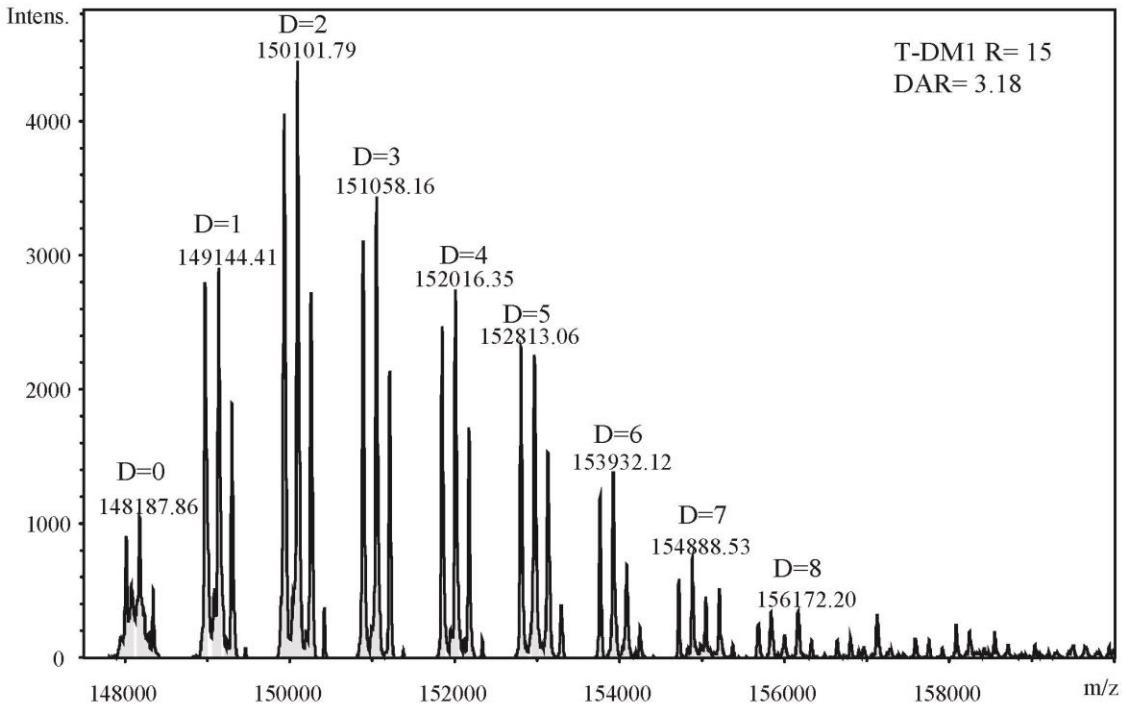

Figure 3.6. ESI/MS spectra of T-DM1 synthesized with 15 molar excess of SMCC-DM1.

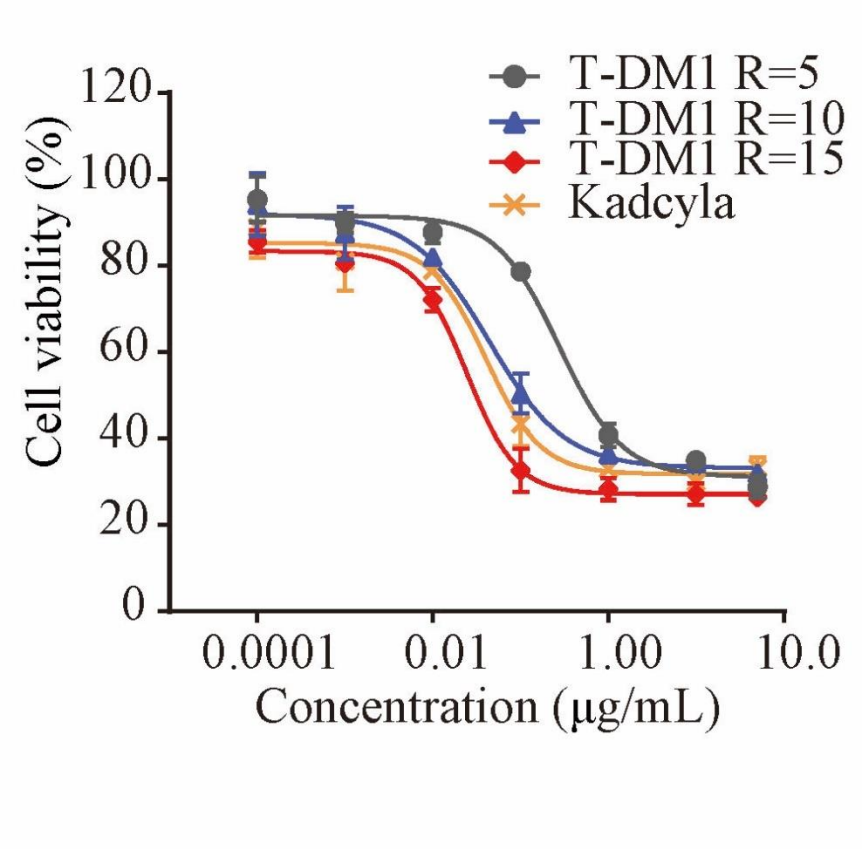

Figure 3.7. Cytotoxicity of Kadcyla® and T-DM1s synthesized with different ratio of SMCC-DM1 in SK-BR-3 cells. The LC50 of T-DM1 R=5, R=10, R=15, and Kadcyla® were 0.275 μg/ml, 0.044 μg/ml, 0.024 μg/ml, and 0.040 μg/ml, respectively. Data presented as mean ± SD.

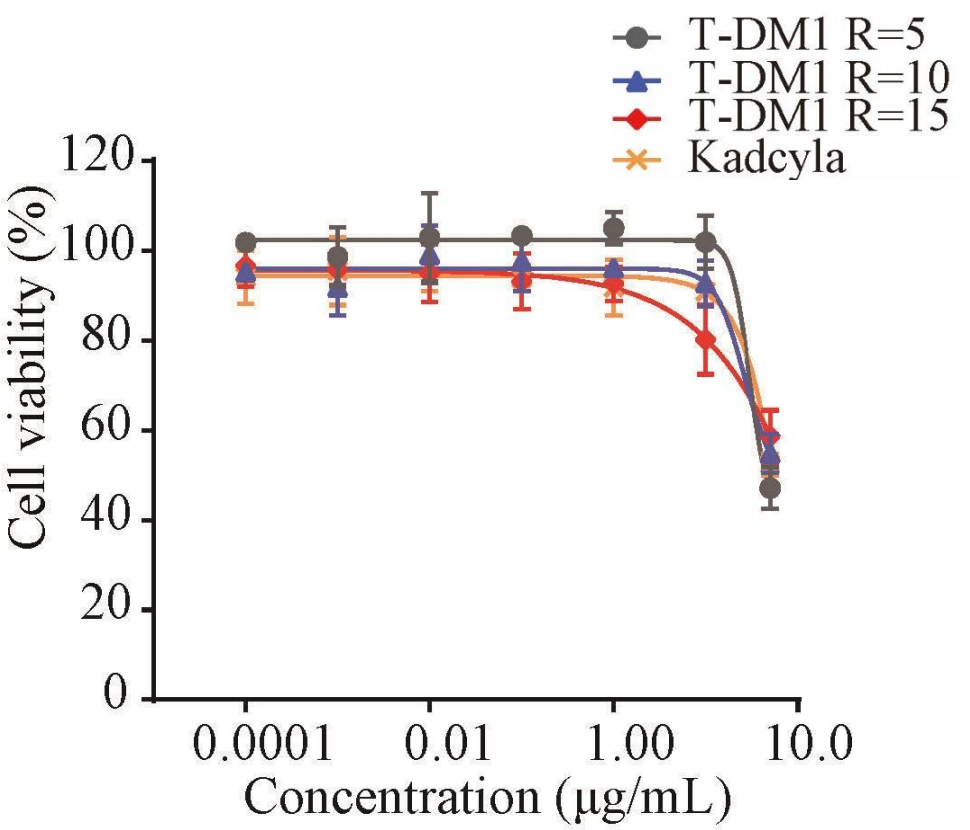

Figure 3.8. Cytotoxicity of Kadcyla® and T-DM1s synthesized with different ratio of SMCC-DM1 in MDA-MB-231 cells. Kadcyla® and T-DM1s only induced nonspecific cancer cell death after 1 μg/ml. Data presented as mean ± SD.

ADCs with high DARs tend to form aggregates, which can cause rapid clearance from the body due to the increased hydrophobicity.[36] The binding activity of recombinant TZ and the synthesized T-DM1 R=10 was compared to that of Herceptin® and Kadcyla® in Her2-positive SK-BR-3 cells and Her2-negative MDA-MB-231 cells, respectively. TZ and T-DM1 prepared in our laboratory showed the same antibody binding activity as Herceptin® and Kadcyla® (Figure 3.9).

3.4.3. Generation of Surface-Engineered Cells

To precisely demonstrate the combined anti-cancer activity of SE-NK/T-DM1 cells, the effects of individual components—DM1, TZ, and NK92 cells—must be identified. Since Jurkat cells are CD3- and CD4-positive T cells that do not have direct cytolytic activities, this cell line was selected as a surrogate negative control for NK92 cells. We therefore prepared Jurkat cells modified with TZ (SE-JK/TZ) or T-DM1 (SE-JK/T-DM1) and NK92 cells modified with TZ (SE-NK/TZ) or T-DM1 (SE-NK/T-DM1) in addition to the unmodified cells.

Jurkat cells were uniformly modified with various amounts of DMPE-TZ to generate the SE-JK/TZ cells (Figure 3.10). The cell viability and proliferation of Jurkat cells were not affected upon modification (Figure 3.11a, b). To investigate the retention time of TZ on the cell membrane in the presence of serum, FITC-labeled goat anti-human (H+L) antibody was used to detect TZ on the SE-JK/TZ cells. Even though the fluorescence intensity decreased partly due to cell proliferation and loss of TZ to the media over time, TZ was detected on the modified cells incubated in the complete growth media over 24 hours (Figure 3.12). Although pharmacokinetic studies remain to be a future

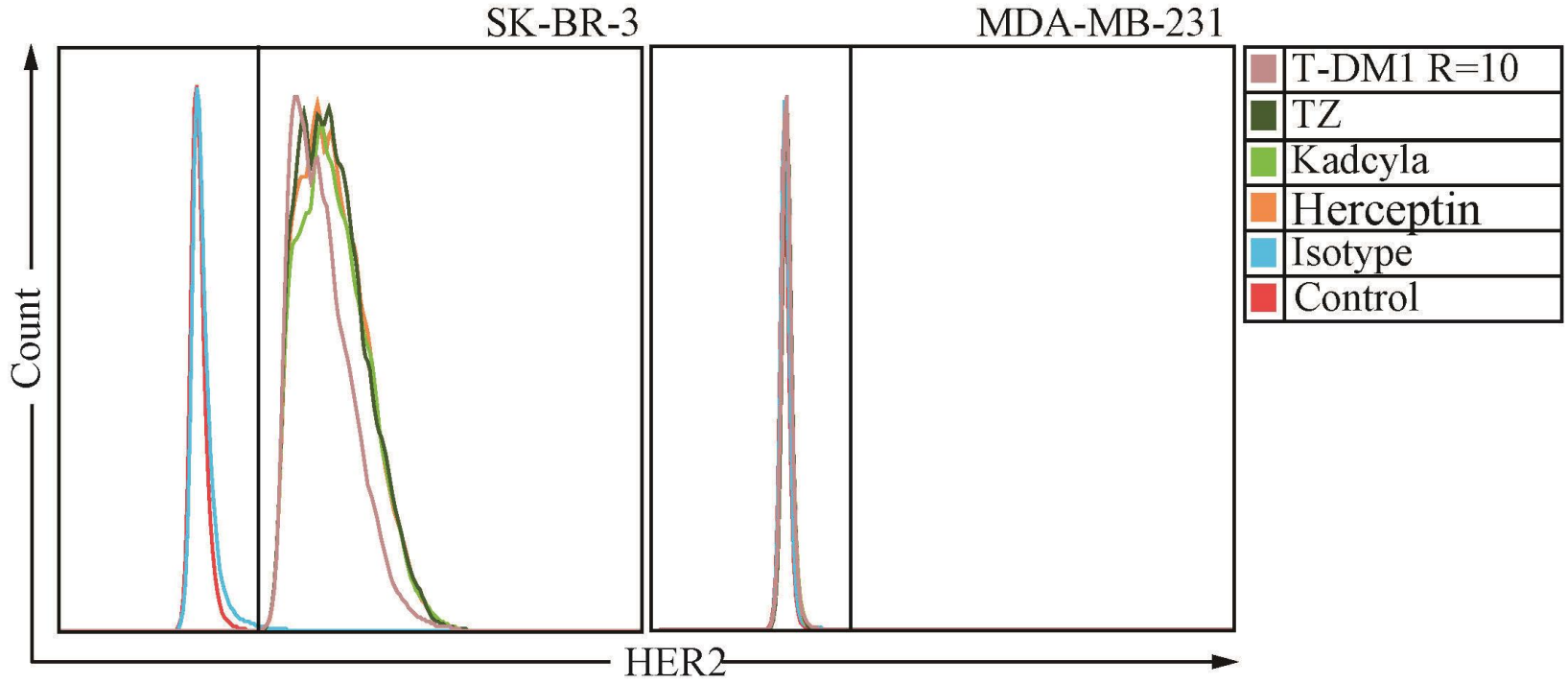

Figure 3.9. Antigen-specific binding of TZ and T-DM1. Antibody binding activities of TZ, T-DM1 R=10, Herceptin®, and Kadcyla® were compared in Her2-positive SK-BR-3 cells or Her2-negative MDA-MB-231 cells. Labeled cells were analyzed by flow cytometry.

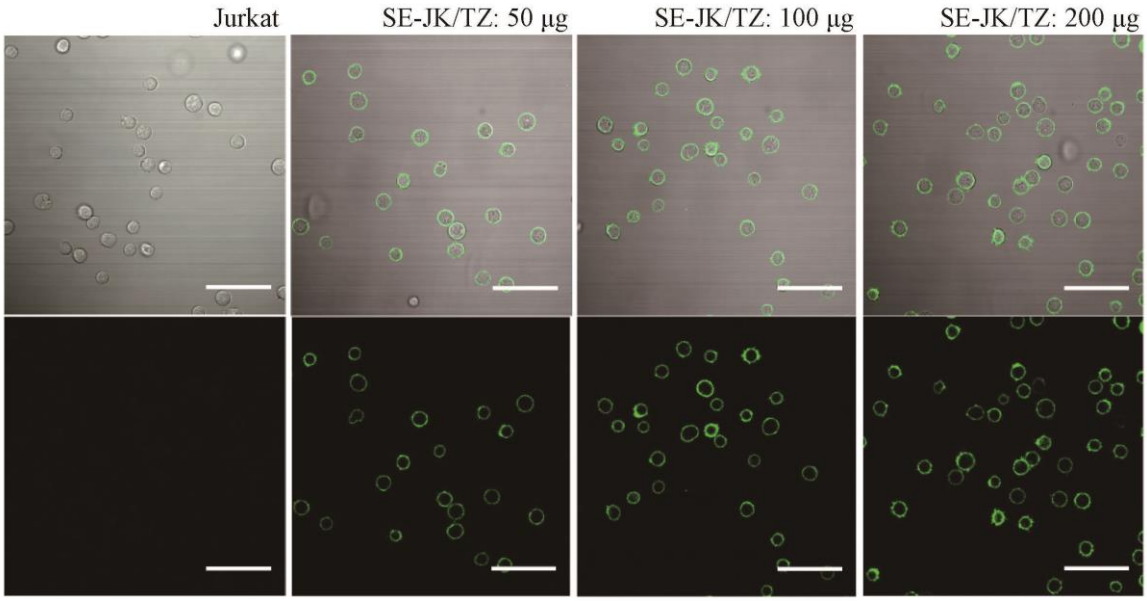

Figure 3.10. Confocal images of SE-JK/TZ cells. Jurkat cells, 5×10^5 cells, were modified with 50, 100 or 200 µg of DMPE-TZ-FITC. Scale bars, 50 µm.

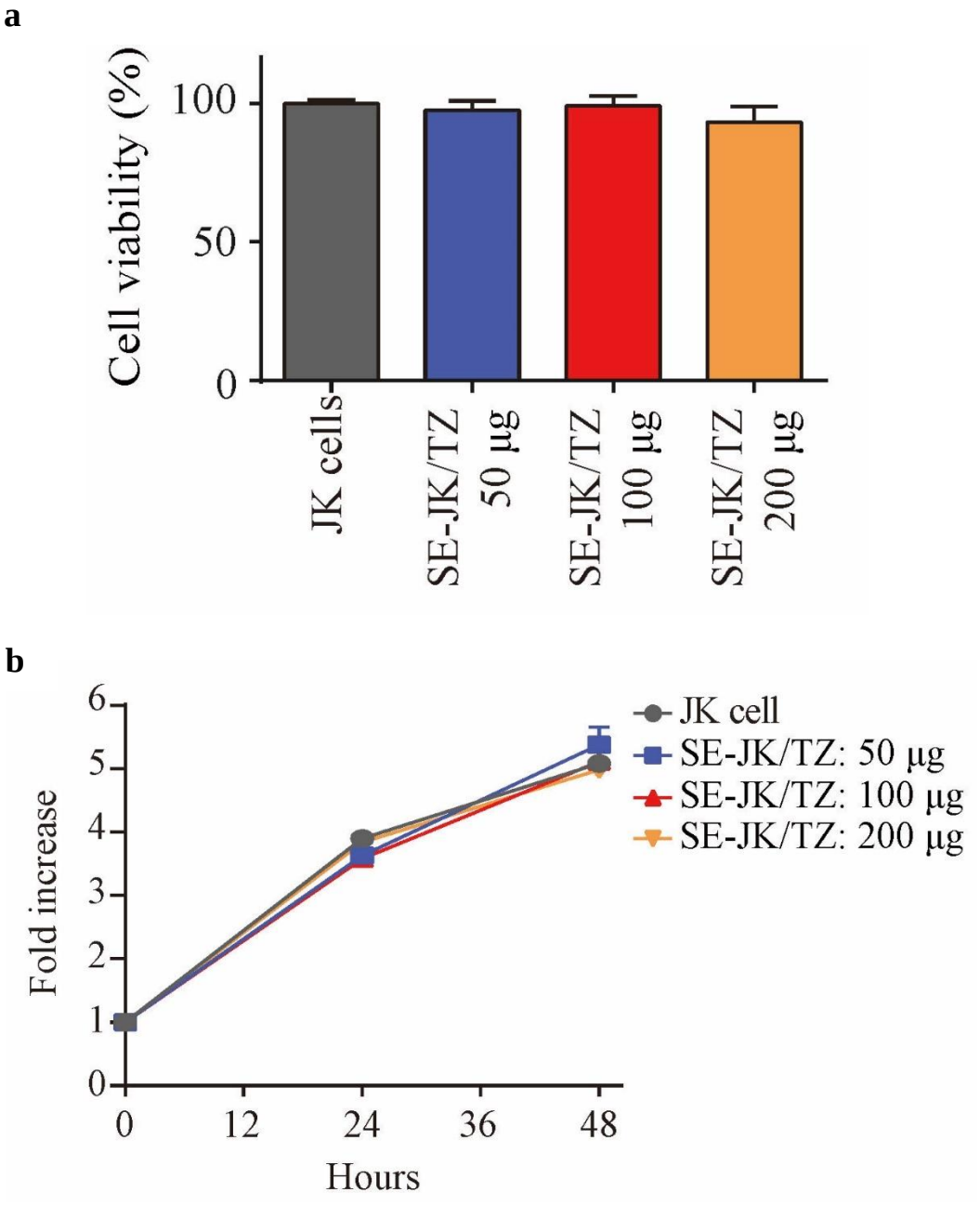

Figure 3.11. Cell viability (a) and cell proliferation (b) of SE-JK/TZ cells compared to unmodified Jurkat cells. Data presented as mean ± SD.

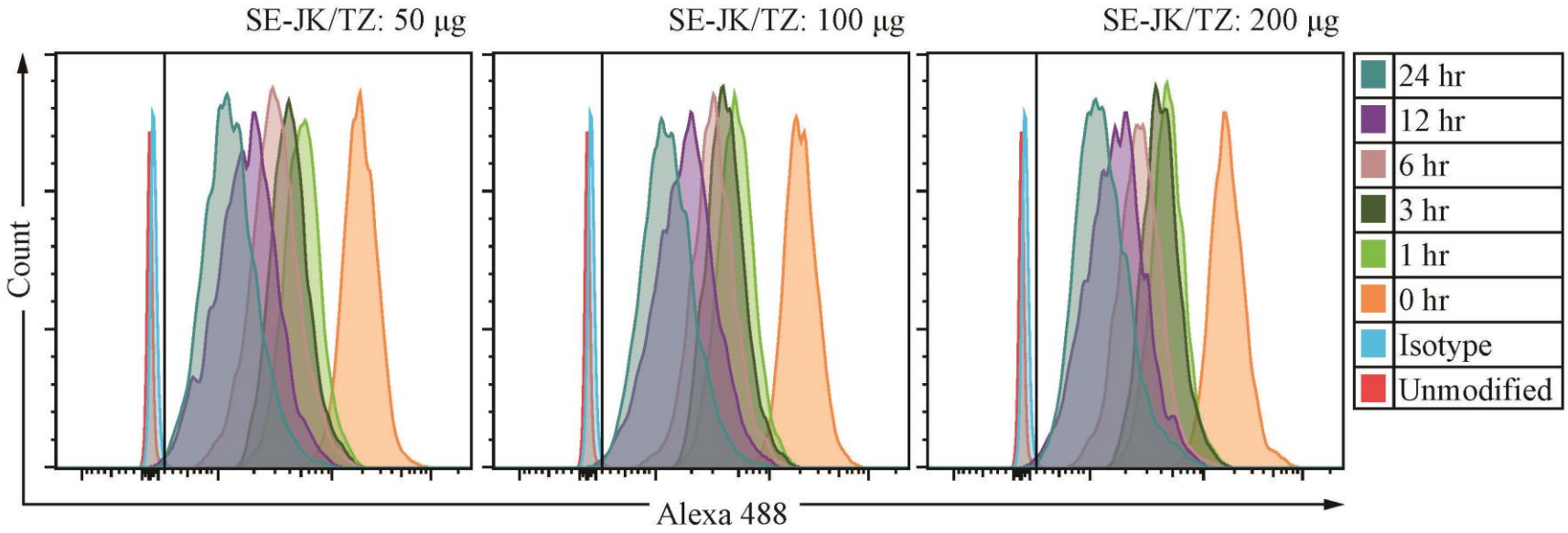

Figure 3.12. Retention time of TZ on the surface of SE-JK/TZ cells in the presence of 10% serum. SE-JK/TZ cells, 1×10^5 cells, were collected at each time point and mixed with FITC-labeled goat anti-human antibodies. Fluorescent intensity was measured by flow cytometry. Plots were selected from two representative experiments.

challenge, this result suggests that the modified cells may circulate in the body long enough to bind to the target tumor tissues. The optimal amount of DMPE-TZ required for reliable modification of 5×10^5 cells was determined to be 100 μg. Jurkat cells and NK92 cells were further modified with DMPE-T-DM1 to generate the SE-JK/T-DM1 cells and SE-NK/T-DM1 cells, respectively (Figure 3.13). Despite the fact that T-DM1 may lead to NK92 cell death, the surface engineering with DMPE-T-DM1 had no influence on the NK92 cell viability and proliferation (Figure 3.14a, b). Unlike other subtypes of NK cells, NK92 cells lack CD16, CD32 and CD64 IgG receptors that can initiate antibody internalization and antibody-dependent cellular cytotoxicity (ADCC).[37] This characteristic receptor expression protects NK92 cells from the membrane-embedded ADCs. Retention time of T-DM1 on the SE-NK/T-DM1 cells was tested beyond 24 hours (Figure 3.15). This result confirms that TZ or T-DM1 could reside on the cell surface for 48 hours. Surface engineering of Jurkat cells or NK92 cells with TZ or T-DM1 was well-tolerated because the TZ or T-DM1, embedded in the cell membrane through the lipid-PEG, did not internalize into the cells.[38]

NK cell-specific receptors should still be available following the surface modification. NK92 cells express a broad spectrum of activating receptors, including NKp30, NKp46, 2B4, NKG2D, NKG2E, and CD56.[39] We observed the availability of two NK cell markers, CD56 and 2B4, on the surface of the SE-NK/T-DM1 cells because those receptors are necessary for cytolytic activity, cell adhesion, and NK92 cell activation.[39] CD56 and 2B4 were available on the SE-NK/T-DM1 cells (Figure 3.16), indicating that the surface engineering of NK92 cells did not interfere with the receptor accessibility and that the inherent cytolytic activity of NK92 cells was maintained in SE-NK/T-DM1 cells.

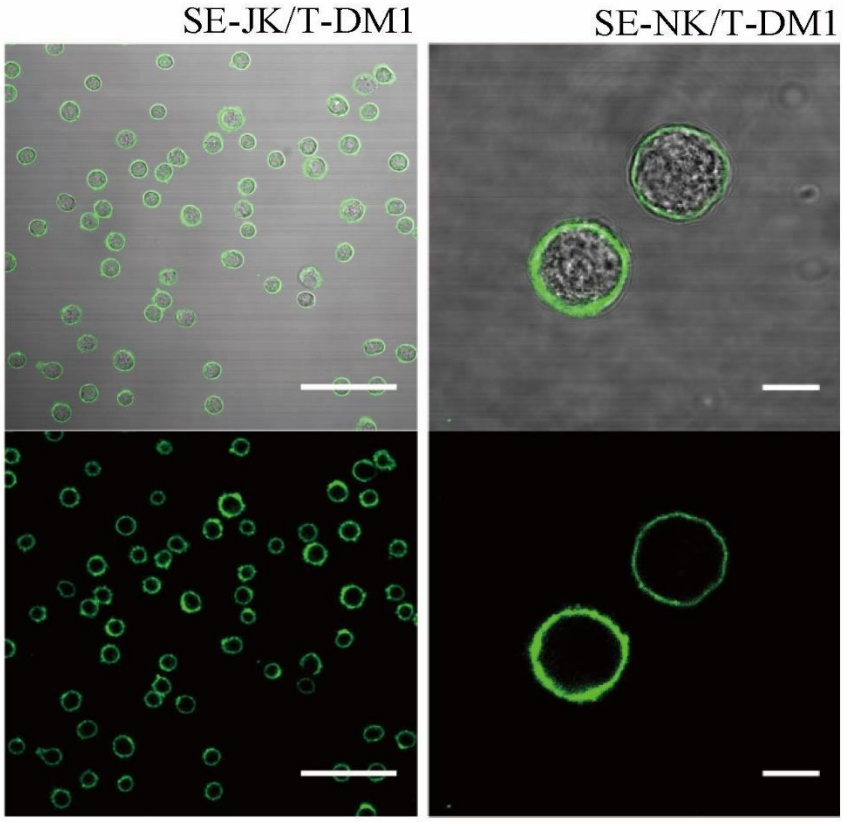

Figure 3.13. Confocal images of SE-JK/T-DM1 cells and SE-NK/T-DM1 cells. NK92 cells or Jurkat cells were modified with 100 μg of DMPE-T-DM1-FITC. Immediately after the washing, cells suspended in HBSS were observed under confocal microscope. Scale bars, 50 μm for the SE-JK/T-DM1 cells and 10 μm for the SE-NK/T-DM1 cells.

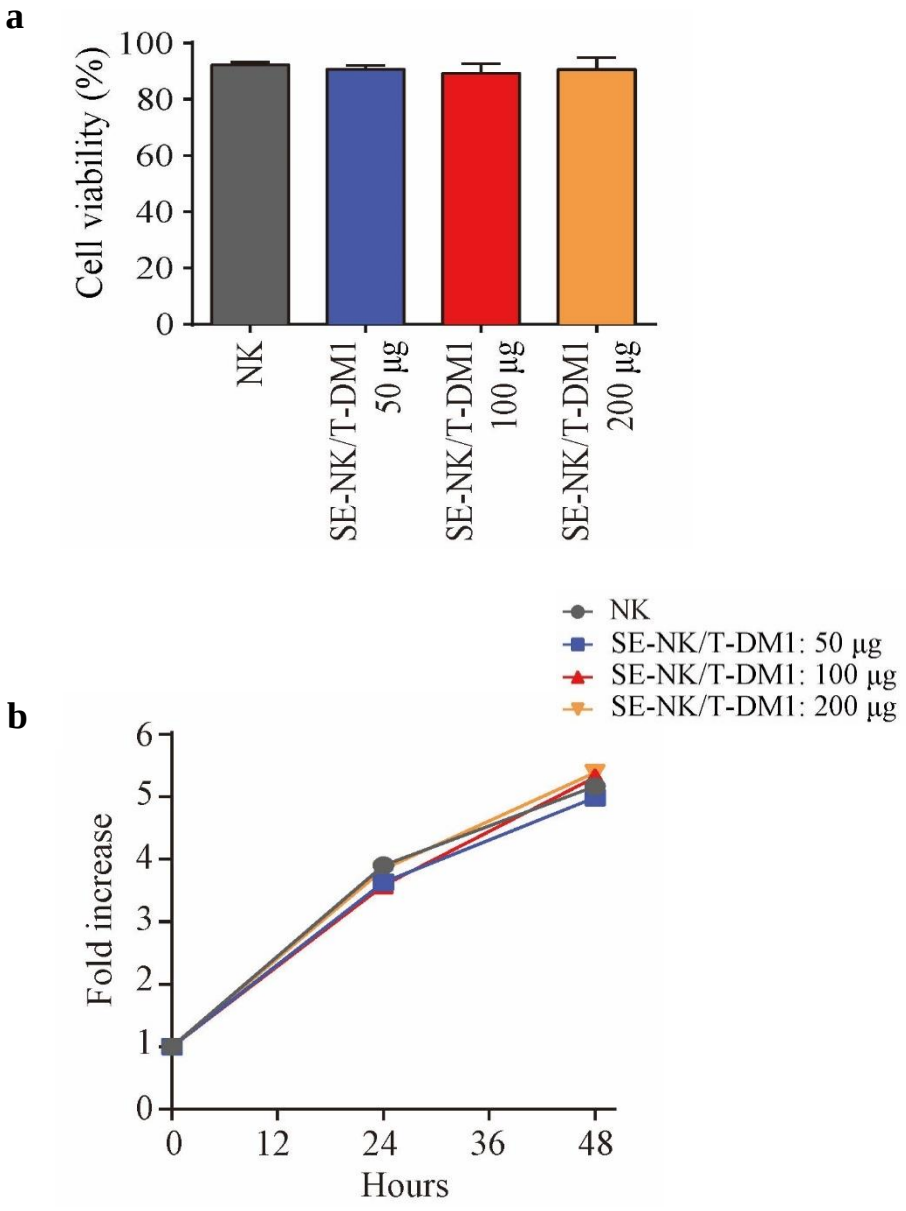

Figure 3.14. Influence of surface modification with T-DM1 on NK92 cell viability and proliferation. (a) Cell viabilities of the SE-NK/T-DM1 cells and unmodified NK92 cells. Data represent mean ± SD. (b) Proliferation of the SE-NK/T-DM1 cells and unmodified NK92 cells. The SE-NK/T-DM1 cells were generated with 50 µg, 100 µg, or 200 µg of DMPE-PEG-T-DM1 and compared to unmodified NK92 cells. Data presented as mean ± SD.

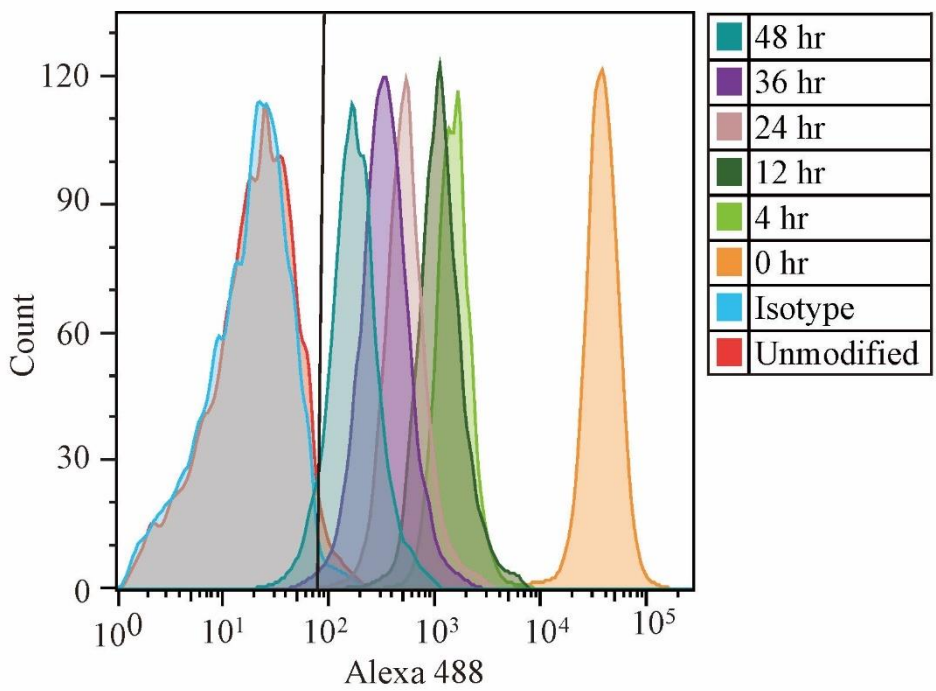

Figure 3.15. Retention time of T-DM1 on the surface of SE-NK/T-DM1 cells. The SE-NK/T-DM1 cells were incubated in the presence of 10% serum. At each time point, 1×10^5 SE-NK/T-DM1 cells were collected and mixed with FITC-labeled goat anti-human (H+L) antibodies for flow cytometry. Plot was selected from two independent experiments.

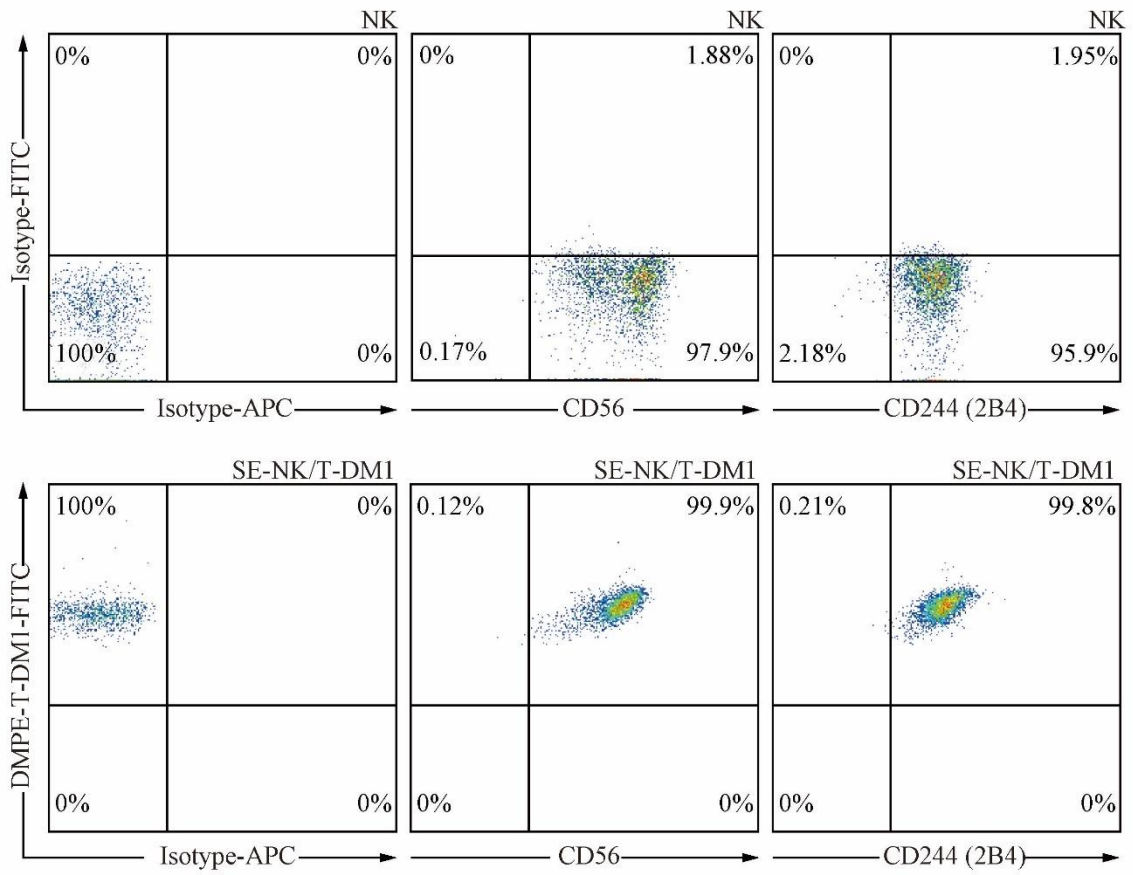

Figure 3.16. Expression of NK92 cell receptors. The availability of CD56 and 2B4 on the cell membrane of SE-NK/T-DM1 cells prepared with 100 μg of DMPE-T-DM1-FITC was determined by flow cytometry. Plots were selected from two independent experiments.

3.4.4. Selective Binding and Transfer of TZ and T-DM1

To demonstrate the specific binding of modified immune cells to Her2-positive cancer, the SE-JK/TZ cells or unmodified Jurkat cells were co-incubated with Her2-positive SK-BR-3 cells or Her2-negative MDA-MB-231 cells at E:T ratio of 5:1 for 2 hours and thoroughly washed to remove unbound Jurkat cells. The ratio of remaining SE-JK/TZ cells to SK-BR-3 cells was significantly higher than that of unmodified Jurkat cells after the washing. No difference was observed between the SE-JK/TZ cells and unmodified Jurkat cells in MDA-MB-231 cells (Figure 3.17a). To expand on this finding, we determined the amount of remaining NK92 cells after co-incubation of SK-BR-3 cells with unmodified NK92 cells, T-DM1+NK92 cells, or SE-NK/T-DM1 cells at E:T ratio 10:1. The remaining E:T ratios of SE-NK/T-DM1 cells, T-DM1+NK92 cells, and unmodified NK92 cells after the removal of unbound cells were approximately 3.8, 0.5, and 0.3, respectively (Figure 3.17b). When the SE-NK/T-DM1 cells were treated at E:T ratio of 5:1, the remaining E:T ratio of SE-NK/T-DM1 cell to SK-BR-3 cells was 1.4. Consistently, negligible numbers of NK92 cells remained bound on Her2-negative MDA-MB-231 cells. These results confirm the specific binding capability of the surface-engineered immune effector cells—modified with TZ or T-DM1—to the target cancer cells.

T-DM1 should transfer from the SE-NK/T-DM1 cells to the target cells in order to exert its anti-cancer activity on cancer cells. The SE-JK/TZ-FITC cells, SE-NK/TZ-FITC cells, SE-NK/T-DM1-FITC cells, unmodified Jurkat cells, or unmodified NK92 cells were co-incubated with SK-BR-3 cells or MDA-MB-231 cells; the transfer of TZ-FITC or T-DM1-FITC was observed by confocal microscopy. Upon the specific binding of

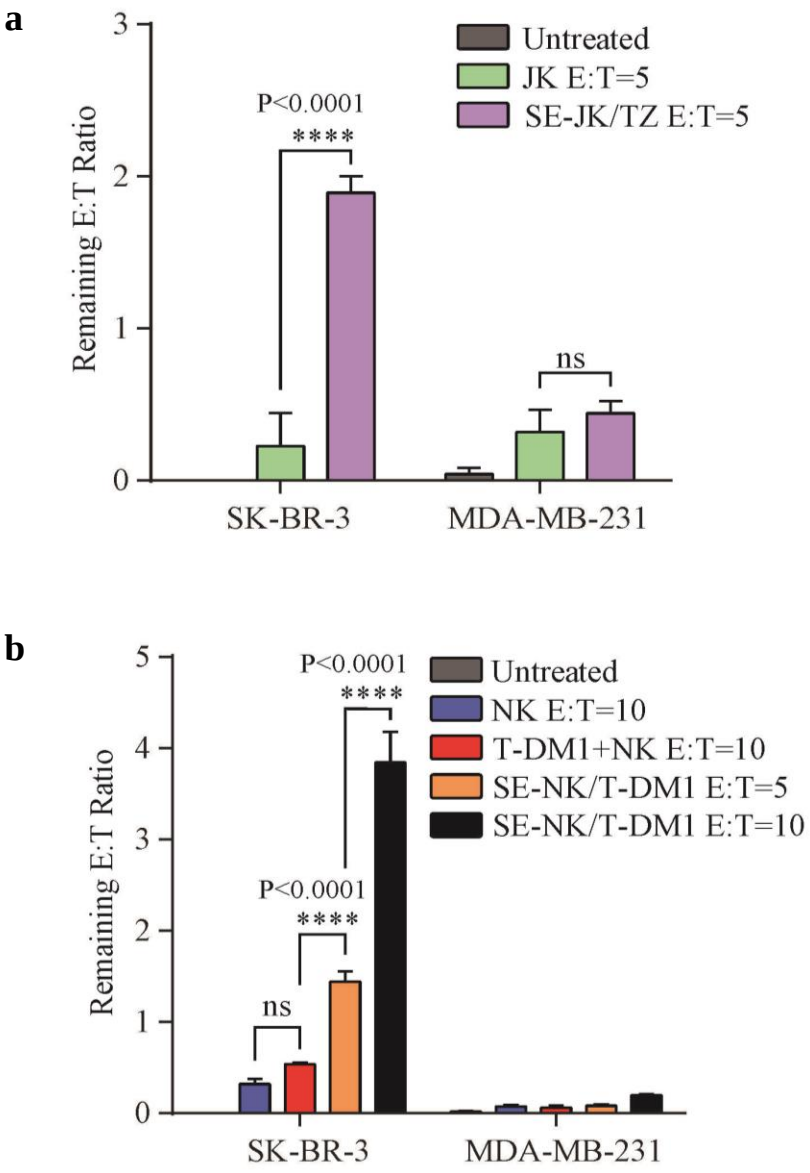

Figure 3.17. TZ and T-DM1 on the surface of SE-JK/TZ cells and SE-NK/T-DM1 cells, respectively, increased the number of cancer-bound Jurkat and NK92 cells. (a) Remaining E:T ratio of cancer-bound Jurkat cells. Higher number of SE-JK/TZ cells remained bound to SK-BR-3 cells. (b) Remaining E:T ratio of cancer-bound NK92 cells. The number of cancer cells-bound NK92 cells was increased when the SE-NK/T-DM1 cells were co-incubated with SK-BR-3 cells. Binding of surface-engineered immune cells to MDA-MB-231 cells was not observed in either study. After the removal of unbound effector cells, the remaining Jurkat cells and NK-92 cells were counted per 1×10^4 cancer cells by flow cytometry. Data presented as mean ± SD (ns, no significant; ****P<0.0001, by two-way ANOVA with Bonferroni post-hoc tests).

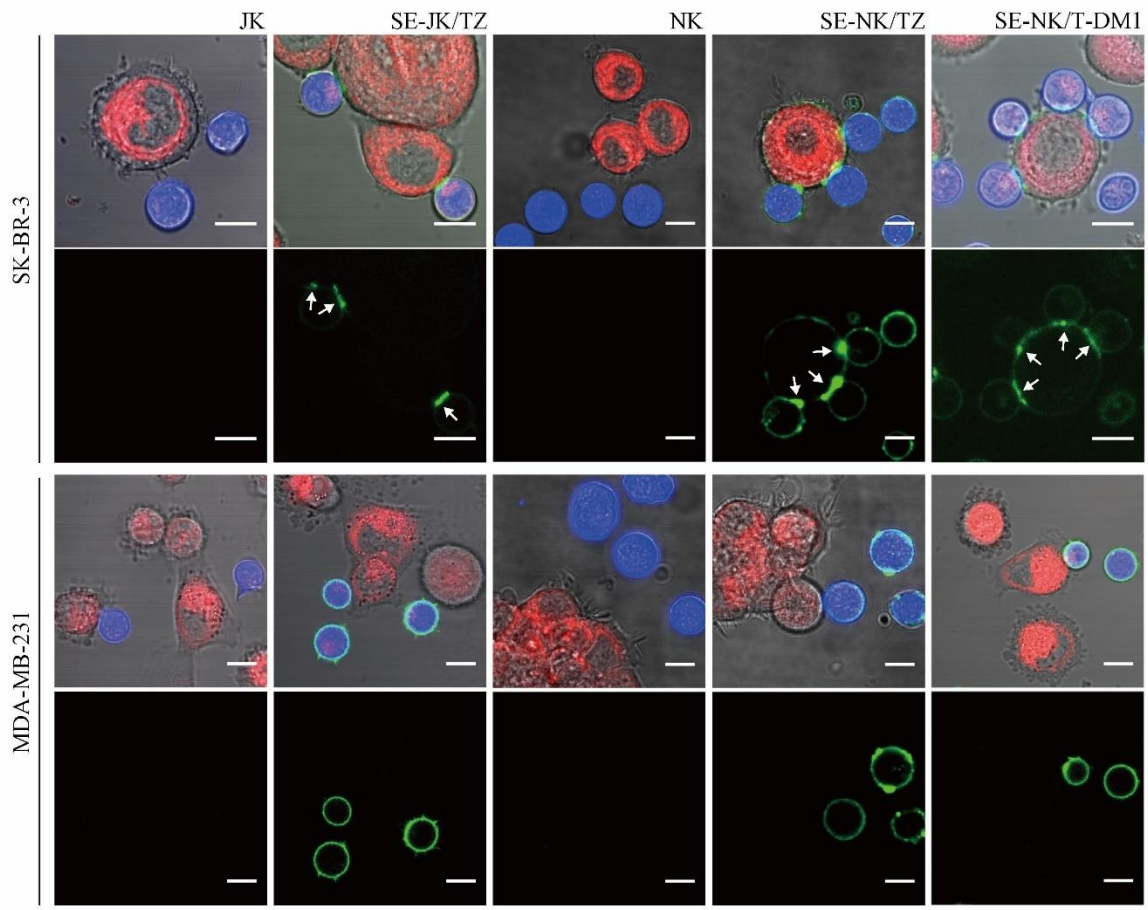

Figure 3.18. Confocal images showing the binding of SE-JK/TZ-FITC cells, SE-NK/TZ-FITC cells, or SE-NK/T-DM1-FITC cells to SK-BR-3 cells or MDA-MB-231 cells. CMTPX-labeled cancer cells (red) were co-incubated with CMAC-labeled effector cells (blue). These fluorescently labeled cells were co-incubated at E:T ratio of 10:1. Unbound effector cells were washed after 30 minutes of co-incubation and the cells were observed under confocal microscopy. Localization of TZ (green) and T-DM1 (green) at the effector cell-to-cancer cell junction is indicated with white arrows. Scale bars, 10 μm. All images are representative of two independent experiments.

surface-engineered immune cells to the target cancer cells (Figure 3.18), TZ and T-DM1 migrated toward the contact area, formed clusters at the effector cell-to-cancer cell junction (Figure 3.18, white arrows), and subsequently transferred to the target cancer cells. This observation suggests the lipid raft involvement of DMPE-TZ and DMPE-T-DM1 anchored on the cell membrane.[40] In contrast, these events did not occur with MDA-MB-231 cells (Figure 3.18). These results reveal that the SE-NK/T-DM1 cells or SE-NK/TZ cells are able to specifically recognize and bind to Her2-positive cancer cells; thereafter, T-DM1 embedded on the surface of NK92 cells can relocate onto the cancer cell membrane.

Internalization of T-DM1, which may occur through receptor-mediated and clathrin-dependent endocytosis, is critical for the anti-cancer efficacy of T-DM1 because DM1 acts on intracellular targets in cancer cells.[23,41] With the knowledge of previously reported observations on cellular uptake of T-DM1, trafficking of T-DM1 to lysosomes, and release of DM1,[42] we have focused on confirming the internalization of T-DM1 that has been transferred from the SE-NK/T-DM1 cells. Distinct fluorescent dots representing the internalized T-DM1 following the transfer from the SE-NK/T-DM1 cells were detected in the cytoplasm (Figure 3.19). To confirm that the fluorescence intensity represents T-DM1, cancer cells—used as a positive control—were co-treated with T-DM1 and geldanamycin (GA), the latter of which is a Hsp90 inhibitor that induces rapid internalization of TZ bound to Her2.[43] The T-DM1 internalization was facilitated in the presence of GA in SK-BR-3 cells as expected (Figure 3.19). Although the fluorescent intensity was low, we confirmed that the fluorescence pattern of T-DM1 observed in the cytosol of cancer cells upon the transfer from the SE-NK/T-DM1 cells was similar to the internalized T-DM1 induced by the addition of GA. No fluorescent activity was observed with MDA-MB-231 cells treated

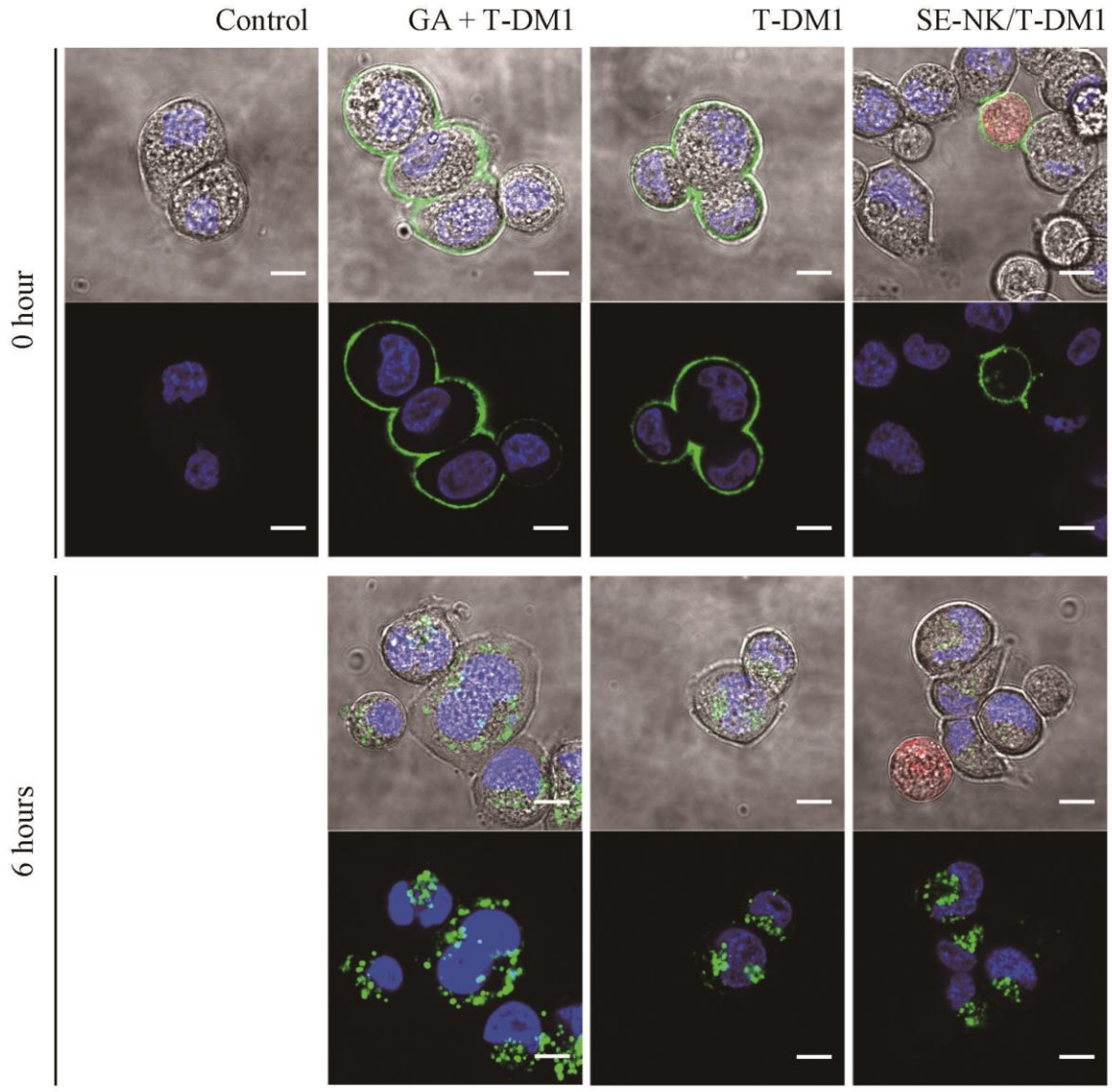

Figure 3.19. Internalization of transferred T-DM1 into Her2-positive SK-BR-3 cells. Cancer cells were labeled with Nucblue® nuclear stain (blue) and NK92 cells were labeled with CMTPX (red). Cancer cells were treated with 5 μg of T-DM1-FITC or SE-NK/T-DM1-FITC cells at E:T ratio of 10:1. Unbound effector cells were removed after 30 minutes of incubation. As a positive control, GA was added at a final concentration of 3 μM. Cells were imaged immediately after removing unbound cells and after 6 hours of incubation by confocal microscopy. Scale bars, 10 μm. All images are representative of two independent experiments.

with the identical conditions used in SK-BR-3 cells (Figure 3.20), confirming the insignificant anti-cancer activity of SE-NK/TZ cells and SE-NK/T-DM1 cells against Her2-negative cancer cells.

3.4.5. Anti-Cancer Activity of SE-NK/T-DM1 Cells

To demonstrate the therapeutic benefits of SE-NK/T-DM1 cells over the co-treatment of NK92 cells with T-DM1 (T-DM1+NK92 cells), we compared the anti-cancer activity of SE-NK/T-DM1 cells to that of T-DM1+NK92 cells. For accurate comparison, we first quantified the amount of T-DM1 on the membrane of surface-engineered cells. The SE-JK/T-DM1 cells or SE-NK/T-DM1 cells were fractionated by differential lysis, and the amount of T-DM1 in the cell membrane fraction was measured (Figure 3.21a, b). Preparation of 1×10^5 SE-NK/T-DM1 cells with 50 μg, 100 μg, 200 μg of DMEP-T-DM1 contained approximately 1.2 μg, 2.1 μg, or 3.3 μg of T-DM1, respectively, on the membrane (Figure 3.21a). Identical numbers of SE-JK/T-DM1 cells modified with 50 μg, 100 μg, or 200 μg of DMEP-T-DM1 contained approximately 1.0 μg, 1.6 μg, or 2.2 μg of T-DM1, respectively, on the membrane (Figure 3.21b). In the subsequent experiments, the amount of TZ or T-DM1 for the co-treatment groups was determined to be 2.1 μg per 1×10^5 surface-engineered effector cells, which is equivalent to the amount of T-DM1 contained on the surface of 1×10^5 SE-NK/T-DM1 cells prepared by 100 μg of DMPE-T-DM1. To confirm if the SE-NK/T-DM1 cells and T-DM1+NK92 cells induce the same levels of cancer cell death, cancer cells were continuously exposed to each formulation for 24 hours. Both SE-NK/T-DM1 cells and T-DM1+NK92 cells exhibited similar levels of anti-cancer activity (Figure 3.22a),

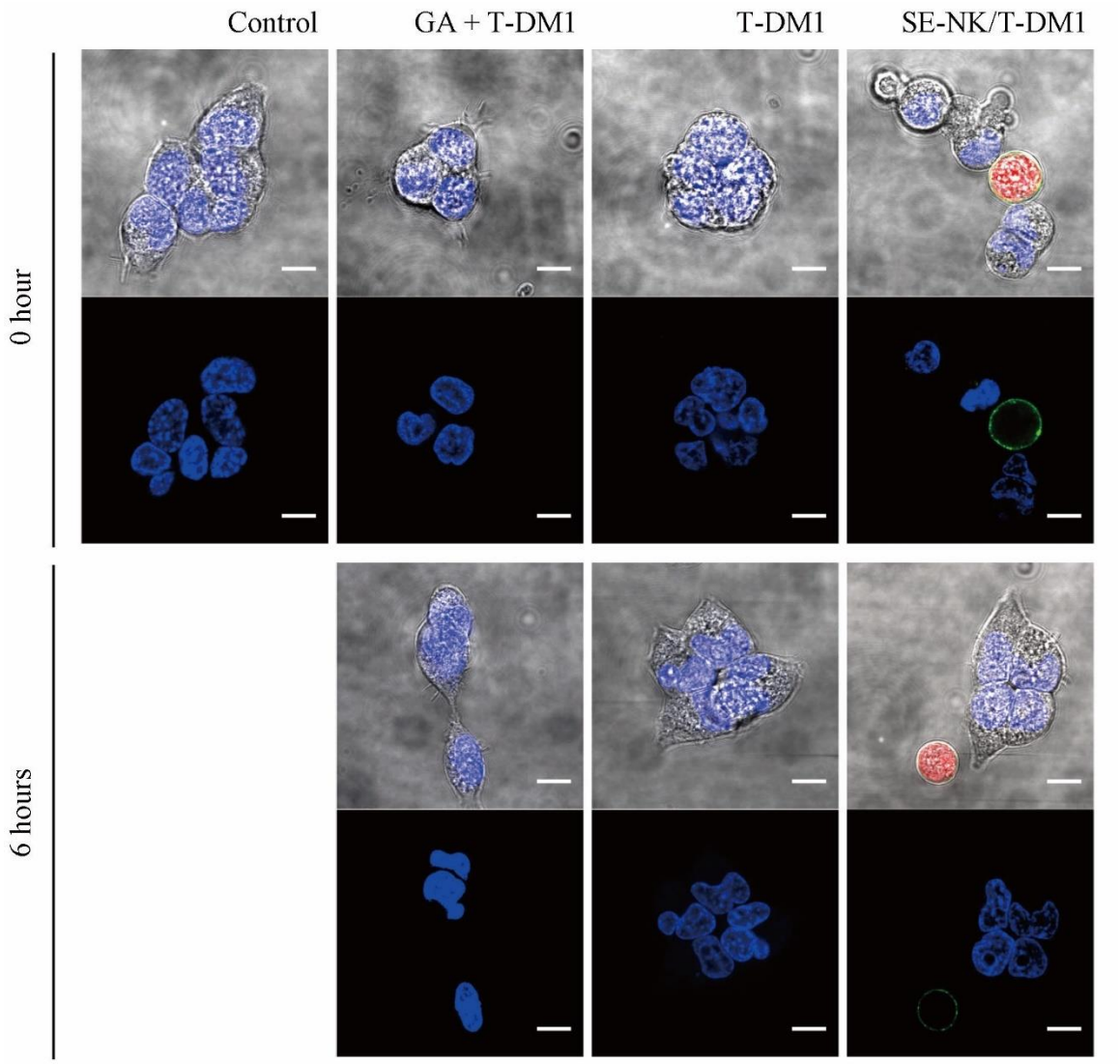

Figure 3.20. Internalization of transferred T-DM1 into Her2-negative MDA-Mb-231 cells. Cancer cells were labeled with Nucblue® nuclear stain (blue) and NK cells were labeled with CMTPX (red). MDA-MB-231 cells were treated with 5 μg of T-DM1-FITC or SE-NK/T-DM1-FITC cells at E:T ratio of 10:1. Unbound effector cells were removed after 30 minutes of incubation. As a positive control, GA was added at a final concentration of 3 μM. Cells were imaged immediately after removing unbound cells and after 6 hours of incubation by confocal microscopy. No intracellular uptake of T-DM1 was observed. Scale bars, 10 μm. All images are representative of two independent experiments.

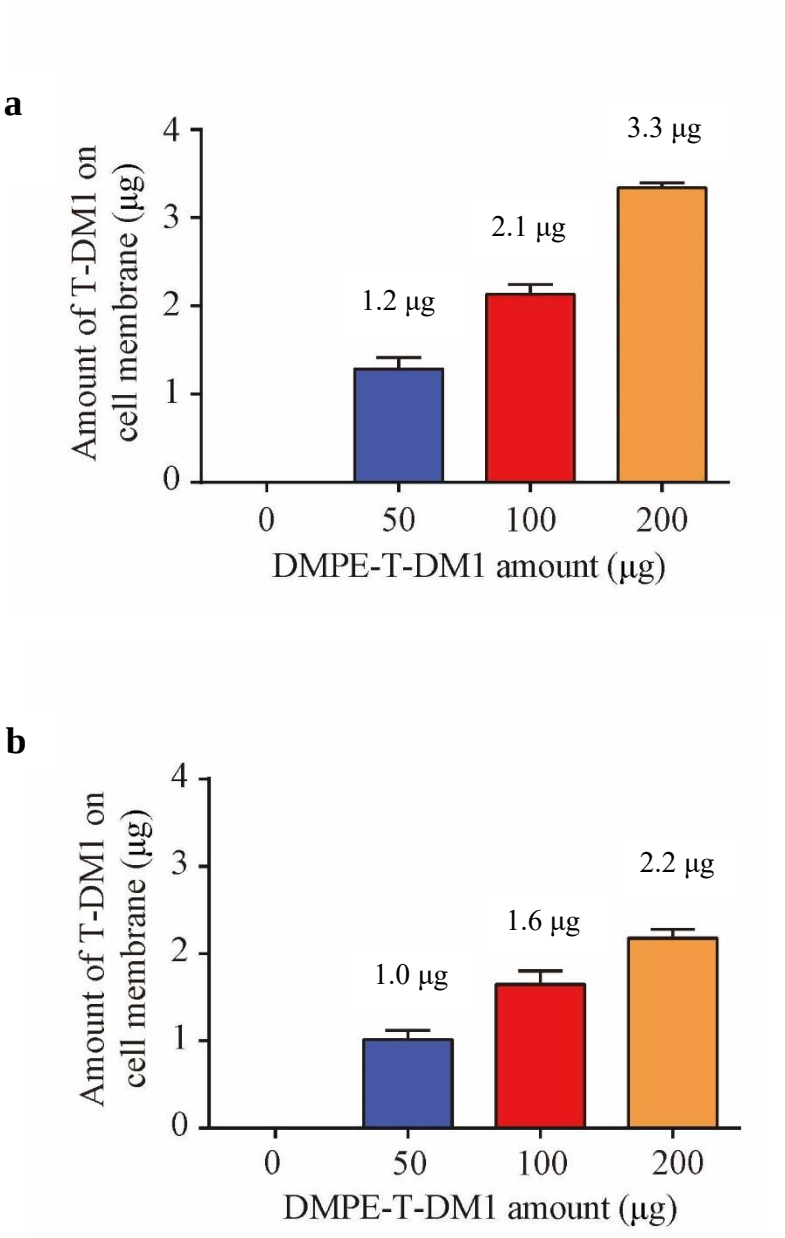

Figure 3.21. Amounts of T-DM1 embedded on the cell membrane. The SE-NK/T-DM1 cells or SE-JK/T-DM1 cells were generated with 50, 100, and 200 μg of DMPE-T-DM1. The membrane faction of cell lysate was collected by the differential lysis of SE-NK/T-DM1 cells or SE-JK/T-DM1 cells (1×10^5 cells). The amount of T-DM1 in the cell membrane fraction of (a) SE-NK/T-DM1 cells or (b) SE-JK/T-DM1 cells was quantified by a human IgG ELISA. Number represents the average amount of T-DM1 on the surface. Data presented as mean ± SD.

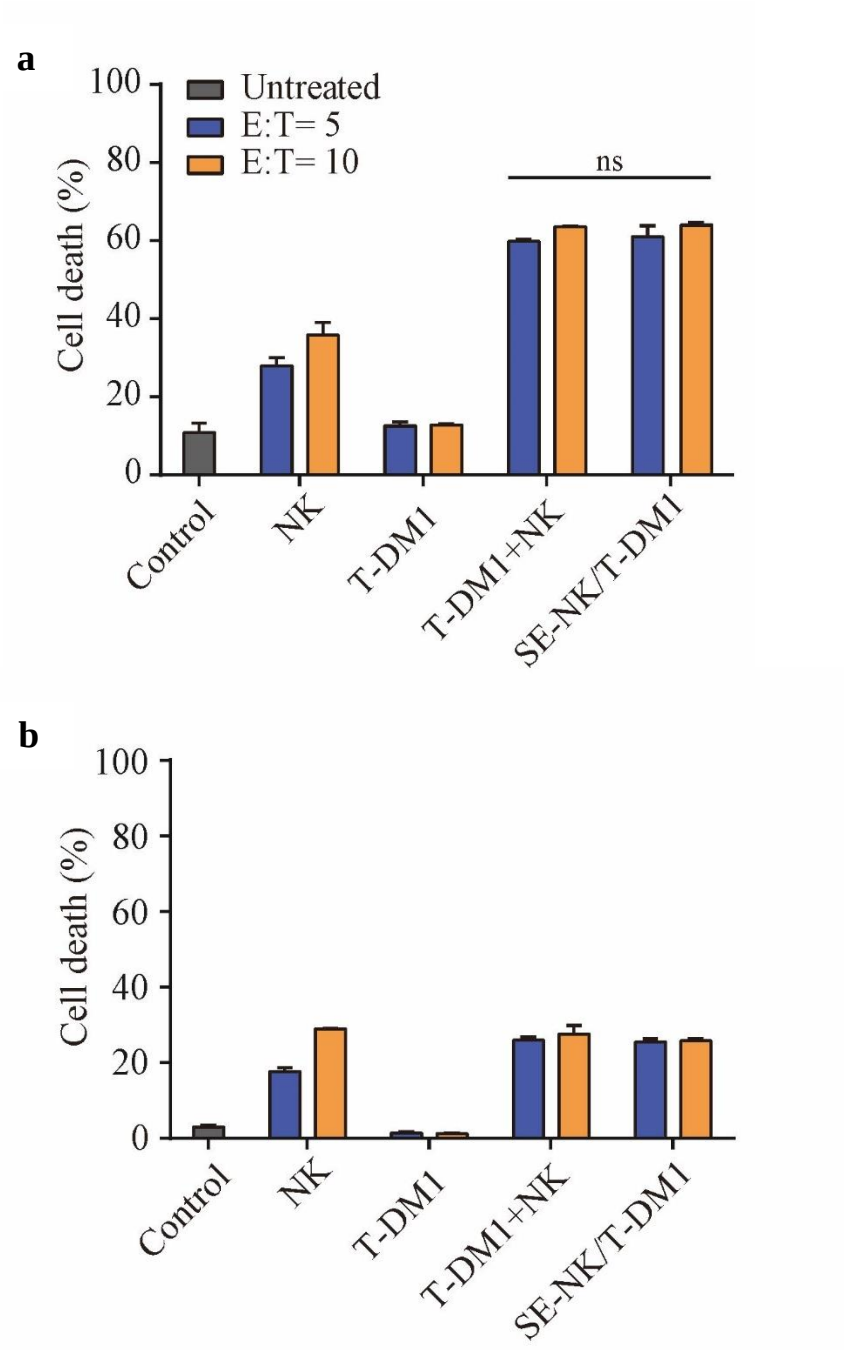

Figure 3.22. Long-term incubation of SE-NK/T-DM1 cells with (a) Her2-positive SK-BR-3 cells or (b) Her2-negative MDA-MB-231 cells. Cancer cells labeled with CMAC were co-incubated with SE-NK/T-DM1 cells, NK92 cells, T-DM1, or T-DM1+NK92 cells at E:T ratio of 5:1 or 10:1. After 24 hours, all cells were collected and Annexin V/PI assays were performed using flow cytometry. Data presented as mean ± SD (ns, not significant, by two-way ANOVA with Bonferroni post-hoc tests).

indicating that there was no difference in the exposed amount ofT-DM1 between groups treated with the SE-NK/T-DM1 cells and those co-treated with T-DM1+NK92 cells. This observation also implied that continuous exposure to the T-DM1+NK92 cells treatment would allow enough time for NK92 cells to identify dying cancer cells affected by T-DM1 in a confined well system. In MDA-MB-231 cells, only the anti-cancer activity of NK92 cells was observed in both treatment groups (Figure 3.22b).

Second, cancer cells were incubated with the effector cells for 2 hours; subsequently, the unbound effector cells were thoroughly removed in order to mimic the *in vivo* cancer homing effect. The remaining cancer-bound effector cells were further incubated with the target cells for 24 hours, and the resulting cancer cell death was recorded. In SK-BR-3 cells, we found that the level of cancer cell death induced by the SE-NK/T-DM1 cells was higher than that induced by the NK92 cell and T-DM1+NK92 cells (Figure 3.23a). This is due to the fact that a higher number of SE-NK/T-DM1 cells remained bound to SK-BR-3 cells, resulting in an augmented anti-cancer activity. Again, no significant cell death was noticed in MDA-MB-231 cells (Figure 3.23b).

Third, we assessed the effect of chemotherapeutic agents on the surface-engineered effector cells on cancer cell viability. The effector cells and cancer cells were co-incubated for 6 hours, and the cancer cell viability was measured. Levels of cancer cell death induced by the SE-JK/TZ cells and SE-JK/T-DM1 cells were compared to identify the anti-cancer effect of DM1. As expected, T-DM1 exhibited a greater cytolytic effect against SK-BE-3 cells than TZ (Figure 3.24a). The resulting cancer cell death was due to the addition of DM1 and Jurkat cells—lacking cytolytic effects—and did not show supportive effects. The identical treatments used on SK-BR-3 cells showed no significant effects on

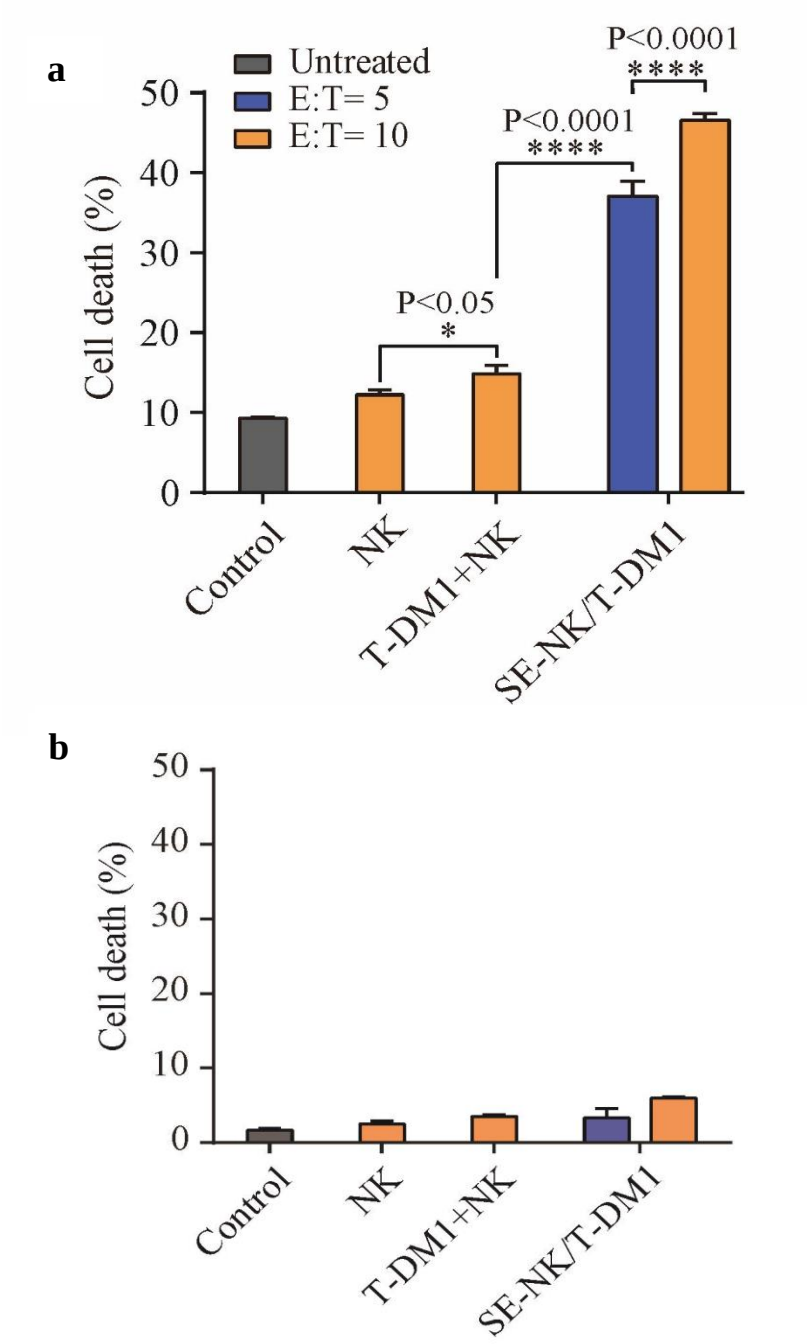

Figure 3.23. Short-term incubation of SE-NK/T-DM1 cells with (a) SK-BR-3 cells and (b) MDA-MB-231 cells demonstrated targeted anti-cancer activity. Cancer cells labeled with CMAC were co-incubated with SE-NK/T-DM1 cells, NK92 cells, or T-DM1+NK92 cells at E:T ratio of 5:1 or 10:1. Unbound cells were thoroughly removed 2 hours after the treatment and the remaining cell mixtures were incubated for additional 24 hours. The cancer cell death was measured by the Annexin V/PI kit and flow cytometry. Data presented as mean ± SD (**P*<0.05, *****P*<0.0001, by two-way ANOVA with Bonferroni post-hoc tests).

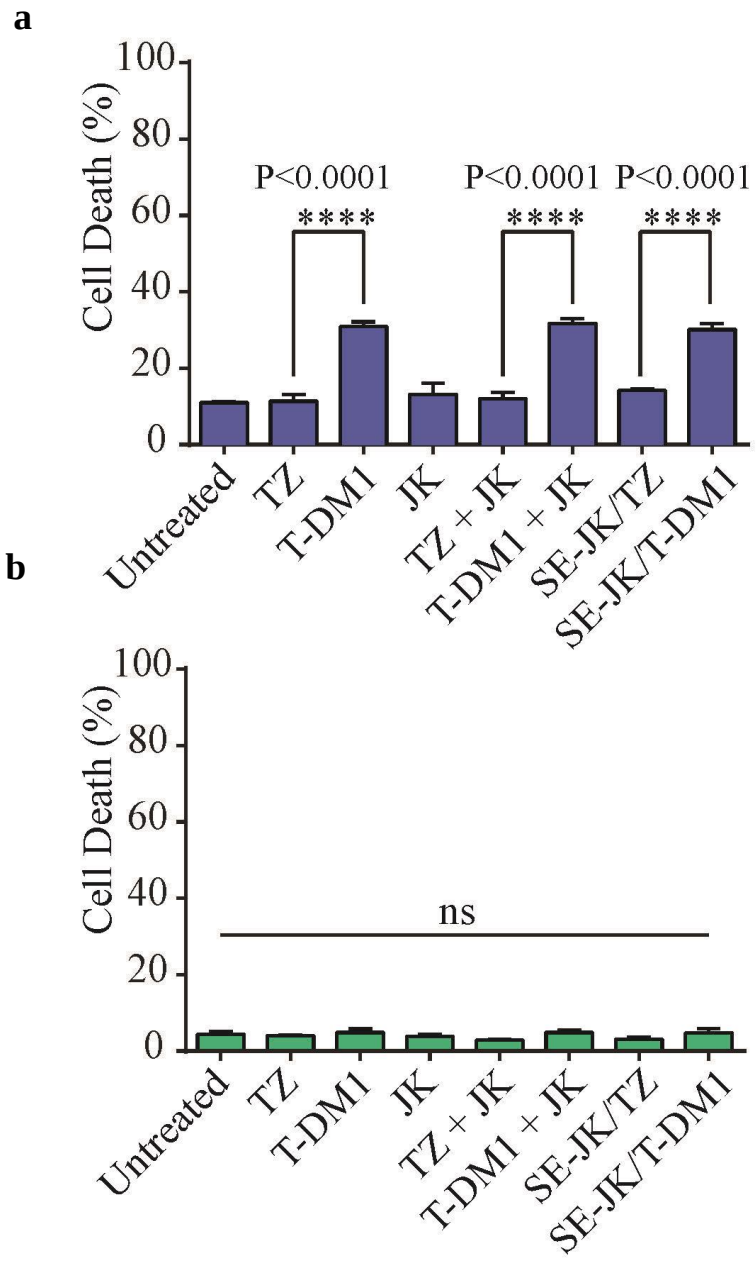

Figure 3.24. Effects of DM1 on cancer cell death. The targeted anti-cancer activity of T-DM1 was isolated by comparing the cancer cell death induced by the treatment of SE-JK/TZ cells and SE-NK/T-DM1 cells in (a) SK-BR-3 cells or (b) MDA-MB-231 cells. All effector cells were co-incubated with CMAC-labeled cancer cells at E:T ratio of 10:1 and the amount of TZ or T-DM1 co-treated with Jurkat cells was equivalent to the T-DM1 amount embedded on the SE-NK/T-DM1 cells as shown in Figure 3.20. All cells were collected after 6 hours of co-incubation. Cancer cell death was determined by the flow cytometry-based Annexin V/PI analysis. Data presented as mean ± SD (ns, not significant, ****P<0.0001, by one-way ANOVA followed by Tukey post-hoc tests).

MDA-MB-231 cells (Figure 3.24b). After changing the effector cells from Jurkat cells to NK92 cells, the SE-NK/TZ cells showed augmented cancer cell deaths in comparison to TZ alone, TZ+NK92 cells, and unmodified NK92 cells (Figure 3.25a). The treatments involving T-DM1 further enhanced the anti-cancer activity against Her2-positive cancer cells, and the SE-NK/T-DM1 cells exhibited a superior anti-cancer activity over all treatments (Figure 3.25a). We postulated that DM1 contained in T-DM1 had induced an increase of approximately 20% in the death of Her2-positive cancer cells. Except for the nonspecific cytolytic activity of NK92 cells, none of the treatments induced significant cytotoxicity in MDA-MB-231 cells (Figure 3.25b). It is thus acceptable to state that the anti-cancer activity of SE-NK/TZ cells or SE-NK/T-DM1 cells against MDA-MB-231 cells is confined to the innate cytolytic functions of NK92 cells with negligible effects from TZ or T-DM1.

Finally, we have identified the cytolytic activity of NK92 cells by comparing the SE-JK/TZ cells to SE-NK/TZ cells and the SE-JK/T-DM1 cells to SE-NK/T-DM1 cells. Unlike Jurkat cells, NK92 cells showed cytolytic activity in SK-BR-3 cells (Figure 3.26a). Comparing the TZ+Jurkat cells to TZ+NK92 cells, NK92 cells were observed to induce roughly 25% more cancer cell death. With surface engineering, the SE-NK/TZ cells showed approximately 47% higher cancer cell death than the SE-JK/TZ cells. In contrast, only the cytolytic activity of NK92 cells was observed when MDA-MB-231 cells (Figure 3.26b) were exposed to the same treatment stated in Figure 3.25a. Similarly, T-DM1+NK92 cells caused nearly 27% more cancer cell death compared to T-DM1+Jurkat cells (Figure 3.27a). The SE-NK/T-DM1 cells induced approximately 58% greater cancer cell death in SK-BR-3 cells compared to the SE-JK/T-DM1 cells.

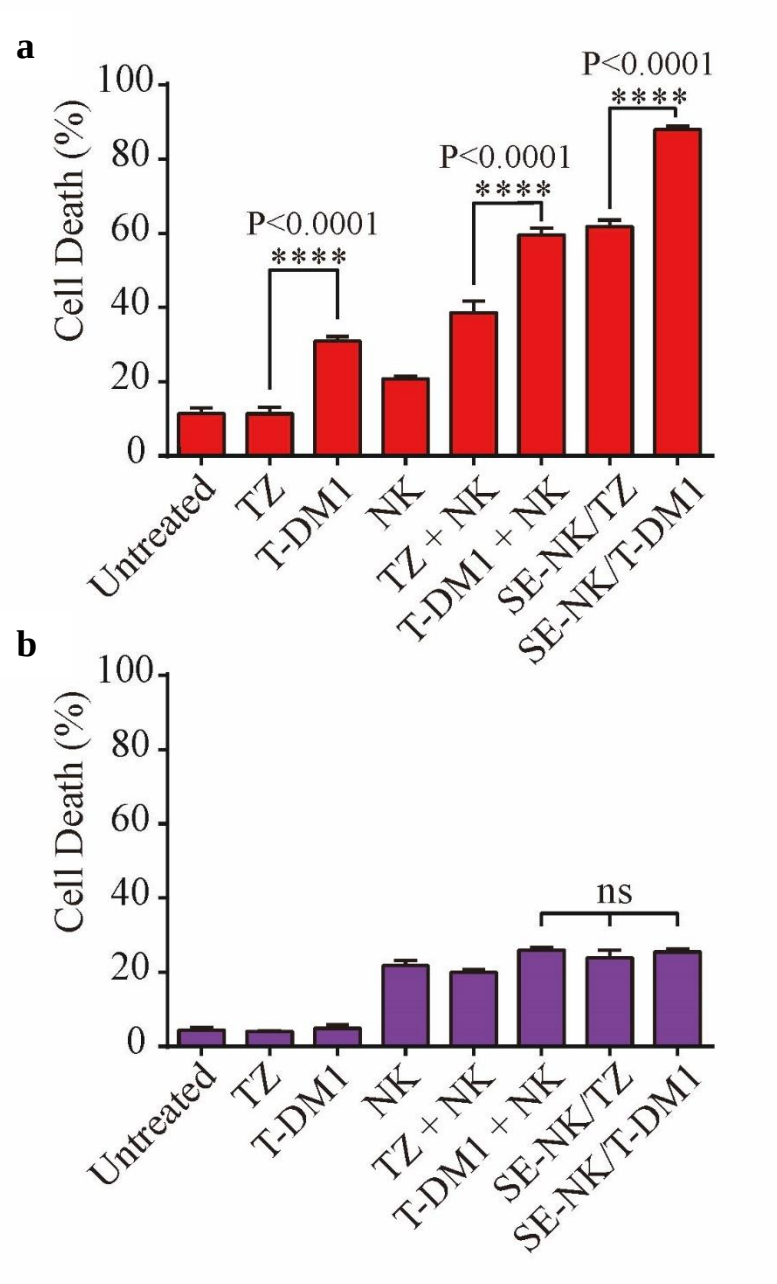

Figure 3.25. Anti-cancer activity of T-DM1 contained in the SE-NK/T-DM1 cells against (a) SK-BR-3 cells and (b) MDA-MB-231 cells. All effector cells were co-incubated with CMAC-labeled cancer cells at E:T ratio of 10:1. The amount of TZ or T-DM1 used for the co-treatment with NK92 cells was identical to the amount T-DM1 found in SE-NK/T-DM1 cells as shown in Figure 3.20. After 6 hours of incubation, all cells were collected and the cancer cell death was analyzed by the flow cytometry-based Annexin V/PI analysis. Data presented as mean ± SD (ns, not significant, ****P<0.0001, by one-way ANOVA followed by Tukey post-hoc tests).

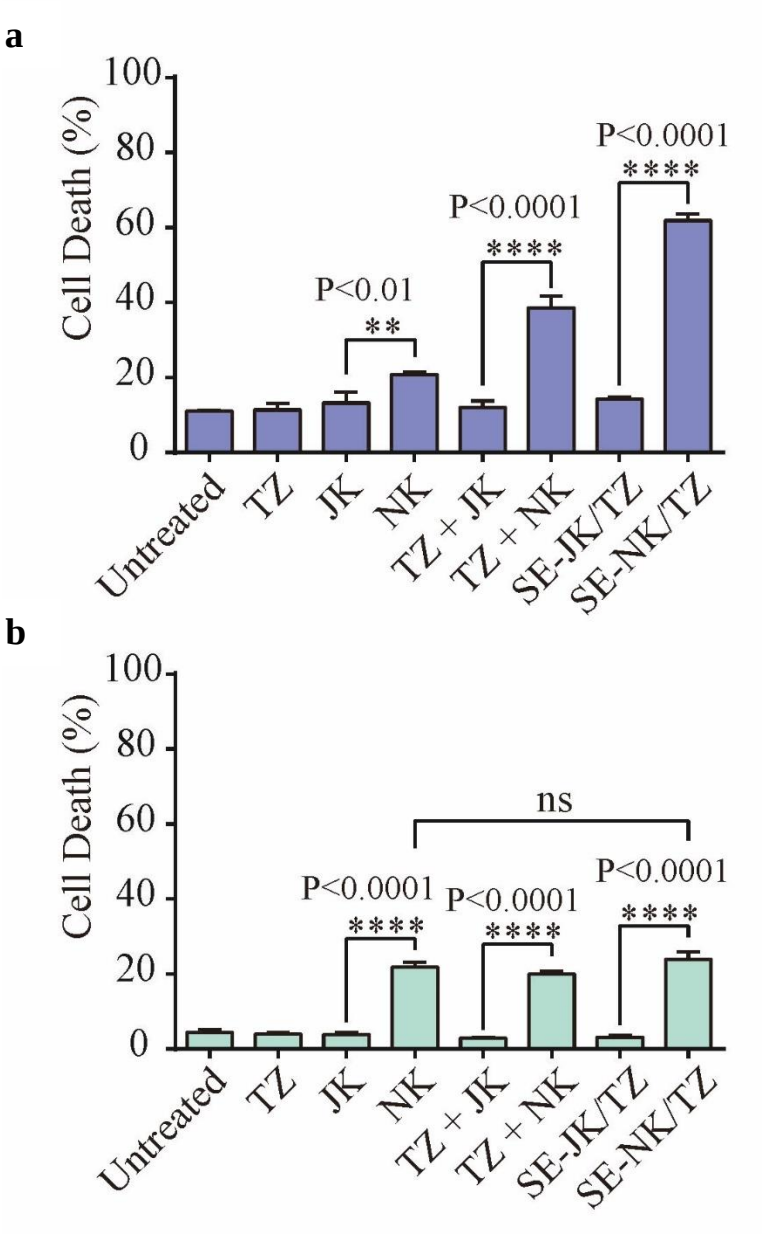

Figure 3.26. Cancer cell death induced by SE-NK/TZ cells and SE-JK/TZ cells in (a) SK-BR-3 cells and (b) MDA-MB-231 cells. All effector cells were co-incubated with CMAC-labeled cancer cells at E:T ratio of 10:1. The amount of TZ co-treated with Jurkat cells or NK92 cells was identical to the amount of T-DM1 found on the SE-NK/T-DM1 cells as shown in Figure 3.20. After 6 hours of incubation, all cells were collected and the cancer cell death was analyzed by the flow cytometry-based Annexin V/PI analysis. Data presented as mean ± SD (ns, not significant, $^{**}P<0.01$, $^{****}P<0.0001$, by one-way ANOVA followed by Tukey post-hoc tests).

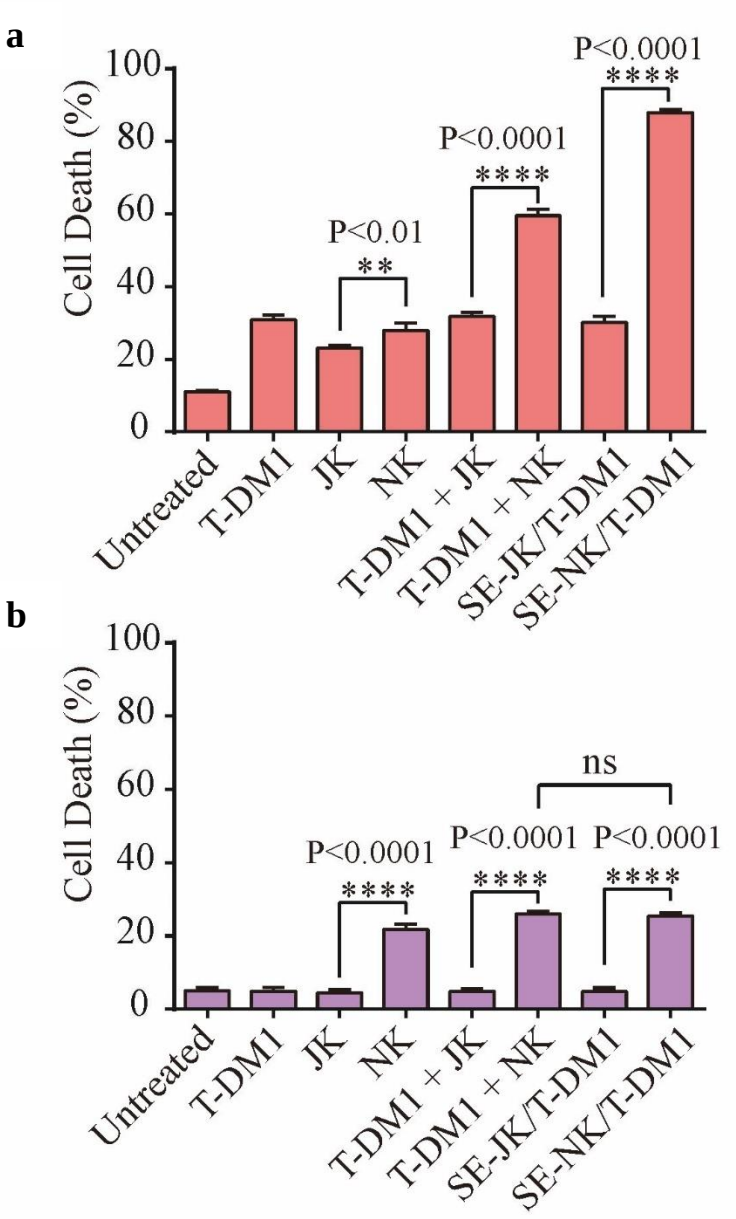

Figure 3.27. Anti-cancer effects of SE-NK/T-DM1 cells and SE-JK/T-DM1 cells against (a) SK-BR-3 cells and (b) MDA-MB-231 cells. All effector cells were co-incubated with CMAC-labeled cancer cells at E:T ratio of 10:1. The amount of T-DM1 co-treated with Jurkat cells or NK92 cells was identical to the amount of T-DM1 found on the SE-NK/T-DM1 cells as shown in Figure 3.20. After 6 hours of incubation, all cells were collected and the cancer cell death was analyzed by the flow cytometry-based Annexin V/PI analysis. Data presented as mean ± SD. (ns, not significant, $^{**}P<0.01$, $^{****}P<0.0001$, by one-way ANOVA followed by Tukey post-hoc tests).

Consistently, no significant differences in cell death beyond the NK92 cell activity were shown in MDA-MB-231 cells (Figure 3.27b). These results confirm that the individual components contained in the SE-NK/T-DM1 cells contributed to the combinatorial anti-cancer effect. Moreover, embedding ADCs in NK92 cells through surface engineering enhanced the anti-cancer efficacy beyond the provided benefits of T-DM1 alone, NK92 cells alone, or T-DM1+NK92 cells.

3.4.6. Mechanistic Studies

To determine whether or not cytokine release plays a crucial role in the combined anti-cancer activity of SE-NK/T-DM1 cells, we assessed the levels of interferon-γ (IFN-γ) released in the presence or absence of IL-2, a key component in retaining the activity of NK92 cells.[44] IL-2 appeared to be essential in enhancing the cytolytic activity of unmodified NK92 cells (Figure 3.28a). However, IL-2 had no influence on the anti-cancer activity of SE-NK/T-DM1 cells. Moreover, the level of IFN-γ released was low throughout all treatment groups in the absence of IL-2 (Figure 3.28b). These findings reveal that IL-2 is not critical for the combined anti-cancer activity of SE-NK/T-DM1 cells.

To elucidate the mechanism of action of SE-NK/T-DM1 cells, expression of CD107a, a marker expressed with the degranulation of NK cells,[45,46] was examined in the SE-NK/T-DM1 cells and unmodified NK92 cells upon interaction with cancer cells. As a positive control, the degranulation of NK92 cells was observed by detecting the appearance of CD107a after the PMA/Ionomycin stimulation (Figure 3.29a). The NK92 cells and T-DM1+NK92 cells expressed CD107a at the basal level when co-incubated with SK-BR-3 cells (Figure 3.29b) and MDA-MB-231 cells (Figure 3.29c). Upon binding to

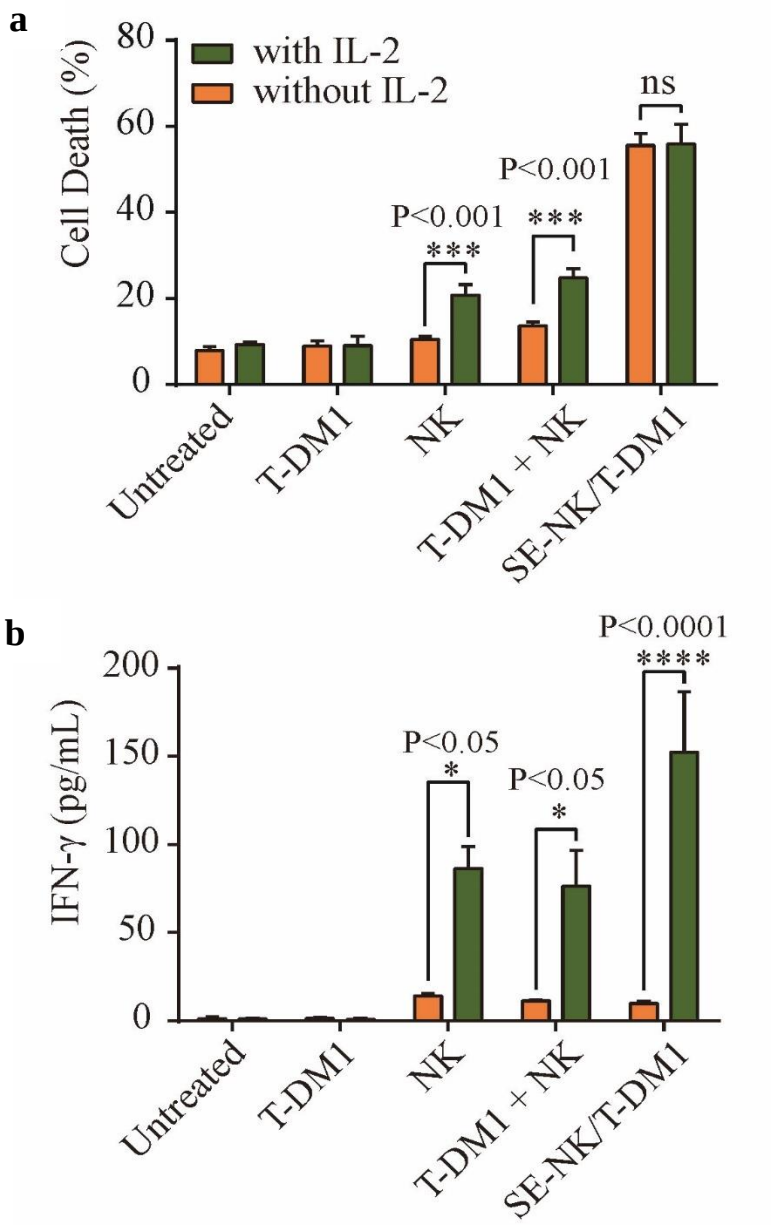

Figure 3.28. Effects of IL-2 on the anti-cancer activity of SE-NK/T-DM1 cells. (a) CMAC-labeled SK-BR-3 cells were co-incubated with SE-NK/T-DM1 cells, T-DM1, NK92 cells, or T-DM1+NK92 cells at E:T ratio of 10:1. NK92 cells were maintained in the absence of IL-2 for 48 hours prior to the surface modification. Unbound cells were removed and the remaining cell mixtures were incubated for 24 hours. Annexin V/PI kit was used to determine the dead cancer cells by Flow cytometry. (b) Level of IFN-γ released from SE-NK/T-DM1 cells. The culture media was sampled from the cytotoxicity study (a) and the amount of IFN-γ in each collected sample was measured using the human IFN-γ ELISA kit (detection limit: 15.6 - 1,000 pg/mL). Bars represent mean ± SD (*P<0.05, ****P<0.0001, by two-way ANOVA with Bonferroni post-hoc tests).

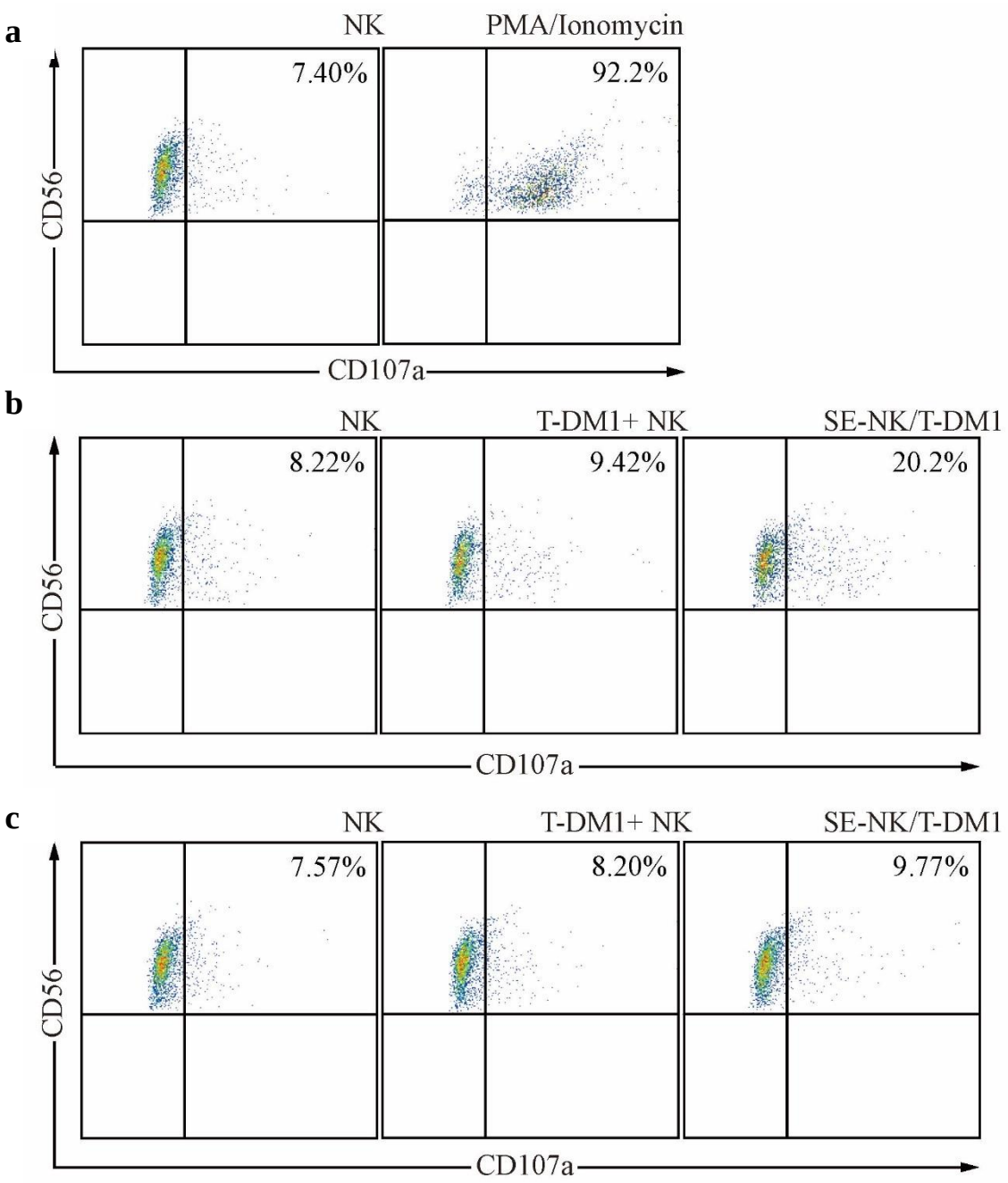

Figure 3.29. Degranulation of NK92 cells. (a) CD107a expression in NK92 cells grown in culture condition or under PMA/Ionomycin stimulation. CD107a expression on NK92 cells, T-DM1+NK92 cells, or SE-NK/T-DM1 cells co-incubated with (b) SK-BR-3 cells or (c) MDA-MB-231 cells. Flow cytometry was conducted to detect the CD107a expression from NK92 cells that have been identified by CD56 expression. Plots were selected from two independent experiments.

cancer cells, the CD107a expression was amplified in the SE-NK/T-DM1 cells co-incubated with SK-BR-3 cells at E:T ratio 10:1 (Figure 3.29b); this increase was absent in MDA-MB-231 cells (Figure 3.29c). We concluded that the degranulation of NK92 cells stimulated by the binding of SE-NK/T-DM1 cells to the target cancer cells is a favorable mechanism of action of the combined anti-cancer activity of SE-NK/T-DM1 cells.

3.4.7. *In Vivo* Efficacy Studies

Because generating Her2-positive breast cancer xenograft models using SK-BR-3 cells is very difficult,[47] we instead developed a Her2-positive lung cancer model with Calu-3 cells. Before initiating the *in vivo* efficacy studies with this animal model, we had verified the *in vitro* anti-cancer activity of SE-NK/T-DM1 cells against Calu-3 cells. Briefly, T-DM1 activity against Calu-3 was determined (Figure 3.30). The SE-NK/T-DM1 cells were able to specifically bind to Calu-3 cells (Figure 3.31). Following the binding event, the fluorescence cluster formation was observed at the effector cell-to-cancer cell junctions, and T-DM1 was transferred from the SE-NK/T-DM1 cells into internal compartments of Calu-3 cells (Figure 3.32). Comparable levels of cancer cell death were observed when Calu-3 cells were continuously exposed to T-DM1+NK92 cells and SE-NK/T-DM1 cells for 24 hours (Figure 3.33). The number of NK92 cells bound to Calu-3 cells increased when cancer cells were co-incubated with the SE-NK/T-DM1 cells for a short period (Figure 3.34). Increased numbers of SE-NK/T-DM1 cells bound to Calu-3 cells resulted in an enhanced anti-cancer activity (Figure 3.35). The SE-NK/T-DM1 cells expressed CD107a upon encountering Calu-3 cells, indicating the degranulation of NK92 cells (Figure 3.36).

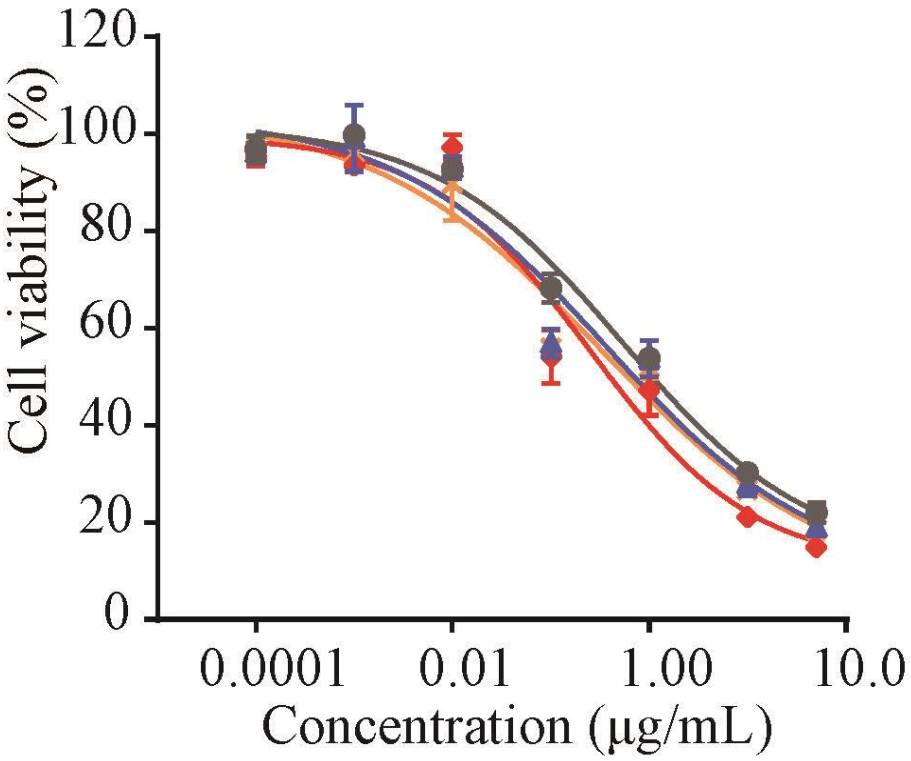

Figure 3.30. Cytotoxicity of Kadcyla® and T-DM1s synthesized with different ratios of SMCC-DM1 in Calu-3 cells. The LC50 of T-DM1 R=5, R=10, R=15, and Kadcyla® was 0.535, 0.365, 0.253, and 0.340 µg/ml, respectively. Data presented as mean ± SD.

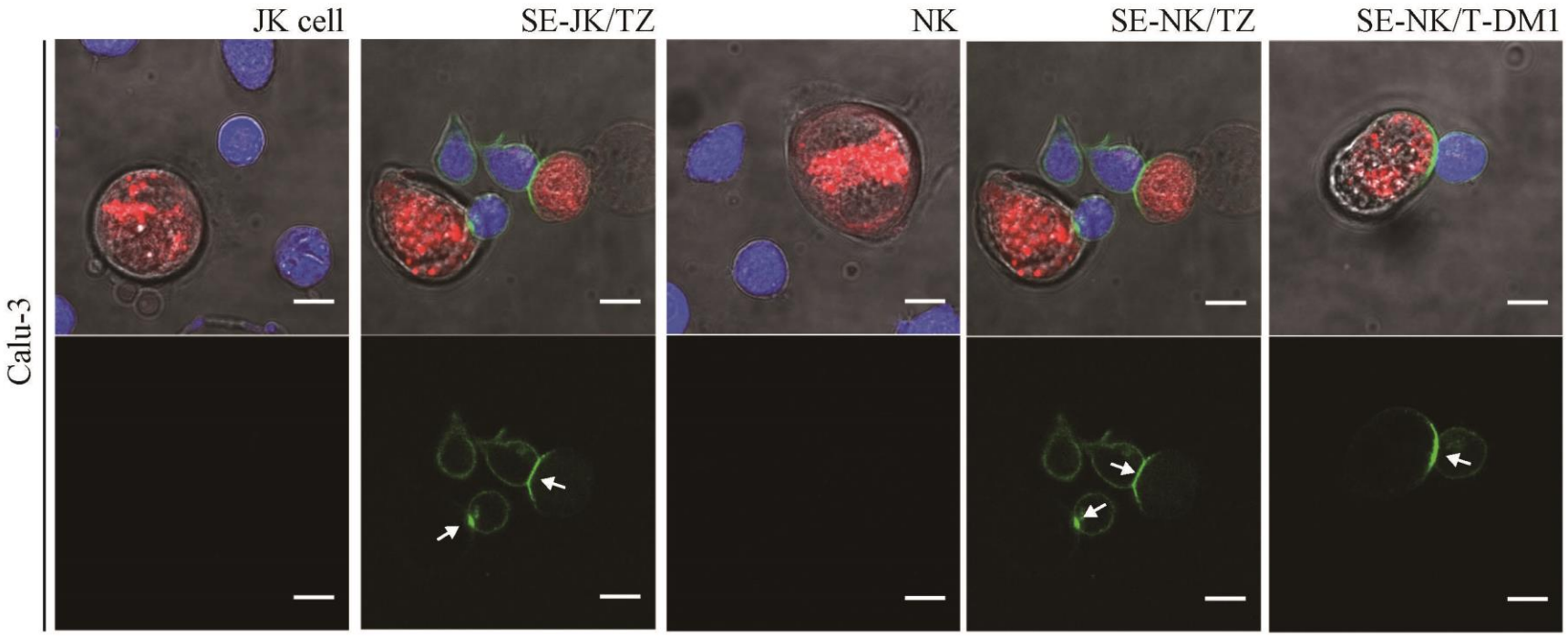

Figure 3.31. Confocal images showing the binding of SE-JK/TZ cells, SE-NK/TZ cells, or SE-NK/T-DM1 cells to Calu-3 cells. CMTPX-labeled Calu-3 cells (red) were co-incubated with CMAC-labeled effector cells (blue). Identical procedure stated in Figure 2.17 was followed. Localization of TZ (green) and T-DM1 (green) at the effector cell-to-cancer cell junction is indicated with white arrows. Scale bars, 10 μm. All images are representative of two independent experiments.

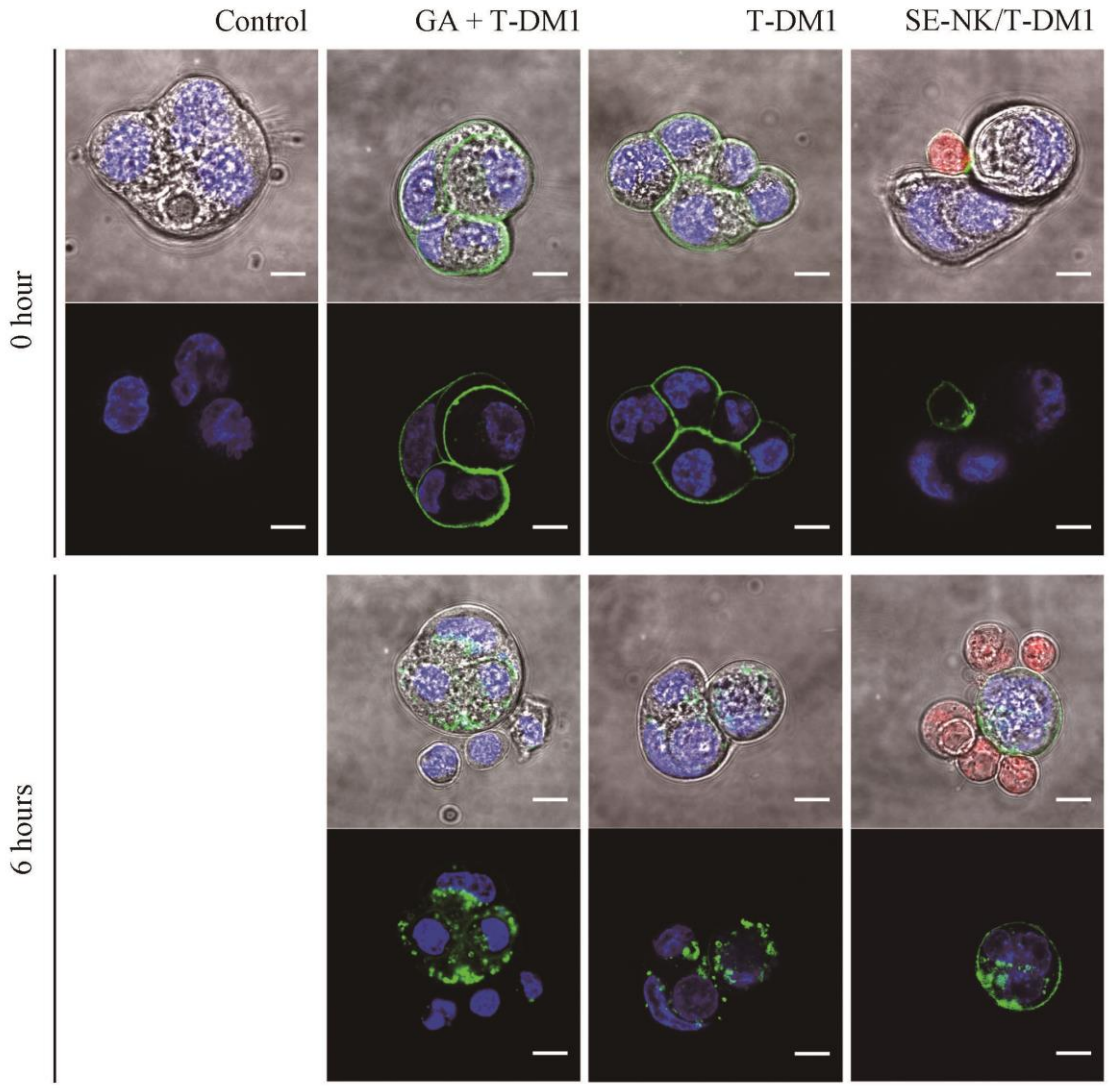

Figure 3.32. Internalization of transferred T-DM1 into Her2-positive Calu-3 cells. Calu-3 cells were labeled with Nucblue® nuclear stain (blue) and NK92 cells were labeled with CMTPX (red). Calu-3 cells were treated with 5 μg of T-DM1-FITC or SE-NK/T-DM1-FITC cells at E:T ratio of 10:1. Unbound effector cells were removed after 30 minutes of incubation. GA was added to T-DM1 treated Calu-3 cells at a final concentration of 3 μM. Cells were imaged immediately after removing unbound cells and after 6 hours of incubation by confocal microscopy. Scale bars, 10 μm. All images are representative of two independent experiments.

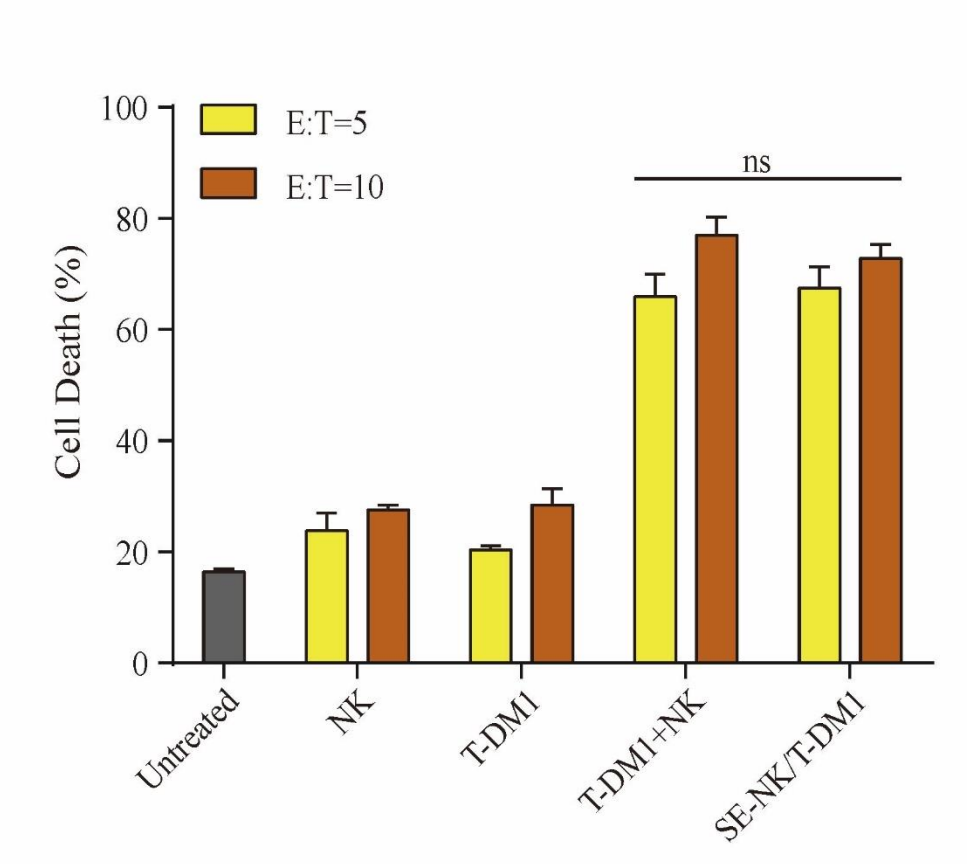

Figure 3.33. Long-term incubation of SE-NK/T-DM1 cells with Calu-3 cells. CMAC-labeled Calu-3 cells were co-incubated with SE-NK/T-DM1 cells, NK92 cells, T-DM1, or T-DM1+NK92 cells at E:T ratio of 5:1 or 10:1. After 24 hours, all cells were collected and Annexin V/PI assays were performed by flow cytometry. Data presented as mean ± SD (ns, not significant, by two-way ANOVA with Bonferroni post-hoc tests).

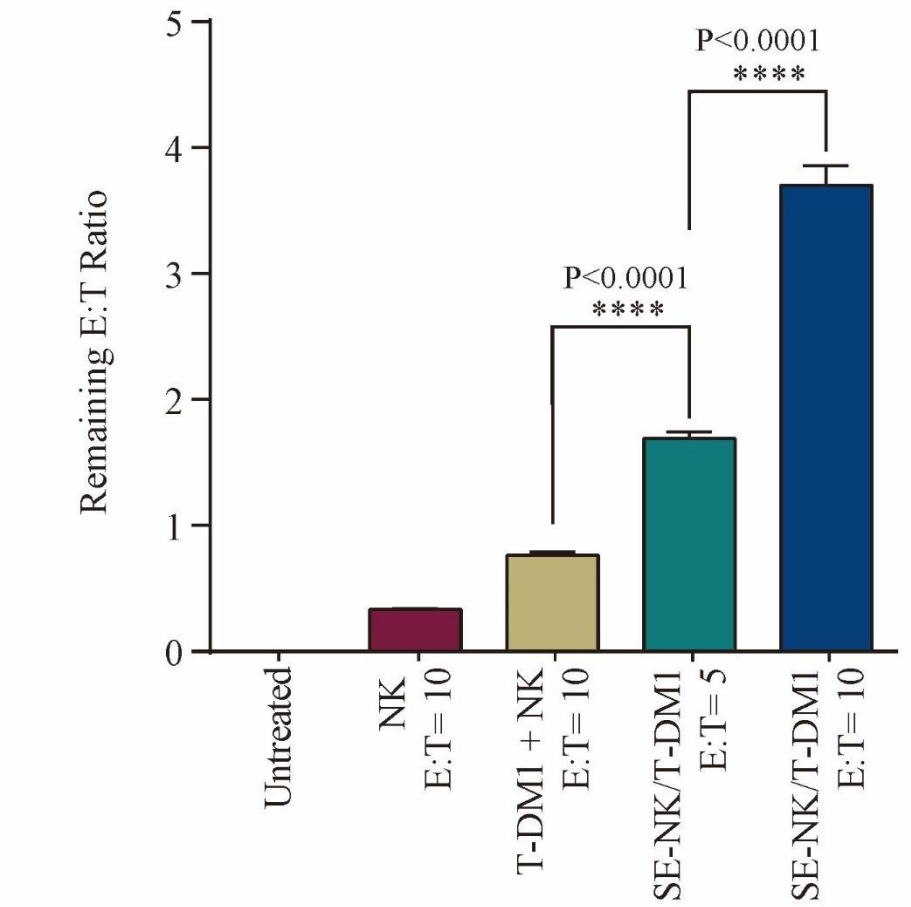

Figure 3.34. Targeted binding of SE-NK/T-DM1 cells to Calu-3 cells. CMTPX-labeled Calu-3 cells were co-incubated with CMAC-labeled effector cells. Calu-3 cells were treated with NK92 cells, T-DM1+NK cells, or SE-NK/T-DM1 cells. After 2 hours, unbound effector cells were removed and remaining cells were collected. NK92 cells were counted per 1×10^4 Calu-3 cells by flow cytometry. Data presented as mean ± SD (****P<0.0001 by one-way ANOVA with Tukey post-hoc tests).

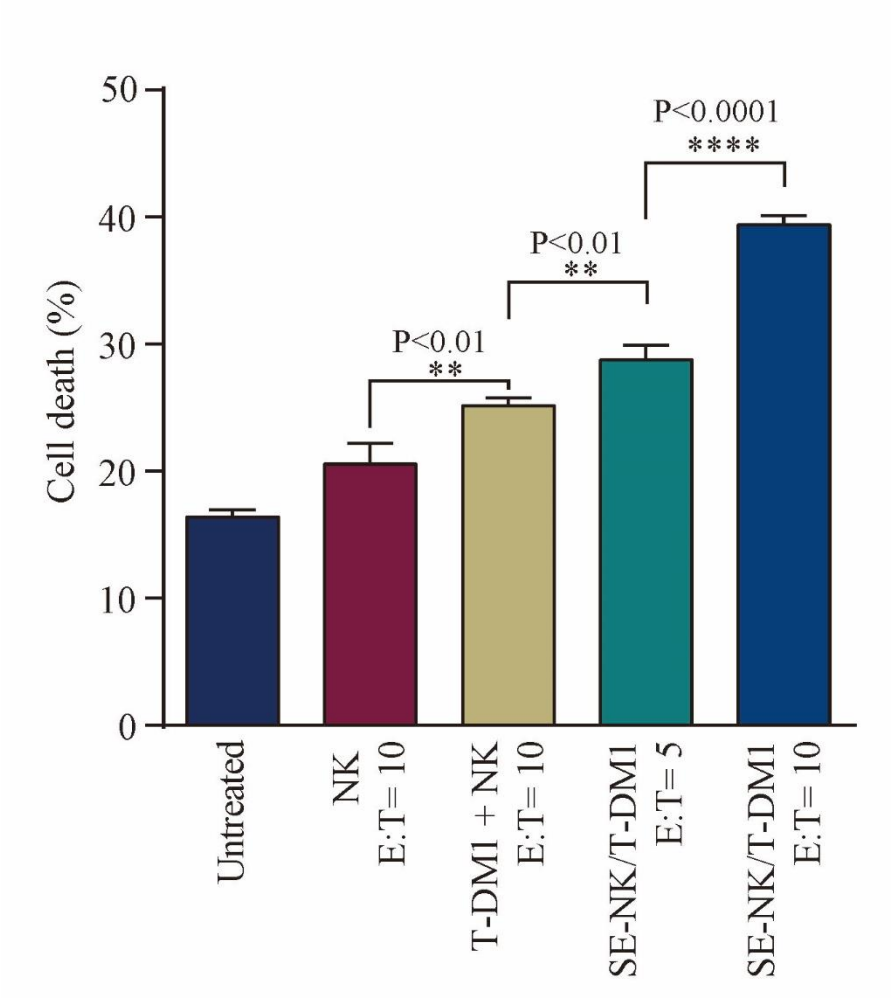

Figure 3.35. Short-term incubation of SE-NK/T-DM1 cells with Calu-3 cells demonstrated the enhanced anti-cancer activity through targeted binding. Calu-3 cells labeled with CMAC were co-incubated with SE-NK/T-DM1 cells, NK92 cells, T-DM1, or T-DM1+NK92 cells at E:T ratio of 5:1 or 10:1. Unbound cells were removed after 2 hours and the remaining cell mixtures are incubated for 24 hours. All cells were collected and Annexin V/PI assay was performed by flow cytometry. Data presented as mean ± SD. (**P<0.01, ****P<0.0001 by one-way ANOVA with Tukey post-hoc tests.)

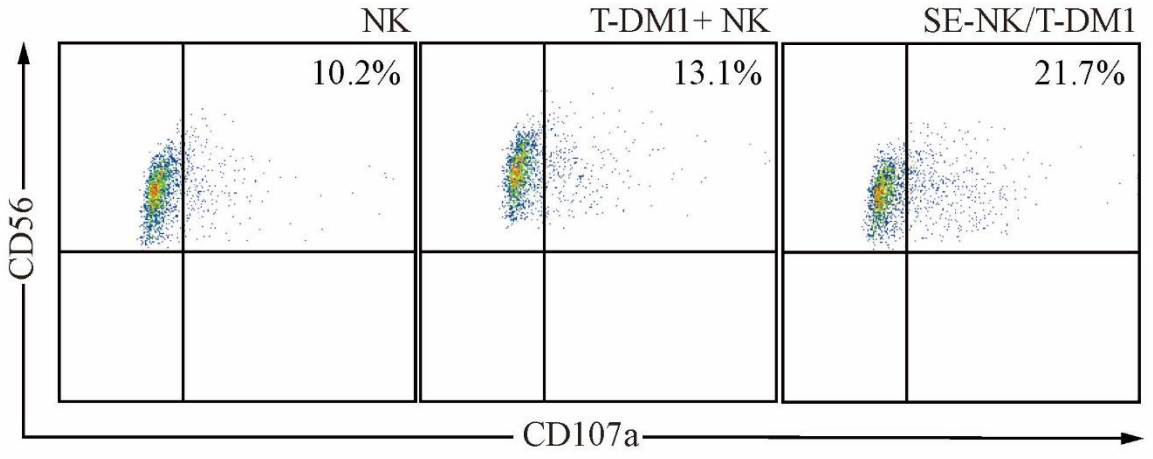

Figure 3.36. Expression of CD107a on NK92 cells, T-DM1+NK92 cells, or SE-NK/T-DM1 cells following the co-incubation with Calu-3 cells. Flow cytometry was conducted to analyze the CD107a expression on NK92 cells that have been identified by CD56 expression. Plots were selected from two representative experiments.

No significant toxicity was reported on NSG mice injected with 1×10^7 Her2-specific CAR-NK cells; therefore, 1×10^7 surface-engineered NK92 cells were injected as the maximum dose.[20] The amount of T-DM1 on 1×10^7 SE-NK/T-DM1 cells (100 μg formulation) was calculated to be 210 μg, which is similar to the recommended dose found in the literature for mice models (7-10 mg/kg).[48]

We have compared the anti-cancer activity of SE-NK/T-DM1 cells to that of T-DM1+NK92 cells using Her2-positive Calu-3 models and Her2-negative MDA-MB-231 models. In the Her2-positive tumor model, SE-NK/T-DM1 cells exhibited the strongest anti-cancer efficacy through the combinatorial effects of TZ, DM1, and NK92 cells (Figure 3.37a). Unmodified NK92 cells were ineffective in inhibiting the tumor growth, while T-DM1 started to suppress the tumor growth after Day 7. The T-DM1+NK92 cells also significantly inhibited the tumor growth compared to the control. At the end-point of the study, both dosages of SE-NK/T-DM1 cells were effective in demonstrating substantially reduced tumor growth compared to the T-DM1+NK92 cells. With the benefit of enhanced anti-cancer activity, the chemoimmunotherapeutic approach using the SE-NK/T-DM1 cells may reduce the time and cost required to obtain sufficient tumor-reactive NK92 cells for patient infusion. In the Her2-negative tumor model, no significant tumor growth suppression was observed among all treatment groups (Figure 3.38a). At the end-point of the study, animals treated with NK92 cells, T-DM1+NK92 cells, and SE-NK/T-DM1 cells showed a minor suppression effect on tumor growth compared to the control group; however, no statistical significance was attained between the treatment groups. No significant body weight change was observed in either the Calu-3 models (Figure 3.37b)

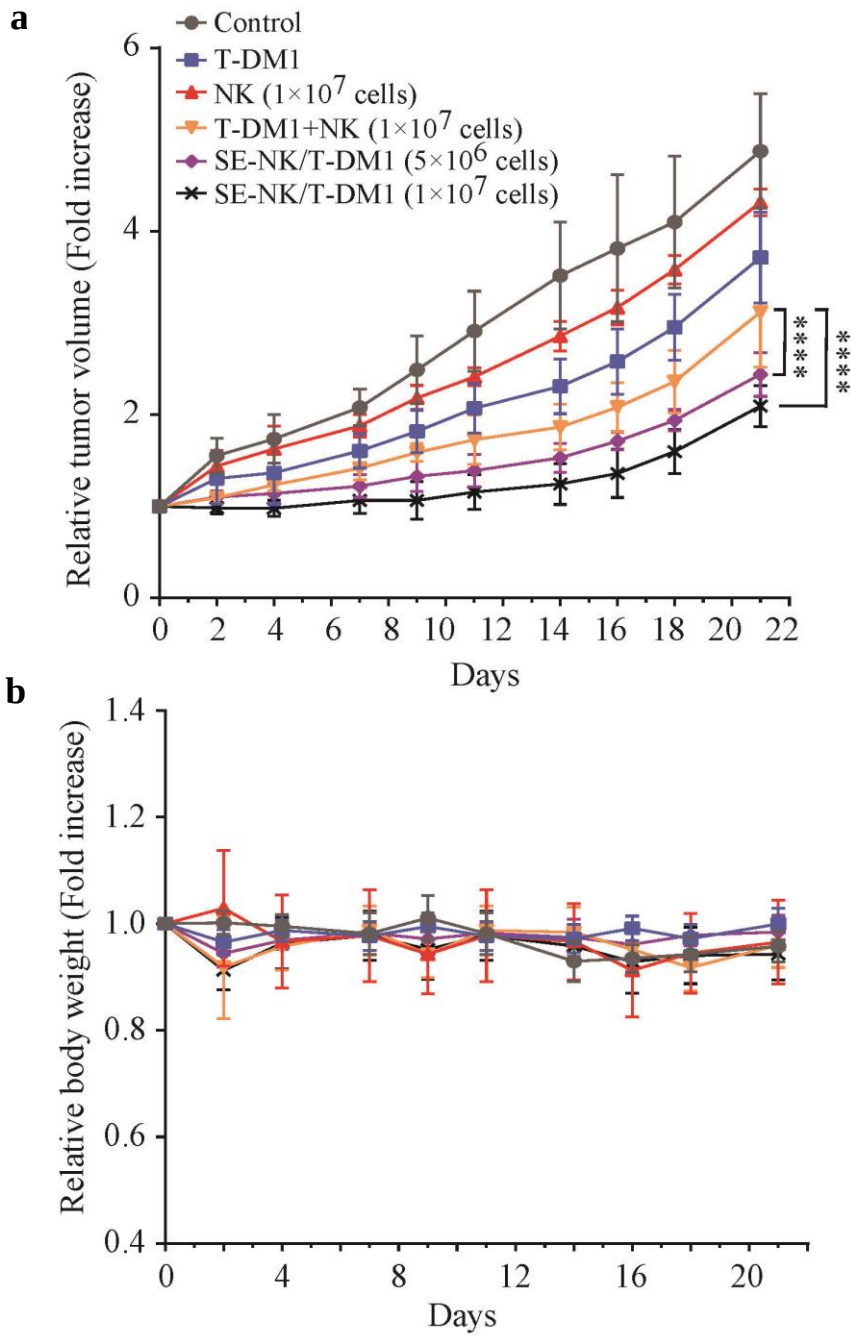

Figure 3.37. *In vivo* anti-cancerr efficacy of SE-NK/T-DM1 cells in Her2-positive Calu-3 models. (a) Tumor growth and (b) body weight of Calu-3 models. Female NSG mice (n=4) were inoculated with 1×10^7 cancer cells and the tumor volume was measured. Animals received weekly treatment of T-DM1, NK92 cells, T-DM1+NK92 cells, or SE-NK/T-DM1 cells for 3 weeks. Relative tumor volume was calculated by normalizing the recorded tumor volume to the initial tumor volume. Data presented mean ± SD (****P<0.0001, two-way repeated measure ANOVA with Bonferroni post-hoc tests).

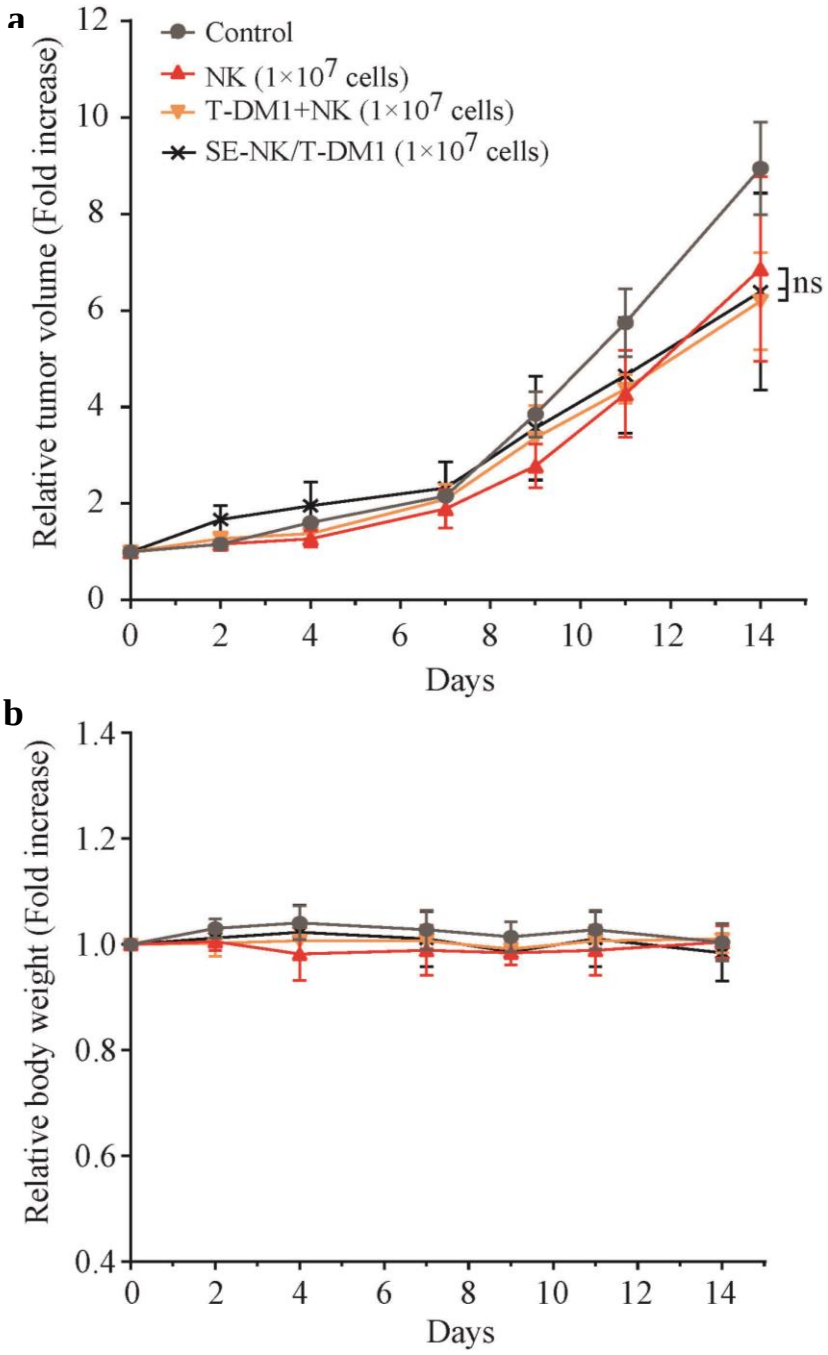

Figure 3.38. *In vivo* anti-cancer efficacy of SE-NK/T-DM1 cells in Her2-negative MDA-MB-231 models. (a) Tumor growth and (b) body weight of MDA-MB-231 models. Female NSG mice (n=3 for control, rest n=4) were inoculated with 1×10^7 cancer cells and the tumor volume was measured. Animals received weekly treatment of NK92 cells, T-DM1+NK92 cells, or SE-NK/T-DM1 cells for 3 weeks. Relative tumor volume was calculated by normalizing the recorded tumor volume to the initial tumor volume. Data presented as mean ± SD (ns, not significant, two-way repeated measure ANOVA with Bonferroni post-hoc tests).

or MDA-MB-231 models (Figure 3.38b), indicating that no severe toxicity was caused by the treatments.

For the biodistribution study, NSG mice bearing Calu-3 tumors were administered unmodified NK92 cells, T-DM1+NK92 cells, or SE-NK/T-DM1 cells. The population of NK92 cells migrated to the major organs, including the heart, kidneys, liver, lung, and spleen; the tumor was quantitatively analyzed by flow cytometry. No accumulation of NK92 cells was observed in the heart, kidneys, or lungs (Figure 3.39). NK92 cells were detected in the liver and spleen; however, no significant difference in the number of NK92 cells was observed among the treatment groups. Compared to the T-DM1+NK92 cells and unmodified NK92 cells, a larger number of NK92 cells were spotted in the tumor tissues of mice that received SE-NK/T-DM1 cells.

3.5. Discussion

The anti-cancer activity of SE-NK/T-DM1 cells as chemoimmunotherapy was extensively investigated to identify the individual activities of TZ, DM1, and NK92 cells. It is clear to note that T-DM1 is more potent to induce cell death than is TZ. The differences in the anti-cancer effects between SE-JK/T-DM1 cells and SE-JK/TZ cells originated solely from the cytotoxicity of DM1 contained in T-DM1 due to the fact that Jurkat cells lack direct cytolytic function.[49] More complicated trends were observed in the SE-NK/T-DM1 cells. In the target cancer cells, unmodified NK92 cells showed noticeable cytolytic activity; however, it was lower than cytotoxicity of T-DM1. The TZ+NK92 cells were more effective in eliminating the target cancer cells than T-DM1 alone. Binding of TZ to Her2 on the cell membrane inhibits the down-stream signaling pathway associated

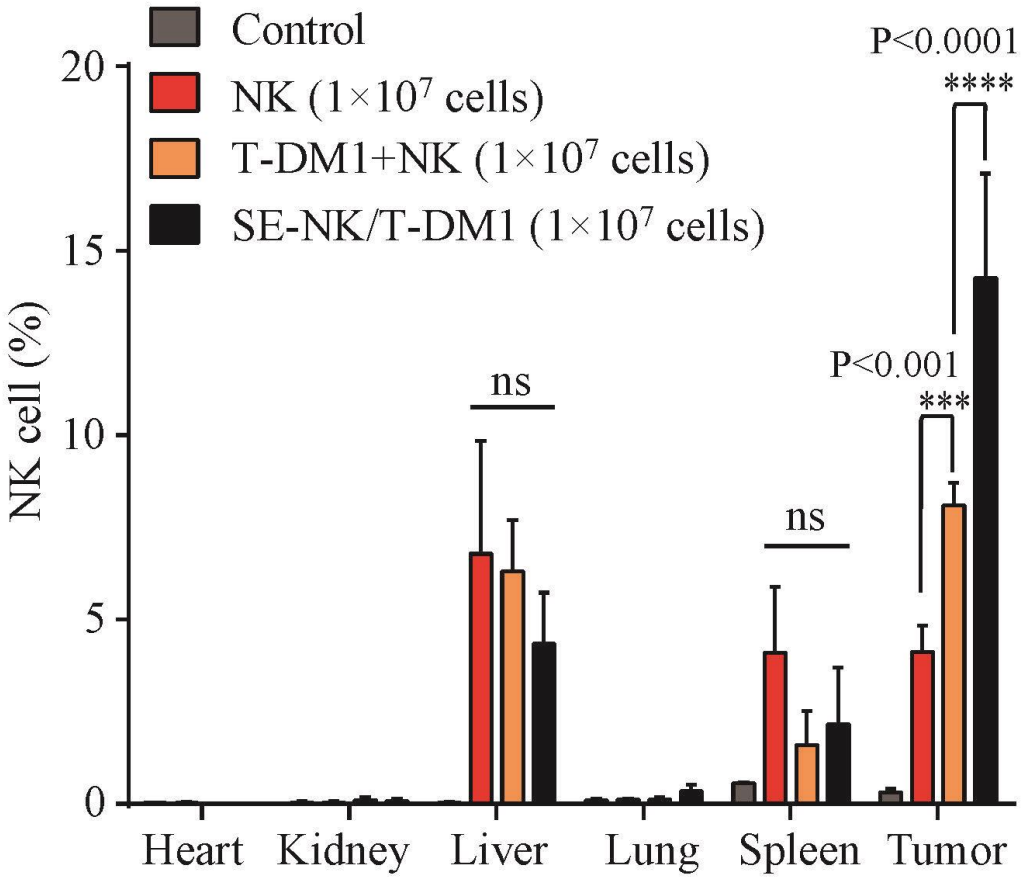

Figure 3.39. Biodistribution of SE-NK/T-DM1 cells in Calu-3 model. Animals (*n*=3) received NK92 cells, T-DM1+NK92 cells, or SE-NK/T-DM1 cells and the vital organs were harvested 24 hours after the injection. Single-cell suspensions were generated through mechanical and enzymatic digestion of the harvested organs and NK92 cells were detected using the anti-CD56 antibody. The NK92 cells were counted among 1×10^5 total cells. Data presented as mean ± SD (ns, not significant; ***P<0.001; ****P<0.0001; two-way ANOVA with Bonferroni post-hoc tests).

with PI3K and AKT, both of which are involved in cell cycle arrest and cell apoptosis.[50] NK92 cells recognized and eradicated the target cancer cells undergoing apoptosis, which was induced by the inhibition of the downstream signaling pathways resulting from the binding of TZ.[51,52] SE-NK/TZ cells displayed stronger anti-cancer activities compared to the TZ+NK92 cells. The TZ grafted on the surface may have directed SE-NK/TZ cells toward the antigen-expressing cancer cells and led to physical contact with the target cancer cells, which in turn increased the chance to stimulate the cytolytic function of NK 92 cells. The SE-NK/T-DM1 cells achieved the greatest anti-cancer activity; the magnitude of the increased anti-cancer efficacy could not be simply explained as the sum of anti-cancer effects of three components—DM1, TZ, and NK92 cells.

The lack of CD16, CD32 and CD64 IgG receptor expression on the surface of NK92 cells indicates that ADCC seems to be inappropriate to explain the mechanism of action of SE-NK/T-DM1 cells.[12,37,39] The NK92 cells that are transferred adoptively are typically supplemented with IL-2—an NK cell activating cytokine—which stimulates NK92 cells to secrete IFN-γ upon encountering the target cells.[53,54] We investigated the effect of IL-2 on IFN-γ secretion from the SE-NK/T-DM1 cells. The NK92 cells and T-DM1+NK92 cells showed increase in targeted cancer cell death with IL-2, whereas SE-NK/T-DM1 cells showed the same activity regardless of the presence of IL-2. Interestingly, the IFN-γ secretion was only increased in the treatment groups supplemented with IL-2. These results demonstrate that although IL-2 increases the cytolytic activity of NK92 cells through enhanced release of IFN-γ,[55,56] the cytolytic activity of SE-NK-T-DM1 cells is independent from IFN-γ secretion and does not require IL-2 supplementation.

The next mechanism we examined was the ability of NK92 cells to release perforins and granzymes,[39] both of which trigger direct killing of foreign, damaged, malignant, and infected cells.[45,57] The detection of degranulation marker, CD107a, has been a widely used method to measure the cytolytic activity of NK cells.[45,46] As NK92 cells engage the target cells, CD107a co-localizes with perforins and granzymes into the secretory lysosomes and translocates to the cell membrane as the lysosomes fuse with the cell membrane for perforin and granzyme release.[58,59] The unmodified NK92 cells and T-DM1+NK92 cells showed basal level of CD107a expression when encountered with the target cancer cells. Compared to the other treatment groups, the appearance of CD107a was increased in the SE-NK/T-DM1 cells following the recognition of target cancer cells; this level of increase in the CD107a expression was found to be similar to the reported levels from Alter et al. and Kwant-Mitchell et al.[58,60] We postulate that, in the SE-NK/T-DM1 cells, T-DM1 pushes target cancer cells towards apoptosis and triggers the expression of damage-associated molecular patterns (DAMP).[51,61-63] Simultaneously, these damaged and/or apoptotic cancer cells are recognized and eliminated by NK92 cells that have been delivered closer to the target tumor tissues by the targeting ability of T-DM1. Finally, the stimulated SE-NK/T-DM1 cells destroy the target cancer cells through the perforin and granzyme pathway. Consequently, these findings confidently claim that the incorporation of ADCs into the surface of NK92 cells not only allows the cancer homing of NK92 cells, but also offers a novel means of combining chemotherapy and immunotherapy in a single immune cell.

Our objective was to demonstrate the therapeutic benefit of ADC-embedded NK92 cells as a new platform for chemoimmunotherapy. Future studies should be conducted to

define the mechanism of action of the surface-engineered effector cells in detail and, more importantly, to facilitate the translation into clinical cancer therapy. Pharmacokinetic studies are necessary to determine the circulation times of SE-NK/T-DM1 cells and the fate of T-DM1 and NK92 cells once the SE-NK/T-DM1 cells dissociate into individual components. Although expression of CD107a provides indirect evidence for the activation of NK92 cells, actual levels of perforins and granzymes released from the activated NK92 cells should be determined. Several supplementary cytokines, such as IL-2, IL-12, IL-15, and IL-18, can enhance the innate cytolytic activity of NK cells.[64-66] Preactivation or co-administration of these activating cytokines can improve the anti-cancer efficacy of SE-NK/T-DM1 cells and allow them to be more favorable for clinical application. It is also important to perform histological analysis to identify SE-NK/T-DM1 cells trafficked to tumors and other organs. Since T-DM1 is approved primarily to treat Her2-positive breast cancers, the efficacy of SE-NK/T-DM1 cells should be evaluated in Her2-positive patient-derived primary breast cancer models for clinical translation. In addition, as the CD19-targeted CAR-T cells have shown impressive results in hematological malignancies,[67] we plan to investigate the therapeutic efficacy of SE-NK/ADC cells generated with anti-CD19 ADCs in B-cell acute lymphoblastic leukemia, chronic lymphocytic leukemia, and B-cell non-Hodgkin lymphoma models for expedited clinical transition.

3.6. Conclusion

Surface engineering of active immune cells with ADCs is composed of a clinically promising strategy to effectively combine immunotherapy and chemotherapy in a single

cell. Our method allows enhanced accumulation of ADCs and active NK92 cells in the target tumor tissue. With the active NK92 cells and ADCs co-localized in proximity at the tumor tissue, NK 92 cells recognize the damaged cancer cells induced by ADCs. These simultaneous anti-cancer activities are the basis for combinatorial anti-cancer efficacy of the ADC-embedded NK92 cells. With our strategy, active targeting of any immune cells—including T cells, DCs, and macrophages—to different types of cancers is achievable through the embedding of various ADCs in the immune cell surface. Currently, many antibodies have been generated for specific diseases and target cells. Most of these antibodies are candidates of new ADCs, and thus the application of SE-NK/ADCs cells may become a readily accessible tool for chemoimmunotherapy. Potent effector cells with a specific tumor-homing capability and chemoimmunotherapeutic anti-cancer activity can be generated instantly by simply mixing the pre-expanded immune cells from cell bank or freshly isolated immune cells from the patients with a ready-to-use DMPE-ADC formulation on the bedside. This single-injection therapy using ADC-embedded immune cells serves as a new platform to develop tailored chemoimmunotherapy for the treatment of many different types of cancers in addition to the breast cancer and the lung cancer introduced here.

3.7. References

1. Zitvogel L, Apetoh L, Ghiringhelli F, Kroemer G. 2008. Immunological aspects of cancer chemotherapy. Nat Rev Immunol **8**(1):59-73.

2. Lake RA, Robinson BW. 2005. Immunotherapy and chemotherapy--A practical partnership. Nat Rev Cancer **5**(5):397-405.

3. Casares N, Pequignot MO, Tesniere A, Ghiringhelli F, Roux S, Chaput N, Schmitt E, Hamai A, Hervas-Stubbs S, Obeid M, Coutant F, Metivier D, Pichard E, Aucouturier P, Pierron G, Garrido C, Zitvogel L, Kroemer G. 2005. Caspase-dependent immunogenicity of doxorubicin-induced tumor cell death. J Exp Med **202**(12):1691-1701.

4. Demaria S, Volm MD, Shapiro RL, Yee HT, Oratz R, Formenti SC, Muggia F, Symmans WF. 2001. Development of tumor-infiltrating lymphocytes in breast cancer after neoadjuvant paclitaxel chemotherapy. Clin Cancer Res **7**(10):3025-3030.

5. Fagnoni FF, Lozza L, Zibera C, Zambelli A, Ponchio L, Gibelli N, Oliviero B, Pavesi L, Gennari R, Vescovini R, Sansoni P, Da Prada G, Robustelli Della Cuna G. 2002. T-cell dynamics after high-dose chemotherapy in adults: Elucidation of the elusive CD8+ subset reveals multiple homeostatic T-cell compartments with distinct implications for immune competence. Immunology **106**(1):27-37.

6. Goldrath AW, Bevan MJ. 1999. Selecting and maintaining a diverse T-cell repertoire. Nature **402**(6759):255-262.

7. Ghiringhelli F, Menard C, Puig PE, Ladoire S, Roux S, Martin F, Solary E, Le Cesne A, Zitvogel L, Chauffert B. 2007. Metronomic cyclophosphamide regimen selectively depletes CD4+CD25+ regulatory T cells and restores T and NK effector functions in end stage cancer patients. Cancer Immunol Immunother **56**(5):641-648.

8. Chang CL, Hsu YT, Wu CC, Lai YZ, Wang C, Yang YC, Wu TC, Hung CF. 2013. Dose-dense chemotherapy improves mechanisms of antitumor immune response. Cancer Res **73**(1):119-127.

9. Verma R, Foster RE, Horgan K, Mounsey K, Nixon H, Smalle N, Hughes TA, Carter CR. 2016. Lymphocyte depletion and repopulation after chemotherapy for primary breast cancer. Breast Cancer Res **18**(1):10.

10. Park B, Yee C, Lee KM. 2014. The effect of radiation on the immune response to cancers. Int J Mol Sci **15**(1):927-943.

11. Cheng M, Chen Y, Xiao W, Sun R, Tian Z 2013. NK cell-based immunotherapy for malignant diseases. Cell Mol Immunol **10**(3):230-252.

12. Klingemann H, Boissel L, Toneguzzo F 2016. Natural killer cells for immunotherapy - Advantages of the NK-92 cell line over blood NK cells. Front Immunol **7**:91.

13. Emens LA. 2010. Chemoimmunotherapy. Cancer J **16**(4):295-303.

14. Bracci L, Schiavoni G, Sistigu A, Belardelli F. 2014. Immune-based mechanisms of cytotoxic chemotherapy: Implications for the design of novel and rationale-based combined treatments against cancer. Cell Death Differ **21**(1):15-25.

15. Morgan RA, Yang JC, Kitano M, Dudley ME, Laurencot CM, Rosenberg SA. 2010. Case report of a serious adverse event following the administration of T cells transduced with a chimeric antigen receptor recognizing ERBB2. Mol Ther **18**(4):843-851.

16. Glienke W, Esser R, Priesner C, Suerth JD, Schambach A, Wels WS, Grez M, Kloess S, Arseniev L, Koehl U. 2015. Advantages and applications of CAR-expressing natural killer cells. Front Pharmacol **6**:21.

17. Arai S, Meagher R, Swearingen M, Myint H, Rich E, Martinson J, Klingemann H. 2008. Infusion of the allogeneic cell line NK-92 in patients with advanced renal cell cancer or melanoma: A phase I trial. Cytotherapy **10**(6):625-632.

18. Suck G. 2006. Novel approaches using natural killer cells in cancer therapy. Semin Cancer Biol **16**(5):412-418.

19. Chang YH, Connolly J, Shimasaki N, Mimura K, Kono K, Campana D. 2013. A chimeric receptor with NKG2D specificity enhances natural killer cell activation and killing of tumor cells. Cancer Res **73**(6):1777-1786.

20. Schonfeld K, Sahm C, Zhang C, Naundorf S, Brendel C, Odendahl M, Nowakowska P, Bonig H, Kohl U, Kloess S, Kohler S, Holtgreve-Grez H, Jauch A, Schmidt M, Schubert R, Kuhlcke K, Seifried E, Klingemann HG, Rieger MA, Tonn T, Grez M, Wels WS. 2015. Selective inhibition of tumor growth by clonal NK cells expressing an ErbB2/HER2-specific chimeric antigen receptor. Mol Ther **23**(2):330-338.

21. Scott AM, Wolchok JD, Old LJ. 2012. Antibody therapy of cancer. Nat Rev Cancer **12**(4):278-287.

22. Chari RV, Miller ML, Widdison WC. 2014. Antibody-drug conjugates: An emerging concept in cancer therapy. Angew Chem Int Ed Engl **53**(15):3796-3827.

23. Peters C, Brown S. 2015. Antibody-drug conjugates as novel anti-cancer chemotherapeutics. Biosci Rep **35**(4).

24. Slamon DJ, Leyland-Jones B, Shak S, Fuchs H, Paton V, Bajamonde A, Fleming T, Eiermann W, Wolter J, Pegram M, Baselga J, Norton L. 2001. Use of chemotherapy plus a monoclonal antibody against HER2 for metastatic breast cancer that overexpresses HER2. N Engl J Med **344**(11):783-792.

25. Kahl B. 2008. Chemotherapy combinations with monoclonal antibodies in non-Hodgkin's lymphoma. Semin Hematol **45**(2):90-94.

26. Eichhorst B, Fink AM, Bahlo J, Busch R, Kovacs G, Maurer C, Lange E, Koppler H, Kiehl M, Sokler M, Schlag R, Vehling-Kaiser U, Kochling G, Ploger C, Gregor M, Plesner T, Trneny M, Fischer K, Dohner H, Kneba M, Wendtner CM, Klapper W, Kreuzer KA, Stilgenbauer S, Bottcher S, Hallek M, Investigators IG, GCLLSG GCSG. 2016. First-line chemoimmunotherapy with bendamustine and rituximab versus fludarabine, cyclophosphamide, and rituximab in patients with advanced chronic lymphocytic leukaemia (CLL10): An international, open-label, randomised, phase 3, non-inferiority trial. Lancet Oncol **17**(7):928-942.

27. Sievers EL, Senter PD. 2013. Antibody-drug conjugates in cancer therapy. Annu Rev Med **64**:15-29.

28. Heath VL, Bicknell R. 2009. Anticancer strategies involving the vasculature. Nat Rev Clin Oncol **6**(7):395-404.

29. Bruno A, Ferlazzo G, Albini A, Noonan DM. 2014. A think tank of TINK/TANKs: Tumor-infiltrating/tumor-associated natural killer cells in tumor progression and angiogenesis. J Natl Cancer Inst **106**(8):dju200.

30. Teicher BA, Chari RV. 2011. Antibody conjugate therapeutics: Challenges and potential. Clin Cancer Res **17**(20):6389-6397.

31. Won YW, Patel AN, Bull DA. 2014. Cell surface engineering to enhance mesenchymal stem cell migration toward an SDF-1 gradient. Biomaterials **35**(21):5627-5635.

32. Lim KS, Lee DY, Valencia GM, Won YW, Bull DA. 2017. Cell surface-engineering to embed targeting ligands or tracking agents on the cell membrane. Biochem Biophys Res Commun **482**(4):1042-1047.

33. Santos EB, Yeh R, Lee J, Nikhamin Y, Punzalan B, Punzalan B, La Perle K, Larson SM, Sadelain M, Brentjens RJ. 2009. Sensitive in vivo imaging of T cells using a membrane-bound Gaussia princeps luciferase. Nat Med **15**(3):338-344.

34. Pittet MJ, Grimm J, Berger CR, Tamura T, Wojtkiewicz G, Nahrendorf M, Romero P, Swirski FK, Weissleder R. 2007. In vivo imaging of T cell delivery to tumors after adoptive transfer therapy. Proc Natl Acad Sci U S A **104**(30):12457-12461.

35. Gonzales C, Yoshihara HA, Dilek N, Leignadier J, Irving M, Mieville P, Helm L, Michielin O, Schwitter J. 2016. In-vivo detection and tracking of T cells in various organs in a melanoma tumor model by 19F-fluorine MRS/MRI. PLoS One **11**(10):e0164557.

36. Hamblett KJ, Senter PD, Chace DF, Sun MM, Lenox J, Cerveny CG, Kissler KM, Bernhardt SX, Kopcha AK, Zabinski RF, Meyer DL, Francisco JA. 2004. Effects of drug loading on the antitumor activity of a monoclonal antibody drug conjugate. Clin Cancer Res **10**(20):7063-7070.

37. Jarahian M, Watzl C, Issa Y, Altevogt P, Momburg F. 2007. Blockade of natural killer cell-mediated lysis by NCAM140 expressed on tumor cells. Int J Cancer **120**(12):2625-2634.

38. Liu H, Kwong B, Irvine DJ. 2011. Membrane anchored immunostimulatory oligonucleotides for in vivo cell modification and localized immunotherapy. Angew Chem Int Ed Engl **50**(31):7052-7055.

39. Maki G, Klingemann HG, Martinson JA, Tam YK. 2001. Factors regulating the cytotoxic activity of the human natural killer cell line, NK-92. J Hematother Stem Cell Res **10**(3):369-383.

40. Wang TY, Leventis R, Silvius JR. 2005. Artificially lipid-anchored proteins can elicit clustering-induced intracellular signaling events in Jurkat T-lymphocytes independent of lipid raft association. J Biol Chem **280**(24):22839-22846.

41. Ritchie M, Tchistiakova L, Scott N. 2013. Implications of receptor-mediated endocytosis and intracellular trafficking dynamics in the development of antibody drug conjugates. MAbs **5**(1):13-21.

42. Erickson HK, Park PU, Widdison WC, Kovtun YV, Garrett LM, Hoffman K, Lutz RJ, Goldmacher VS, Blattler WA. 2006. Antibody-maytansinoid conjugates are activated in targeted cancer cells by lysosomal degradation and linker-dependent intracellular processing. Cancer Res **66**(8):4426-4433.

43. Austin CD, De Maziere AM, Pisacane PI, van Dijk SM, Eigenbrot C, Sliwkowski MX, Klumperman J, Scheller RH. 2004. Endocytosis and sorting of ErbB2 and the site of action of cancer therapeutics trastuzumab and geldanamycin. Mol Biol Cell **15**(12):5268-5282.

44. Thornton S, Kuhn KA, Finkelman FD, Hirsch R. 2001. NK cells secrete high levels of IFN-gamma in response to in vivo administration of IL-2. Eur J Immunol **31**(11):3355-3360.

45. Bryceson YT, March ME, Ljunggren HG, Long EO. 2006. Activation, coactivation, and costimulation of resting human natural killer cells. Immunol Rev **214**:73-91.

46. Krzewski K, Gil-Krzewska A, Nguyen V, Peruzzi G, Coligan JE. 2013. LAMP1/CD107a is required for efficient perforin delivery to lytic granules and NK-cell cytotoxicity. Blood **121**(23):4672-4683.

47. Holliday DL, Speirs V. 2011. Choosing the right cell line for breast cancer research. Breast Cancer Res **13**(4):215.

48. Phillips GD, Fields CT, Li G, Dowbenko D, Schaefer G, Miller K, Andre F, Burris HA, 3rd, Albain KS, Harbeck N, Dieras V, Crivellari D, Fang L, Guardino E, Olsen SR, Crocker LM, Sliwkowski MX. 2014. Dual targeting of HER2-positive cancer with

trastuzumab emtansine and pertuzumab: Critical role for neuregulin blockade in antitumor response to combination therapy. Clin Cancer Res **20**(2):456-468.

49. Bartelt RR, Cruz-Orcutt N, Collins M, Houtman JC. 2009. Comparison of T cell receptor-induced proximal signaling and downstream functions in immortalized and primary T cells. PLoS One **4**(5):e5430.

50. Valabrega G, Montemurro F, Aglietta M. 2007. Trastuzumab: Mechanism of action, resistance and future perspectives in HER2-overexpressing breast cancer. Ann Oncol **18**(6):977-984.

51. Chan CJ, Smyth MJ, Martinet L. 2014. Molecular mechanisms of natural killer cell activation in response to cellular stress. Cell Death Differ **21**(1):5-14.

52. Baychelier F, Vieillard V. 2013. The modulation of the cell-cycle: A sentinel to alert the NK cells of dangers. Front Immunol **4**:325.

53. Roda JM, Parihar R, Magro C, Nuovo GJ, Tridandapani S, Carson WE, 3rd. 2006. Natural killer cells produce T cell-recruiting chemokines in response to antibody-coated tumor cells. Cancer Res **66**(1):517-526.

54. Anegon I, Cuturi MC, Trinchieri G, Perussia B. 1988. Interaction of Fc-receptor (Cd16) ligands induces transcription of interleukin-2 receptor (Cd25) and lymphokine genes and expression of their products in human natural-killer cells. J Exp Med **167**(2):452-472.

55. Cooper MA, Fehniger TA, Caligiuri MA. 2001. The biology of human natural killer-cell subsets. Trends Immunol **22**(11):633-640.

56. Nagler A, Lanier LL, Cwirla S, Phillips JH. 1989. Comparative studies of human Fcriii-positive and negative natural-killer cells. J Immunol **143**(10):3183-3191.

57. Geller MA, Miller JS. 2011. Use of allogeneic NK cells for cancer immunotherapy. Immunotherapy **3**(12):1445-1459.

58. Alter G, Malenfant JM, Altfeld M. 2004. CD107a as a functional marker for the identification of natural killer cell activity. J Immunol Methods **294**(1-2):15-22.

59. Bryceson YT, March ME, Barber DF, Ljunggren HG, Long EO. 2005. Cytolytic granule polarization and degranulation controlled by different receptors in resting NK cells. J Exp Med **202**(7):1001-1012.

60. Kwant-Mitchell A, Pek EA, Rosenthal KL, Ashkar AA. 2009. Development of functional human NK cells in an immunodeficient mouse model with the ability to provide protection against tumor challenge. PLoS One **4**(12):e8379.

61. Inoue H, Tani K. 2014. Multimodal immunogenic cancer cell death as a consequence of anticancer cytotoxic treatments. Cell Death Differ **21**(1):39-49.

62. Garg AD, Martin S, Golab J, Agostinis P. 2014. Danger signalling during cancer cell death: Origins, plasticity and regulation. Cell Death Differ **21**(1):26-38.

63. Bianchi ME. 2014. Killing cancer cells, twice with one shot. Cell Death Differ **21**(1):1-2.

64. Ni J, Miller M, Stojanovic A, Garbi N, Cerwenka A. 2012. Sustained effector function of IL-12/15/18-preactivated NK cells against established tumors. J Exp Med **209**(13):2351-2365.

65. Morvan MG, Lanier LL. 2016. NK cells and cancer: You can teach innate cells new tricks. Nat Rev Cancer **16**(1):7-19.

66. Agaugue S, Marcenaro E, Ferranti B, Moretta L, Moretta A. 2008. Human natural killer cells exposed to IL-2, IL-12, IL-18, or IL-4 differently modulate priming of naive T cells by monocyte-derived dendritic cells. Blood **112**(5):1776-1783.

67. Park JH, Geyer MB, Brentjens RJ. 2016. CD19-targeted CAR T-cell therapeutics for hematologic malignancies: Interpreting clinical outcomes to date. Blood **127**(26):3312-3320.

CHAPTER 4

RESULTS, CONCLUSIONS, AND FUTURE STUDIES

4.1. Summary of Chapter 2

4.1.1. Study Motivation

Cell surface regulates the behavior of cells toward their surrounding environment. As discussed in Chapter 1, cell surface engineering is a powerful tool for cell therapy because remodeling of cell surface with biomaterials can change the cell adhesion, migration, cellular activities, and cell-to-cell interaction for specific purposes. Indeed, genetic modification, which is the most advanced strategy available today, has revolutionized the field of cell therapy through the generation of tailor-made therapeutic cells. Although a large number of genetically modified cells have entered oncology clinical trials in the past decade, smoother clinical transition of these cells has been blocked by their stigma related to safety and lengthy production time.[1-3] One of the disadvantages of genetic engineering is that it can only generate proteins, receptors, and biomolecules within the realm of cellular biosynthesis with variable expression efficiency. In other words, genetic modification limits the manipulative freedom of modifying cells. Therefore, surface modification methods—aside from the genetic engineering discussed in Chapter 1—should be applied to incorporate many therapeutic and diagnostic materials, including small molecule drugs, polymers, proteins, nanoparticles, fluorescent tags, and

imaging agents. In Chapter 2, studies were designed to demonstrate the use of hydrophobic interactions to modify cells for enhanced cell migration and improved cell tracking.

4.1.2. Hypothesis

Cell surface engineering with hydrophobic interaction allows noninvasive and nontoxic incorporation of biomaterials into the cell membrane. This technology allows homogeneous and rapid modification of the cell membrane. Because any biomaterials hydrophobized with lipid conjugation can theoretically be embedded into the cell membrane, applications of cell surface engineering through hydrophobic interaction would allow cells to be modified with a small protein or a magnetic resonance imaging (MRI) contrast agent.

4.1.3. Key Study Results

Mesenchymal stem cells (MSCs) expressing chemokine receptors CXCR4 migrate toward the SDF-1 gradient established by injured cardiomyocytes in the ischemic heart.[4,5] As described in Chapter 1, SDF-1 expression decreases after 4-7 days of myocardial infarction (MI). Thus, surface engineering of MSCs with CXCR4, as demonstrated by Won et al., can enhance the migration of *ex vivo* expanded MSCs for early cardiac muscle repair.[6] As the expression of SDF-1 decreases over time, cardiomyocytes in the infarct border zone begin to express CXCR4.[7] It has been reported that the delivery of cell mixtures containing whole bone marrow mononuclear cells and SDF-1 expressing MSCs has improved the cardiac function in MI patients who missed the SDF-1 therapeutic window for the delivery of MSCs expressing CXCR4.[8] This observation

indicated that the surface engineering of MSCs with SDF-1 could be beneficial for homing MSCs to the ischemic heart in later stages of acute MI. In order to test the enhanced migration, MSCs were first modified with DMPE-PEG-SDF-1. Different amounts of DMEP-PEG-SDF-1 uniformly modified the MSCs. Similar to the results reported by Won et al., SDF-1 modified MSCs showed enhanced migration when exposed to increasing concentrations of CXCR4.

Next, Jurkat cells were surface-engineered with MRI contrast agents to test the possibility of real-time visualization. Superparamagnetic iron oxide nanoparticles (SPIONs) are popular imaging agents for MRI due to their ability to produce sharp image contrasts. Internalization of surface-coated SPIONs is often required to label therapeutic cells for *in vivo* tracking.[9,10] With this approach, the risk of releasing iron ions from the SPION core increases as the internalized surface-coated SPIONs undergo endocytosis and experience the low pH environment of lysosomal compartments.[11,12] Ultimately, dismantled surface-coated SPIONs may alter the cell homeostasis and induce cytotoxicity.[10,13] To overcome this challenge, fluorescently labeled surface-coated SPIONs were hydrophobized with DMPE-PEG molecules and subsequently applied onto Jurkat cells. Surface modification with DMPE-PEG-SPION-FITC did not affect the viability or cell proliferation. Most importantly, Jurkat cells modified with different amounts of DMPE-PEG-SPION-FITC showed dosage-dependent MRI signal intensity.

4.1.4. Conclusion

Cell surface engineering with hydrophobic interaction instantaneously changes the properties of cells without sacrificing cell viability and cellular functions. As demonstrated

by the SDF-1-embedded MSCs and SPION-modified Jurkat cells, surface modification through hydrophobic interaction reliably transforms ordinary cells for enhanced target site-homing effects and real-time cell tracking. Many different types of cells can be modified with a wide range of biomaterials through hydrophobic interaction, and these therapeutic cells with special functions can be employed to improve the therapeutic benefits of cell therapy.

4.2. Summary of Chapter 3

4.2.1. Study Motivation

Historically, many conventional chemotherapeutic agents have been thought to impair host immunosurveillance against tumors. Recent combinational cancer therapies have shown that the ability of low dose chemotherapeutic agents to work in concert with the host innate and adaptive immune systems is essential to stimulate potent anti-cancer activity inducing cancer cell death.[14-17] Many combinatorial therapies have introduced monoclonal antibodies in order to bridge the anti-cancer activities of chemotherapeutic agents with the host immune system; hence chemoimmunotherapy has been in the spotlight.[18-22] Antibodies are particularly proficient in this role because of their high specificities against tumor-associated antigens (TAAs), minimal off-target effects, low risk of immunogenicity, high rate of promoting immunologic memory, and circulation longevity. Antibodies in action will bind to the TAAs expressed on cancer cells and subsequently initiate cell death signaling, antibody-dependent cellular cytotoxicity (ADCC), antibody dependent phagocytosis, and complement-dependent cytotoxicity (CDC).[23] A summary of the immunomodulatory mechanisms of chemotherapeutic agents

and antibodies is provided in Table 4.1. The interaction of cytotoxic agents and antibodies with the immune system has fueled the development of a delivery strategy that can tie all three components together.

To achieve stronger anti-cancer activity, decades of research aimed to enhance the potency of antibodies have successfully conjoined chemotherapy with antibodies to generate the antibody-drug conjugates (ADCs).[24] In addition to the distinctive characteristics of antibodies, these new therapeutic antibodies specifically deliver toxic chemotherapeutic agents to certain types of cancer cells for the interest of maximizing the therapeutic benefits with low off-target effects. Several ADCs, including Trastuzumab-DM1 (T-DM1) and Brentuximab vedotin, are available in the market, and other ADCs are currently undergoing clinical investigation.[25,26]

Chemotherapeutic agents, antibodies, and ADCs as immunomodulators recruit a number of different effector cells—including natural killer (NK) cells, dendritic cells (DCs), tumor-specific T cells, and tumor-associated macrophages—to the tumor site as shown in Table 4.1.[14,15,27] As a crucial component of the innate immune system, NK cells have been involved in preventing abnormal neoplastic growth.[27] Unfortunately, tumor cells often evade the immunosurveillance by establishing a supportive microenvironment for undisturbed tumor growth. Cytolytic activity of autologous NK cells is thus suppressed as the cells encounter self-MHC expressing tumor cells and weakened by preexisting diseases.[28] Moreover, patients experiencing a high dose chemotherapy and ionizing radiotherapy display a significantly reduced NK cell population.[29,30] In order to achieve sufficient anti-cancer efficacy, an adequate number of immune effector cells must be maintained.[31,32] Although infusion of allogeneic NK cells shows beneficial

Table 4.1 Immunomodulatory functions of chemotherapeutic agents and antibodies

Drug	Effect on Tumor	Effect on Immune System
Sunitinib	• Blocks multiple tumor-associated tyrosine kinases, including VEGFR and PDGFR	• Blocks STAT3 • Decreases numbers and effectiveness of MDSCs and T_{Reg} cells • Blocks VEGF signaling
Imatinib	• Blocks multiple tumor-associated tyrosine kinases, including ABL and KIT • Increases TRAIL expression	• Blocks IDO • Decreases number and effectiveness of T_{Reg} cells • Promotes DC–NK cell crosstalk • Increases the number of B-1 B cells (without memory) • Increases the amount of 'natural' anti-cancer carbohydrate antibodies
Trastuzumab	• Blocks growth signaling through HER2	• Primes anti-cancer CTLs • Boosts NK cell secretion of IFN-γ and ADCC
Bevacizumab	• Blocks angiogenesis	• Increases DC maturation • Promotes DC differentiation toward mature DCs instead of MDSCs • Increases DC priming of T cells
Temsirolimus, rapamycin and other mTOR inhibitors	• Blocks mTOR pathway	• Enhances $CD8^+$ T cell activation and IFN-γ production, • Augments $CD8^+$ T cell differentiation into memory T cells • Impairs the homeostasis of T_{Reg} cells • Decreases IDO expression • Augments the responsiveness of T_{Reg} cells to antigen
JAK2 inhibitors	• Blocks JAK2 signaling in tumor cells	• Enhances DC maturation • Bolsters DC-mediated antigen presentation and T cell priming • Decreases immunosuppressive STAT3 signaling, decreases IAP expression and decreases tumor cell PDL1 expression

Table 4.1 (Continued)

Drug	Effect on Tumor	Effect on Immune System
HSP90 inhibitors	• Blocks HSP90, which increases unfolded protein-associated stress in tumor cells • Increases expression of NKG2D ligands	• Recognition of NKG2D ligand on tumor cells by CTL • Decreases cytokine secretion from macrophages and T cells • Decreases expression of co-stimulatory molecules on DCs and • Decreases antigen presentation by DCs
PI3K-AKT inhibitors	• Decreases PI3K-AKT signaling in tumor cells • Decreases prosurvival signaling • Decreases tumor-promoting inflammation	• Increases tumor susceptibility to perforin and granzyme-mediated lysis by CTLs and NK cells
IAP inhibitors	• Sensitizes tumor cells to apoptosis	• Increases T cell, NK cell and NKT cell responses to stimulation
Gemcitabine	• Antigen presentation • Inhibition of MSCs and B cells	• Increases antigen cross-presentation • Partial activation of dendritic cells • Priming of APCs for CD40 signal • Killing subsets of APC • Inhibition of regulatory cells
Anthracyclines	• HMGB1 release • Cell-surface calreticulin	• Increases antigen uptake T-cell activation • Increases T cell-dependent anti-cancer effects
Oxaliplatin	• HMGB1 release	• Increases T cell activation • Increases T cell-dependent anti-cancer effects

Table 4.1 (Continued)

Drug	Effect on Tumor	Effect on Immune System
5-Fluorouracil	• Increases HSP production	• Increases local tumor-antigen cross-presentation • T-cell activation • Suppresses T_{Reg} cells
Cisplatin	• Decreases succinate dehydrogenase activity • Increases CD95 expression	• Increases local tumor-antigen cross-presentation • T-cell activation • MDSCs suppression
Taxanes	• Inhibition of M2 macrophages • Upregulation of mannose-6-phosphate receptors	• Inhibition of regulatory cells • Perforin and granzyme-mediated lysis by CTLs and NK cells • Macrophage induced DC, NK, and T cell activation
Cyclophosphamide	• Inhibition of T_{Reg} cells Self-peptide–MHC class I complexes	• Inhibition of regulatory cells • Generation of memory T cells • Increases NK cell activation

Abbreviation:
ADCC, antibody-dependent cellular cytotoxicity; APC, antigen presenting cells; CTL, cytotoxic T lymphocyte; DC, dendritic cell; HSP90, heat shock protein 90; IAP, inhibitor of apoptosis protein; IDO, indoleamine-pyrrole 2,3-dioxygenase; JAK2, janus kinase 2; MDSC, myeloid-derived suppressor cell; MHC, major histocompatibility complex; mTOR, mammalian target of rapamycin NK, natural killer; NKG2D, natural killer group 2, member D; PDGFR, platelet-derived growth factor receptor; PDL1, PD1 ligand 1; STAT3, signal transducer and activator of transcription 3; T_{Reg} cells, regulatory T cells; TRAIL, tumour-necrosis-factor-related apoptosis-inducing ligand; VEGF, vascular endothelial growth factor; VEGFR, VEGF receptor.

Adapted from Zitvogel et al.,[16] Vanneman et al.,[33] and Bracci et al.[15]

graft-versus leukemia (GVL) effects with minimal risk of inducing graft-versus-host diseases (GVHD),[34] the supply of large amounts of NK cells is limited due to the low number of NK cells present in the donor's blood.[28] Fortunately, several NK cell lines, such as NK92, HANK-1, KHYG-1, NK-YS, NKG, YT, YTS, and NKL have been developed; however, NK92 cells constitute the only cell line approved for testing that demonstrates reliable *ex vivo* expansion and consistent cytotoxicity against target cells.[27,28,34] Comparisons among T cells, peripheral blood NK cells and NK92 cells are shown in Table 4.2. Despite the optimism surrounding NK92 development, clinical studies with NK92 have shown at most mild responses in patients with solid tumors.[27,28,35-37] Nevertheless, NK92 cells have increasingly become favorable cell-based immunotherapeutic agents while the method of redirecting cytolytic activity of T cells using the chimeric antigen receptors (CARs) has continued to show fatal adverse effects.[28,34,38-40] Currently, genetic modification to express CARs, CD16, and NKG2D—in order to empower NK92—has been studied to improve the anti-cancer responsiveness of NK92 cells.[41-44] These genetically engineered NK92 cells also bear limitations—such as inefficient gene transfer efficiency, development of endogenous immune responses against the viral components, possibility of mutagenesis, uncontrolled persistence of genetically modified NK, inability to administrate repeatedly, and inability to achieve systemic dose escalation—that allow us to conclude that preserving the transient anti-cancer activity of NK92 cells is much safer than the genetic modification approach.[34,45-48] Nonetheless, NK92 cells lack functionality to specifically target cancer cells; therefore, a new method for cancer targeted delivery of NK92 cells must be developed for effective chemoimmunotherapy.

Table 4.2. Comparison of T cells, peripheral blood NK cells, and NK92 cells

Parameter	T cells	NK cells	NK92 cells
Collection	Leukopheresis	Leukopheresis	Continuously growing activated NK cells
Preparation	Activation of cells with anti-CD3/CD28 beads MHC must be matched for allogeneic donor cells	Low population of NK cells Enrichment required for autologus NK cells MHC must be matched for allogeneic donor cells or alloreactive T cells must be depleted.	No processing necessary prior to surface engineering or CAR engineering
Expansion	Flasks, bags or wave® expansion system	Feeder cells are required with IL-2 Flasks, bags or bioreactors	Serum-free media without feeder cells IL-2 required
Gene Transduction	Lentiviral system 30% transduction	Low transduction efficiency with viral vectors	Roughly 50% transfection efficiency
Cytotoxic mechanisms	Expression of CAR is required Inactivated when tumor antigen is lost	Multiple cytolytic receptors Fc receptor dependent cytotoxicity	Multiple cytolytic receptors
Adverse events	CAR-T cells "off target" effects Prolonged survival in the patient circulation increases the risk of adverse effects. Can induce cytokine storm	Limited life span in patients No concern about persistence	Limited life span in patients No concern about persistence
Clinical results	CAR-T cells: Phase I studies have shown clinical benefits CAR-T cells Phase II ongoing	Prof of clinical benefits pending	Prof of clinical benefits pending
Off-the-shelf formulation	Autologus T cells require separate preparation for each patients	Donor NK cell cryopreservation is possible but recovery is poor	Cryopreservation is well-tolerated Easily expanded upon thawing

Adapted from Klingemann.[47]

ADC technology has certainly revolutionized cancer immunotherapy. Nevertheless, it has a critical limitation to be a stand-alone treatment: only a small percentage of administrated ADCs localizes at the tumor site.[49] The host immune system may not be able to recognize and exert anti-cancer effects due to low numbers of antibodies bound on cancer cells intended to induce apoptosis. Because the number of tumor-infiltrating NK cells has been shown to be indistinguishable from the NK cell population in normal tissues,[50] the probability of observing the benefits of chemoimmunotherapy using ADCs alone may depend on the sensitivity of host immune system. Therefore, an innovative strategy to concurrently deliver activated allogenic NK92 cells with ADCs is necessary in order to reach the full therapeutic capacity of chemoimmunotherapy.

4.2.2. Hypothesis

Lipid-conjugated ADCs can modify NK92 cells through hydrophobic interaction to generate surface-engineered NK92 cells with ADCs (SE-NK/ADC cells). The study was designed to investigate the following hypotheses: (1) SE-NK/ADC cells would specifically migrate toward the target tumor site through the recognition of target cancer cells by ADCs, (2) ADCs would induce apoptosis in the target cancer cells, (3) NK92 cells concurrently delivered at the tumor tissues with ADCs would recognize the apoptotic cancer cells, and (4) NK92 cells would further destroy the dying cancer cells. In order to test these hypotheses, NK92 cells were surface-engineered with T-DM1 (SE-NK/T-DM1 cells), and the *in vitro* and *in vivo* effects of SE-NK/T-DM1 cells on Her2-positive and Her2-negative cancer cells were analyzed.

4.2.3. Key Study Results

T-DM1 was generated by conjugating trastuzumab (TZ) with 10 molar excess of linker-conjugated DM1. When tested against Her2-positive SK-BR-3 cells, synthesized T-DM1 showed comparable cytotoxicity to Kadcyla® (ado-trastuzumab emtansine). The SE-NK/T-DM1 cells were prepared by incubating NK92 cells with lipid-conjugated T-DM1. Incubation of SE-NK/T-DM1 cells or co-treatment of T-DM1 and NK92 cells (T-DM1+NK92 cells) with Her2-positive SK-BR-3 cells for 24 hours showed increased cancer cell death compared to the individual effects of T-DM1 or NK92 cells. There were no differences detected between the treatments of SE-NK/T-DM1 cells and T-DM1+NK92 cells when both treatments were incubated for 24 hours. However, when SE-NK/T-DM1 cells and T-DM1+NK92 cells were incubated for short period of time, washed to remove unbound NK92 cells, and incubated for 24 hours, the SE-NK/T-DM1 cells induced a significantly greater number of cancer cell deaths than did the co-treatment. This result indicates that the surface embedded T-DM1 was able to deliver NK92 cells toward the Her2-positive cancer cells. In Her2-negative MDA-MB-231 cells, only the cytolytic activity of NK92 cells was observed. In order to examine the individual effects of NK92 cells and T-DM1 on SE-NK/T-DM1cells, NK92 cells were modified with TZ (SE-NK/TZ cells), and Jurkat cells were modified with TZ (SE-JK/TZ cells) and T-DM1 (SE-JK/T-DM1 cells). Jurkat cells did not show cytolytic activity against SK-BR-3 cells or MDA-MB-231 cells. When SE-JK/T-DM1 cells, SE-JK/TZ cells, and T-DM1 were treated with SK-BR-3 cells, only the cytotoxicity of T-DM1 was observed. When SE-NK/TZ cells, SE-NK/T-DM1 cells, and T-DM1 were incubated with SK-BR-3 cells, NK92 cells amplified the effects of TZ and T-DM1. As

expected, the treatment of SE-NK/T-DM1 cells induced the greatest number of cancer cell deaths compared to other treatments. Next, the cytolytic activity of NK92 cells was identified by comparing SE-JK/TZ cells and SE-NK/TZ cells. When incubated with SK-BR-3 cells, SE-NK/TZ cells induced a greater number of cancer cell deaths compared to SE-JK/TZ cells. Similarly, the cytotoxicity of SE-JK/T-DM1 cells and SE-NK/T-DM1 cells were compared *via* incubation with SK-BR-3 cells. Again, SE-NK/T-DM1 cells showed the greatest anti-cancer activity, and only the anti-cancer activity of NK92 cells was visible in Her2-neative MDA-MB-231 cells when they were incubated with the same treatments. These results indicated that the cytotoxicity of SE-NK/T-DM1 cells results from a combination of anti-cancer activities of T-DM1 and NK92 cells.

The mechanism of NK92 cell activity was examined. Addition of interleukin-2 (IL-2) induced the release of interferon-γ (IFN-γ) from NK92 cells and improved the cytolytic activity of unmodified NK92 cells against SK-BR-3 cells. Although IL-2 induced the SE-NK/T-DM1 cells to release IFN-γ, there was no difference in cytotoxicity against SK-BR-3 cells between SE-NK/T-DM1 cells with or without IL-2. This indicates that the cytotoxicity did not result solely from the release of cytokines from NK92 cells. Perforin and granzyme release was indirectly measured by analyzing the expression level of degranulation marker CD107a. Compared to the control and T-DM1+NK92 cells, the SE-NK/T-DM1 cells expressed a higher level of CD107a when incubated with SK-BR-3 cells. No significant expression of CD107a was observed when the SE-NK/T-DM1 cells were incubated with MDA-MB-231 cells. These results indicate that the cytotoxic activity of NK92 cells in SE-NK/T-DM1 cell formulation was attributable to the perforin and granzyme release.

In vivo efficacy of SE-NK/T-DM1 cells was examined in female NOD scid gamma (NSG, NOD-*scid* IL2Rg^{null}) mice. NSG mice bearing Her2-positive Calu-3 tumors were injected weekly with T-DM1, 1×10^7 NK cells, 1×10^7 T-DM+NK92 cells, 1×10^6 SE-NK/T-DM1 cells, and 1×10^7 SE-NK/T-DM1 cells for 3 weeks. At the end point, SE-NK/T-DM1 cells significantly suppressed the Calu-3 tumor growth when compared to the T-DM1+NK92 cells. Adverse effects related to the administration of SE-NK/T-DM1 cells were not observed, for body weights did not change over the treatment course. When MDA-MB-231 cells were exposed to similar treatments, only the effects of NK92 cells were observed. A biodistribution study was conducted 24 hours after the administration of 1×10^7 NK92 cells, 1×10^7 T-DM1+NK92 cells, and 1×10^7 SE-NK/T-DM1 cells. NK92 cells were detected by flow cytometry from the single-cell suspension prepared from each harvested organ. Animals treated with SE-NK/T-DM1 cells showed significantly higher accumulation of NK92 cells in the tumor site than other treatments.

4.2.4. Conclusion

Chemotherapy and immunotherapy were successfully integrated to generate SE-NK/T-DM1 cells. Surface engineering of T-DM1 on NK92 cells did not induce cytotoxicity. Although T-DM1 dissociated from the SE-NK/T-DM1 cells over time, a significant amount of T-DM1 was available on the NK92 cell membrane for up to 48 hours. *In vitro* and *in vivo* experiments have demonstrated the antigen-specific cytolytic activity of SE-NK/T-DM1 cells. The cytotoxicity of SE-NK/T-DM1 cells resulted from the combined activities of T-DM1 and NK92 cells. Moreover, SE-NK/T-DM1 cells

significantly suppressed the tumor growth in Her2-positive Calu-3 animal models compared to T-DM1+NK92 cells. The *in vivo* biodistribution study confirmed that T-DM1 on the surface of NK92 cells enhanced the tumor-targeted migration of SE-NK/T-DM1 cells. As demonstrated by SE-NK/T-DM1 cells, transient surface modification with ADCs could redirect active immune cells toward tumor tissue with enhanced anti-cancer efficacy. As ADC technology continues to develop, surface-engineered immune cells with ADCs may progressively act as potent chemoimmunotherapeutic agents directed toward various tumor antigens.

4.3. Future Studies

As stated throughout this dissertation, cell surface engineering with hydrophobic interaction is a noninvasive, nontoxic, reliable, and rapid surface chemistry that provides transient modifications to various types of cells. Any synthetic and natural biomaterials that can be hydrophobized with lipid conjugations can potentially be incorporated into the cell membrane. Experimental studies presented in Chapter 2 and Chapter 3 demonstrated proof of the concept that cells can be remodeled for a specific purpose by modifying the cell surface with bioactive materials. While the objectives of each study have been accomplished, additional studies must be conducted to provide a comprehensive analysis of the surface-engineered therapeutic cells for possible clinical transition.

4.3.1. Risk of Differentiation and *In Vivo* Migration of SDF-1 Modified MSCs

Lipid-conjugated SDF-1 uniformly modified the MSCs in Chapter 2. The effects of membrane-anchored SDF-1 were not thoroughly investigated. Tang et al. reported that

MSCs could differentiate into endothelial-like cells when exposed to 50 ng/mL of SDF-1 for 14 days.[51] Although the retention time of membrane-embedded SDF-1 is short, the effects of grafting SDF-1 onto the MSC membrane should be evaluated in terms of cell differentiation. Tang et al. stated that MSC differentiation due to SDF-1 exposure could be suppressed by treating the MSCs with the inhibitor N^G-nitro-L-arginine methyl ester (L-NAME).[51] Transient modification with SDF-1 with surface engineering may be beneficial to avoid the differentiation of MSCs.

In order to investigate the potential MSC differentiation due to the surface-embedded SDF-1, unmodified MSCs; SDF-1 surface-engineered MSCs; MSCs with equivalent amount of free SDF-1; MSCs with free SDF-1 (50 ng/mL); SDF-1 surface-engineered MSCs with L-NAME; SDF-1 with equivalent free SDF-1 and L-NAME; and MSCs with free SDF-1 (50 ng/mL) and L-NAME should be incubated for 14 days. After the differentiation period, the expression levels of endothelial cell markers, such as CD31 and VIII-related factor, on the collected cells should be evaluated through flow cytometry and western blotting.[51]

Enhanced migration of surface-engineered MSCs with SDF-1 was demonstrated using a transwell system. SDF-1 modified MSCs demonstrated enhanced chemotaxis toward increasing CXCR4 concentrations. As reported in the literature, delivery of MSCs to the ischemic left ventricles takes advantage of the CXCR4/SDF-1 axis.[51-55] In earlier stages of acute myocardial infarction (MI), injured cardiomyocytes express SDF-1 in order to recruit the CXCR4-expressing MSCs for cardiac repair. However, the expression of SDF-1 declines in the injured sites, and the expression of CXCR4 on MSCs increases in later stages of acute MI. Won et al. demonstrated the enhanced migration of

CXCR4-modified MSCs toward SDF-1 at an early stage of acute MI.[6] Conversely, the SDF-1-modified MSCs, as introduced in Chapter 2, can be employed at the later stage of acute MI for enhanced migration toward CXCR4. In order to determine the benefits of enhanced MSC migration toward the ischemic heart, both systems should be evaluated in animal models of MI, preferably in rat models with rat MSCs, SDF-1 and CXCR4. Sprague-Dawley rats anesthetized with ketamine and xylazine should be intubated and ventilated for left anterior descending (LAD) artery ligation.[7,51,56] Successful performance of ligation can be confirmed by the blanching of myocardium distal to the ligation and electrocardiography.[57] To evaluate the homing effects of rCXCR4 and rSDF-1 at early and late stages of MI, the ligated animals should be administered CXCR4-modified rMSCs or rSDF-1-modified rMSCs at 24 hours or a week after the ligation procedure through tail vein infusion. Control groups should receive a thoracotomy with or without the injection of unmodified rMSCs, CXCR4-modified MSCs, or SDF-1-modified MSCs. Because of the characteristic CXCR4 and SDF-1 expressions at the infarcted sites as described above, rCXCR4-modified rMSCs are expected to accumulate in the injured heart in early stage MI, and rSDF-1 modified rMSCs should migrate toward the injured heart in late stage MI. The migration of surface-modified rMSCs and accumulation at the infarct site can be visualized using single-photon emission computed tomography (SPECT) or MRI by prelabeling the rMSCs with radioisotopes or MRI contrast agents.[58,59] Cardiac function parameters—including left ventricular ejection fraction (LVEF), left ventricular end-diastolic volume (LVEDV), left ventricular end-systole volume (LVESV), left ventricular stroke volume (LVSV), left ventricular cardiac output (LVCO), left ventricular cardiac index (LVCI), and left ventricular mass end diastolic (LVMASS-ED)—will be

analyzed by MRI before and 4 weeks after the administration of rMSCs.[60] Also, the heart will be harvested from each animal to compare the presence of cardiomyocytes and the degree of restored cardiac functions before and after the treatment through immunohistological staining, using antibodies specific for cardio Troponin I, GLUT1, GLUT4, PFK, GAPDH and p70s6k antibodies.[60] The presence of cardiomyocytes, glucose transporters, and glucose metabolism-related enzymes will indicate the regeneration of the damaged heart.

4.3.2. Relaxivity of SPIONs on Surface Modified Jurkat Cells

In Chapter 2, SPION-modified Jurkat cells were imaged using T2*-weighted sequence for MRI analysis. The primary objective was to visualize the presence of SPION-modified Jurkat cells using MRI. Other properties of SPION-modified Jurkat cells as MRI contrast agents have not been studied in this dissertation. One of the important properties of MRI contrast agents is relaxivity. Relaxivity indicates the ability of magnetic agents to increase the relaxation rate of the surrounding water proton spins.[61] In other words, relaxivity measures the sensitivity of the contrast agent to produce more distinguished MRI images. Because the relaxivity of identical contrast agents can be different due to temperature, field strength, and delivery methods, SPION-modified Jurkat cells may show different levels of relaxivity from free SPIONs. Unfortunately, MRI study designs and results of SPION-modified Jurkat cells are insufficient to calculate the relaxivity. The efficacy of an MRI contrast agent is not only determined by the pharmacokinetic properties but also by magnetic properties; hence, it is important to provide T1- and T2-relaxivities for SPION-modified Jurkat cells.[62]

Following the experimental designs described by Rohrer et al. and Shevtsov et al., relaxation rates R1 and R2 will be measured from agar phantoms containing a constant number of Jurkat cells modified with various amounts of SPIONs.[62,63] R1 of Jurkat cells with various concentrations of surface-modified SPIONs will be measured with a saturation recovery sequence. From the collected data, relaxation time T1 can be calculated with Equation 4.1 where S is the measured signal and S_o is a constant signal at equilibrium. Relaxation time T2 can be measured by multiple echoes on Jurkat cells

$$S = S_o\,(1\text{-}e^{(-TR/T1)}) \tag{4.1}$$

with various concentrations of surface-modified SPIONs. The collected data can be represented as an exponential decay with Equation 4.2. R1 and R2 can be acquired from

$$S = S_o\,(e^{(-TE/T2)}) \tag{4.2}$$

T1 and T2 using the inverse relationship (R1= 1/T1 and R2= 1/T2). Finally, linear plots can be obtained using the Equation 4.3 and 4.4 with the slopes of each plot, r1 and r2, representing the T1- and T2-relaxivities.

$$1/\Delta T1 = r1*[\text{SPIONs on Jurkat cells}] \tag{4.3}$$

$$1/\Delta T2 = r2*[\text{SPIONs on Jurkat cells}] \tag{4.4}$$

4.3.3. Internalization of Surface-Embedded SPIONs through Endocytosis

Surface-engineered SPIONs on Jurkat cells remained on the cell membrane; however, the long-term fate of membrane-embedded SIPONs has not been studied. In order to investigate the endocytosis of surface-embedded SIPONs, the presence of internalized SPIONs on unmodified Jurkat cells, Jurkat cells with surface-engineered SPIONs, and Jurkat cells with internalized SPIONS, should be determined over time. Jurkat cells with internalized SPIONs can be prepared by incubating Jurkat cells with SPIONs overnight in cell culture conditions. Unmodified Jurkat cells, Jurkat cells with surface-engineered SPIONs, and Jurkat cells with internalized SPIONs cells collected at different time points will be fixed and stained with Prussian blue dye to identify the endocytosed SPIONs.[64] Moreover, as Lim et al. demonstrated the visualization of endocytosed nanoclusters through TEM images; endocytosis of SPIONs by Jurkat cells can also be observed with TEM imaging.[65] Jurkat cells with surface-engineered SPIONs and Jurkat cells exposed to SPIONs for 30 minutes will be fixed and processed for TEM observation. Formation of macropinosomes, ruffle closures, cup closures, and presence of intracellular vesicles and endosomal vesicles may indicate the endocytosis of SPIONs by Jurkat cells.

4.3.4. Real-Time Tracking of Therapeutic Cells Modified with SPIONs

In Chapter 2, Jurkat cells were modified with the lipid-conjugated SPIONs and seeded on a phantom gel. MRI contrast agents on the cell surface were able to produce sharp contrast images. Prior to testing the real-time tracking ability of SPION-modified cells, the fate of dissociated SPIONs had to be determined. Dissociated SPIONs may have

followed the distribution pattern of SPION microbubbles that Barrefelt and coworkers have described.[66] Free SPIONs may have predominately accumulated in the lungs initially and then gradually shifted to the spleen and liver.[66] Macrophages in the lung displayed increased iron accumulation; however, macrophages of other organs followed the same pattern. Large accumulation of SPIONs in the organs was resolved over time, and signs of severe adverse effects were absent.[66]

In order to examine the dissociation of SPION-modified Jurkat cells into SPIONs and Jurkat cells, SPION-modified Jurkat cells will be generated using ^{125}I-labeled SPIONs. EDC/NHS-activated SPIONs can be radiolabeled with sulfo-SHPP and iodination reagent kit (Thermo Fisher Scientific, Waltham, MA) following the manufacture's protocol to generate ^{125}I-labeled SPIONs. Mice will be injected with ^{125}I-labeled SPION-modified Jurkat cells and blood samples will be collected at different time points up to 72 hours after the injection. Cells and serum will be separated by a density gradient centrifugation using Ficoll-Paque™ (Miltenyi Biotec, Bergisch Gladbach, Germany). Radioactivity of dissociated ^{125}I-labeled SPION will be detected in the serum faction using a liquid scintillation counter. Anti-human CD3 antibodies conjugated with magnetic beads will isolate Jurkat cells from the cell fraction, and the radioactivity from Jurkat cells will be measured. Attenuation of radioactivity in the cell faction indicates the loss of SPIONs from the Jurkat cell surface. Lastly, histological samples of major organs will be analyzed to examine the presence of dissociated SPIONs and Jurkat cells. After understanding the effects of dissociated SPIONs, real-time tracking of SPION-modified therapeutic cells can be evaluated in animal models.

4.3.5. Degree of DMPE-PEG Conjugation on SPIONs and T-DM1

The degree of DMPE-PEG conjugation on SPIONs and T-DM1 has not been analyzed. DMPE-PEG-NH_2 was conjugated on carboxyl-terminated SPIONs through EDC/NHS chemistry, and DMPE-PEG-NHS was attached to available primary amines of T-DM1. In order to complete the characterization of DMPE-PEG-SIPONs and DMPE-PEG-T-DM1 and to present them as "ready-to-use" tools, the degree of DMPE-PEG conjugation on both SPIONs and T-DM1 should be determined to provide consistent chemical properties. The degree of DMPE-PEG conjugation on SPIONs can be measured by comparing the concentrations of free carboxylic acid groups before and after the conjugation. Toluidine blue O dye absorption assay (TBO assay) is often used to determine the degree of carboxylation.[67] DMPE-PEG-SPIONs and unmodified SPIONs incubated with TBO solution should be repeatedly washed to remove excess TBO dyes. TBO dye can be desorbed from SPIONs *via* incubation in 20% SDS solution at 40°C for 30 minutes. The resulting supernatant can be measured at 625 nm to determine the concentration of free carboxylic aids.

The degree of DMPE-PEG conjugation on T-DM1 can be measured by comparing the concentrations of free primary amines before and after the conjugation. Colorimetric tests using 2,4,6-trinitrobenzene sulfonic acid (TNBSAor TNBS) quantitate free primary amines on proteins.[68] DMPE-PEG-T-DM1 and unmodified T-DM1 should be incubated with dilute TNBSA in 37°C for 2 hours. After the addition of 10% SDS stop solution, the change in absorbance can be measured at 335 nm.

Alternatively, the concentrations of conjugated DMPE-PEGs on SPIONs and T-DM1 can be determined by measuring the concentration of lipid chains after the modification.[69]

Fatty acid assay quantitatively measures the amount of free lipids with alkyl chains of 8-carbon or more. When analyzed with the assay, DMPE-PEG-SPIONs and DMPE-PEG-T-DM1 will generate colorimetric changes that can be measured at 570 nm. The absorbance measurements can be converted to the conjugated amount of lipids using a standard curve obtained with free DMPE.

4.3.6. Concentration-Dependent DMPE-PEG Toxicity

SDF-1-modified MSCs, SPION-modified Jurkat cells, and SE-NK/T-DM1 cells were generated by applying a small amount of DMPE-PEG conjugates onto a fixed number of cells. The tested amounts of DMPE-PEG conjugates did not show signs of cytotoxicity when applied to cells; however, the maximum tolerated amount of DMPE-PEG conjugates should be reported for safety assessment. As a study model, the cytotoxicity of increasing amounts of DMPE-PEGs and DMPE-PEG-T-DM1 up to 1 mg/mL should be evaluated on NK92 cell modification. The changes in cell viability and stress level can be examined through viability assay and lactate dehydrogenase (LDH) assay. Flow cytometric analysis of live and dead NK92 cells after the modification can be identified with calcein-AM and ethidium homodimer-1 dyes after the modification. LDH assay measures the level of LDH released from the cells with a damaged membrane. LDH released from the damaged cells converts resazurin into fluorescent resorufin, which can be detected with a fluorescent reader (560 nm/590 nm). LDH levels of NK92 cells after the modification, with increasing concentrations of DMPE-PEGs and DMPE-PEG-T-DM1, may represent the adverse effects occurring at the cell membrane.

4.3.7. Quantification of Internalized T-DM1

Upon binding to Her2, T-DM1 was transferred from the SE-NK/T-DM1 cells to target cancer cells. Although fluorescent imaging confirmed the presence of internalized T-DM1 in the cytoplasm of target cancer cells, a more quantitative approach to measure the concentration of T-DM1 in the cytoplasm should be conducted. Following the experimental procedures described in Chapter 3, Her2-positive and Her2-negative cancer cells should be treated with T-DM1, T-DM1 with geldanamycin, and SE-NM/T-DM1 cells for 30 minutes and the unbound cells should be removed. Cancer cells will be detached from the plate at 1-hour and 6-hour post-treatment and lysed *via* differential lysis. Fractions from the membrane and cytosol will be applied to human IgG ELISA. Colorimetric changes will be plotted to determine the amount of internalized T-DM1. Also, anti-human Fc antibodies will be used to detect the presence of T-DM1 in each lysate by western blotting. The efficiency of T-DM1 internalization *via* Her2 binding can be analyzed by comparing the T-DM1 concentrations on the membrane and in the cytosol.

4.3.8. Mechanism of SE-NK/T-DM1 Cells

Experimental results in Chapter 3 demonstrated that the incubation of SE-NK/T-DM1 cells with Her2-positive SK-BR-3 cells induced the expression of degranulation marker, CD107a, on NK92 cells. This observation indicates that NK92 cells released perforins and granzymes upon engaging apoptotic cancer cells. In a normal state, CD107a co-localizes with perforin/granzyme containing secretory lysosomes.[70,71] Upon NK92 cell activation, the lysosomes migrate towards the membrane and release perforin and granzymes *via* membrane fusion.[70,71] During this process, CD107a integrates into the

cell membrane for a brief moment and recycles back into the lysosome. Therefore, the expression of CD107a is indirect evidence of perforin and granzyme release. However, physical evidence of perforin and granzyme release needs to be provided. Quantitative analysis of released perforins and granzyme can be attained by analyzing the expression level of perforin, using flow cytometry, and then measuring the concentration of released granzymes with ELISA.

4.3.9. Pharmacokinetics of SE-NK/T-DM1 Cells

It is anticipated that the administered SE-NK/T-DM1 cells will dissociate into trastuzumab, DM1, and NK92 cells. Because NK92 cells are carrying T-DM1, all pharmacokinetic parameters of T-DM1—especially the drug exposure and clearance—may be different from T-DM1 as a single agent. Pharmacokinetics of NK92 cells may be difficult to obtain due to the fact that NK92 cells are living drugs. However, several studies have indirectly gathered some of the pharmacokinetic parameters, including organ accumulation time and circulation time, by analyzing the accumulation of NK92 cells in the organs by MRI imaging.[72-75] As demonstrated by CAR-T cells,[76] the circulating time of NK92 cells can also be determined by isolating the NK92 cells in the bloodstream of animals treated with SE-NK/T-DM1 cells. Pharmacokinetic properties of SE-NK/T-DM1 may be different from individual NK92 cells due to the membrane-anchored T-DM1. Therefore, studies to evaluate the *in vivo* stability of SE-NK/T-DM1 cells and their dissociation into NK92 cells, trastuzumab, and DM1 should be conducted to provide a better understanding of the *in vivo* behaviors of surface-engineered effector cells. Ponte et al. have conducted extensive

pharmacokinetic studies using [^{3}H]DM1 and have reported that the thiosuccinimide linkage in ADCsis less labile *in vivo* with only fractional loss of SMCC-DM1.[77] Similar experimental designs can be used to study the *in vivo* stability and pharmacokinetic of SE-NK/T-DM1. Radioactive T-[^{3}H]DM1 obtained from Creative Biolabs (NY, USA) can be hydrophobized with DMPE-PEG-NHS for surface engineering of NK92 cells. Blood samples should be collected at different time points after the administration of SE-NK/T-[^{3}H]DM1 cells. Serum and cells should be separated with a density gradient centrifugation using Ficoll-Paque™. Serum fractions can be applied on protein L-coated plates to detect the dissociated T-[^{3}H]DM1 and trastuzumab. After immobilizing T-[^{3}H]DM1 and trastuzumab on each well, radioactivity of each well should be measured with liquid scintillation counter to detect T-[^{3}H]DM1. Subsequently, anti-human Fc antibodies conjugated with HRP should be applied to collected supernatants from each well to quantify both T-[^{3}H]DM1 and trastuzumab. The radioactivity of collected supernatant can be measured to determine the amount of released [^{3}H]DM1. NK92 cells enriched from the cell fraction—using anti-human CD56 antibodies conjugated with magnetic beads—should be counted by flow cytometry. NK92 cells retaining T-[^{3}H]DM1 on the surface can be identified by applying fluorescently labeled anti-human Fc antibodies and measuring radioactivity. Moreover, histological studies should be conducted to evaluate the accumulation of SE-NK/T-DM1 cells or each individual component in all major organs. It is important to obtain these pharmacokinetic profiles in order to predict the *in vivo* behavior and estimate the appropriate dosage of SE-NK/T-DM1 cells.

4.3.10. Chou-Talalay Method of Combinatorial Effects

The anti-cancer efficacy of SE-NK/T-DM1 cells is a summed effect of T-DM1 and NK92 cells. The combinatorial effects of T-DM1 and NK92 cells in SE-NK/T-DM1 cells can be defined as synergism, additive effect, or antagonism through the Chou-Talalay method.[78,79] Many drug combinations proposed for cancer have been evaluated for synergetic effects with the Chou-Talalay method.[80-83] Although current employment of the Chou-Talalay method is fairly limited to examine the combinatorial effects of small molecular drugs and proteins, several studies have utilized the Chou-Talalay method to analyze synergetic effects of oncolytic herpes simplex viruses (HSV) and therapeutic proteins.[81,84,85] The experimental methods described by Cheema et al. can be modified to determine the synergy between T-DM1 and NK92 cells in SE-NK/T-DM1 cells; however, both *in vitro* and *in vivo* study results of SE-NK/T-DM1 cells reported in Chapter 3 are insufficient to conduct the Chou-Talalay analysis. In order to evaluate the combinatorial effects in SE-NK/T-DM1 cells, the anti-cancer effects of various concentrations of T-DM1 and different numbers of NK92 cells should be obtained as separate agents. Also, the anti-cancer effects of changing the concentration of T-DM1 and the number of NK92 cells in SE-NK/T-DM1 cells should be analyzed. The results acquired from each experiment can be used to obtain individual and combined dosage response curves and EC50 values that can be fit to Chou-Talalay models. Chou-Talalay combination indices (CIs) can be calculated for each fraction affected (Fa), i.e., level of cancer cell death using Equation 4.5, where Dx1 and Dx2 are the dosages of T-DM1 and NK92 cells required to reach a particular Fa, respectively, and D1 and D2 are the dosages of SE-NK/T-DM1 cells required to

reach the same Fa.[85] CI=1, CI>1, and CI<1 represent additive effect, antagonism, and synergism, respectively. CompuSyn software is available for computerized analytical simulations using the Chou-Talalay method.[78]

$$CI = (D1/Dx1) + (D2/Dx2) + (D1)(D2)/[(Dx1)(Dx2)] \quad (4.5)$$

4.3.11. Improving Cytotoxicity of NK92 Cells

The *in vivo* tumor efficacy study of Chapter 3 was conducted without any cytokine supplement. The anti-cancer activity of SE-NK/T-DM1 cells can be enhanced with supplementary cytokines, such as IL-2, IL-12, IL-15 and IL-18.[86-88] These cytokines regulate NK cell survival, proliferation and function. Ni et al. have reported that mouse NK cells preactivated with murine IL-12, IL-15, and IL-18 expressed high levels of IL-2Rα.[86] In the presence of $CD4^+$ T cells that secrete IL-2 tumor, high numbers of NK cells persisted and accumulated in the tumor tissue.[86] Similarly, Leong and colleagues have preactivated human NK cells with IL-12, IL-15, and IL-18 and adoptively transferred them to NSG mice.[89] With co-administration of IL-2, these preactivated NK cells showed enhanced survival, proliferation, IFN-γ production, and cytotoxicity. Therefore, administering NK92 cells with cytokine supplements can increase the persistence and effectiveness of the SE-NK/T-DM1 cells. As reported by Romee et al., NK92 cells should be preactivated in culture media containing 10 ng/mL of IL-12, 50 ng/mL of IL-18, and 1 ng/mL of IL-15 for 16 hours.[90] The *in vivo* anti-cancer efficacy and toxicity of SE-NK/T-DM1 cells should be compared with and without preactivation of NK92 cells. Once the effects of preactivated NK92 cells in SE-NK/T-DM1 cells are defined, coadministration of activating cytokines

and SE-NK/T-DM1 cells without the preactivation should be carefully conducted in animal models to develop a supplementary activation cocktail for the enhanced anti-cancer therapy of SE-NK/T-DM1 cells.[78,81]

4.3.12. Her2-Positive Breast Cancer and Hematological Cancers

Although SE-NK/T-DM1 demonstrated tumor growth suppression in Her2-positive Calu-3 lung cancer models, the studies were originally designed to test their efficacy in Her2-positive breast cancer models. Unfortunately, it was difficult to generate breast cancer models using Her2-positive cell lines due to poor tumorigenic potentials of SK-BR-3 cells.[91] Despite the difficulty in model generation, the SE-NK/T-DM1 cells should be tested against breast cancer since T-DM1 has been consistently supported with evidence as a treatment of breast cancer. In order to investigate the potential clinical impact, the anti-cancer activity of SE-NK/T-DM1 cells should be tested in patient-derived breast cancer xenograft models. DeRose et al. described an effective method to generate patient-derived tumor models that retain essential features of the original tumors.[92] Following the protocol, patient-derived breast cancer xenograft models may be generated by implanting a mixture of patient-derived Her2-positive cancer cells and MSCs onto the mammary fat pad of NOD-SCID mice.

CAR-T cells have advanced to provide therapeutic breakthrough for solid cancers. Current approaches of cancer-targeted drug delivery are limited to certain types of cancers with overexpressed tumor antigens. Because most of the antigens expressed in cancer cells are also expressed at low levels in healthy tissues, adverse on-target off-tumor effects may increase.[93] These observations indicate that continuous research is required to treat solid

tumors. Due to this fact, a significant number of CAR-T cell clinical trials continue to be focused on hematological cancers, such as lymphoma, acute lymphoblastic leukemia (ALL), chronic lymphocytic leukemia (CLL), B-cell acute lymphoblastic leukemia (B-ALL), non-Hodgkin's lymphoma (NHL), and diffuse large cell lymphoma (DLCL).[1,2,93] For the treatment of these malignant diseases, CAR-T cells targeting CD19, CD20, and CD22 have been developed and shown significant clinical success.[1,93,94] For the cell surface engineering approach, coltuximab ravtansine (SAR3419), an anti-CD19 monoclonal antibody conjugated with maytansinoid DM4, can be anchored on NK92 cells.[95] Recent reports on a Phase II study stated that coltuximab ravtansine was well tolerated with a low clinical response rate in ALL patients.[96] Alternatively, currently available CD19 antibodies for diagnostics can be conjugated with SMCC-DM1 to generate CD19-speicifc ADCs. Similar to T-DM1, these CD19-specific ADCs can be hydrophobized with DMPE-PEG for the surface engineering of NK92 cells.

4.4. References

1. Kershaw MH, Westwood JA, Darcy PK. 2013. Gene-engineered T cells for cancer therapy. Nat Rev Cancer **13**(8):525-541.

2. Kershaw MH, Westwood JA, Slaney CY, Darcy PK. 2014. Clinical application of genetically modified T cells in cancer therapy. Clin Transl Immunology **3**(5):e16.

3. Geyer MB, Brentjens RJ. 2016. Review: Current clinical applications of chimeric antigen receptor (CAR) modified T cells. Cytotherapy **18**(11):1393-1409.

4. Penn MS. 2009. Importance of the SDF-1:CXCR4 axis in myocardial repair. Circ Res **104**(10):1133-1135.

5. Penn MS, Pastore J, Miller T, Aras R. 2012. SDF-1 in myocardial repair. Gene Ther **19**(6):583-587.

6. Won YW, Patel AN, Bull DA. 2014. Cell surface engineering to enhance mesenchymal stem cell migration toward an SDF-1 gradient. Biomaterials **35**(21):5627-5635.

7. Zhang M, Mal N, Kiedrowski M, Chacko M, Askari AT, Popovic ZB, Koc ON, Penn MS. 2007. SDF-1 expression by mesenchymal stem cells results in trophic support of cardiac myocytes after myocardial infarction. Faseb J **21**(12):3197-3207.

8. Assmus B, Fischer-Rasokat U, Honold J, Seeger FH, Fichtlscherer S, Tonn T, Seifried E, Schachinger V, Dimmeler S, Zeiher AM, Registry T-C. 2007. Transcoronary transplantation of functionally competent BMCs is associated with a decrease in natriuretic peptide serum levels and improved survival of patients with chronic postinfarction heart failure: Results of the TOPCARE-CHD Registry. Circ Res **100**(8):1234-1241.

9. Li L, Jiang W, Luo K, Song HM, Lan F, Wu Y, Gu ZW. 2013. Superparamagnetic iron oxide nanoparticles as MRI contrast agents for non-invasive stem cell labeling and tracking. Theranostics **3**(8):595-615.

10. Singh N, Jenkins GJ, Asadi R, Doak SH. 2010. Potential toxicity of superparamagnetic iron oxide nanoparticles (SPION). Nano Rev **1**.

11. Arbab AS, Wilson LB, Ashari P, Jordan EK, Lewis BK, Frank JA. 2005. A model of lysosomal metabolism of dextran coated superparamagnetic iron oxide (SPIO) nanoparticles: Implications for cellular magnetic resonance imaging. NMR Biomed **18**(6):383-389.

12. Chen CC, Ku MC, D MJ, Lai JS, Hueng DY, Chang C. 2013. Simple SPION incubation as an efficient intracellular labeling method for tracking neural progenitor cells using MRI. PLoS One **8**(2):e56125.

13. Bulte JW, Douglas T, Witwer B, Zhang SC, Strable E, Lewis BK, Zywicke H, Miller B, van Gelderen P, Moskowitz BM, Duncan ID, Frank JA. 2001. Magnetodendrimers allow endosomal magnetic labeling and in vivo tracking of stem cells. Nat Biotechnol **19**(12):1141-1147.

14. Emens LA. 2010. Chemoimmunotherapy. Cancer J **16**(4):295-303.

15. Bracci L, Schiavoni G, Sistigu A, Belardelli F. 2014. Immune-based mechanisms of cytotoxic chemotherapy: Implications for the design of novel and rationale-based combined treatments against cancer. Cell Death Differ **21**(1):15-25.

16. Zitvogel L, Apetoh L, Ghiringhelli F, Kroemer G. 2008. Immunological aspects of cancer chemotherapy. Nat Rev Immunol **8**(1):59-73.

17. Chen G, Emens LA. 2013. Chemoimmunotherapy: reengineering tumor immunity. Cancer Immunol Immunother **62**(2):203-216.

18. Kahl B. 2008. Chemotherapy combinations with monoclonal antibodies in non-Hodgkin's lymphoma. Semin Hematol **45**(2):90-94.

19. Shebzukhov YV, Koroleva EP, Khlgatian SV, Lagarkova MA, Meshcheryakov AA, Lichinitser MR, Karbach J, Jager E, Kuprash DV, Nedospasov SA. 2005. Humoral immune response to thymidylate synthase in colon cancer patients after 5-FU chemotherapy. Immunol Lett **100**(1):88-93.

20. Eichhorst B, Fink AM, Bahlo J, Busch R, Kovacs G, Maurer C, Lange E, Koppler H, Kiehl M, Sokler M, Schlag R, Vehling-Kaiser U, Kochling G, Ploger C, Gregor M, Plesner T, Trneny M, Fischer K, Dohner H, Kneba M, Wendtner CM, Klapper W, Kreuzer KA, Stilgenbauer S, Bottcher S, Hallek M, Investigators IG, GCLLSG GCSG. 2016. First-line chemoimmunotherapy with bendamustine and rituximab versus fludarabine, cyclophosphamide, and rituximab in patients with advanced chronic lymphocytic leukaemia (CLL10): An international, open-label, randomised, phase 3, non-inferiority trial. Lancet Oncol **17**(7):928-942.

21. Heath VL, Bicknell R. 2009. Anticancer strategies involving the vasculature. Nat Rev Clin Oncol **6**(7):395-404.

22. Kay NE, Strati P, LaPlant BR, Leis JF, Nikcevich D, Call TG, Pettinger AM, Lesnick CE, Hanson CA, Shanafelt TD. 2016. A randomized phase II trial comparing chemoimmunotherapy with or without bevacizumab in previously untreated patients with chronic lymphocytic leukemia. Oncotarget **7**(48):78269-78280.

23. Scott AM, Wolchok JD, Old LJ. 2012. Antibody therapy of cancer. Nat Rev Cancer **12**(4):278-287.

24. Sievers EL, Senter PD. 2013. Antibody-drug conjugates in cancer therapy. Annu Rev Med **64**:15-29.

25. Diamantis N, Banerji U. 2016. Antibody-drug conjugates--An emerging class of cancer treatment. Br J Cancer **114**(4):362-367.

26. Peters C, Brown S. 2015. Antibody-drug conjugates as novel anti-cancer chemotherapeutics. Biosci Rep **35**(4).

27. Cheng M, Chen Y, Xiao W, Sun R, Tian Z. 2013. NK cell-based immunotherapy for malignant diseases. Cell Mol Immunol **10**(3):230-252.

28. Klingemann H, Boissel L, Toneguzzo F. 2016. Natural Killer Cells for Immunotherapy - Advantages of the NK-92 Cell Line over Blood NK Cells. Front Immunol **7**:91.

29. Verma R, Foster RE, Horgan K, Mounsey K, Nixon H, Smalle N, Hughes TA, Carter CR. 2016. Lymphocyte depletion and repopulation after chemotherapy for primary breast cancer. Breast Cancer Res **18**(1):10.

30. Park B, Yee C, Lee KM. 2014. The effect of radiation on the immune response to cancers. Int J Mol Sci **15**(1):927-943.

31. Fagnoni FF, Lozza L, Zibera C, Zambelli A, Ponchio L, Gibelli N, Oliviero B, Pavesi L, Gennari R, Vescovini R, Sansoni P, Da Prada G, Robustelli Della Cuna G. 2002. T-cell dynamics after high-dose chemotherapy in adults: Elucidation of the elusive CD8+ subset reveals multiple homeostatic T-cell compartments with distinct implications for immune competence. Immunology **106**(1):27-37.

32. Goldrath AW, Bevan MJ. 1999. Selecting and maintaining a diverse T-cell repertoire. Nature **402**(6759):255-262.

33. Vanneman M, Dranoff G. 2012. Combining immunotherapy and targeted therapies in cancer treatment. Nat Rev Cancer **12**(4):237-251.

34. Glienke W, Esser R, Priesner C, Suerth JD, Schambach A, Wels WS, Grez M, Kloess S, Arseniev L, Koehl U. 2015. Advantages and applications of CAR-expressing natural killer cells. Front Pharmacol **6**:21.

35. Tonn T, Becker S, Esser R, Schwabe D, Seifried E. 2001. Cellular immunotherapy of malignancies using the clonal natural killer cell line NK-92. J Hematother Stem Cell Res **10**(4):535-544.

36. Arai S, Meagher R, Swearingen M, Myint H, Rich E, Martinson J, Klingemann H. 2008. Infusion of the allogeneic cell line NK-92 in patients with advanced renal cell cancer or melanoma: A phase I trial. Cytotherapy **10**(6):625-632.

37. Suck G. 2006. Novel approaches using natural killer cells in cancer therapy. Semin Cancer Biol **16**(5):412-418.

38. Brudno JN, Kochenderfer JN. 2016. Toxicities of chimeric antigen receptor T cells: Recognition and management. Blood **127**(26):3321-3330.

39. Morgan RA, Yang JC, Kitano M, Dudley ME, Laurencot CM, Rosenberg SA. 2010. Case report of a serious adverse event following the administration of T cells transduced with a chimeric antigen receptor recognizing ERBB2. Mol Ther **18**(4):843-851.

40. DeFrancesco L. 2017. CAR-T's forge ahead, despite Juno deaths. Nat Biotechnol **35**(1):6-7.

41. Clemenceau B, Valsesia-Wittmann S, Jallas AC, Vivien R, Rousseau R, Marabelle A, Caux C, Vie H. 2015. In vitro and in vivo comparison of lymphocytes transduced with a human CD16 or with a chimeric antigen receptor reveals potential off-target interactions due to the IgG2 CH2-CH3 CAR-spacer. J Immunol Res **2015**:482089.

42. Chang YH, Connolly J, Shimasaki N, Mimura K, Kono K, Campana D. 2013. A chimeric receptor with NKG2D specificity enhances natural killer cell activation and killing of tumor cells. Cancer Res **73**(6):1777-1786.

43. Schonfeld K, Sahm C, Zhang C, Naundorf S, Brendel C, Odendahl M, Nowakowska P, Bonig H, Kohl U, Kloess S, Kohler S, Holtgreve-Grez H, Jauch A, Schmidt M, Schubert R, Kuhlcke K, Seifried E, Klingemann HG, Rieger MA, Tonn T, Grez M, Wels WS. 2015. Selective inhibition of tumor growth by clonal NK cells expressing an ErbB2/HER2-specific chimeric antigen receptor. Mol Ther **23**(2):330-338.

44. Esser R, Muller T, Stefes D, Kloess S, Seidel D, Gillies SD, Aperlo-Iffland C, Huston JS, Uherek C, Schonfeld K, Tonn T, Huebener N, Lode HN, Koehl U, Wels WS. 2012. NK cells engineered to express a GD2-specific antigen receptor display built-in ADCC-like activity against tumour cells of neuroectodermal origin. J Cell Mol Med **16**(3):569-581.

45. Levine BL. 2015. Performance-enhancing drugs: Design and production of redirected chimeric antigen receptor (CAR) T cells. Cancer Gene Ther **22**(2):79-84.

46. Hinrichs CS, Restifo NP. 2013. Reassessing target antigens for adoptive T-cell therapy. Nat Biotechnol 31(11):999-1008.

47. Klingemann H. 2014. Are natural killer cells superior CAR drivers? Oncoimmunology **3**:e28147.

48. Romanski A, Uherek C, Bug G, Seifried E, Klingemann H, Wels WS, Ottmann OG, Tonn T. 2016. CD19-CAR engineered NK-92 cells are sufficient to overcome NK cell resistance in B-cell malignancies. J Cell Mol Med **20**(7):1287-1294.

49. Teicher BA, Chari RV. 2011. Antibody conjugate therapeutics: Challenges and potential. Clin Cancer Res **17**(20):6389-6397.

50. Bruno A, Ferlazzo G, Albini A, Noonan DM. 2014. A think tank of TINK/TANKs: Tumor-infiltrating/tumor-associated natural killer cells in tumor progression and angiogenesis. J Natl Cancer Inst **106**(8):dju200.

51. Tang J, Wang J, Yang J, Kong X, Zheng F, Guo L, Zhang L, Huang Y. 2009. Mesenchymal stem cells over-expressing SDF-1 promote angiogenesis and improve heart function in experimental myocardial infarction in rats. Eur J Cardiothorac Surg **36**(4):644-650.

52. Askari AT, Unzek S, Popovic ZB, Goldman CK, Forudi F, Kiedrowski M, Rovner A, Ellis SG, Thomas JD, DiCorleto PE, Topol EJ, Penn MS. 2003. Effect of stromal-cell-derived factor 1 on stem-cell homing and tissue regeneration in ischaemic cardiomyopathy. Lancet **362**(9385):697-703.

53. Tang YL, Zhu W, Cheng M, Chen L, Zhang J, Sun T, Kishore R, Phillips MI, Losordo DW, Qin G. 2009. Hypoxic preconditioning enhances the benefit of cardiac progenitor cell therapy for treatment of myocardial infarction by inducing CXCR4 expression. Circ Res **104**(10):1209-1216.

54. Jane-wit D, Altuntas CZ, Johnson JM, Yong S, Wickley PJ, Clark P, Wang Q, Popovic ZB, Penn MS, Damron DS, Perez DM, Tuohy VK. 2007. Beta 1-adrenergic receptor autoantibodies mediate dilated cardiomyopathy by agonistically inducing cardiomyocyte apoptosis. Circulation **116**(4):399-410.

55. Dong F, Harvey J, Finan A, Weber K, Agarwal U, Penn MS. 2012. Myocardial CXCR4 expression is required for mesenchymal stem cell mediated repair following acute myocardial infarction. Circulation **126**(3):314-324.

56. Won YW, McGinn AN, Lee M, Bull DA, Kim SW. 2013. Targeted gene delivery to ischemic myocardium by homing peptide-guided polymeric carrier. Mol Pharm **10**(1):378-385.

57. Tang J, Wang J, Yang J, Kong X. 2008. Adenovirus-mediated stromal cell-derived-factor-1alpha gene transfer induces cardiac preservation after infarction via angiogenesis of CD133+ stem cells and anti-apoptosis. Interact Cardiovasc Thorac Surg **7**(5):767-770.

58. Yang Y, Schumacher A, Yang Y, Liu J, Shi X, Hill WD, Hu TC. 2011. Monitoring bone marrow-originated mesenchymal stem cell traffic to myocardial infarction sites using magnetic resonance imaging. Magn Reson Med **65**(5):1430-1436.

59. Kraitchman DL, Tatsumi M, Gilson WD, Ishimori T, Kedziorek D, Walczak P, Segars WP, Chen HH, Fritzges D, Izbudak I, Young RG, Marcelino M, Pittenger MF, Solaiyappan M, Boston RC, Tsui BM, Wahl RL, Bulte JW. 2005. Dynamic imaging of allogeneic mesenchymal stem cells trafficking to myocardial infarction. Circulation **112**(10):1451-1461.

60. Cai M, Shen R, Song L, Lu M, Wang J, Zhao S, Tang Y, Meng X, Li Z, He ZX. 2016. Bone Marrow Mesenchymal Stem Cells (BM-MSCs) improve heart function in swine myocardial infarction model through paracrine effects. Sci Rep **6**:28250.

61. Jacques V, Dumas S, Sun WC, Troughton JS, Greenfield MT, Caravan P. 2010. High-relaxivity magnetic resonance imaging contrast agents. Part 2. Optimization of inner- and second-sphere relaxivity. Invest Radiol **45**(10):613-624.

62. Rohrer M, Bauer H, Mintorovitch J, Requardt M, Weinmann HJ. 2005. Comparison of magnetic properties of MRI contrast media solutions at different magnetic field strengths. Invest Radiol **40**(11):715-724.

63. Shevtsov MA, Nikolaev BP, Yakovleva LY, Marchenko YY, Dobrodumov AV, Mikhrina AL, Martynova MG, Bystrova OA, Yakovenko IV, Ischenko AM. 2014. Superparamagnetic iron oxide nanoparticles conjugated with epidermal growth factor (SPION-EGF) for targeting brain tumors. Int J Nanomed **9**:273-287.

64. Kalber TL, Ordidge KL, Southern P, Loebinger MR, Kyrtatos PG, Pankhurst QA, Lythgoe MF, Janes SM. 2016. Hyperthermia treatment of tumors by mesenchymal stem cell-delivered superparamagnetic iron oxide nanoparticles. Int J Nanomedicine **11**:1973-1983.

65. Lim KS, Lee DY, Valencia GM, Won YW, Bull DA. 2015. Nano-self-assembly of nucleic acids capable of transfection without a gene carrier. Adv Funct Mater **25**(34):5445-5451.

66. Barrefelt A, Saghafian M, Kuiper R, Ye F, Egri G, Klickermann M, Brismar TB, Aspelin P, Muhammed M, Dahne L, Hassan M. 2013. Biodistribution, kinetics, and biological fate of SPION microbubbles in the rat. Int J Nanomedicine **8**:3241-3254.

67. Rodiger S, Ruhland M, Schmidt C, Schroder C, Grossmann K, Bohm A, Nitschke J, Berger I, Schimke I, Schierack P. 2011. Fluorescence dye adsorption assay to quantify carboxyl groups on the surface of poly(methyl methacrylate) microbeads. Anal Chem **83**(9):3379-3385.

68. Simard E, Sollradl T, Maltais JS, Boucher J, D'Orleans-Juste P, Grandbois M. 2015. Receptor for advanced glycation end-products signaling interferes with the vascular smooth muscle cell contractile phenotype and function. PLoS One **10**(8):e0128881.

69. Domingo-Espin J, Lindahl M, Nilsson-Wolanin O, Cushman SW, Stenkula KG, Lagerstedt JO. 2016. Dual actions of apolipoprotein A-I on glucose-stimulated insulin secretion and insulin-independent peripheral tissue glucose uptake lead to increased heart and skeletal muscle glucose disposal. Diabetes **65**(7):1838-1848.

70. Krzewski K, Gil-Krzewska A, Nguyen V, Peruzzi G, Coligan JE. 2013. LAMP1/CD107a is required for efficient perforin delivery to lytic granules and NK-cell cytotoxicity. Blood **121**(23):4672-4683.

71. Cohnen A, Chiang SC, Stojanovic A, Schmidt H, Claus M, Saftig P, Janssen O, Cerwenka A, Bryceson YT, Watzl C. 2013. Surface CD107a/LAMP-1 protects natural killer cells from degranulation-associated damage. Blood **122**(8):1411-1418.

72. Meier R, Golovko D, Tavri S, Henning TD, Knopp C, Piontek G, Rudelius M, Heinrich P, Wels WS, Daldrup-Link H. 2011. Depicting adoptive immunotherapy for prostate cancer in an animal model with magnetic resonance imaging. Magn Reson Med **65**(3):756-763.

73. Daldrup-Link HE, Meier R, Rudelius M, Piontek G, Piert M, Metz S, Settles M, Uherek C, Wels W, Schlegel J, Rummeny EJ. 2005. In vivo tracking of genetically engineered, anti-HER2/neu directed natural killer cells to HER2/neu positive mammary tumors with magnetic resonance imaging. Eur Radiol **15**(1):4-13.

74. Mallett CL, McFadden C, Chen Y, Foster PJ. 2012. Migration of iron-labeled KHYG-1 natural killer cells to subcutaneous tumors in nude mice, as detected by magnetic resonance imaging. Cytotherapy **14**(6):743-751.

75. Brand JM, Meller B, Von Hof K, Luhm J, Bahre M, Kirchner H, Frohn C. 2004. Kinetics and organ distribution of allogeneic natural killer lymphocytes transfused into patients suffering from renal cell carcinoma. Stem Cells Dev **13**(3):307-314.

76. Bai Y, Kan S, Zhou S, Wang Y, Xu J, Cooke JP, Wen J, Deng H. 2015. Enhancement of the in vivo persistence and antitumor efficacy of CD19 chimeric antigen receptor T cells through the delivery of modified TERT mRNA. Cell Discov **1**:15040.

77. Ponte JF, Sun X, Yoder NC, Fishkin N, Laleau R, Coccia J, Lanieri L, Bogalhas M, Wang L, Wilhelm S, Widdison W, Pinkas J, Keating TA, Chari R, Erickson HK, Lambert JM. 2016. Understanding how the stability of the thiol-maleimide linkage impacts the pharmacokinetics of lysine-linked antibody-maytansinoid conjugates. Bioconjug Chem **27**(7):1588-1598.

78. Chou TC. 2010. Drug combination studies and their synergy quantification using the Chou-Talalay method. Cancer Res **70**(2):440-446.

79. Chou TC. 2006. Theoretical basis, experimental design, and computerized simulation of synergism and antagonism in drug combination studies. Pharmacol Rev **58**(3):621-681.

80. Lin SF, Gao SP, Price DL, Li S, Chou TC, Singh P, Huang YY, Fong Y, Wong RJ. 2008. Synergy of a herpes oncolytic virus and paclitaxel for anaplastic thyroid cancer. Clin Cancer Res **14**(5):1519-1528.

81. Liu TC, Castelo-Branco P, Rabkin SD, Martuza RL. 2008. Trichostatin A and oncolytic HSV combination therapy shows enhanced antitumoral and antiangiogenic effects. Mol Ther **16**(6):1041-1047.

82. Zhang R, Yang J, Sima M, Zhou Y, Kopecek J. 2014. Sequential combination therapy of ovarian cancer with degradable N-(2-hydroxypropyl)methacrylamide copolymer paclitaxel and gemcitabine conjugates. Proc Natl Acad Sci U S A **111**(33):12181-12186.

83. Zhang C, Zhai S, Li X, Zhang Q, Wu L, Liu Y, Jiang C, Zhou H, Li F, Zhang S, Su G, Zhang B, Yan B. 2014. Synergistic action by multi-targeting compounds produces a potent compound combination for human NSCLC both in vitro and in vivo. Cell Death Dis **5**:e1138.

84. Adusumilli PS, Stiles BM, Chan MK, Chou TC, Wong RJ, Rusch VW, Fong Y. 2005. Radiation therapy potentiates effective oncolytic viral therapy in the treatment of lung cancer. Ann Thorac Surg **80**(2):409-416; discussion 416-407.

85. Cheema TA, Kanai R, Kim GW, Wakimoto H, Passer B, Rabkin SD, Martuza RL. 2011. Enhanced antitumor efficacy of low-dose Etoposide with oncolytic herpes simplex virus in human glioblastoma stem cell xenografts. Clin Cancer Res **17**(23):7383-7393.

86. Ni J, Miller M, Stojanovic A, Garbi N, Cerwenka A. 2012. Sustained effector function of IL-12/15/18-preactivated NK cells against established tumors. J Exp Med **209**(13):2351-2365.

87. Morvan MG, Lanier LL. 2016. NK cells and cancer: You can teach innate cells new tricks. Nat Rev Cancer **16**(1):7-19.

88. Agaugue S, Marcenaro E, Ferranti B, Moretta L, Moretta A. 2008. Human natural killer cells exposed to IL-2, IL-12, IL-18, or IL-4 differently modulate priming of naive T cells by monocyte-derived dendritic cells. Blood **112**(5):1776-1783.

89. Leong JW, Chase JM, Romee R, Schneider SE, Sullivan RP, Cooper MA, Fehniger TA. 2014. Preactivation with IL-12, IL-15, and IL-18 induces CD25 and a functional high-affinity IL-2 receptor on human cytokine-induced memory-like natural killer cells. Biol Blood Marrow Transplant **20**(4):463-473.

90. Romee R, Schneider SE, Leong JW, Chase JM, Keppel CR, Sullivan RP, Cooper MA, Fehniger TA. 2012. Cytokine activation induces human memory-like NK cells. Blood **120**(24):4751-4760.

91. Holliday DL, Speirs V. 2011. Choosing the right cell line for breast cancer research. Breast Cancer Res **13**(4):215.

92. DeRose YS, Wang G, Lin YC, Bernard PS, Buys SS, Ebbert MT, Factor R, Matsen C, Milash BA, Nelson E, Neumayer L, Randall RL, Stijleman IJ, Welm BE, Welm AL. 2011. Tumor grafts derived from women with breast cancer authentically reflect tumor pathology, growth, metastasis and disease outcomes. Nat Med **17**(11):1514-1520.

93. Fesnak AD, June CH, Levine BL. 2016. Engineered T cells: The promise and challenges of cancer immunotherapy. Nat Rev Cancer **16**(9):566-581.

94. Maude SL, Teachey DT, Porter DL, Grupp SA. 2015. CD19-targeted chimeric antigen receptor T-cell therapy for acute lymphoblastic leukemia. Blood **125**(26):4017-4023.

95. Hong EE, Erickson H, Lutz RJ, Whiteman KR, Jones G, Kovtun Y, Blanc V, Lambert JM. 2015. Design of coltuximab ravtansine, a CD19-targeting antibody-drug conjugate (ADC) for the treatment of B-cell malignancies: Structure-activity relationships and preclinical evaluation. Mol Pharm **12**(6):1703-1716.

96. Kantarjian HM, Lioure B, Kim SK, Atallah E, Leguay T, Kelly K, Marolleau JP, Escoffre-Barbe M, Thomas XG, Cortes J, Jabbour E, O'Brien S, Bories P, Oprea C, Hatteville L, Dombret H. 2016. A phase II study of coltuximab ravtansine (SAR3419) monotherapy in patients with relapsed or refractory acute lymphoblastic leukemia. Clin Lymphoma Myeloma Leuk **16**(3):139-145.

APPENDIX

DIRECT INCORPORATION OF FUNCTIONAL PEPTIDE INTO M-DNA THROUGH LIGAND-TO-METAL CHARGE TRANSFER[†]

A.1. Abstract

Conventional nonviral gene delivery methods suffer from the toxicity of cationic polymer carriers. There is a significant need for a new method of gene delivery that overcomes the limitations and allows targeted gene delivery. In this study, we have developed a new method to incorporate functional peptides into DNA without the need of chemical conjugations by utilizing the ligand-to-metal charge transfer (LMCT) transition, which occurs between the divalent metal ions and the sulfhydryl group in cysteine. To apply the LMCT transition to incorporate cysteine-containing targeting peptides into DNA, divalent metal ions must be first introduced to DNA. Zn^{2+} ions spontaneously intercalate into DNA base pairs at pH 7.0 - 8.5, resulting in the conversion of normal B-DNA to metal-bound DNA (M-DNA). We found that the Zn^{2+} ions present in M-DNA could interact with the sulfhydryl groups in cysteines of targeting peptides through the LMCT transition and the M-DNA/peptide complex could specifically transfect the target cells.

[†] Modified with the permission from KS Lim, GM Valencia, YW Won, and DA Bull. ACS Macro Letters 2017; 6: 98-102. Copyright © 2017 American Chemical Society. Lee and Lim co-managed this project and co-authored the research article. Lee contributed to the transfection of PEI/M-DNA polyplex and behavior of C-RGD-C/M-DNA complex. Lim contributed to the characterization of PEI/M-DNA polyplex and behavior of C-9R-C/M-DNA complex. Bull and Won are the PIs responsible for the project.

A.2. Introduction

Successful gene therapy is reliant upon the transfer of safe and efficient therapeutic nucleic acids to their target cells.[1-3] Gene delivery vehicles can be divided into two categories: viral vectors and nonviral carriers.[4,5] Each of these methods, however, suffers from the limitations imposed by the immunogenicity of viral compartments or the toxicity of cationic polymeric carriers.[6-8] In particular, the development of nonviral polymer carriers utilizes one or more of the following principles: 1) electrostatic interaction, 2) encapsulation, and 3) absorption.[3,4,9] For efficient gene transfection, these methods require the use of high concentrations of cationic polymers, which can cause cytotoxicity.[6,8] Thus, there is a need for a new method of nonviral gene delivery that reduces the polymer use and allows targeted gene delivery without compromising transfection efficiency.

We have focused on the ligand-to-metal charge transfer (LMCT) between Zn^{2+} ions and sulfhydryl groups of cysteines to directly bind functional peptides to nucleic acids.[10,11] This LMCT transition between Zn^{2+} ions and the cysteinyl residues of peptides occurs at nanomolar and/or picomolar levels of affinity.[12-15] To apply this LMCT transition to the modification of DNA with cysteine-containing peptides, Zn^{2+} ions must first be introduced to DNA. It is known that divalent metal ions, such as Zn^{2+}, lead to the conversion of normal B-DNA to metal-bound DNA (M-DNA) by intercalating into the DNA base pairs at pH 7.0 – 8.5.[13,15] Although the binding of divalent metal ions can drive the self-assembly of DNA,[13,16] this conformational change does not affect the integrity and activity of DNA.

In the present study, M-DNA was generated using Zn^{2+} ions, and the resulting M-DNA was further modified with a cancer targeting peptide, C-RGD-C, or a cell

penetrating peptide (CPP), C-9R-C, through the LMCT transition. The Zn^{2+} ions present in M-DNA interact with the sulfhydryl groups of cysteines present in these peptides (Figure A.1). The C-RGD-C peptide attached to M-DNA enhanced the gene transfection into the target cancer cells. Similarly, the LMCT transition and the electrostatic interaction simultaneously contributed to the enhanced binding of CPPs to M-DNA, which in turn reduced the amount of peptide necessary to achieve high levels of gene transfection. This method can serve as a strategy to modify DNA with any functional peptide.

A.3. Materials and Methods

A.3.1. Materials

$ZnCl_2$, MTT, and PEI were purchased from Sigma-Aldrich (St. Louis, MO). Plasmid DNA expressing luciferase and luciferase assay kits were obtained from Promega (Madison, WI). Yoyo-1 dye was purchased from Thermo Fisher scientific (Waltham, MA). Peptides were synthesized by the DNA/peptide Core at the University of Utah. All cell culture supplies were purchased from Life Technologies (Invitrogen, Grand Island, NY).

A.3.2 Preparation of M-DNA

M-DNA was prepared as described previously with some modifications.[14,16,17] Plasmid DNA, 10 µg, was mixed with the $ZnCl_2$ stock solution at final Zn^{2+} concentrations ranging from 1.83 mM to 7.32 mM. Thereafter, the pH of the mixture was adjusted to 7.4 or below 7.0 by adding NaOH. This mixture was incubated for 20 minutes at room temperature to generate M-DNA.

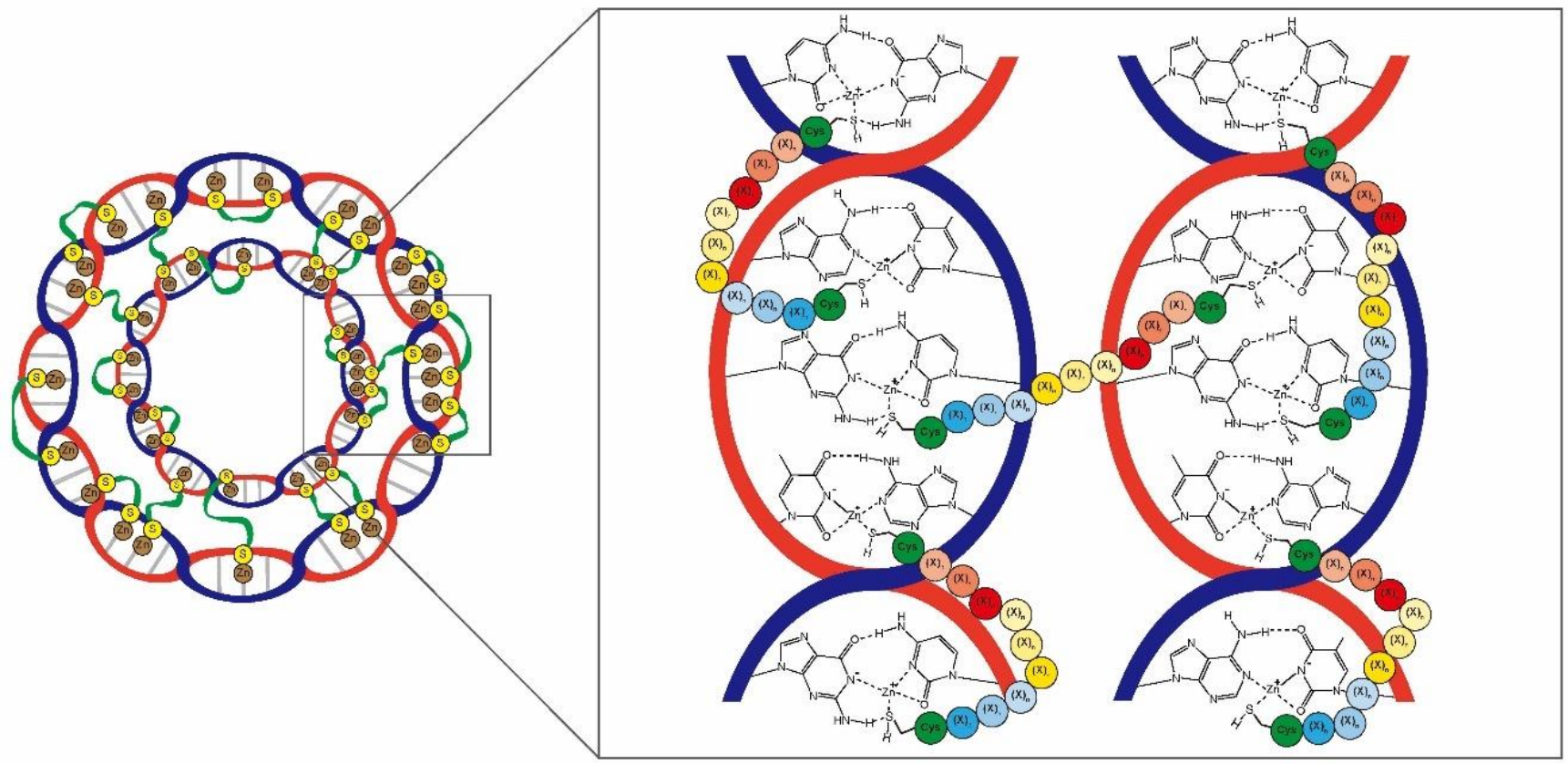

Figure A.1. Schematic illustration showing the binding of cysteine-contained peptides to plasmid DNAs through the LMCT transition.

A.3.3. Ethidium Fluorescence Assay

$ZnCl_2$ was added to DNA dissolved in MOPS buffer in the presence of ethidium bromide (EtBr). The fluorescence intensity of the mixture was recorded over time. The M-DNA prepared as described above or its parent B-DNA was diluted in MOPS buffer containing EtBr at a final concentration of 4 μg/mL. Resulting EtBr-labeled M-DNA and B-DNA were mixed with different amounts of PEI. During the incubation at room temperature, fluorescence intensity was measured using a fluorescence photometer at excitation and emission wavelengths of 516 nm and 598 nm, respectively, every 5 minutes up to 40 minutes.

A.3.4. Preparation of Peptide/M-DNA Complex and PEI/M-DNA Polyplex

Each peptide was dissolved in water and added to M-DNA at peptide-to-DNA (peptide/DNA) weight ratios of 0.125, 0.25, 0.5, and 1.0. The pH was adjusted to 7.4 or below 7.0. The mixture was reacted for 30 minutes at room temperature. Similarly, PEI was added to preformed M-DNA at PEI-to-DNA (PEI/DNA) weight ratios ranging from 0.01 to 1.0. For the control, M-DNA was reconverted to B-DNA by lowering pH to 5.0 and mixed with PEI at different PEI/DNA weight ratios to form a polyplex. Natural B-DNA was also added with PEI at different PEI/DNA weight ratios for polyplex formation.

A.3.5 Characterization

Five micrograms of C-RGD-C were added to 1 mL of 7.32 mM $ZnCl_2$ solution with or without 10 μg DNA. The pH of the mixture was adjusted to 7.4 by adding NaOH and then incubated for 10 minutes. The sizes and zeta potentials of C-RGD-C/$ZnCl_2$ complex,

C-RGD-C/M-DNA complex, and M-DNA were determined by dynamic light scattering (Malvern Zetasizer Nano-ZS; Malvern Instruments, UK) with three parallel measurements.

A.3.6. UV Spectrophotometry

Absorption spectra of the peptides, peptide/M-DNA complex, and M-DNA from 200 nm to 450 nm were recorded at 25 °C using a Tecan Infinite 200 PRO NanoQuant spectrophotometer (Teacan Group Ltd, Switzerland) in 1 cm quartz cuvettes. Stock solutions of peptides in 0.01 M HCl were diluted to final concentrations of 1 μM with 50 mM borate at pH 7.4 in the presence of 50 μM TCEP.

A.3.7. Transfection and Cellular Uptake

MDA-MB-231 and HEK293 cells were maintained according to the protocols provided from the ATCC. The MDA-MB-231 cell line was chosen to test the targeting ability of the C-RGD-C/M-DNA complex because this cell line is widely used in targeted gene delivery studies with the RGD-containing peptide. HEK293 cells were used in all other transfection studies because this cell line has been readily used in general gene transfection studies. For *in vitro* transfection studies, M-DNA was prepared with the plasmid DNA encoding luciferase; then, PEI or peptides were added to form the PEI/M-DNA polyplex, C-9R-C/M-DNA complex, and C-RGD-C/M-DNA complex. Cells were incubated for 48 hours after the transfection, and the luciferase activity in cell lysates was determined according to the manufacturer's protocol. Cell viability was determined 48 hours after the transfection using MTT assay. Yoyo-labeled plasmid DNA was prepared according to the manufacturer's instruction and processed to form M-DNA and peptide- or

polymer-incorporated M-DBA complexes for flow cytometry (FACSCanto; BD Bioscience, USA).

A.4. Results and Discussion

A.4.1. M-DNA Formation and Toxicity

The M-DNA formation was verified through an ethidium fluorescence assay.[14,17] The effects of Zn^{2+} concentration and time on the conversion of B-DNA to M-DNA were studied at pH 7.5 (Figure A.2). M-DNA was partially generated by the incubation with ≤3.66 mM $ZnCl_2$, while complete conversion to M-DNA was observed in the presence of ≥5.49 mM $ZnCl_2$. In the absence of Zn^{2+}, no conformational change in DNA was observed. It was verified that the M-DNA generated in this study was nontoxic to cells (Figure A.3).

A.4.2. Comparison of PEI/M-DNA Complex and PEI/B-DNA Polyplex

To compare our new method utilizing the LMCT transition to conventional electrostatic interaction, M-DNA was first condensed by the most commonly used cationic polymer: branched poly(ethylenimine) 25 kDa (PEI). When different amounts of PEI were mixed with M-DNA at pH 7.4, the migration of M-DNA was completely retarded at a PEI/DNA weight ratio of 0.1 (Figure A.4a), whereas the migration of reconverted B-DNA—generated by lowering the pH to 5.0—was retarded at a PEI/DNA weight ratio of 0.6 (Figure A.4b). The formation of PEI/B-DNA polyplex was completed at a PEI/DNA weight ratio of 0.5 (Figure A.4c). The M-DNA showed approximately 50% of fluorescence quenching compared to the parent B-DNA, and the addition of PEI decreased it further in a PEI-amount dependent manner (Figure A.5). At PEI/DNA weight ratio of 0.1,

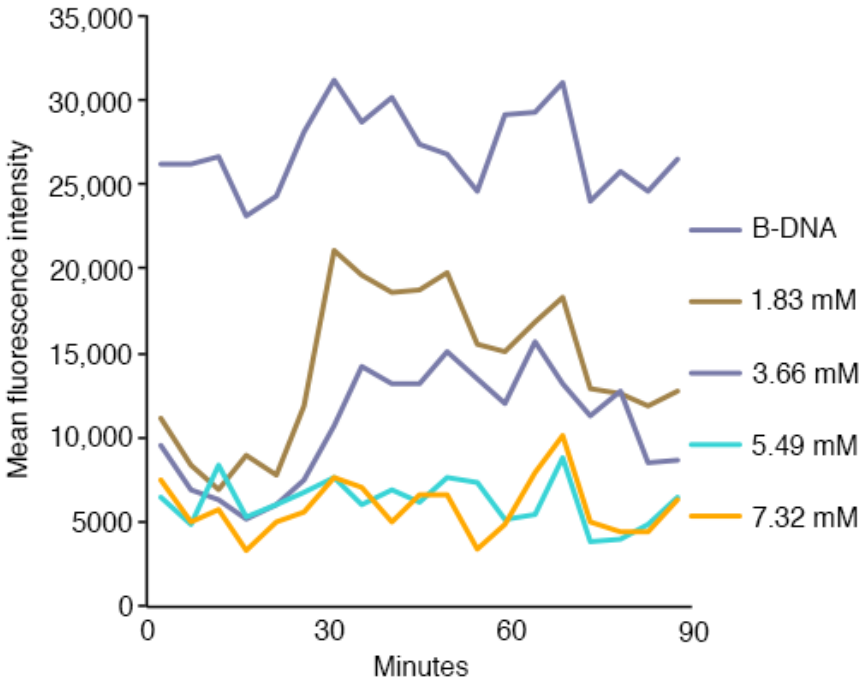

Figure A.2. Effects of Zn^{2+} concentration and incubation time on M-DNA formation. Plasmid DNA encoding luciferase was incubated with various concentrations of $ZnCl_2$ in the presence of EtBr for 90 minutes. The fluorescence intensities were recorded over time.

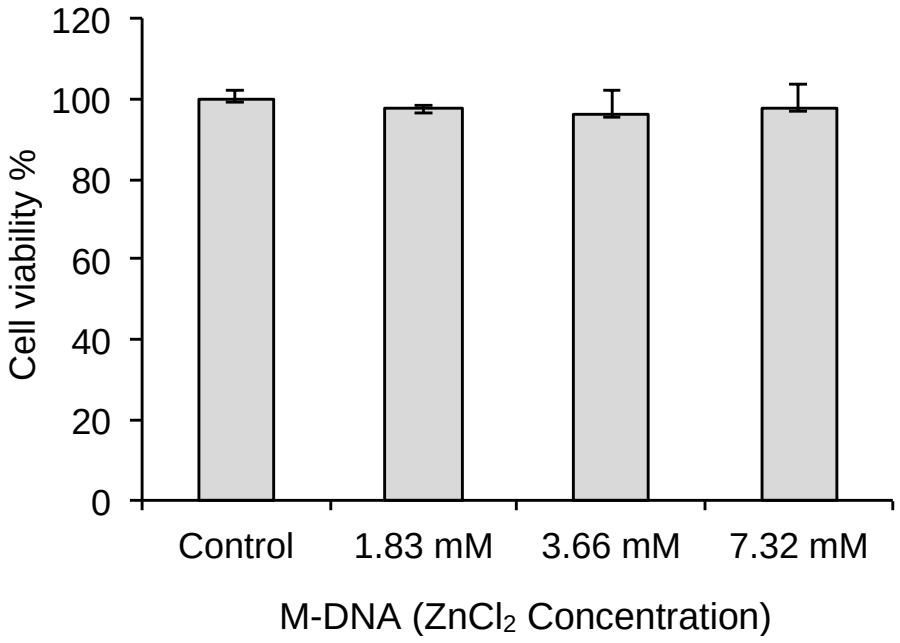

Figure A.3. Cytotoxicity of M-DNA generated using various concentrations of $ZnCl_2$. HEK293 cells were treated with M-DNA and the cell viability was determined by MTT assay at 48 hours post-treatment.

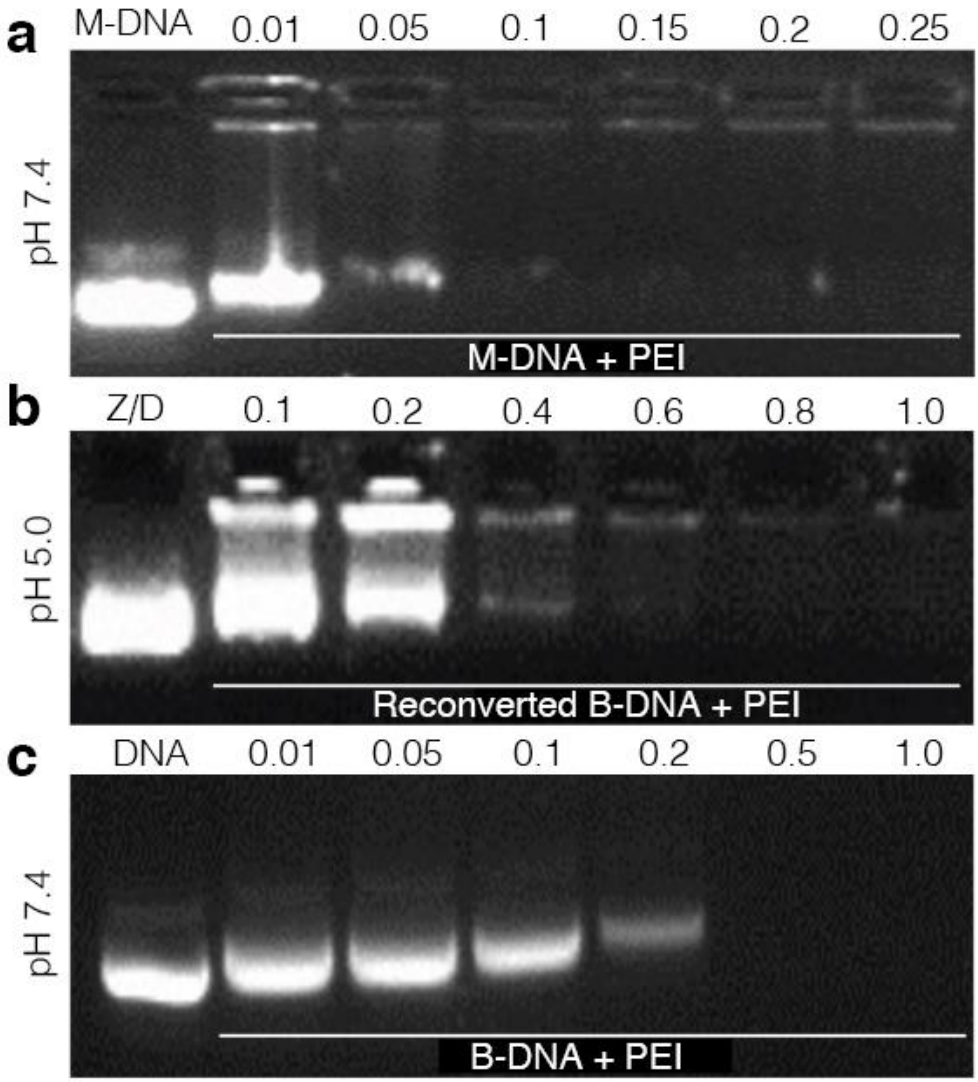

Figure A.4. Characterization of PEI/M-DNA polyplex. Gel retardation assay of (a) PEI/M-DNA polyplex at pH 7.4, (b) reconverted B-DNA mixed with PEI at pH 5.0, and (c) PEI/B-DNA polyplex at pH 7.4. Numbers indicate the PEI/DNA weight ratios.

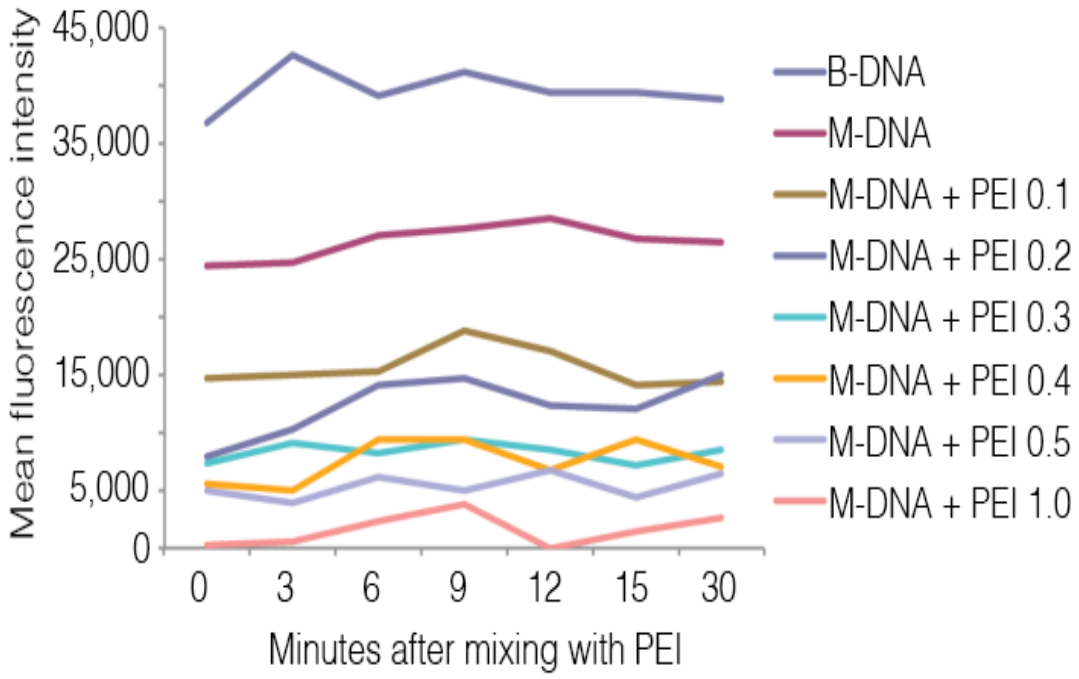

Figure A.5. EtBr replacement assays of PEI/M-DNA polyplex. Numbers in the indices (e.g., PEI 0.1) indicate the PEI/DNA weight ratios.

the fluorescence of M-DNA was approximately 30% of B-DNA, and it was stable over time. The fluorescence intensity continued to decrease with increasing PEI concentration and finally dropped to below 10% of B-DNA at the PEI/DNA weight ratio of 1.0. Without the M-DNA formation, however, the highest PEI/DNA weight ratio could not reduce the fluorescence intensity to below 10% of the parent B-DNA (Figure A.6), and the fluorescence increased over time with PEI/B-DNA polyplexes generated at PEI/DNA weight ratios of 0.1 and 0.2. These results suggest that the PEI/DNA weight ratio of 0.1 appeared to be sufficient to completely condense the M-DNA.

The formation of PEI/M-DNA polyplex achieved higher levels of gene expression compared to the M-DNA (Figure A.7). The PEI/M-DNA polyplex prepared at a PEI/DNA weight ratio of 0.5 showed the same transfection efficiency as the PEI/B-DNA polyplex prepared at a PEI/DNA weight ratio of 1.0. The PEI/M-DNA polyplex at a PEI/DNA weight ratio of 0.1 showed almost the same levels of gene expression as the PEI/B-DNA polyplex at a PEI/DNA weight ratio of 0.5, indicating that the formation of M-DNA could reduce the minimal amount of PEI to 20%. Moreover, these results imply that the electrostatic interaction alone is insufficient to dramatically reduce the amount of cationic polymer required for efficient gene transfection.

A.4.3. Behavior of C-9R-C/M-DNA Complex

C-9R-C peptide, a well-known CPP,[18-20] is expected to interact with M-DNA through the combination of LMCT transition and electrostatic interaction, while the control CPP, G-9R-G, can bind to M-DNA electrostatically. The 9R moiety binds to M-DNA through electrostatic interaction while the cysteines located at both ends of C-9R-C interact

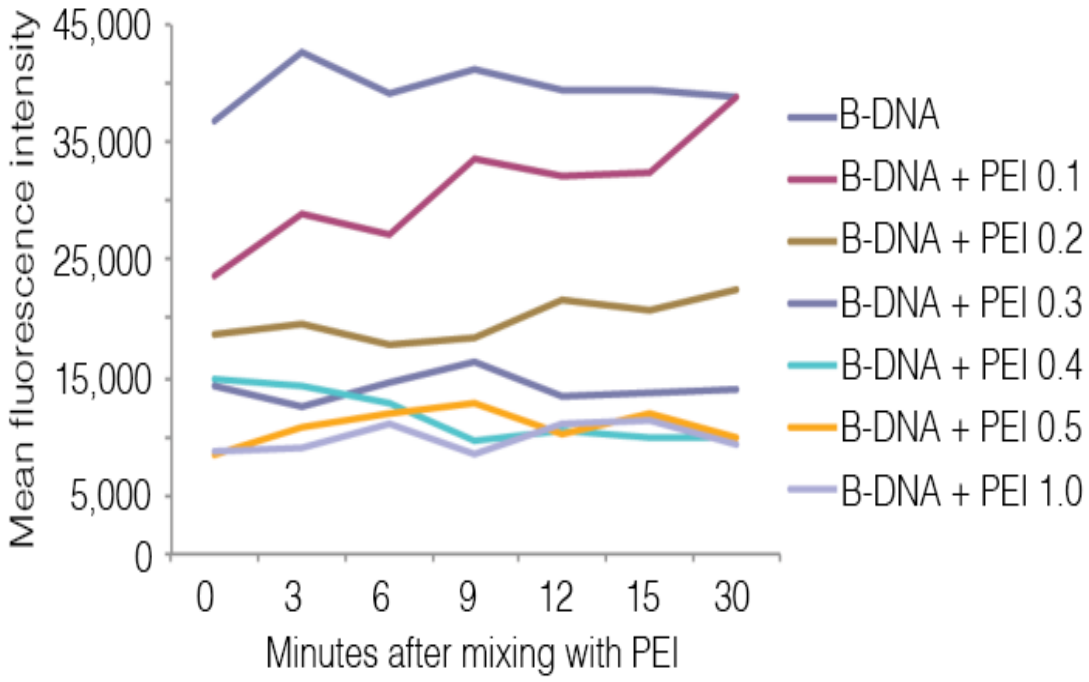

Figure A.6. EtBr replacement assays of PEI/B-DNA polyplex. Numbers in the indices (e.g., PEI 0.1) indicate the PEI/DNA weight ratios.

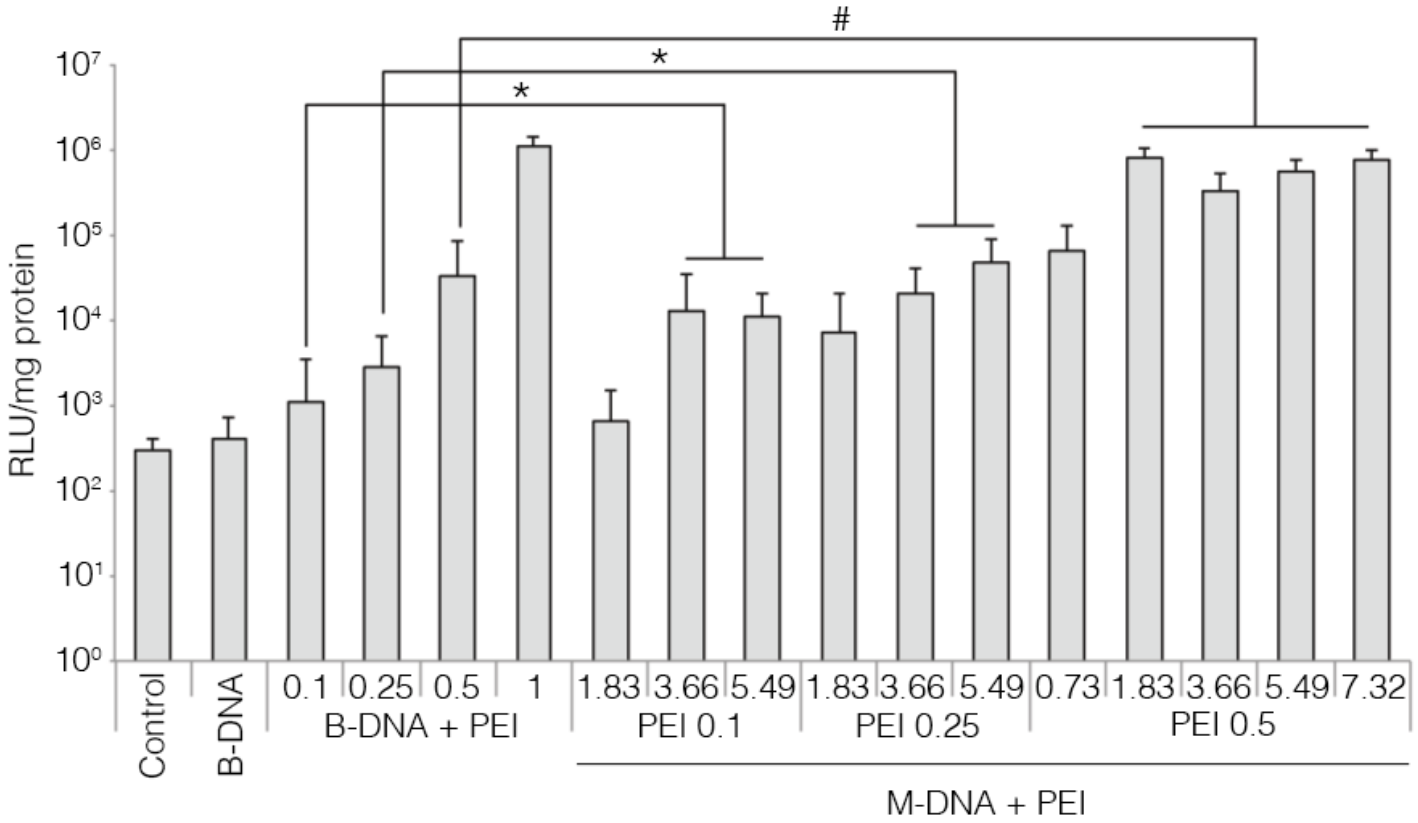

Figure A.7. Luciferase gene transfection by PEI/M-DNA polyplex or PEI/B-DNA polyplex. The numbers in the B-DNA+PEI group indicate the PEI/DNA weight ratios. The numbers in other groups indicate the $ZnCl_2$ concentrations ranging from 0.73 mM to 7.32 mM used to generate M-DNA. In the PEI/M-DNA complex groups, PEI 0.1, 0.25, and 0.5 indicate the PEI/DNA weight ratios (*p<0.05, #p<0.01; one-way ANOVA.

with Zn^{2+} ions present in the M-DNA *via* the LMCT transition.[12,21] On the other hand, the G-9R-G peptide reacts with M-DNA only through a charge-interaction due to the absence of cysteine. Compared to G-9R-G peptide, C-9R-C peptide would, therefore, form a stronger bond with the M-DNA.

Scanning of electronic absorption spectrum in the far UV region was performed to verify the binding of Zn^{2+} to the thiol groups in C-9R-C peptide. This scan demonstrated that the LMCT transition was centered near 230 nm (Figure A.8). A bathochromic shift of the center of the bands was also observed by the analysis of UV spectra recorded with a fixed amount of C-9R-C throughout the titration of Zn^{2+} ions. Ellman's assay—performed to determine the amount of free cysteine present in the mixture—demonstrated that there was a significant difference in the levels of free cysteine between the concentration of added cysteines and the concentration of free cysteines following interaction with the M-DNA (Figure A.9). The gradients for each plot in Figure A.8 were 0.8531 for the C-9R-C only, 0.5936 for the C-9R-C+Zn^{2+}, and 0.6908 for the C-9R-C+M-DNA, confirming that the amount of free cysteine was decreased by the LMCT transition. This result further verified the occurrence of LMCT transition between M-DNA and C-9R-C peptide.

We sought to determine the minimal amount of C-9R-C peptide necessary for the complete condensation of M-DNA. The migration of M-DNA was completely retarded at a C-9R-C-to-DNA (C9RC/DNA) weight ratio of 0.08 (Figure A.10a), whereas the retardation of B-DNA by the formation of C-9R-C/B-DNA complex was observed at a C9RC/DNA weight ratio of 1.0 (Figure A.10b). G-9R-G, which can bind to M-DNA solely through electrostatic interaction, retarded the migration of M-DNA at a G-9R-G-to-DNA

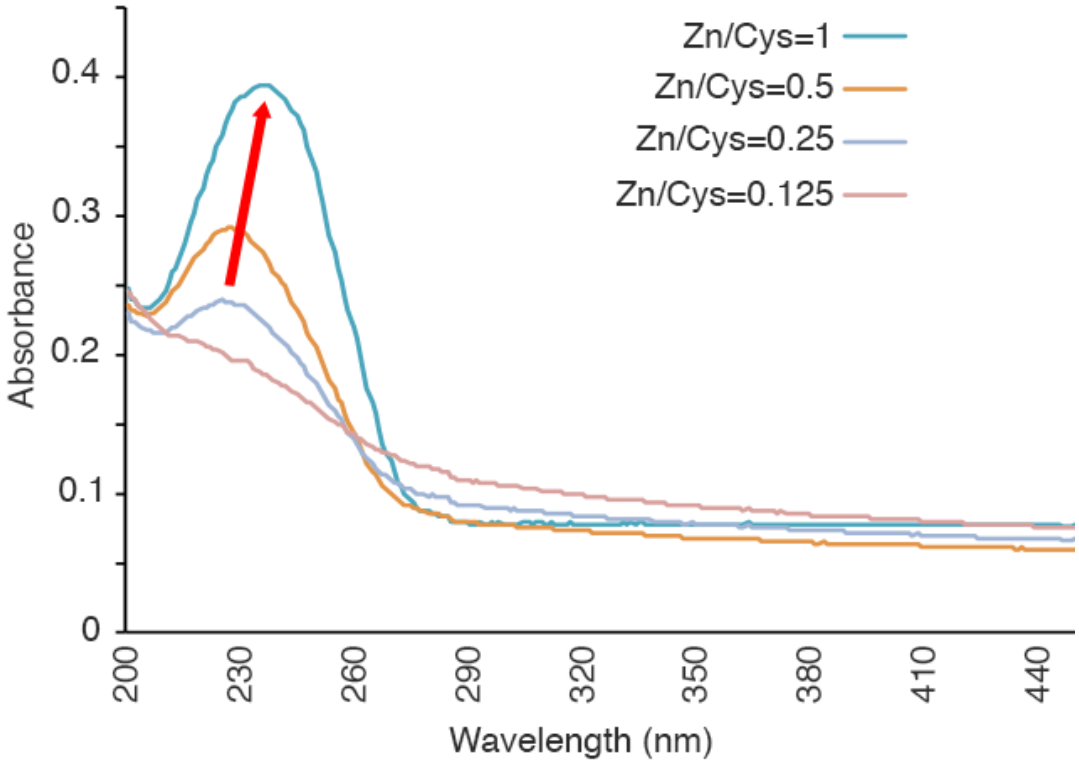

Figure A.8. Spectrophotometric titration of C-9R-C with Zn^{2+}. UV spectra obtained by the incremental addition of $ZnCl_2$. The arrow indicates the bathochromic shift.

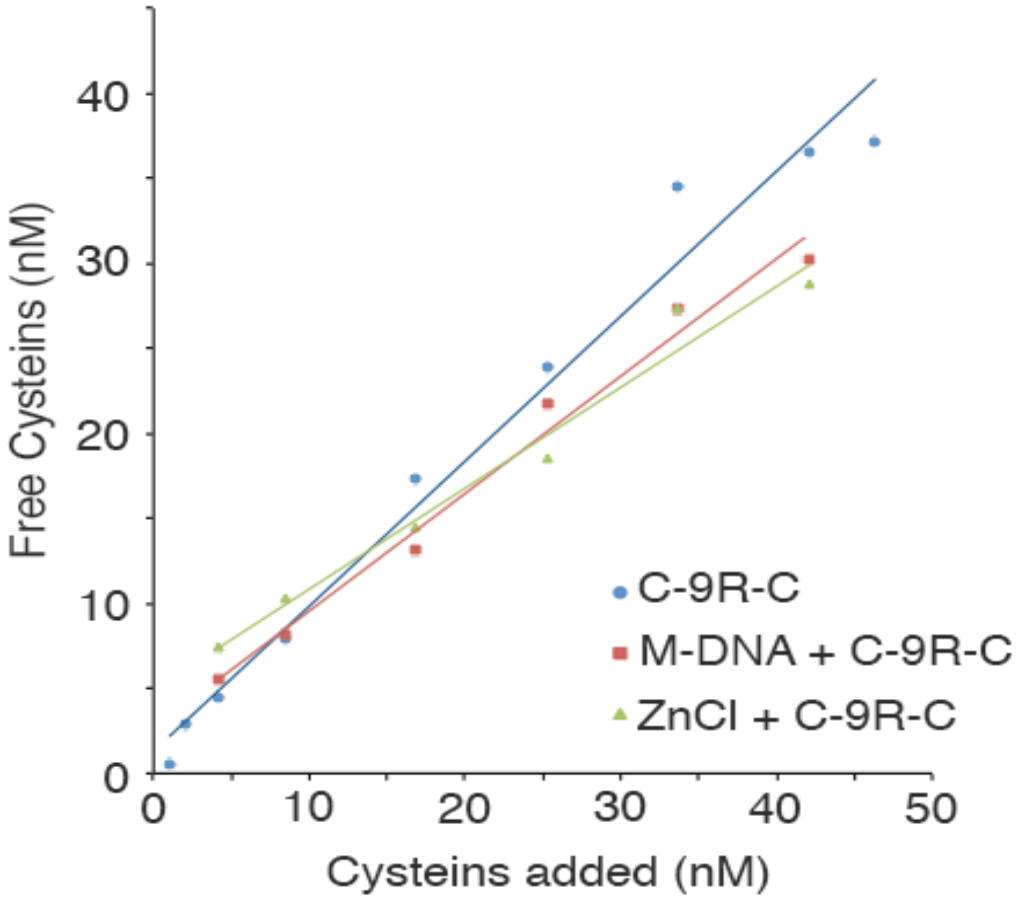

Figure A.9. The free cysteine concentration in C-9R-C and the free cysteine concentration after the addition of different amounts of C-9R-C peptide to M-DNA, or $ZnCl_2$ containing reaction buffers. M-DNA was prepared in the presence of 7.32 mM $ZnCl_2$ and the same concentration of $ZnCl_2$ without DNA was used as a control.

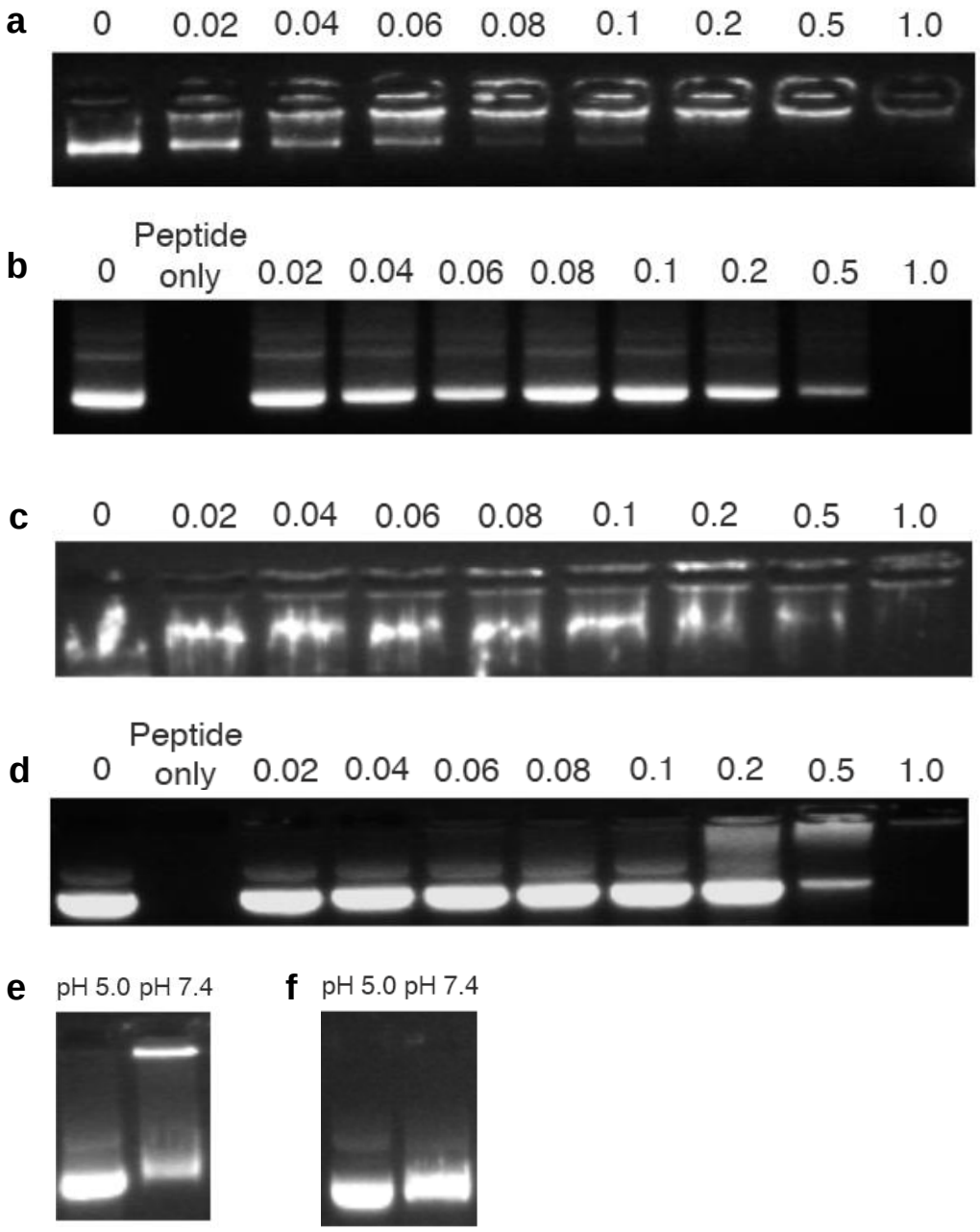

Figure A.10. Agarose gel electrophoresis of C-9R-C/M-DNA complex and G-9R-G/M-DNA complex. (a) C-9R-C/M-DNA complex, (b) C-9R-C/B-DNA complex, (c) G-9R-G/M-DNA complex, and (d) G-9R-G/B-DNA complex. The numbers indicate the peptide/DNA weight ratios. Gel retardation of (e) C-9R-C/M-DNA complex and (f) G-9R-G/M-DNA at pH 7.4 or at pH 5.0. Both complexes were formed at a peptide/DNA weight ratio of 0.05.

(G9RG/DNA) weight ratio of 1.0 (Figure A.10c). This G9RG/DNA weight ratio is the same ratio at which the parent B-DNA was condensed by G-9R-G (Figure A.10d). The M-DNA was incubated with C-9R-C (Figure A.10e) or G-9R-G (Figure A.10f) at pH 5.0 or at pH 7.4 because LMCT transition does not occur below pH 7.0,[12] while the guanidine side groups of arginine retain their positive charge even below pH 7.0. Both peptides can interact with M-DNA through electrostatic interaction at pH below 7.0, but C-9R-C binds to M-DNA through LMCT transition at pH 7.4 in addition to the electrostatic interaction. C-9R-C retarded migration of the M-DNA at a C9RC/DNA weight ratio of 0.05 at pH 7.4. This retardation of M-DNA migration was not observed at pH 5.0 (Figure A.10e). There was no difference in migration, regardless of the pH, when the M-DNA was condensed by G-9R-G at an identical ratio (Figure A.10f).

The transfection efficiency (Figure A.11) and cellular uptake (Figure A.12) of the C-9R-C/M-DNA complex were directly proportional to the amount of C-9R-C added and were consistently greater than those of the C-9R-C/B-DNA complex without affecting the cell viability (Figure A.13). Interestingly, the C-9R-C/M-DNA complex prepared at a C9RC/DNA weight ratio of 0.1 exhibited the same level of gene expression as the C-9R-C/B-DNA complex prepared at a C9RC/DNA weight ratio of 2.0. In addition, we compared the transfection efficiency of the C-9R-C/M-DNA complex to that of the G-9R-G/M-DNA complex prepared at pH 7.4 or at pH 5.0. The transfection efficiency of C-9R-C/M-DNA complex relative to that of G-9R-G/M-DNA complex increased continuously with an increasing C9RC/DNA weight ratio at pH 7.4, while no difference in the relative transfection was observed at pH 5.0 (Figure A.14). These results indicate that the C-9R-C peptide capable of interacting with the M-DNA through LMCT transition and

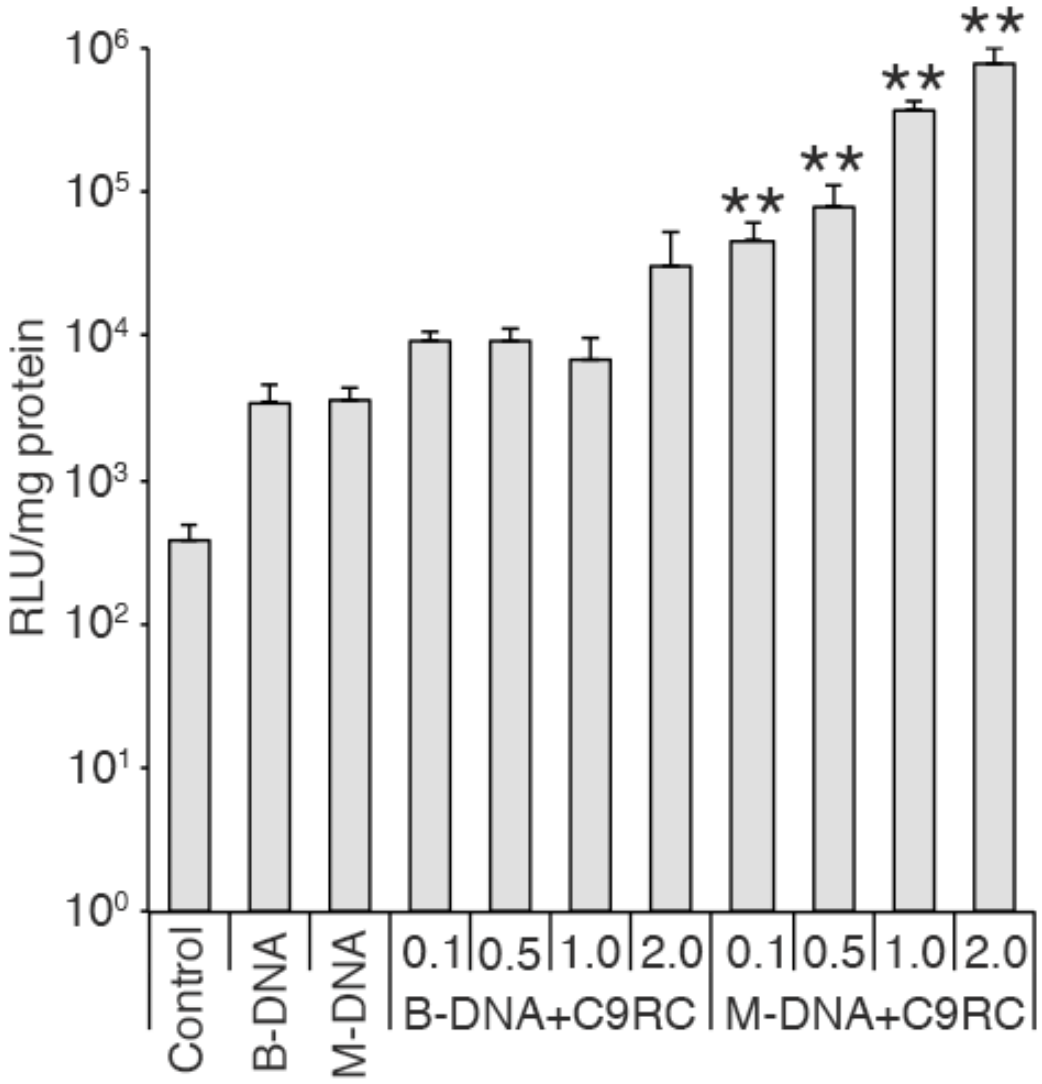

Figure A.11. Transfection of HEK293 cells with C-9R-C/M-DNA complex and C-9R-C/B-DNA complex. Luciferase activity was analyzed 48 hours after the transfection (**p<0.01, M-DNA *vs*. B-DNA). The numbers indicate the C9RC/DNA weight ratios. M-DNA was prepared in the presence of 7.32 mM $ZnCl_2$.

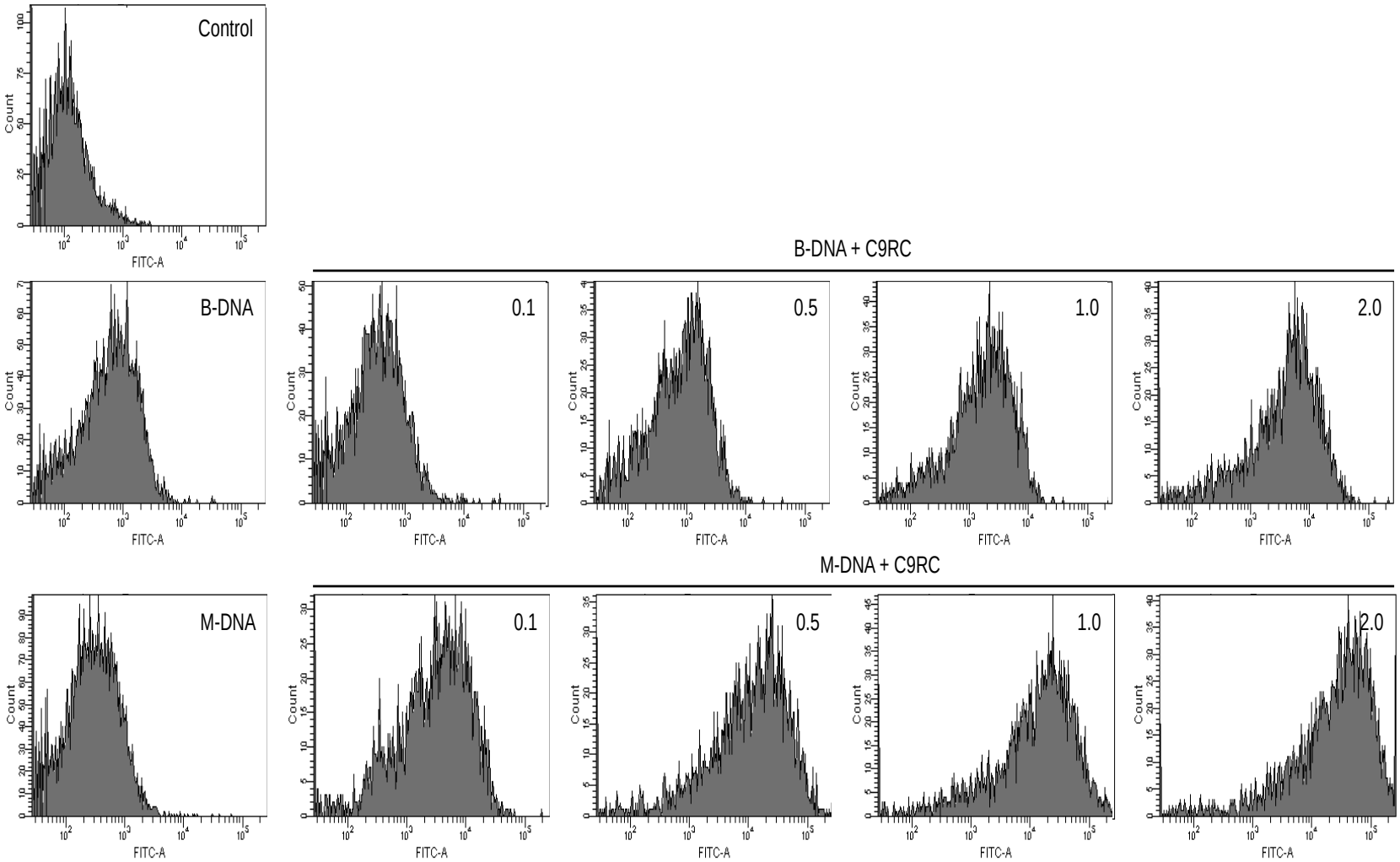

Figure A.12. Cellular uptake of C-9R-C/B-DNA complex or C-9R-C/M-DNA complex in HEK293 cells. The numbers represent peptide/DNA weight ratio

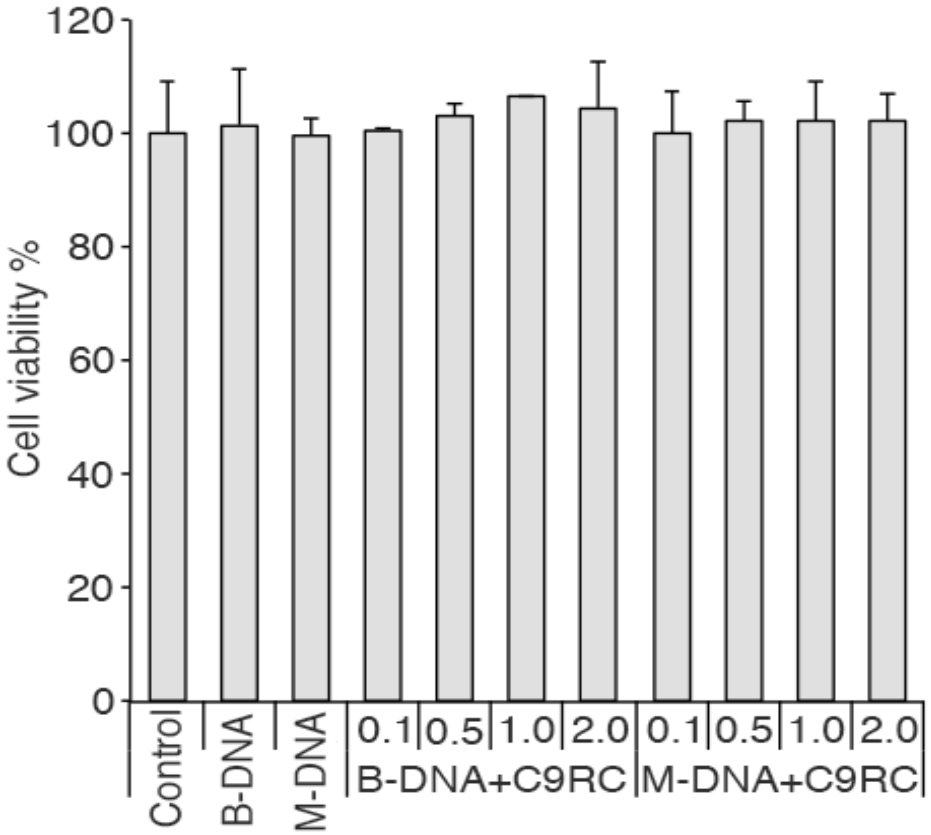

Figure A.13. HEK293 cell viability following the transfection with C-9R-C/M-DNA complex or C-9R-C/B-DNA complex. The numbers indicate the C9RC/DNA weight ratios. M-DNA was prepared in the presence of 7.32 mM $ZnCl_2$.

electrostatic interaction reduces the amount of peptide necessary for a high gene transfection efficiency to less than 5% of the peptide amount required for regular polyplex formation with a cationic peptide.

A.4.4. Behavior of C-RGD-C/M-DNA Complex

In order for the LMCT transition method to be broadly applicable to gene delivery, there must be a capacity for targeted gene transfection. Conjugation of targeting peptides to nonviral vectors is one of the most well-established approaches for the development of targeted gene delivery.[22,23] Since the direct conjugation of targeting moieties to nucleic acids can lead to the loss of nucleic acid activity,[24,25] the direct introduction of targeting peptides to nucleic acids through conventional conjugation-based methodologies is not a viable approach. Moreover, negatively or slightly positively charged targeting peptides are unable to directly interact with nucleic acids through electrostatic interaction. We, therefore, hypothesized in the beginning that the LMCT transition could allow the incorporation of any peptides containing cysteine to M-DNA without the need for either chemical conjugation or a positively charged mediator. To prove our hypothesis, a noncyclic C-RGD-C peptide, one of the most validated targeting peptides for cancer, was introduced to M-DNA through the LMCT transition.

The parent B-DNA or M-DNA was mixed with C-RGD-C peptide at different C-RGD-C-to-DNA (CRGDC/DNA) weight ratios and then electrophoresed on an agarose gel. Migration of B-DNA was not retarded even at the highest CRGDC/DNA weight ratio. Addition of C-RGD-C peptide to the M-DNA, however, partially retarded the M-DNA migration as the amount of the peptide increased (Figure A.15). We recorded the electronic

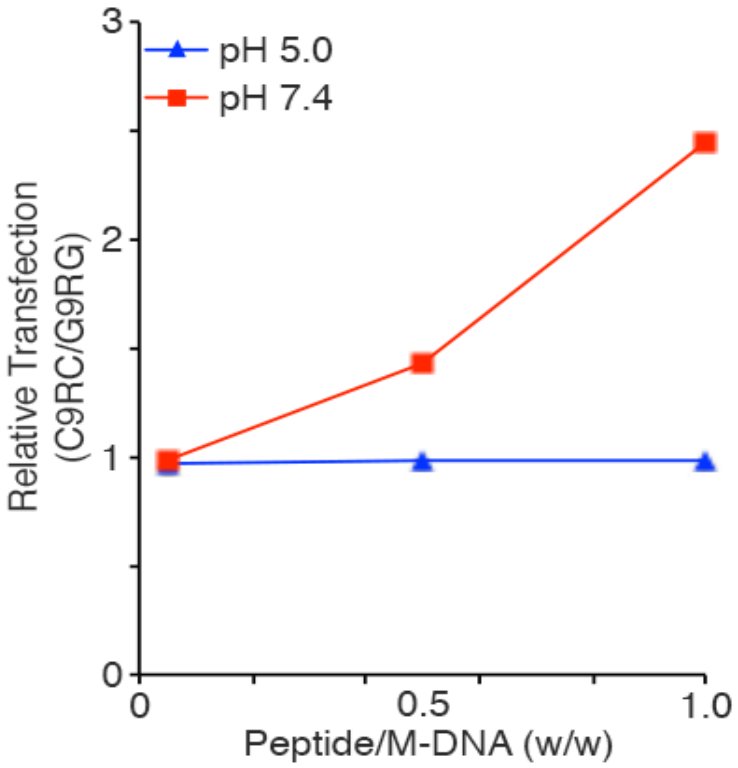

Figure A.14. Transfection efficiency of C-9R-C/M-DNA complex relative to that of G-9R-G/M-DNA complex in HEK293 cells. Peptide/DNA complexes were prepared at pH 7.4 or at pH 5.0.

absorption spectrum in the far UV region to verify the LMCT transition between C-RGD-C peptide and Zn^{2+} ions present in M-DNA, which is centered near 230 nm (Figure A.16a). The UV spectra recorded with a fixed amount of C-RGD-C peptide throughout the Zn^{2+} titration was analyzed to confirm the LMCT transition between C-RGD-C peptide and Zn^{2+}. The incremental additions of Zn^{2+} to C-RGD-C peptide up to Zn/Cys ratio of 0.5 led to an increase in absorbance values near 230 nm. The absorbance spectra of C-RGD-C/M-DNA complex acquired by subtracting the background absorbance from each spectrum showed that the LMCT transition reached a steady state at Zn/Cys ratio of 0.5 (Figure A.16b). The absorption at 230 nm, where the bathochromic shift of the center of the bands was observed, was increased as a function of the Zn/Cys binding (Figure A.17). These results provided evidence for the binding of C-RGD-C to M-DNA through the LMCT transition.

Finally, we verified the capacity for targeted gene expression by the C-RGD-C/M-DNA complex in cancer cells. MDA-MB-231 cells, a breast cancer cell line, and HEK293 cells—both of which have been used widely in general gene transfection studies—were transfected with one of the following groups: 1) C-RGD-C/M-DNA complex; 2) parent B-DNA mixed with C-RGD-C peptide; and 3) M-DNA. Hydrodynamic diameters and zeta potentials of the M-DNA, Zn/C-RGD-C complex, and C-RGD-C/M-DNA are shown in Table A.1. In MDA-MB-231 cells, the levels of gene expression relative to M-DNA transfection was increased as the CRGDC/DNA weight ratio increased in the C-RGD-C/M-DNA complex group, whereas addition of C-RGD-C peptide to the B-DNA did not lead to a meaningful increase in gene expression (Figure A.18a). The viability of cells was not affected by the transfection

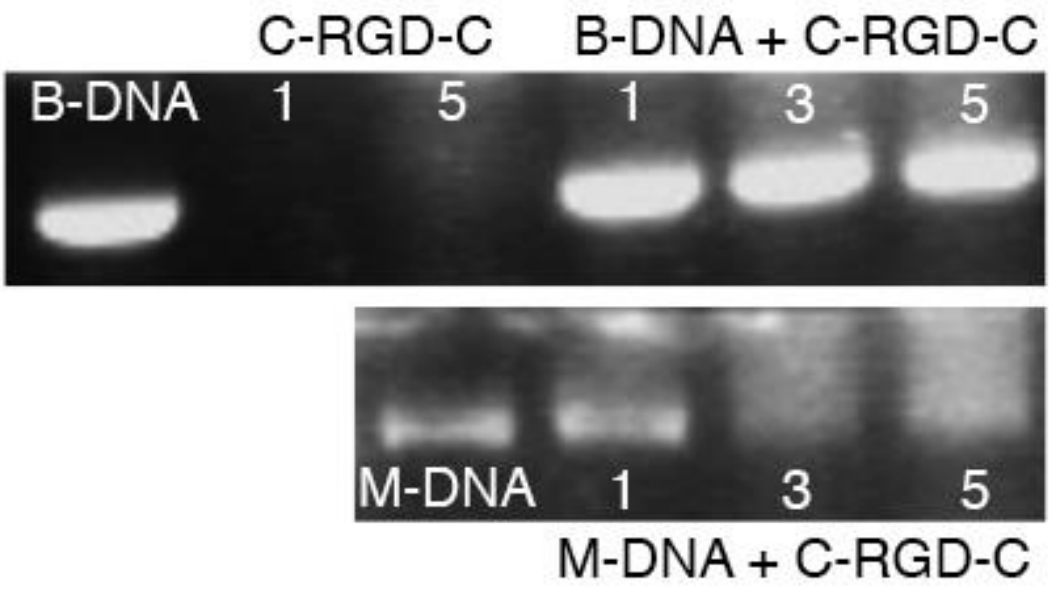

Figure A.15. Agarose gel electrophoresis of M-DNA or B-DNA modified with C-RGD-C peptide. The M-DNA prepared with 7.32 mM $ZnCl_2$ was reacted with C-RGD-C peptide at different CRGDC/DNA weight ratios. The numbers indicate CRGDC/DNA weight ratios.

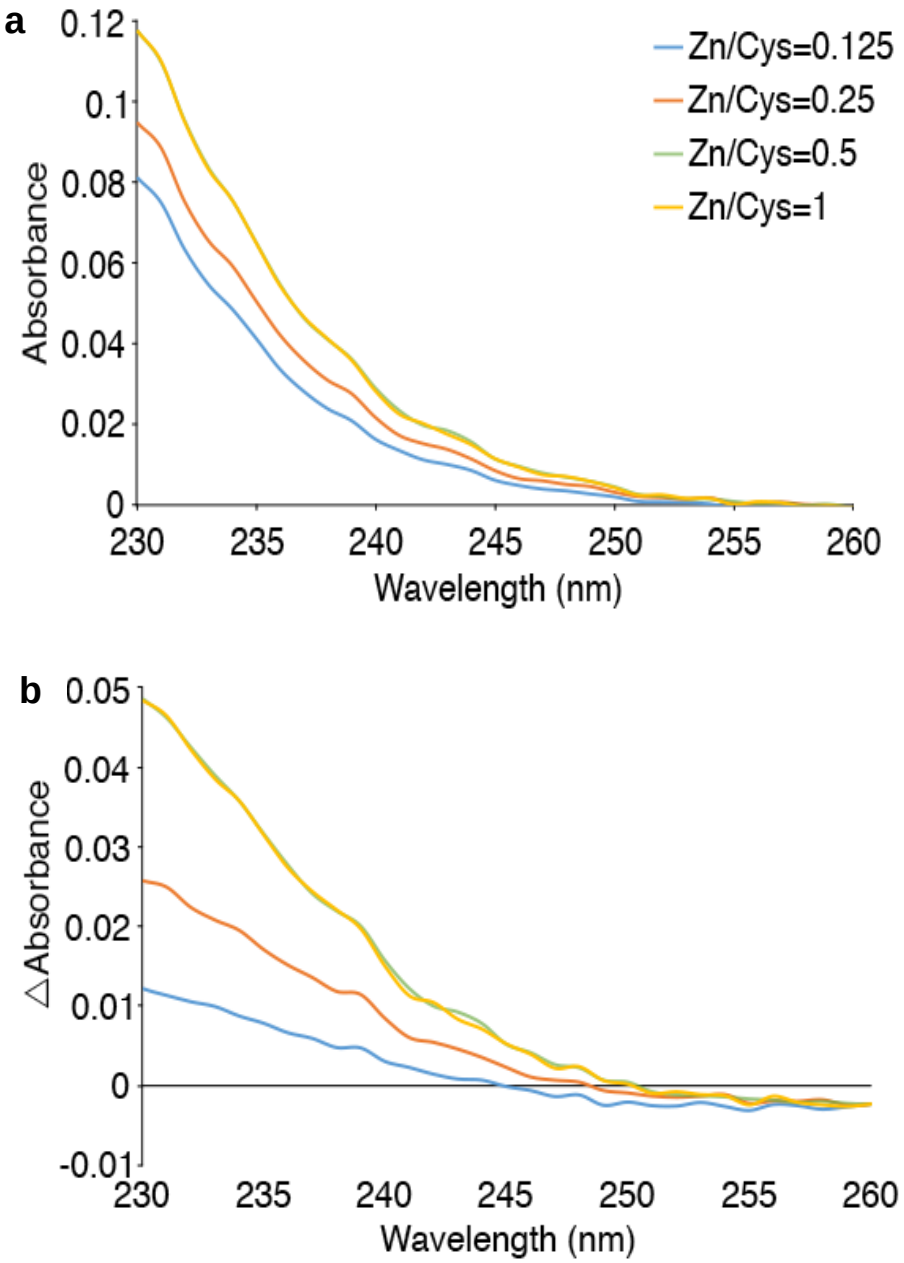

Figure A.16. Spectrophotometric analysis of C-RGD-C/M-DNA complex formation. (a) UV spectra of C-RGD-C/M-DNA complex at CRGDC/DNA weight ratio 0.5/1.0. These results indicate that C-RGD-C peptide binds to Zn^{2+} added on top of M-DNA. (b) UV-difference spectra generated by subtracting the absorbance of peptide from each spectrum from (a). These findings indicate that the LMCT occurs with Zn^{2+} containing M-DNA as seen in Figure A.8 (Line Zn/Cys=1 is superimposed on line Zn/Cys=0.5).

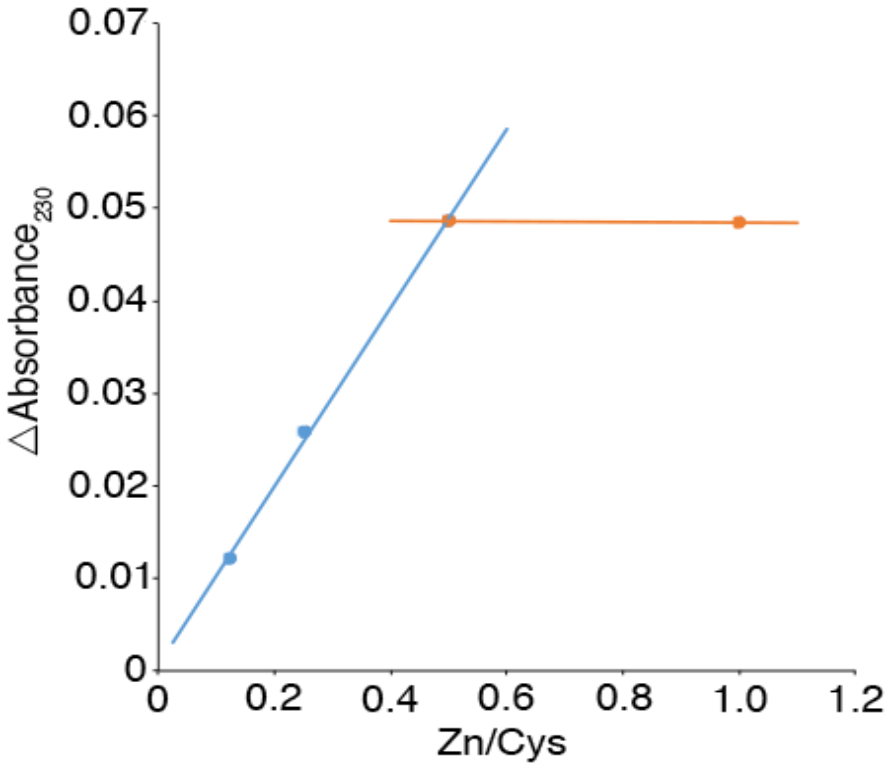

Figure A.17. Changes in absorbance at 230 nm as a function of Zn/Cys ratio.

Table A.1**.** Size and zeta potential

	Size		Zeta potential
	d.nm	PDI	
M-DNA	186.97 ± 5.80	0.25 ± 0.01	-33.36 ± 1.76
C-RGD-C/M-DNA (0.5/1.0)	131.70 ± 8.00	0.54 ± 0.02	-23.25 ± 0.49
Zn/C-RGD-C	3789 ± 241	0.43 ± 0.09	-16.85 ± 0.64

of the C-RGD-C/M-DNA complex (Figure A.18b). This indicates that the gene expression increased as a consequence of C-RGD-C/M-DNA complex formation, which had not been observed by the addition of C-RGD-C peptide to B-DNA. The transfection studies on HEK293 cells further confirm the targeting ability of the C-RGD-C/M-DNA complex. In the HEK293 cells, there was no difference in the levels of luciferase activity between the treatments of C-RGD-C/M-DNA complex and M-DNA (Figure A.19a, b), indicating that the integration of C-RGD-C peptide into M-DNA had no effect on the gene transfection into the nontargeted HEK293 cells. In addition, we compared the cellular uptake of C-RGD-C/M-DNA complex to that of C-RGD-C+B-DNA in MDA-MB-231 cells and HEK293 cells (Figure A.20). The C-RGD-C/M-DNA complex internalized into the cancer cells more efficiently than the B-DNA mixed with C-RGD-C peptide, whereas no difference in cellular uptake was observed between C-RGD-C/M-DNA and C-RGD-C+B-DNA in the normal cells.

A.5. Conclusion

We have explored the feasibility of LMCT transition as a novel means of directly incorporating functional peptides, regardless of their charge density, within DNA. Cationic peptides containing cysteines can facilitate and strengthen the binding to M-DNA through the LMCT transition in combination with electrostatic interaction. Using this strategy, the minimal amount of C-9R-C peptide necessary for reliable gene expression was significantly reduced in comparison to conventional polyplex formation. The LMCT transition method has been further employed to enable the direct incorporation of targeting peptides, such as C-RGD-C, within the M-DNA. The increased gene transfection efficiency

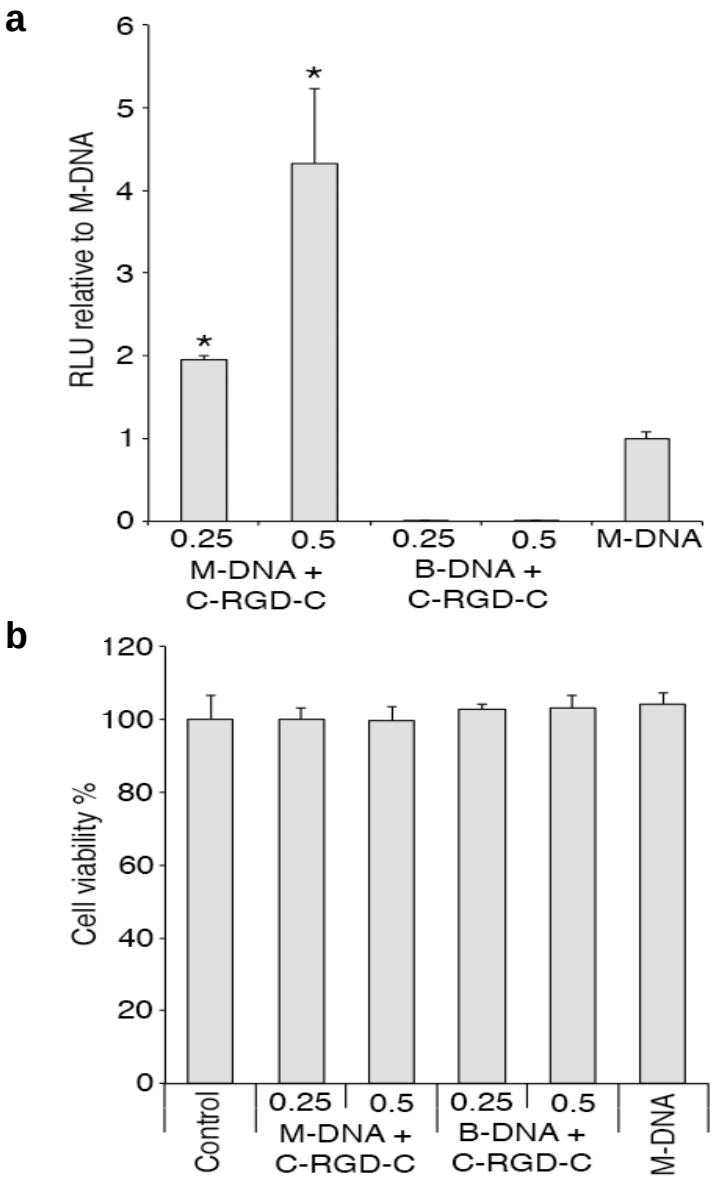

Figure A.18. Luciferase activity (a) and cell viability (b) of MDA-MB-231 cells transfected with C-RGD-C/M-DNA complex. The M-DNA prepared with 7.32 mM $ZnCl_2$ was reacted with C-RGD-C peptide at CRGDC/DNA weight ratio of 0.25 or 0.5. The B-DNA mixed with C-RGD-C peptide served as a negative control (*p<0.05 *vs*. M-DNA).

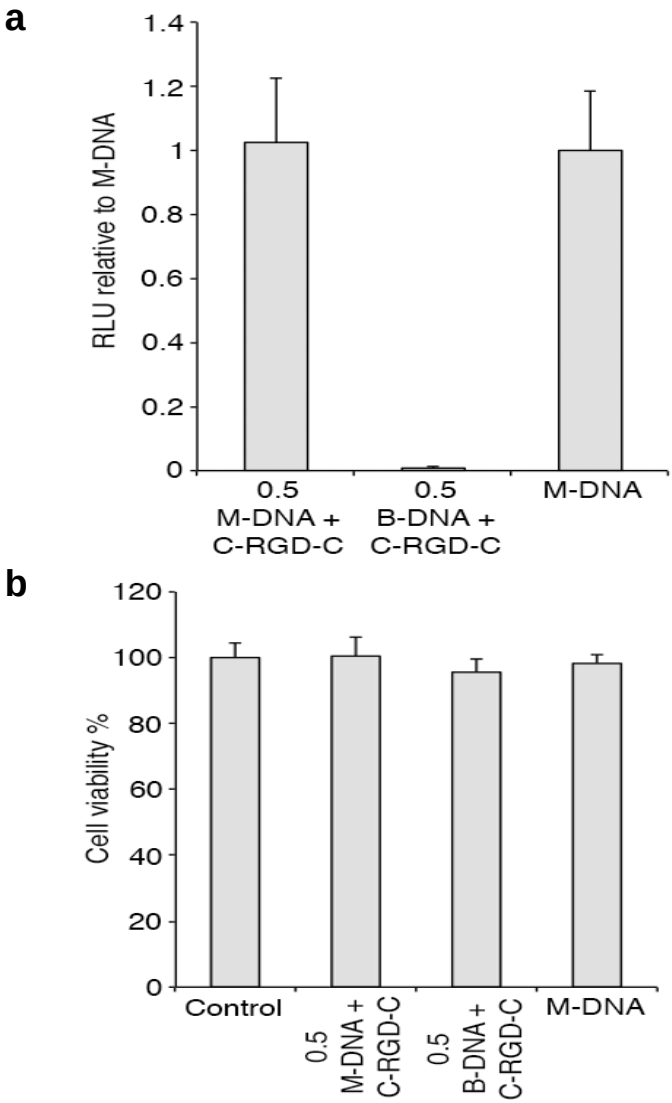

Figure A.19. Luciferase activity (a) and cell viability (b) of HEK293 cells transfected with C-RGD-C/M-DNA complex. The M-DNA prepared with 7.32 mM $ZnCl_2$ was reacted with C-RGD-C peptide at CRGDC/DNA weight ratio of 0.5. The B-DNA mixed with C-RGD-C peptide served as a negative control (*p<0.05 *vs*. M-DNA).

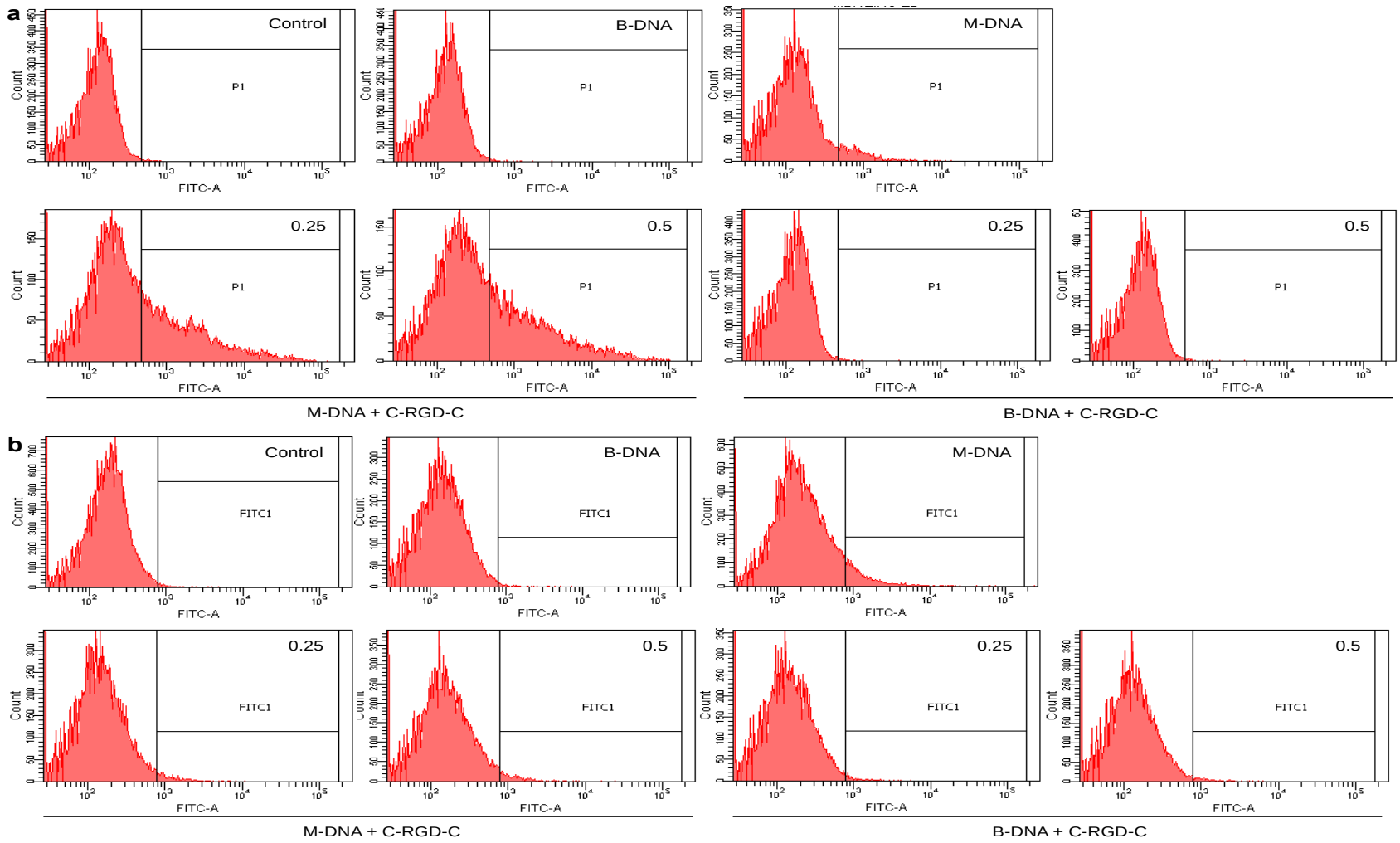

Figure A.20. Cellular uptake of C-RGD-C/B-DNA complex or C-RGD-C/M-DNA complex in (a) MDA-MB-231 cells or (b) HEK293 cells. The numbers represent peptide/DNA weight ratios

in the target cancer cells upon treatment with the C-RGD-C/M-DNA complex indicates that the direct introduction of targeting peptides to M-DNA is a feasible technique for targeted gene delivery. Consequently, the LMCT transition is a promising strategy to modify metal-bound nucleic acids without the requirement for chemical conjugation or electrostatic interaction.

A.6.References

1. Medina-Kauwe LK, Xie J, Hamm-Alvarez S. 2005. Intracellular trafficking of nonviral vectors. Gene Ther **12**(24):1734-1751.

2. Putnam D. 2006. Polymers for gene delivery across length scales. Nat Mater **5**(6):439-451.

3. Whitehead KA, Langer R, Anderson DG. 2009. Knocking down barriers: Advances in siRNA delivery. Nat Rev Drug Discov **8**(2):129-138.

4. Wong SY, Pelet JM, Putnam D. 2007. Polymer systems for gene delivery—Past, present, and future. Prog Polym Sci **32**(8–9):799-837.

5. Park TG, Jeong JH, Kim SW. 2006. Current status of polymeric gene delivery systems. Adv Drug Deliv Rev **58**(4):467-486.

6. Zhou J, Liu J, Cheng CJ, Patel TR, Weller CE, Piepmeier JM, Jiang Z, Saltzman WM. 2012. Biodegradable poly(amine-co-ester) terpolymers for targeted gene delivery. Nat Mater **11**(1):82-90.

7. Lee JB, Hong J, Bonner DK, Poon Z, Hammond PT. 2012. Self-assembled RNA interference microsponges for efficient siRNA delivery. Nat Mater **11**(4):316-322.

8. Lv H, Zhang S, Wang B, Cui S, Yan J. 2006. Toxicity of cationic lipids and cationic polymers in gene delivery. J Control Release **114**(1):100-109.

9. Pack DW, Hoffman AS, Pun S, Stayton PS. 2005. Design and development of polymers for gene delivery. Nat Rev Drug Discov **4**(7):581-593.

10. Henehan CJ, Pountney DL, Zerbe O, Vasak M. 1993. Identification of cysteine ligands in metalloproteins using optical and NMR spectroscopy: Cadmium-substituted rubredoxin as a model [Cd(CysS)4]2- center. Protein Sci **2**(10):1756-1764.

11. Koch M, Bhattacharya S, Kehl T, Gimona M, Vasak M, Chazin W, Heizmann CW, Kroneck PM, Fritz G. 2007. Implications on zinc binding to S100A2. Biochim Biophys Acta **1773**(3):457-470.

12. Krezel A, Maret W. 2007. Dual nanomolar and picomolar Zn(II) binding properties of metallothionein. J Am Chem Soc **129**(35):10911-10921.

13. Aich P, Labiuk SL, Tari LW, Delbaere LJ, Roesler WJ, Falk KJ, Steer RP, Lee JS. 1999. M-DNA: A complex between divalent metal ions and DNA which behaves as a molecular wire. J Mol Biol **294**(2):477-485.

14. Wood DO, Dinsmore MJ, Bare GA, Lee JS. 2002. M-DNA is stabilised in G*C tracts or by incorporation of 5-fluorouracil. Nucleic Acids Res **30**(10):2244-2250.

15. Muntean CM, Nalpantidis K, Feldmann I, Deckert V. 2009. Zn2+–DNA interactions in aqueous systems: A Raman spectroscopic study. J Spectrosc **23**(3-4):155-163.

16. Lim KS, Lee DY, Valencia GM, Won Y-W, Bull DA. 2015. Nano-self-assembly of nucleic acids capable of transfection without a gene carrier. Adv Funct Mater **25**(34):5445-5451.

17. Lee JS, Latimer LJ, Reid RS. 1993. A cooperative conformational change in duplex DNA induced by Zn2+ and other divalent metal ions. Biochem Cell Biol **71**(3-4):162-168.

18. Won YW, Kim HA, Lee M, Kim YH. 2010. Reducible poly(oligo-D-arginine) for enhanced gene expression in mouse lung by intratracheal injection. Mol Ther **18**(4):734-742.

19. Won YW, Yoon SM, Lee KM, Kim YH. 2011. Poly(oligo-D-arginine) with internal disulfide linkages as a cytoplasm-sensitive carrier for siRNA delivery. Mol Ther **19**(2):372-380.

20. Won YW, Adhikary PP, Lim KS, Kim HJ, Kim JK, Kim YH. 2014. Oligopeptide complex for targeted non-viral gene delivery to adipocytes. Nat Mater **13**(12):1157-1164.

21. Maret W, Li Y. 2009. Coordination dynamics of zinc in proteins. Chem Rev **109**(10):4682-4707.

22. Won YW, McGinn AN, Lee M, Bull DA, Kim SW. 2013. Targeted gene delivery to ischemic myocardium by homing peptide-guided polymeric carrier. Mol Pharm **10**(1):378-385.

23. Won YW, Bull DA, Kim SW. 2014. Functional polymers of gene delivery for treatment of myocardial infarct. J Control Release **195**:110-119.

24. Tanimoto M, Kamiya H, Minakawa N, Matsuda A, Harashima H. 2003. No enhancement of nuclear entry by direct conjugation of a nuclear localization signal peptide to linearized DNA. Bioconjug Chem **14**(6):1197-1202.

25. van der Aa MA, Koning GA, d'Oliveira C, Oosting RS, Wilschut KJ, Hennink WE, Crommelin DJ. 2005. An NLS peptide covalently linked to linear DNA does not enhance transfection efficiency of cationic polymer based gene delivery systems. J Gene Med **7**(2):208-217.